Title
THE PERFORMANCE AND ELECTROCHEMICAL BEHAVIOR OF FLUIDIZED BED ELECTRODES

Author
Huh, T.

Publication Date
1985-05-01

Lawrence Berkeley Laboratory
UNIVERSITY OF CALIFORNIA

Materials & Molecular
Research Division

THE PERFORMANCE AND ELECTROCHEMICAL BEHAVIOR OF FLUIDIZED BED ELECTRODES

T. Huh
(Ph.D. Thesis)

May 1985

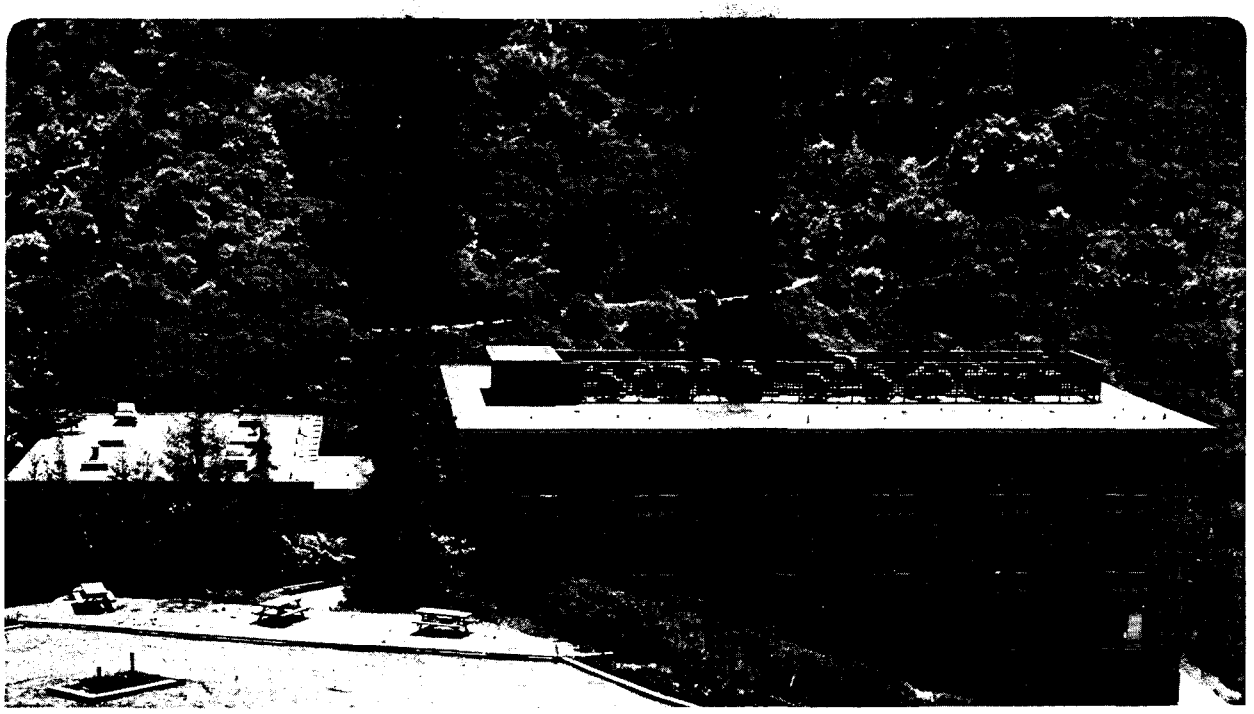

Prepared for the U.S. Department of Energy under Contract DE-AC03-76SF00098

DISCLAIMER

LBL-19621

The Performance and Electrochemical Behavior of Fluidized Bed Electrodes

Taeyoung Huh
Ph.D. Thesis

Lawrence Berkeley Laboratory
University of California
Berkeley, California 94720

May 1985

THE PERFORMANCE AND ELECTROCHEMICAL BEHAVIOR
OF FLUIDIZED BED ELECTRODES

Taeyoung Huh

Ph.D.

Materials Science and Mineral
Engineering Department

James W. Evans

James W. Evans
Chairman of Committee

ABSTRACT

The fluidized bed electrode has been studied to characterize its behavior and evaluate its possible application to the electrowinning of precious metals and to the energy storage system. Its performance and electrochemical behavior has been analyzed in terms of various operating parameters.

The first part of the study is concerned mainly with the overall performance of a fluidized bed electrode for silver recovery from aqueous cyanide solution. The effects of applied current density, bed expansion and electrode materials have been considered and it is found that the performance is free of operating problems and is superior to the Zadra type cell, which is commonly used for precious metal recovery.

The second part is concerned with the internal behavior of fluidized bed electrode. The particle and electrolyte potentials and overpotentials in fluidized bed electrodes of two different types have

been measured and analyzed by means of the probability density distribution and the power spectral density distribution. The resistance of such electrodes are also measured.

The potential transients are observed to depend on current, bed expansion and position in the bed (for copper particles) and each potential can be regarded as a time averaged value onto which two kinds of "noise", low frequency "flicker" noise and white noise, are added. Difference between the two types of electrode is explained by the existence of bubbles in the bed.

The distribution of time averaged overpotential within the Sorapec particle bed is in qualitative agreement with predictions of prior mathematical models.

THE PERFORMANCE AND ELECTROCHEMICAL BEHAVIOR
OF FLUIDIZED BED ELECTRODES

Taeyoung Huh

TABLE OF CONTENTS

ACKNOWLEDGEMENTS

The work and successful outcome represented by this dissertation could only have been done with the support of a large number of people.

My appreciation is gratefully extended to Professor J. W. Evans for his ongoing support, guidance and for his always being available for consultation during the course of this work; to Professor D. W. Fuerstenau for his valuable advice and guidance during my stay at Berkeley; to Professor C. W. Tobias for his introduction to the world of electrochemistry and reviewing this manuscript kindly. In addition, the support given by my fellow students past and present, especially Don and Rajiv, and by the department staff was invaluable and is gratefully acknowledged.

I am greatly indebted to my family. I would like to thank my wife, Youngju, who shared my life, for her gentle patience, constant encouragement and infinite moral support; my father and mother for their immeasurable support, invaluable encouragement and for giving me the opportunity for higher education; my father-in-law for his love, support and careful mind which were expressed by his weekly letters. My family have all been a constant source of inspiration to me and therefore have immensely contributed to this achievement in my life.

Last but not least of all, I wish to thank my God the Father in the Heaven.

This work was supported partially by Homestake Mining Corporation under Service to Industry Contract ES7705 and partially by the Assistant

Secretary for Conservation and Renewable Energy, Office of Energy System Research, Energy Storage Division of the U. S. Department of Energy under Contract number DE-AC03-76SF00098.

I. INTRODUCTION

The fluidized bed electrode has been a focus of many electrochemical and/or extractive metallurgical research projects for the last decade or so.

A cell with a fluidized bed electrode consists of two compartments separated by a porous diaphragm. The solid sheet electrode of the conventional cell is replaced by a bed of conducting particles contained in one compartment. A solid current feeder provides electrical connection with the external circuit, and electrolyte flowing upward from the bottom of the chamber provides the fluidization. The second compartment contains a counter electrode rather similar to the conventional sheet electrode.

The main advantage of the fluidized bed electrode is its very large effective electrode surface area per unit volume. This increases the effective current capacity beyond that of a conventional cell.

However, this electrode has suffered from an unexpected disadvantage, higher power consumption than that of a conventional electrode during the electrowinning process. This is mainly due to the conventional type of anode typically employed as a counter electrode. Due to the high current density at the anode, there exists high oxygen overpotential, and highly evolved oxygen at the anode forms a stream of bubbles between anode and diaphragm. The consequent high cell potential is directly related to the power consumption.

Research has been directed toward characterizing the behavior of a

fluidized bed electrode in terms of operating parameters, to determine the feasibility of its use in extractive metallurgical processes.

Even though considerable successful results have been reported on the performance and gross behavior of the fluidized bed electrode, it has not yet been used in commercial metal production. This is due to insufficient understanding of the electrical and electrochemical behavior of such electrodes compared to conventional electrodes.

The present research is concerned with two topics. The first is determining operating parameters of the fluidized bed electrode for precious metal recovery from aqueous cyanide solution. The second is acquiring basic knowledge of its internal behavior, to support various applications. Potential transients in such electrodes are inherent because of the dynamic behavior of the two media, particle and electrolyte. These variations affect the kinetics of the electrochemical reactions occurring in the cell and the morphology of the electrode; thereby the overall performance of the cell is affected.

In this dissertation, the same parameters will be expressed in two different ways for their respective applications. For example, the superficial current density will be expressed in A/m^2 for the electrowinning process and mA/cm^2 for battery application because these units are usual in their respective fields. Also voltage (overvoltage, cell voltage) for the former is the same as potential (overpotential, cell potential) for the latter.

II. PREVIOUS INVESTIGATIONS

In the late 1960's, Trupp[1] and Bordet[2] et al. investigated the dynamics of liquid fluidized beds to provide data for assessing the technical feasibility of a liquid fluidized bed nuclear reactor. Those results (without electrochemical reactions) are relevant to the idea of particle-particle interactions in fluidized bed electrodes. LeGoff[3] et al. cited the possible advantage of associating fluidization and electrolysis by analyzing the works in two different phenomena.

In 1969, a group of British researchers[4] initiated the investigation of fluidized bed electrodes by studying the cathode reduction of m-nitro benzene sulfonic acid to metanilic acid in aqueous sulfuric acid. Since then, many research projects have been carried out on the fluidized bed electrode.

Fleischmann[5,6] and Goodridge[7] and their respective co-workers have developed a fluidized bed theory, based on a postulated convective charge transfer mechanism. This mechanism consists of charge sharing by the collision of particles (charged at the current feeder) with uncharged particles. Their models employ a charge transfer coefficient which is dependent upon hydrodynamic condition, particle size, electrolyte composition and electrode kinetics. Fleischmann et al[5,6] have attempted to determine the charge transfer coefficient, but their calculated values do not agree well with values obtained experimentally.

Sabacky[8] and Sabacky and Evans[10] applied the porous electrode model by Newman and Tobias[11] to the fluidized bed electrode and determined the

potentials distribution through the bed. By using AC current they also determined the effective bed resistivity of fluidized bed electrodes. Their results indicate that charge is transported by simple electronic conduction through chains and/or clusters of the particles that are in contact, this conduction path proceeding as far as the current feeder. Their conclusions support the results of Beenackers[12].

Goodridge[13] has proposed bipolar behavior for the fluidized bed electrode, where the particle potential is near rest potential and behaves anodically on one side and cathodically on the other. Goodridge, King and Wright[14] reported on the performance of bipolar fluidized bed electrodes in the production of hypobromide, the electrolysis of sea water and the synthesis of dimethyl sebacate. More recently Plimley and Wright[15] have extended the bipolar mechanism to current flow through a fluidized bed electrode in copper electrowinning by measuring the local overpotential distributions for a certain time period. They showed that the nodes of potential histograms moved from cathodic potential to rest potential as the point of observation moved from current feeder (cathodic) toward the interior. But the explanation of charging the particles at the current feeder was the same as that of the conductive mechanism. Figure II-1 shows the possible charge transfer mechanisms in fluidized bed electrodes proposed by various researchers.

Sabacky[8] and Sabacky and Evans[9] reported the conductivity of fluidized bed electrode to be relatively independent of particle size and electrolyte conductivity. The conductivity of the bed was mainly

i) Collision mechanism

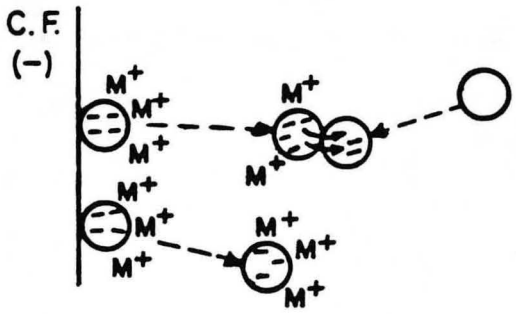

ii) Conductive mechanism

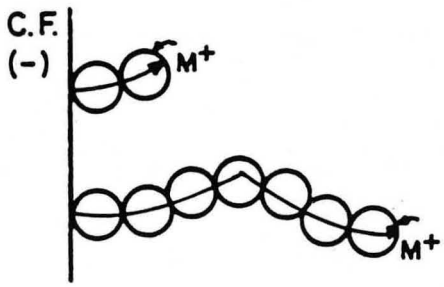

iii) Bipolar mechanism

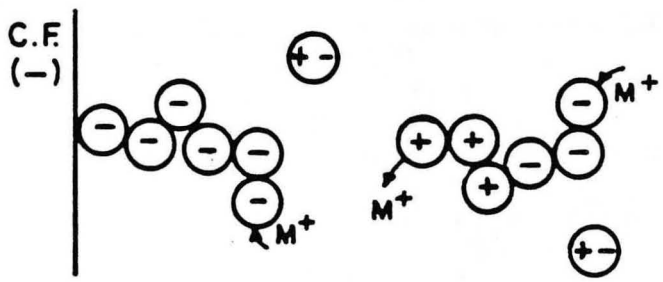

Figure II-1 Possible charge transfer mechanisms in fluidized bed electrodes

dependent on bed expansion, i.e., particle volume fraction. Turner[16] and Handley and Eardley[17] also measured the conductivity of liquid fluidized bed electrodes and Turner[16] applied an empirical two parameter model to fit experimental data. They concluded that the major means of electrical conduction in the liquid fluidized bed was particle to particle linkages.

Two different fluidized bed electrode designs have been used. One is the plane parallel configuration and the other is side by side design. In the former, the macroscopic current flow is parallel to the flow of electrolyte and in the latter, the flows are perpendicular.

Investigations on the general behavior of fluidized bed electrode during metal electrowinning reactions are of the greatest importance and of interest to extractive metallurgists.

Salt[18] proposed a laboratory apparatus for electrodepositing iron on stainless steel particles in a fluidized bed, to solve the compaction and sintering problem of stainless steel powders due to the presence of persistent oxide film on the particles. Flett[19] was the first researcher to use the fluidized bed electrode in the electrowinning of metals from dilute solutions. He used copper coated ballotini particles as a cathode to electrowin copper from dilute copper sulfate solutions. Flett[25] used copper particles in his second investigation to electro-deposit copper from dilute aqueous solutions and also used a fluidized bed anode in an electrorefining cell. He proposed a flowsheet to produce high quality copper with fluidized bed electrowinning and electrorefining from dilute aqueous leaching solutions. He also

reported an increase in current efficiency with an increase in current density in fluidized bed electrowinning operations.

Fleischman[20,21] and Goodridge[22,23], with respective co-workers, measured particle and electrolyte potentials distributions through the fluidized bed cathode during copper electrowinning and compared their measurements with mathematical predictions. However in view of the complexity of the system and the necessary simplifying assumptions, it was not surprising that on the whole their calculated values do not agree well with those obtained experimentally.

Wilkinson and Haines[26,27] conducted some pilot plant scale experiments for long time periods extending up to 100 hours on the use of a fluidized bed copper cathode in electrowinning from dilute aqueous solutions. They showed some operating difficulties in treating leach liquors directly and analyzed the way to overcome those difficulties.

Many investigations have been performed on copper electrowinning with a fluidized bed cathode. Cabin and Gabe[28,29] studied the effects of various operating conditions on the performance of fluidized bed copper electrowinning from acid sulfate solutions. Monhemius and Costa[30] also investigated the electrodeposition of copper from dilute copper solutions using copper coated glass spheres, but they used a fluidized bed that was probably too shallow to eliminate end effects[31]. Simpson[32] determined whether copper produced in one step by fluidized bed electrolysis of an untreated dilute heap leach liquor, would be of sufficient quality to avoid the need of costly repurification steps.

Hutin and Coeuret[33] determined overpotential distribution through

the fluidized bed electrode during copper deposition from concentrated solutions using a fluidized cathode of a plane parallel shape, and mentioned the existence of dissolution zones (anodic regions) within the electrode. This may limit the use of plane parallel design of fluidized bed electrodes. Sabacky and Evans[34] conducted copper electrowinning from acidified concentrated copper sulfate solution with a laboratory scale cell equipped with a fluidized bed cathode. They reported power consumptions higher than that of the conventional electrowinning process, a behavior resulting mainly from excessive consumptions in the anode chamber and cell diaphragm. They found that a major problem associated with the fluidized bed electrode was the "welding" of particles to the porous partition and to the current feeders. With a mathematical model , they explained that these problems are aggravated by high local deposition rates due to extremes of bed resistivity. Masterson[35] and Masterson and Evans[36] constructed a pilot scale fluidized bed electrode of 1000 Amp nominal current to test the technical feasibility of copper electrowinning. They also determined the effect of the presence of an oxidizing agent in electrolytes on the potential distribution, by their mathematical model, and found that there existed an anodic region in the central part of the bed and this region was not eliminated by increasing the current density. Ziegler[37] and Ziegler et al.[38] tested various anodes to reduce power consumption in the anode chamber during copper electrowinning, and Dubrovsky et al.[39] designed anode chambers with DSA (a titanium mesh with an electrocatalytic coating, Eltech Corp.) directly against the diaphragm.

Table II-1 : Summary of some of previous research

Investigators	Ref.No.	Metal	Cell*	Electrolytes	C.D.+
Germain & Goodridge	23	Cu	rec side	2g/l Cu 100g/l H_2SO_4	220-3000
Simpson	32	Cu	rec side	2g/l Cu 100g/l H_2SO_4	550-1100
Fleischmann et al.	21	Cu	cyn side	1g/l Cu 100g/l H_2SO_4	...
Cabin & Gabe	29	Cu	cyn plane	0.2-4g/l Cu 0.5g/l H_2SO_4	...
Wilkinson & Haines	26	Cu	rec side	2g/l Cu 100g/l H_2SO_4	1000-5000
Flett	25	Cu	cyn side	2g/l Cu 100g/l H_2SO_4	...
Fleischmann & Kelsal	56	Cu	cyn plane	...	...
Monhemius & Costa	30	Cu	cyn plane	2g/l Cu 100g/l H_2SO_4	...
Coeuret & Hutin	33	Cu	cyn plane	5-40g/l Cu 10-100g/l H_2SO_4	450-3500
Sabacky & Evans	34	Cu	cyn side	20g/l Cu 100g/l H_2SO_4	2200-6600
Goodridge & Vance	24	Cu	rec side	2.5g/l Cu 100g/l H_2SO_4	1000-5000
Sherwood et al.	40	Ni	cyn side	2-4g/l Ni 60g/l Na_2SO_4 pH 3	220-2000
Masterson & Evans	36	Cu	rec side	25g/l Cu 100g/l H_2SO_4	1000-8800
Ziegler et al.	38	Cu	rec side	25g/l Cu 100g/l H_2SO_4	1000-5000

Table II-1 continued

Dubrovsky & Evans	41	Co	rec side	4.8-100g/l Co	1000-9100
Goodridge & Vance	42	Zn	rec side	20-80g/l zinc sulfate 0.2-5g/l H_2SO_4	2000-6500
Kreysa & Heitz	52	Ag	cyn plane	3-5g/l silver nitrate	250
Jiricny & Evans	43	Zn	rec side	30-50g/l zinc sulfate 0 - 50g/l H_2SO_4	1000-9000

* Cell configuration, rec: rectangular
cyn: cylindrical
side: side by side
plane: Plane parallel

+ Superficial current density, A/m^2

With this anode they reported that power consumption was less than that of the conventional cell even with much higher current densities (Figure II-2).

The performance of fluidized bed electrodes was judged by the current efficiency and energy consumption for electrowinning of certain metals. For the copper, typical values for conventional electrowinning would be a current efficiency of 90 to 95 percent and an energy consumption of 2.2 kWh/kg Cu. Dubrovsky et al.[39] reduced the energy consumption to less than 2 kWh/kg Cu and reported the current efficiency to be well over 90 percent until copper was depleted down to a few ppm.

Most of the researchers who have studied fluidized bed copper electrowinning from dilute aqueous solutions generally agree that current efficiency increases with an increase of current density.

Studies of the other metals have been few compared to those of copper. Sherwood et al.[40] studied nickel, Dubrovsky and Evans[41] cobalt, Goodridge and Vance[42] zinc, and recently Jiricny and Evans[43] studied zinc electrowinning from neutral and acid solutions and reported the effects of added impurities on the performance of the fluidized bed electrode.

LeRoy[44,45] analyzed the particle size distribution of a fluidized bed electrode during continued electrowinning of metals in two different operating modes, one of which included the time variation of the current density for a prolonged period of time, the other being a constant current mode.

Recovery of precious metals will be mentioned in Chapter III.

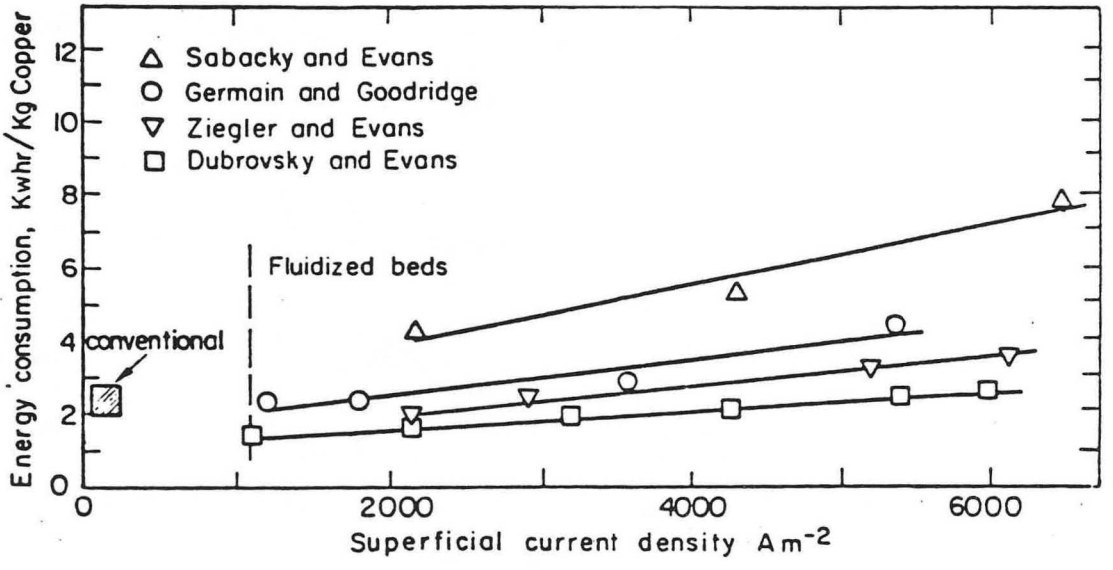

Figure II-2 Improvements in energy consumption in fluidized bed electrowinning of copper

Symbol	Ref. No.
△	34
○	23
▽	38
□	39

Other miscellaneous investigations of mass transfer have been made by Cabin and Gabe[46,48] and Pickett[47].

Even though the fluidized bed electrowinning of metals has been the subject of extensive investigations, there has been only one reported successful commercial operation of this electrode. Akzo Zout Chemie Netherland B.V[49] has installed fluidized bed electrodes to treat waste water by electrochemicallly removing heavy metallic ions.

III. SILVER ELECTROWINNING

A. Introduction and Previous Research

Several new processes have recently been developed for the extraction and recovery of precious metals. One of the most successful is the Carbon-in-Pulp (CIP) process, developed by the U. S. Bureau of Mines [50] and first implemented at the Homestake Mining Company[51]. Electrowinning has become the industrial standard for recovering gold and silver from carbon strip solutions, which typically have less than 1000 ppm of noble metal concentration.

The Zadra cell is commonly used to electrowin silver from aqueous cyanide solutions[51]. This cell employs an extended surface area cathode consisting of steel wool and is operated in a semi-batch mode with periodic shutdown for manual removal of the silver and replacement of the steel wool. The cell suffers from the disadvantage that the cathode degrades as it undergoes a cementation reaction with the silver in solution. Consequently the silver obtained from the cell is in the form of particles admixed with fragments of steel wool and must be subjected to further processing to yield bullion. A cell equipped with a cathode of fluidized silver particles appears to be an attractive alternative to the Zadra cell. The former might be charged and discharged automatically and yield a silver product of the desired purity. The purpose of the investigation described here was to test the feasibility of this idea on a bench scale by studying the effects of various cathode

particles, different anode materials and electrolyte compositions on the overall performance of fluidized bed electrode for silver electrowinning from aqueous cyanide solution.

Kreysa and Heitz[52] have investigated the fluidized bed electrowinning of silver from silver nitrate solutions at lower current density than most of those used in the present study. Paul et al.[53] designed a packed bed electrowinning cell for the recovery of gold from aqueous cyanide solution. More recently Watterman and his coworkers[54] studied the effects of various operating conditions on the fluidized bed electrowinning of gold from cyanide solutions and compared the results with a laboratory scale Zadra type cell.

B. Experimental Apparatus and Procedure

Figure III-1 depicts the 50 Amp cell used in this investigation. The cell was reactangular in geometry and the fluidized bed cathode had horizontal dimensions of 63mm wide and 19mm deep. The depth is in the direction of current flow. Separate cathode and anode chambers were made and bolted together with the diaphragm positioned between the anode and cathode chamber. When expanded the fluidized bed height was around 150mm. In all runs, 25% bed expansion was used. Fluidization was maintained by pumping the silver containing electrolytes up through the bed.

To the left of the fluidized bed is the current feeder which serves as the electrical connection to the particles. Throughout this

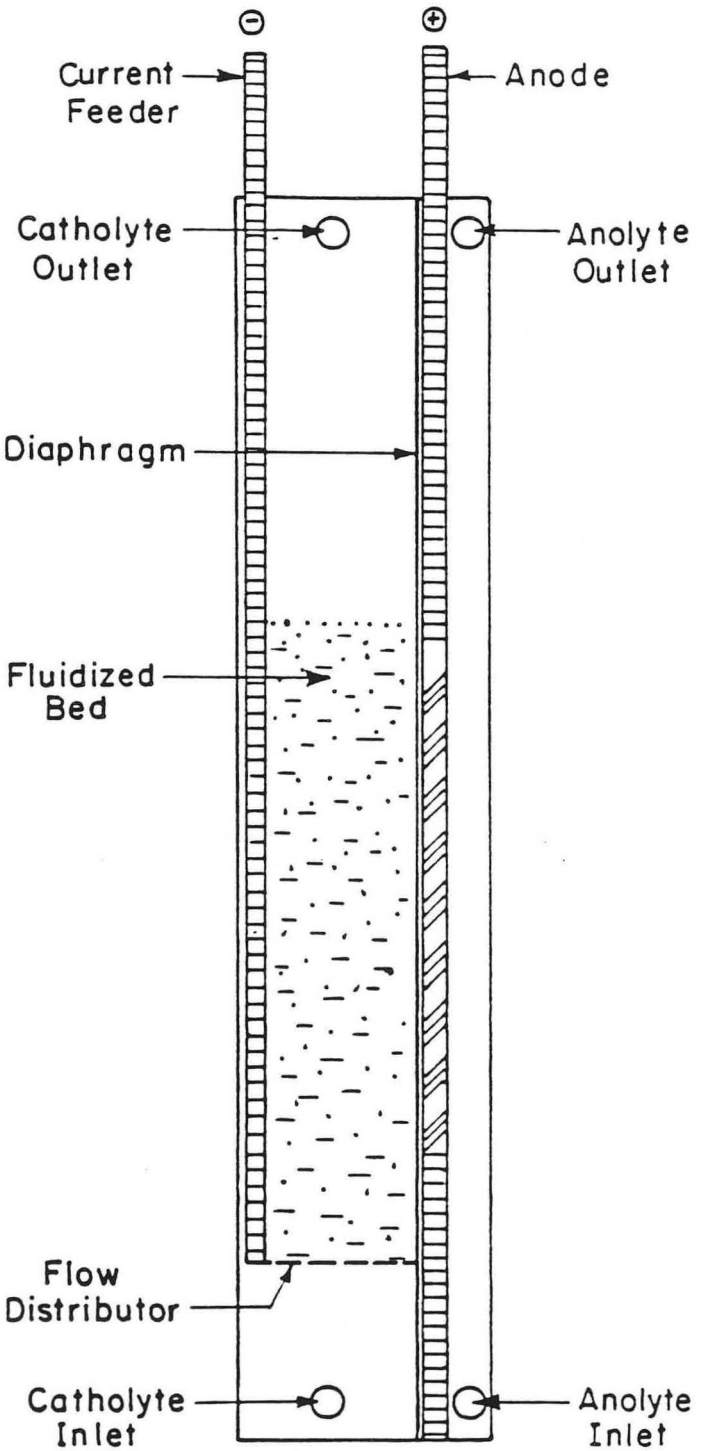

Figure III-1 Side view of laboratory scale cell with fluidized cathode

investigation a 4mm thick graphite sheet was used as a current feeder. Occasionally in fluidized bed electrowinning a problem of metal deposition on the current feeder is observed, but no such problem was encountered in this investigation. To the right of the fluidized bed is the anode chamber which is separated from the fluidized bed by a porous diaphragm. The diaphragm was a synthetic material called "Daramic" (W. R. Grace Corp.) in most runs.

Throughout most of the investigation the catholyte was based on a solution (EW Feed 10-18-81) provided by Homestake Mining Corporation. The Homestake analysis of this solution appears as Table III-1. This was mixed with a 15g/l silver cyanide solution, which was produced by dissolving pure silver plate in a potassium cyanide solution containing 10g/l of KCN (Reagent grade, Mallinckrodt Inc), to bring the silver concentration up to higher levels so that a greater range of silver concentration could be studied. The anolyte used in the investigation was prepared by dissolving sodium hydroxide (Reagent grade, Mallinckrodt Inc) in a known amount of distilled water to achieve the desired pH. For the anolyte containing Na_2SO_4, anhydrous Na_2SO_4 (Reagent grade, J. T. Baker Chemical Co) was dissolved in a known amount of distilled water to make 0.5M Na_2SO_4 solution and then NaOH was added to achieve the desired pH. The experiments were conducted in a batch fashion, pumping catholyte and anolyte from reservoirs, through the cell and back to the reservoirs. Figure III-2 is the apparatus schematic.

The experimental procedure consisted of filling each reservoir with catholyte and anolyte, respectively. The pumps were turned on and the

Table III-1 : Analysis of Homestake Cyanide Solution (EW Feed 10-18-81)

Ag	Cu	Pb	Zn	Co	Cl	Al
200.	81.	3.6	840.	0.9	I	0.3

Ni	As	Sb	Bi	Fe	NaOH
3.4	I	2.1	<0.02	810.	2414.

Total CN	Free CN
4660.	2240.

Note : all are in mg/l

I : Interference precludes determination of As and Cl

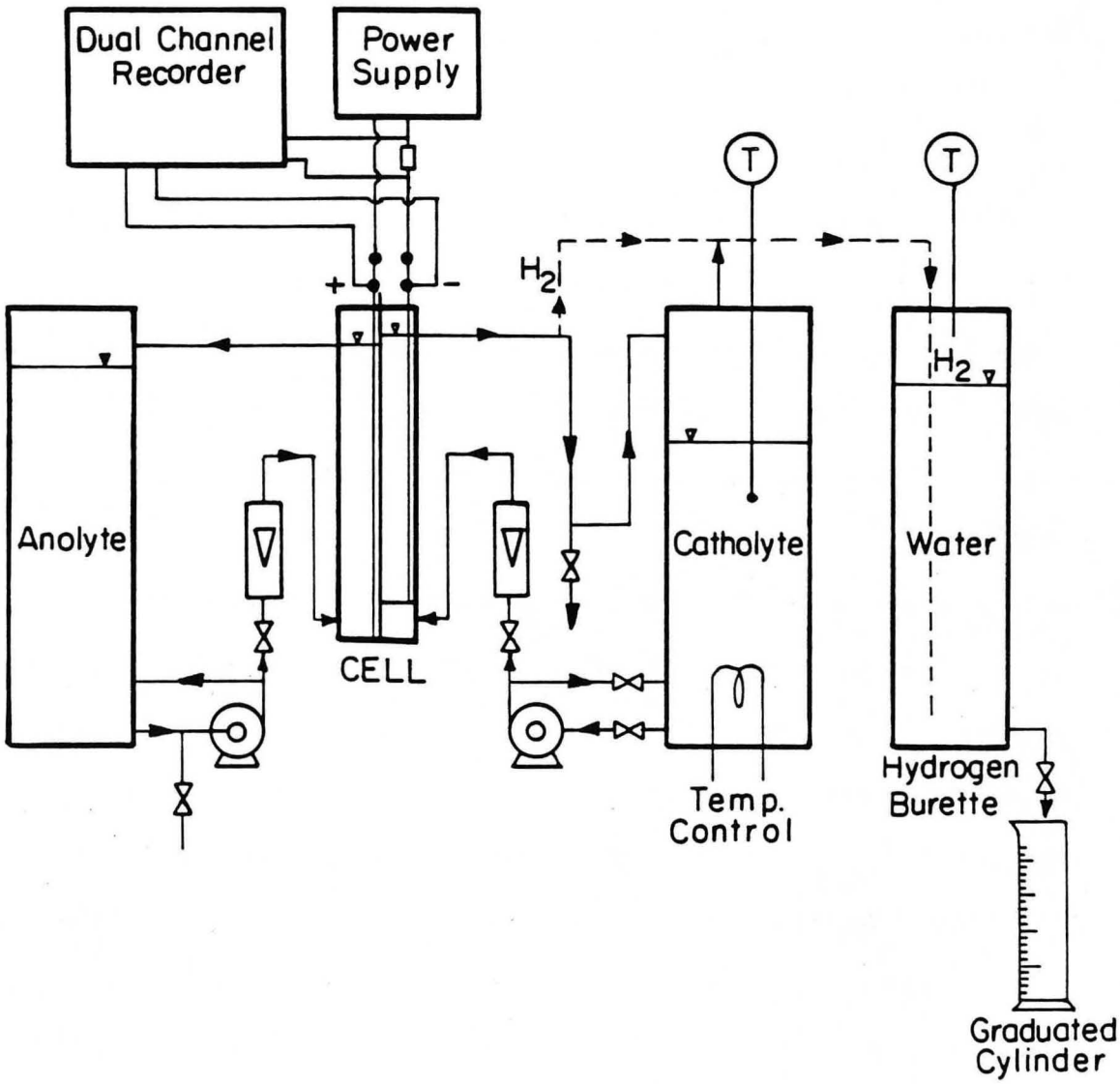

Figure III-2 Experimental apparatus schematic

particles were added to the cathode chamber. The catholyte flow rate was then adjusted to bring the bed expansion to the desired level. The current to the cell (supplied by a Hewlett Packard 6261 B DC power supply) was then turned on and electrolysis commenced. All experiments were run in a constant current mode. The catholyte was sampled periodically and the samples were analyzed by Atomic Absorption Spectrophotometry (Perkin-Elmer 603). Electrolysis was stopped when hydrogen evolution in the cathode became severe. The cell current efficiency was obtained by calculation from silver depletion of the catholyte.

The cell current/voltage relationship was obtained by simply varying the current and noting the voltage as measured on a standard strip chart recorder. These measurements were of short duration and could therefore be carried out at essentially constant catholyte composition. To measure cathode potential drop, the saturated calomel reference electrode was connected to the cell by a luggin capillary with the tip located at the center of active window area of diaphragm in the cathode chamber. This measurement was also recorded on strip chart recorder.

To study the behavior of major impurities, concentration of those impurities were also measured by Atomic Absorption Spectrophotometry and deposited silver particle surfaces were analyzed by Energy Dispersive Analysis by X-ray (EDAX).

Various anodes and cathode particles were used in this investigation. Details concerning these are discussed later.

C. Results and Discussions

Table III-2 summarizes the results for silver electrowinning experiments. Figure III-3 shows a cell voltage and applied current density relationship of a fluidized bed electrode, with silver coated copper particles as a cathode and a platinized titanium mesh as an anode. Catholyte was a synthesized pure silver cyanide solution. The superficial current density is the current density of the active window area of the diaphragm.

As a preliminary step, Nafion (Type 214, E.I.dePont) was tried as an alternative for the cell divider. Figure III-4 shows the cell voltage vs. superficial current density curves with two different diaphragm materials. Except for the diaphragm, all conditions were kept the same. Because of higher cell potential, as well as weldment of particles on Nafion due to surface roughness, all subsequent experiments were performed with the Daramic as a cell divider.

1. Behavior of Various Cathode Particles

In a commercial fluidized bed cell, silver would be electrowon onto silver seed particles, perhaps starting with a 0.5mm seed and growing the particle to 2.5 mm. Such a growth represents an increase in mass by a factor of 125 and therefore only a limited need for seeds. In the early stage of this investigation, difficulty was experienced in obtaining silver particles and a number of alternatives were tried. The

Table III-2 : Summary of Experimental Results

	1	2	3	4	5	6	7	8	9
Catholyte*									
Ag Conc. (ppm)	3270	1700	1130	1520	1860	1980	1460	1500	1770
pH	11.6	11.7	10.3	10.9	10.9	10.7	10.6	10.4	10.6
Anolyte**	1	1	1	2	2	2	2	1	2
pH	13.4	12.7	12.4	12.5	12.4	12.5	12.7	13.5	12.7
Superficial Current Density (A/m^2)	900	450	225	900	450	1350	450	450	900
Actual Current (Amp)	4	2	1	4	2	6	2	2	4
Final Ag Conc.(ppm)	78	2	1	13	2	472	1.5	1	1
Overall Current Efficiency(%)	70	72	68	58	66	61	63	63	63
Cell Voltage (Volts)	4.5	3.0	2.6	5.2	3.6	4.6	3.5	3.4	4.2
Energy Consumption (kWh/kg Ag)	1.6	1.1	0.9	2.1	1.3	1.9	1.4	1.6	1.6
Cathode Particle***	SN	SCC	SCC	SCC	SCC	SCC	SS	SCC	SS
Anode Material†	DSA	DSA	Pt	PT	316	316	Pt	316	Pt
Remarks	a				b	b			

* Others are Homestake solution enriched with silver

** 1 = NaOH only; 2 = MaOH + ½ M Na_2SO_4

*** SN = Silver needle shape particles; SCC = Silver-coated copper particles
SS = Silver shots

† DSA = Dimensionally stable anode ; Pt = Platinized Ti mesh anode ; 316 = 316 stainless Steel anode, perforated

a = H_2 evolution matches to concentration drop; b = stainless steel oxidized

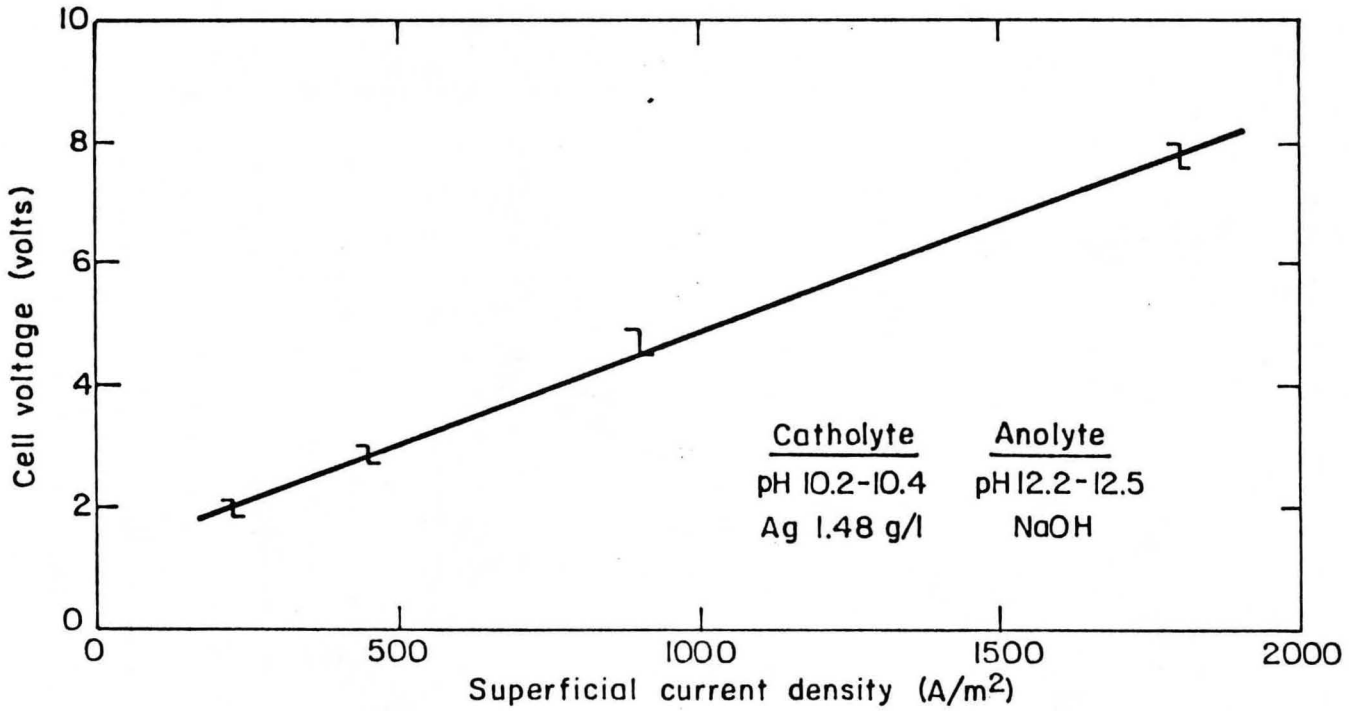

Figure III-3 Cell voltage and superficial current density relationship of fluidized bed electrode (Cathode: silver coated copper particles, Anode: platinized Ti mesh)

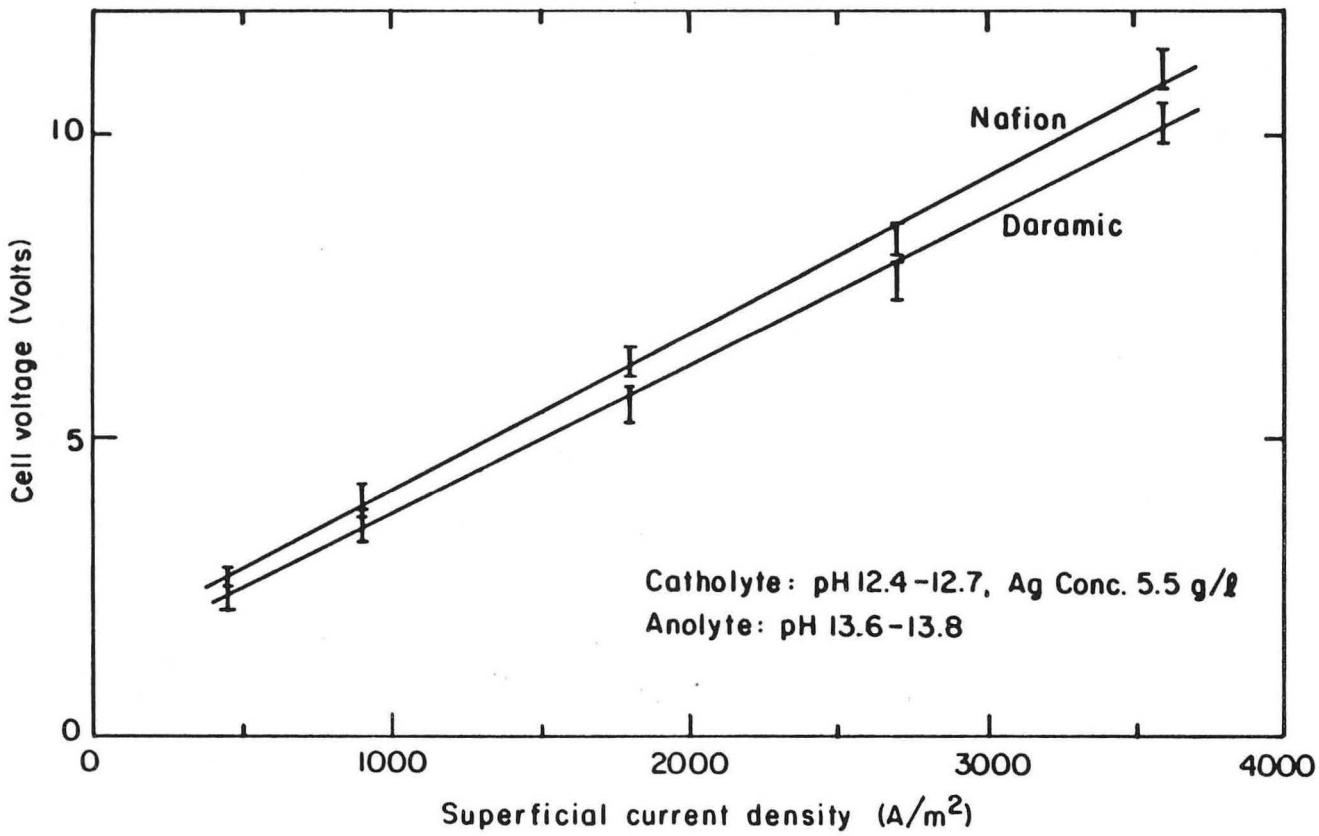

Figure III-4 Effect of different diaphragms on cell voltage

best alternative was copper particles (nominal diameter 0.5mm, Alkan Metal Powders) on to which silver had been deposited in a prior cementation reaction. With a few atomic layers of silver on its surface and additional electrodeposited silver as the experiment proceeds, such a particle would behave electrochemically in a way similar to a pure silver particle. Henceforth, these particles are referred to as silver-coated copper particles. The copper particles as supplied had surface coatings which it was necessary to remove before use. The particles were prepared by cleaning in a dilute nitric acid solution, rinsing in water, drying in a oven and finally screening into the desired size range. Before using, these particles were cleaned with a dilute sulfuric acid solution to remove sulface oxides and then silver was deposited by cementation reaction in pure silver cyanide solution.

An attempt was made to use silver needles (nominal size 0.6x1.2mm, Engelhard Corp.), but difficulty was experienced in fluidizing such particles. Since prior investigations have shown that uniform fluidization is desirable for long term operation of a cell, no further work was done on such particles.

Graphite particles (nominal diameter 0.65mm, Poco Graphite Co.) were also tried. The concept here is that these particles could be easily removed, without contamination of the product, during silver melting subsequent to electrolysis. Further, the particles are "worthless" and their use would minimize security problems. While silver could be deposited on the particles, the deposit was dendritic, rather than smooth, and after some deposition of silver the particles

become difficult to fluidize. No further attention was devoted to these particles.

Some spherical particles were eventually obtained from Johnson Mathey in the size range 0.5-1mm. The purity claimed by the supplier was 99.9%. The particles underwent fluidization and electrodeposition of silver without problems.

Figure III-5 shows the silver-coated copper particles and silver particles used in this study. Figure III-6 shows the cell voltage and cathode voltage drop of fluidized bed electrodes with silver and silver coated copper particles. It is seen that the two kinds of particles differ little in their cell voltage characteristics.

2. Current Efficiency

In the pure silver cyanide solution, two possible major cathodic reactions are as follows:

$$Ag(CN)_2^- + e^- = Ag + 2\,CN^- \qquad E^o=-0.30\ V \qquad \text{(III-1)}$$

$$H_2O + e^- = 1/2\,H_2 + OH^- \qquad E^o=-0.828V \qquad \text{(III-2)}$$

Current efficiency for silver electrowinning can be explained as a ratio of charge consumed by reaction (III-1) to total charge applied. Current efficiency was calculated from the measured silver concentration drop in the catholyte. With the pure silver cyanide solution, this calculation agreed quite well with the current efficiency measured by volume of hydrogen evolved.

Figure III-7 shows a plot of the current efficiency vs. silver concentration for various superficial current densities. Inefficiency

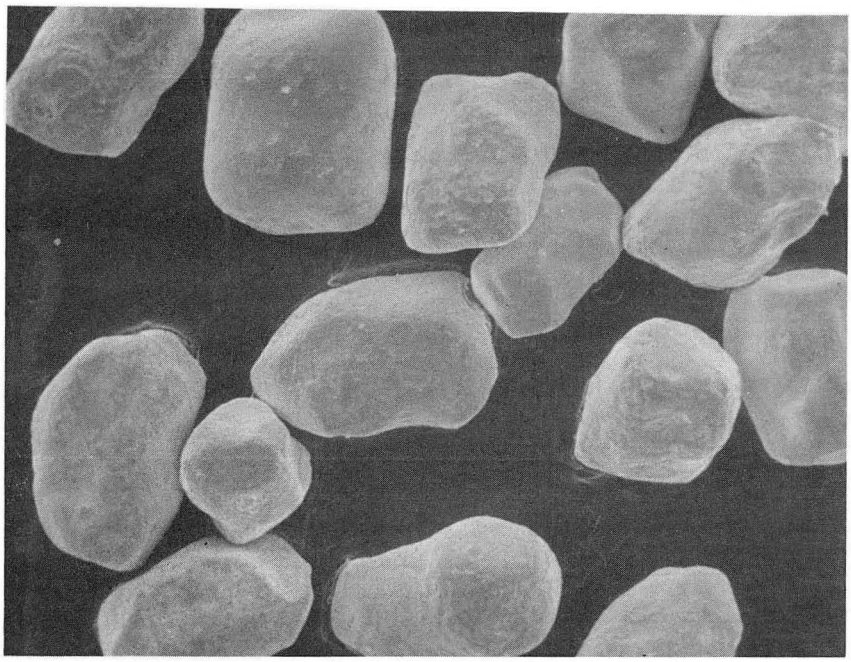

a) silver coated copper particles(x50)

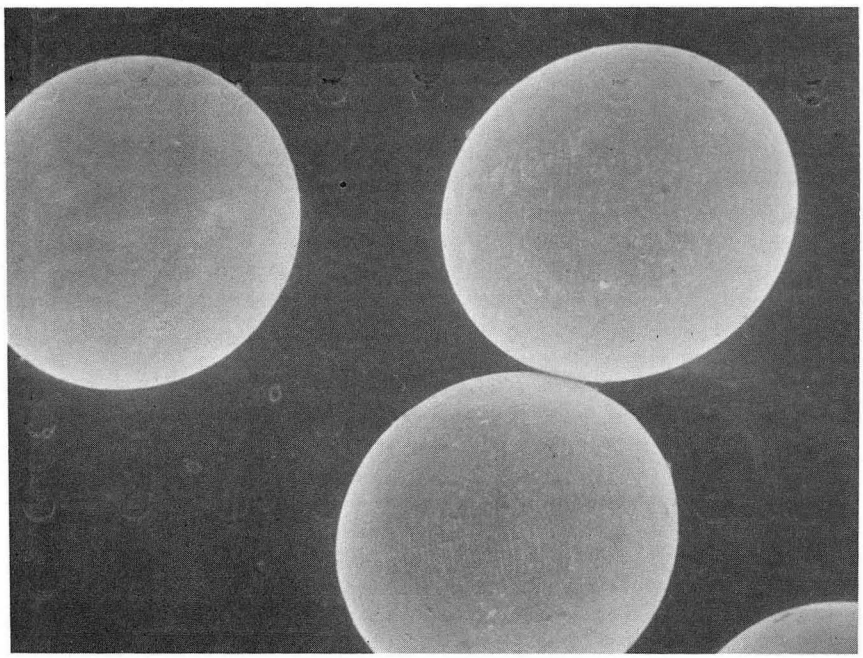

b) silver particles(x50)

XBB 854-2749

Figure III-5 Scanning Electron Microscope photographs of the particles used in this investigation.

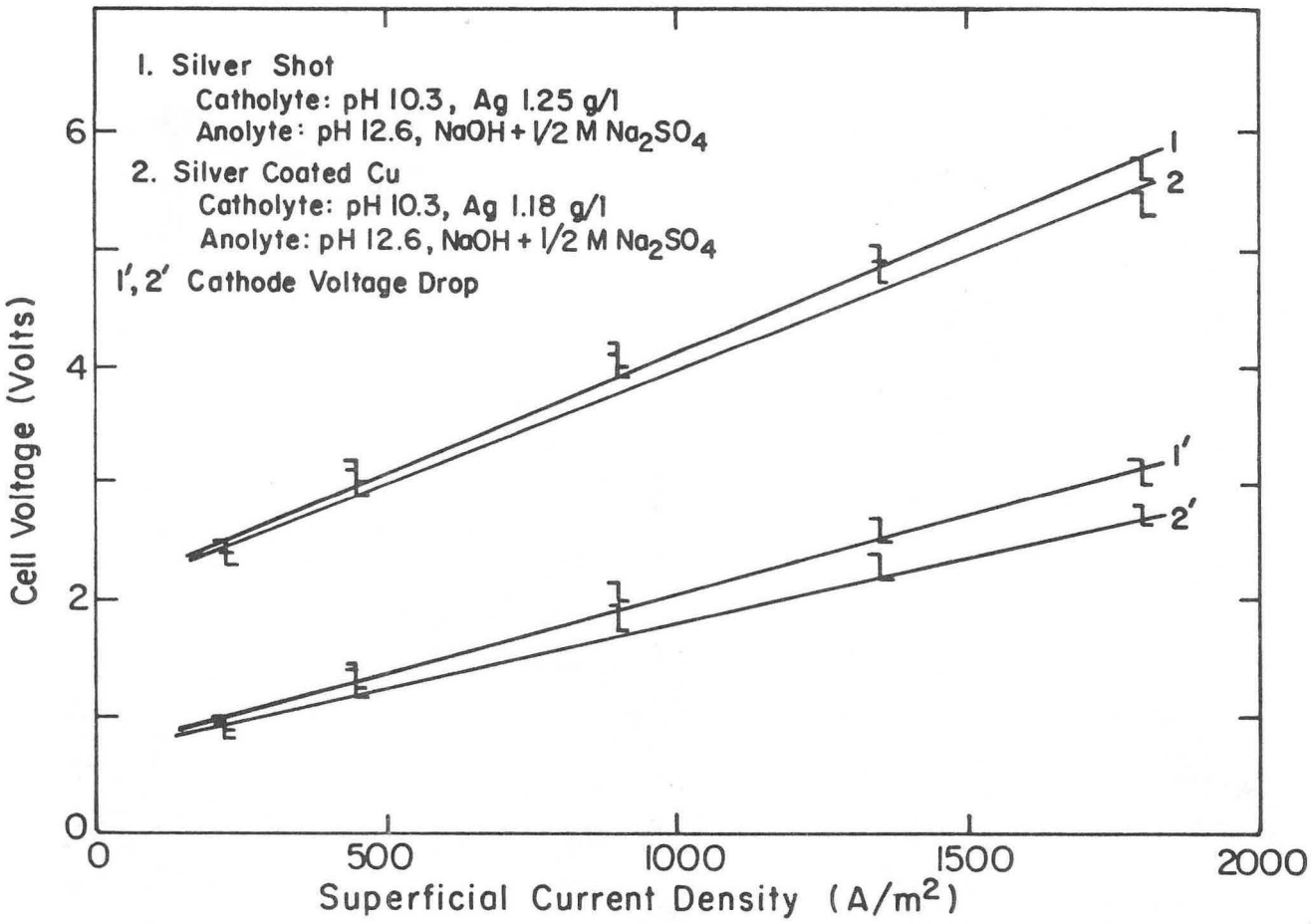

Figure III-6 Effect of particle type and superficial current density on total cell voltage and voltage drop across the cathode (Anode: platinized Ti mesh)

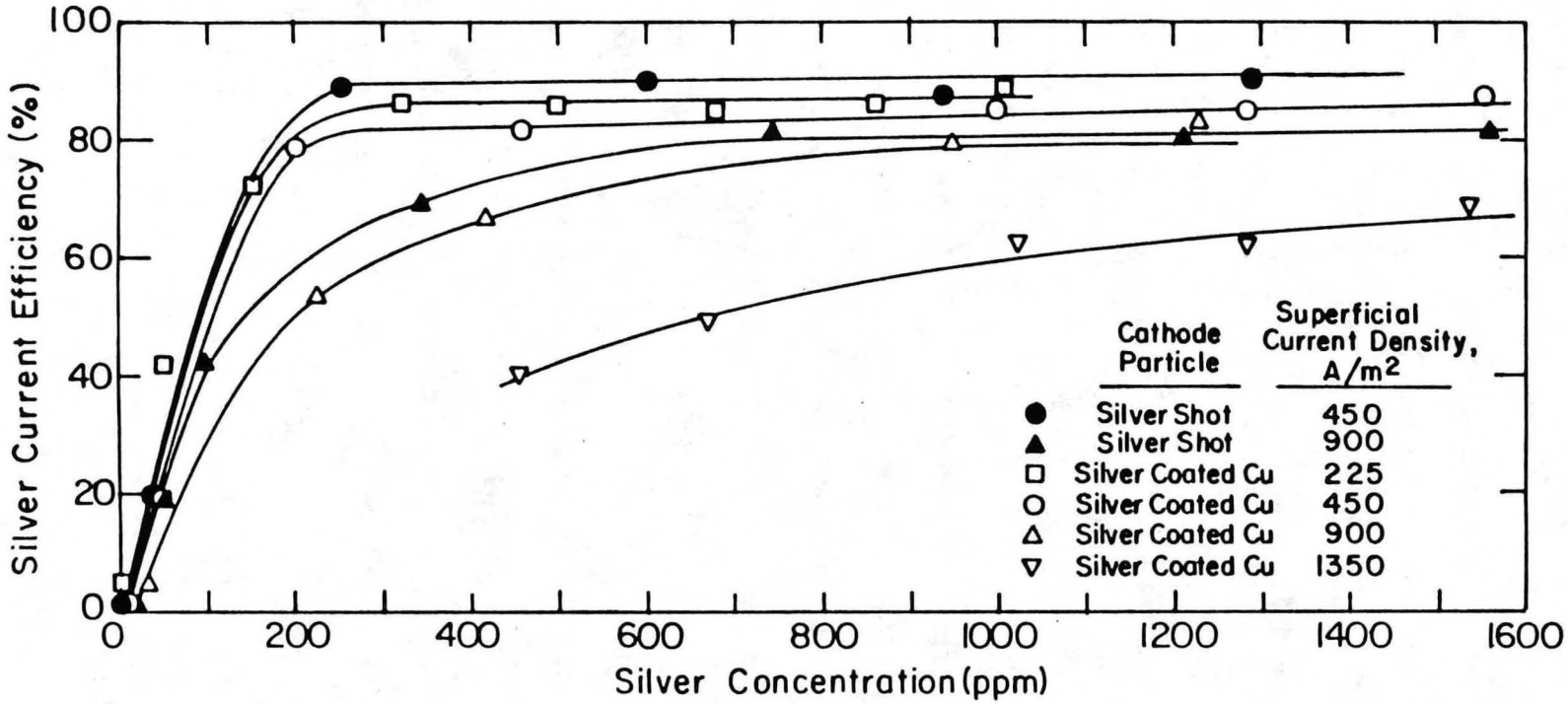

Figure III-7 Plots of current efficiency versus silver concentration at various superficial current densities and two kinds of particles

at low silver concentrations is mainly caused by hydrogen evolution and it is expected that the current efficiency could be increased by an increase in catholyte pH. Nevertheless silver concentrations could be reduced to a final value of a few ppm. Current inefficiency at higher concentrations (>= 400 ppm) is probably due to the reduction of the ferric ions to ferrous ions in the catholyte since no hydrogen evolution was observed in the bed at these higher concentrations. This will be explained in detail later.

The current efficiencies of the silver particles were a little higher than those of silver coated copper particles, perhaps because of higher electrolyte flow rate and therefore improved mass transfer around the larger and denser particles. The dependence of current efficiency for silver electrowinning on the applied current density is shown by the decrease of current efficiency with an increase in superficial current density. This means the silver electrowinning reaction under these conditions is controlled by mass transfer of silver cyanide ions, i.e. is at or close to the limiting current. By comparison with the report of Zadra cell operation at Homestake Mining Co,[51] the percent extraction of silver and current efficiencies of fluidized bed electrode are higher than in the Zadra cell.

3. Anodes

A significant part of this investigation has been devoted to finding a suitable anode for the cell. Prior work in this laboratory has shown that the anode chamber has little effect on current efficiency

but greatly effects the cell voltage and therefore power consumption[38]. Previous work at Berkeley has been focused on electrowinning of copper[34,36] cobalt[41] and zinc[39], where acid electrolytes are common, and in those investigations a dimensionally stable anode(DSA, Eltech Corp.) has been successfully used. This anode is a titanium mesh with a proprietary coating which catalyzes oxygen evolution, i.e., reduces the oxygen evolution overpotential. Although the diaphragm of the cell effectively separates catholyte and anolyte, safety considerations probably rule out operation with an acid anolyte. Consequently, alkaline anolytes were used in this investigation.

Six anode types were used: DSA, pure lead, 304 stainless steel mesh, platinum plated titanium mesh, 316 stainless steel plate and a grooved graphite plate. Meshes and grooves provided for the ready escape of the oxygen generated at the anode. Prior work has shown that the cell voltage can be greatly reduced by facilitating such escape. The 316 stainless steel plate was drilled with 3.97mm diameter holes for the same reason.

Not unexpectedly, the lead anode and the 304 stainless steel mesh corroded rapidly in preliminary experiments and were ruled out from further consideration. The DSA was useful for only a few preliminary runs, at which point its coating had dissolved.

Figure III-8 shows the cell voltage vs. superficial current density for various anodes. As will be seen below, electrolyte composition has an effect on cell voltage. Strictly speaking, the three lines in Figure III-8 are at slightly different electrolyte compositions, and therefore

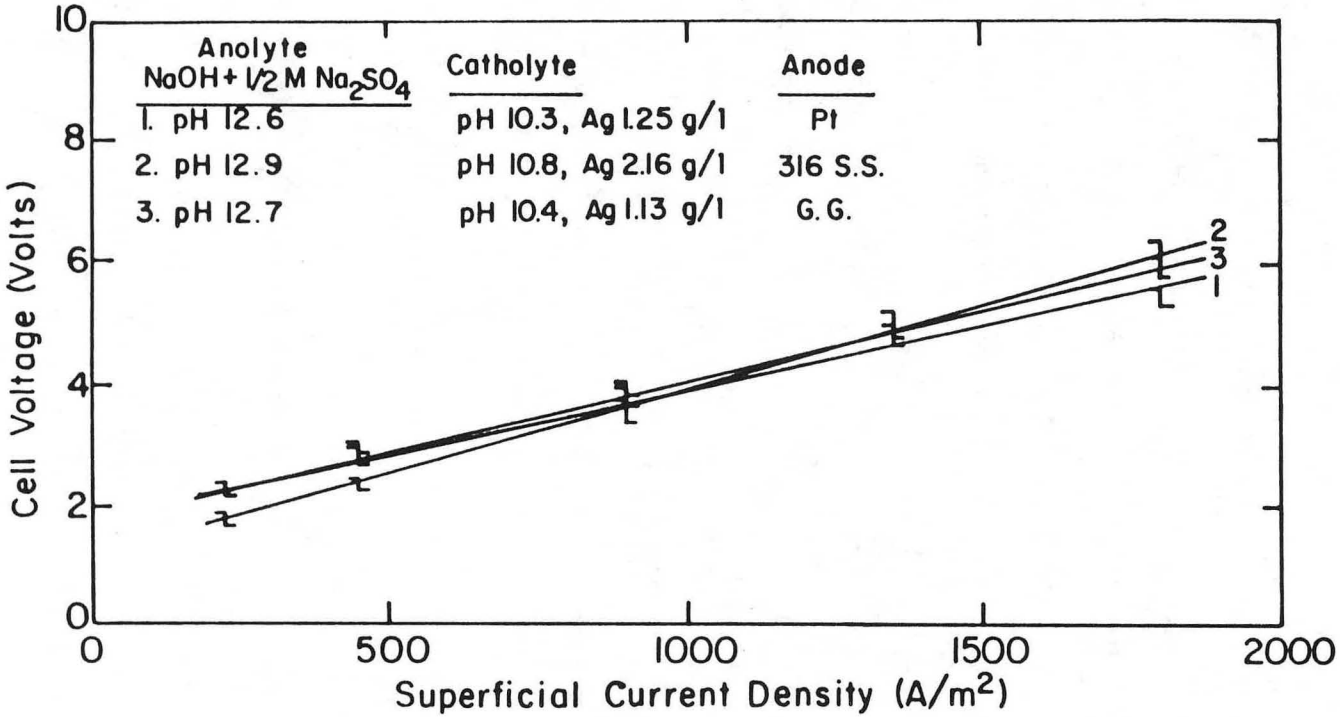

Figure III-8 Effect of anode material on cell voltage (Cathode: silver coated copper particles)

an exact comparison is not possible. However, it is possible to conclude that from a cell voltage viewpoint the 316 stainless steel anode (referred to as stainless steel anode) is marginally inferior to the other two; it yields cell voltage comparable to the others in an electrolyte that is more conductive.

4. Anolyte Composition.

By using the stainless steel anode and silver coated copper particles, the effect of anolyte composition was determined. Figure III-9 represents the results. Quite small increases in pH reduce the cell voltage by making the anolyte more conductive. This results were confirmed by using the other types of anodes. Addition of sodium sulfate also increases the conductivity of anolyte and reduces the cell voltage. However, some oxidation of the stainless steel anode was noted for anolytes containing sodium sulfate.

5. Behavior of Impurities.

The Homestake electrolyte contains significant amount of copper, zinc and iron as impurities. Codeposition of such impurities with the silver would seriously impair the attractiveness of fluidized bed electrowinning since a major attraction of the approach is product purity comparable to that of the Zadra cell.

The possible reduction reactions of these major impurities in cyanide solutions are as follow:

$$Fe(CN)_6^{-3} + e^- = Fe(CN)_6^{-4} \qquad E^o=0.36V \qquad \text{(III-3)}$$

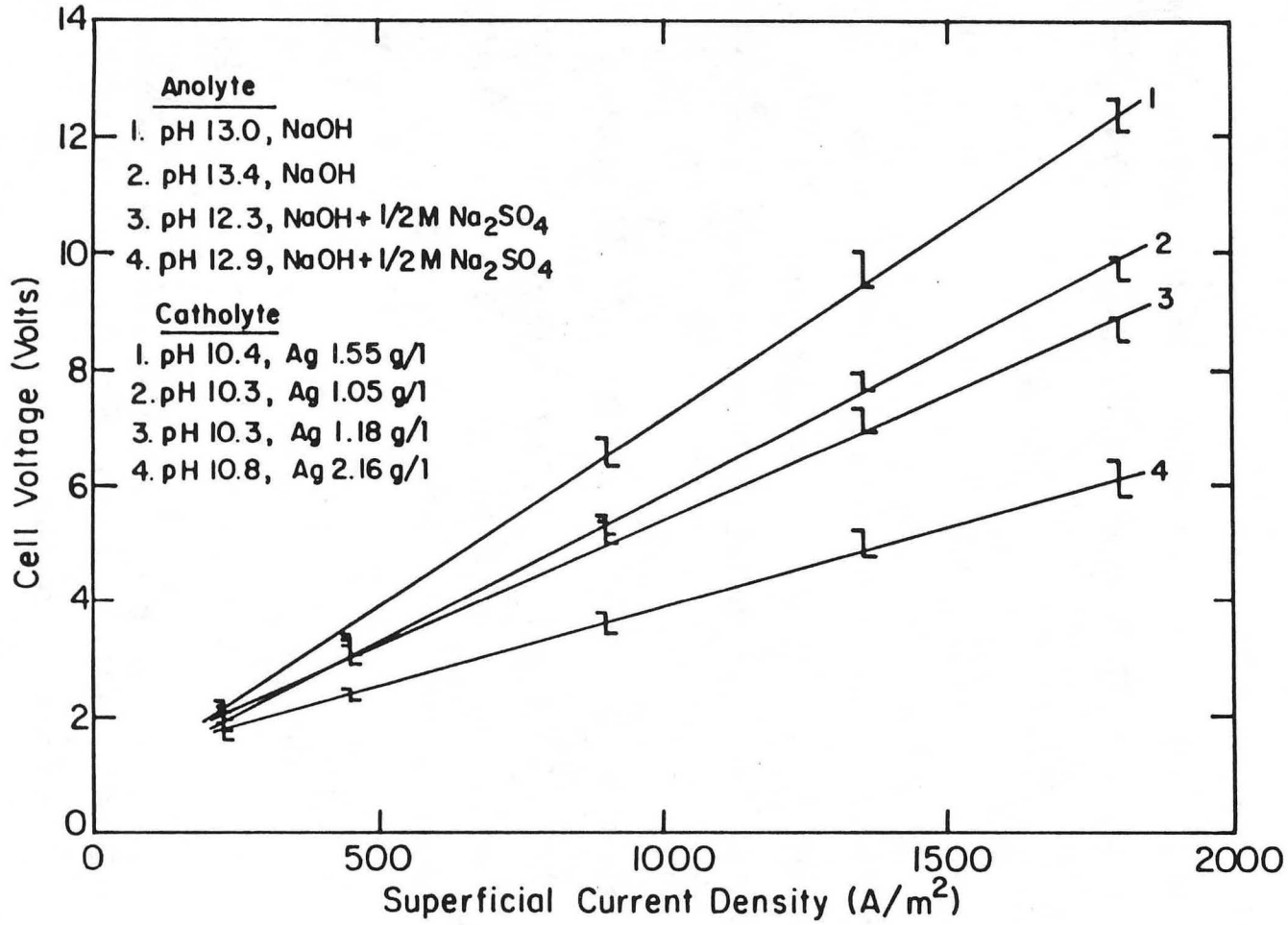

Figure III-9 Effect of sodium sulfate addition and pH of anolyte on the cell voltage (Anode: perforated 316 stainless steel sheet)

$$Cu(CN)_2^- + e^- = Cu + 2\,CN^- \qquad E^o=-0.43V \qquad \text{(III-4)}$$

$$Zn(CN)_4^{--} + 2\,e^- = Zn + 4\,CN^- \qquad E^o=-1.26V \qquad \text{(III-5)}$$

As shown, the reduction reaction of ferric cyanide to ferrous cyanide is more favorable than the silver electrowinning reaction and this can explain the inefficiency at higher silver concentration. Of particular concern is copper since its standard reaction potential is closest to that of silver, and it is therefore the most likely to codeposit.

Catholyte samples from the cell were therefore analysed for copper and zinc in addition to the silver analysis mentioned earlier. Figure III-10 shows the catholyte copper content vs. silver content. It is seen that over the course of the run copper concentration does not change. Variations of the starting copper contents are due to variations in the degree of admixture of pure silver cyanide solution to the Homestake solution. Figure III-11 presents the corresponding lines for the zinc content. This is strong, but indirect, evidence for the purity of the silver product. More direct evidence was obtained by an EDAX analysis. The EDAX technique analyzes a surface layer approximately 2,000 Angstrom units thick. Both the original silver shot and silver shot onto which silver had been deposited, were free of peaks corresponding to copper, zinc and iron. The silver-coated copper particles showed small copper peaks presumably originating in some way from the copper substrate.

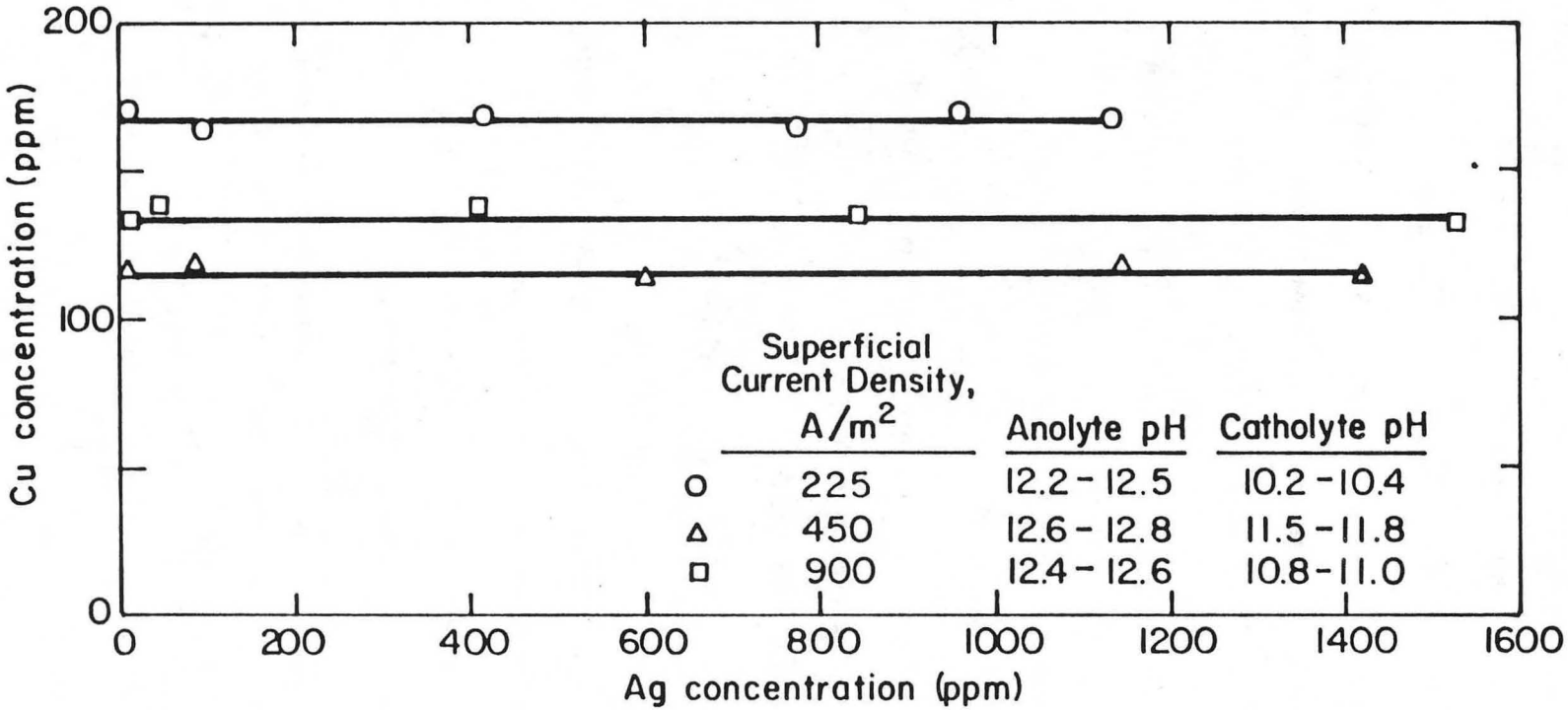

Figure III-10 Analytical results suggesting that copper in solution is not deposited along with the silver

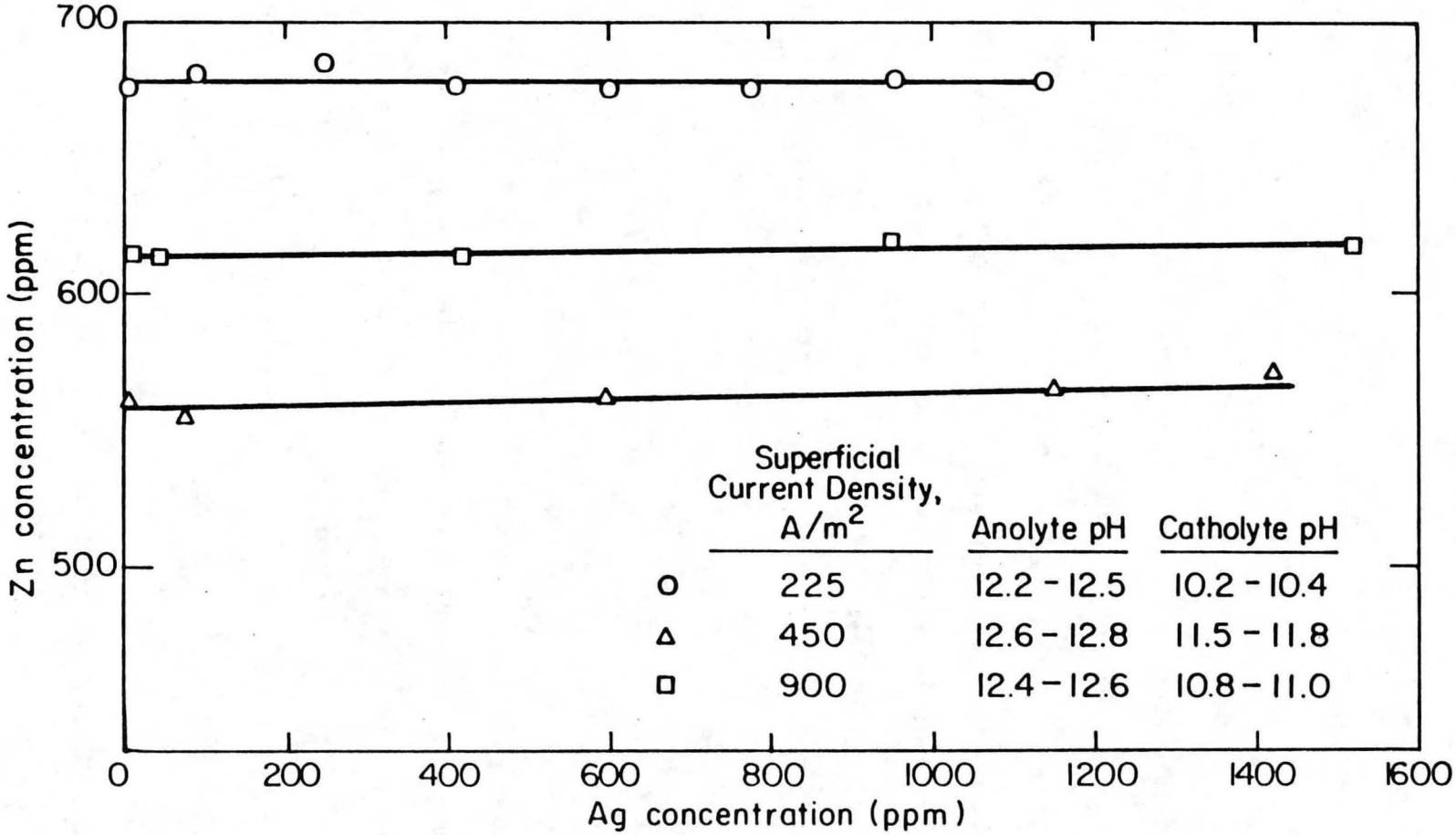

Figure III-11 Analytical results suggesting that electrodeposition of silver is not accompanied by deposition of zinc

IV. TRANSIENT BEHAVIOR

A. Introduction and Previous Research.

The high surface area per unit mass and high mass transfer rate make particulate electrodes attractive where electrochemical reactions are to be conducted at high space-time yields. In the context of energy storage (battery), this means an electrode with high specific power.

The acceptability of an electric vehicle depends on the development of a battery of high specific power, low initial capital cost and construction from readily available raw materials. The idea of Zinc/Air cell has been very attractive because of its high theoretical specific energy.

$$Zn + 1/2\ O_2 \rightarrow ZnO \qquad E^{o}=1.6V, \qquad 1310\ Wh/kg \qquad (IV\text{-}1)$$

The zinc electrode discharge products are very soluble in alkaline battery electrolytes. The high solubility inhibits zinc passivation and contributes to the high rate capabilities of the electrode. However it causes difficulties in controlling zinc morphology on charge and zinc redistribution on cycling. Therefore conventional zinc sheet electrode suffers from short cycle life due to the dendritic growth of zinc deposit during recharging.

The particulate electrode is generally regarded as being easier to generate than other electrodes since structural integrity is not

required. The slurry electrode was based on this idea[55]. However in practice the particle size distribution and morphology must not change significantly.

Even though considerable research has been carried out on the gross behavior of the particulate electrodes, especially fluidized bed electrodes, research on the transient behavior of such electrodes is still sparse. Due to the characteristic hydrodynamic behavior of the two media, particles and electrolyte, in the particulate electrode, potential transients are inherent. Not only is the overall electrode performance affected by the potential transients, but the electrochemical reaction rates as well, because the electrochemical reaction taking place at the particle surface is proceeding under an unsteady state condition. Particle to particle electronic conduction is necessary in order for a particulate electrode to function and has a significant effect on electrode performance. Such conduction is poorly understood at present, although there is evidence that the conductivity drops as the particle volume fraction drops (as mentioned in Chapter II). Hence, the slurry electrode, which has a lower particle volume fraction than a fluidized bed electrode, may not be the best electrode.

The purpose of the investigation described here was to study the transient and local electrochemical behavior of fluidized bed electrode to improve such electrode so as to make it a practical counter electrode to the air electrode. Table IV-1 shows the preliminary engineering analysis of zn fluidized bed / air electrode cell.

To achieve that goal, the potential transients were measured and

Table IV-1 : Preliminary Engineering Analysis of Zn Fluidized Bed/ Air Cell

Energy Basis : 15 kWh

System	Volume(l)	Weight(kg)	
Particle	6	18[a]	43[b]
Electrolyte*	56	78	78
Total	62	96[a]	121[b]
Energy Density (Wh/kg)		156[a]	124[b]

Power Basis

Cell Potential : 1 V

Current Density : 500 mA/cm^2

Cell Active Area : 500 cm^2

Power/Cell : 250 W

50 Cell/System

Total Power : 12.5 kW

Power Density : 130 W/kg^a, 103 W/kg^b

Pumping Power : 1 W^a, 14 W^b

* containing 50 l reservior
a Sorapec particle
b Zn particle

analyzed and also (to yield macroscopic information on the electronic conduction of such electrode) effective resistivities were measured as functions of bed expansion, applied sine wave frequency and electrolyte conductivity.

Fleishman and Kelsall[56] reported briefly on potential fluctuations of fluidized bed electrode during copper elctrowinning. A considerable amount of research has been carried out on the behavior of the conventional zinc electrode in alkaline solutions. McBreen and Cairns[57] reviewed the zinc electrode thoroughly from solution chemistry to it's applications. For use in batteries, potassium hydroxide electrolyte which has concentrations in the range of 4 to 12M are widely accepted. The zincate ion, $Zn(OH)_4^{--}$ is the only one of importance in KOH battery electrolytes.

$$Zn + 4OH^- \rightarrow Zn(OH)_4^{--} + 2e^- \qquad \text{(IV-2)}$$

Fordyce and Baum[58] have conformed the tetrahedral structure of this complex ion by spectroscopic measurement.

On the anodic behavior of zinc electrode in alkaline solution, early investigations involved galvanostatic measurements on zinc sheet[59-61] and porous zinc[62]. In KOH electrolytes, it has been found that when a zinc sheet is anodized at a particular current the overpotential remains relatively constant. With the onset of passivation a rapid, large increase in overpotential occurs. This research confirmed the relationship

$$(i - i_l)\, t^{1/2} = k \qquad \text{(IV-3)}$$

where i is the applied current density and t is the time to passivation. Both i_l and k are constants which are dependent on KOH concentration and on the nature of electrolyte movement.

About the passivation mechanism, investigations using various techniques[63-66] lead to the tentative conclusion that three types of processes may inhibit zinc dissolution in alkaline electrolytes;

i) at overpotentials of about 30 mV passive films with thickness of about a monolayer can form and inhibit dissolution

ii) on continued dissolution these films can grow to greater thicknesses. As they become thicker they tend to crack and peel from the substrate

iii) in quiescent electrolytes a nonadherent deposit of zinc oxide forms on the electrolyte side of film formed by ii)

Two mechanisms have been proposed for the formation of passivating monolayers. One is an adsorption mechanism[67] and the other is two-dimensional nucleation[64].

Several empirical correlations have been proposed between utilization and porous structure of zinc electrodes. Coates et al.[62] reported that there was no relationship in general between the surface area of porous electrode and the specific rate of polarization but Shephard and Langelan[68] concluded that electroporosity had a major

influence on zinc utilization and also Marshall et al.[76] found that a considerable degree of supersaturation occured during the discharge process of zinc slurry electrode by measuring zinc concentrations of the final electrolytes obtained from discharged cells.

Drury, Marshall and Hampton[69,70] investigated the effect of silicate addition to electrolytes and concluded that silicate promotes discharge capacity of the Zn/KOH electrode.

The most important cathodic reaction of zinc electrode in alkaline solutions is zinc deposition. Controlled zinc deposition during charge-discharge cycle is the key to long cell life. When zinc is deposited from alkaline solutions, it is reported that three types of deposits are encountered[71];

i) smooth deposit are formed with a vigorous stirring of the electrolytes

ii) at low overpotentials, dark gray porous deposits (also referred as a mossy deposit) are formed in quiscent electrolytes

iii) at high overpotentials, the deposit is dendritic

The transition from moss to dendrites corresponds to the onset of mass transport control and is characterized by a critical current density which is temperature dependent[71] and is dependent on the hydrodynamic conditions at the electrode surface[72]. Bockris, Nagy and Damjanovic[73] proposed zinc deposition reaction mechanism as follows on the basis of estimates of the activation energies involved:

$$Zn(OH)_4^{--} \rightarrow Zn(OH)_3^{-} + OH^{-} \qquad (IV-4)$$

$$Zn(OH)_3^- + e^- \rightarrow Zn(OH)_2^- + OH^- \quad \text{(IV-5)}$$

$$Zn(OH)_2^- + e^- \rightarrow Zn(OH) + OH^- \quad \text{(IV-6)}$$

$$Zn(OH) + e^- \rightarrow Zn + OH^- \quad \text{(IV-7)}$$

By analysis of the electrodic parameters they reported that reaction (IV-5) is the rate determining step. Also they found the dependency of exchange current density on zincate concentration.

The capacities of zinc-KOH interfaces were studied by galvanostatic pulse current technique[74] and kinetics and thermodynamics of $Zn/Zn^{++},OH^-$ system were investigated at the potentials around the equilibrium value[75].

Discharge characteristics of slurry electrode[76] and packed bed elctrode [77] were studied and it was suggested that the high energy density cell can be obtained by using the particulate bed electrode. Since the invention of the slurry electrode[55], Appleby and Jacquier[78,79] extensively investigated the zinc slurry/air battery for a practical vechicle power source. Their results revealed that this system is capable of 110 Wh/kg, 80 W/kg in a 1 tonne urban vehicle with lifetimes up to twice those for lead-acid system. Similar research was performed in France and the other places. These were reviewed thoroughly by Clarke and Wasson[80] recently.

B. Experimental Apparatus and Procedure

1. Potential Transient Measurement.

a. Apparatus

To measure the potential fluctuations a dual probe, a luggin capillary for electrolyte potential measurement and a captive particle for particle potential measurement, was employed. Figure IV-1 depicts a schematic of a potential measuring probe. It consists of two wires insulated by thin glass tubes and sealed with epoxy at the ends and there are exposed tips about 1mm long. One exposed tip remained inside the luggin capillary and the other placed outside and left exposed to behave as a captive particle. The function of the probe can be explained as follow: Let ϕ_e and ϕ_p be the electrolyte and particle potential respectively at any position of the bed. The local electrode potential, ϕ, at the same position will be

$$\phi = \phi_p - \phi_e \qquad \text{(IV-8)}$$

By making contact with particles in its immediate vicinity the captive particle will sense ϕ_p directly. However the internal tip will be at equilibrium with electrolyte, hence its potential ϕ_e' will be related to the electrolyte potential, ϕ_e, and the local equilibrium potential, ϕ_o, by the equation

$$\phi_o = \phi_e' - \phi_e \qquad \text{(IV-9)}$$

Thus the potential difference between two wires will be

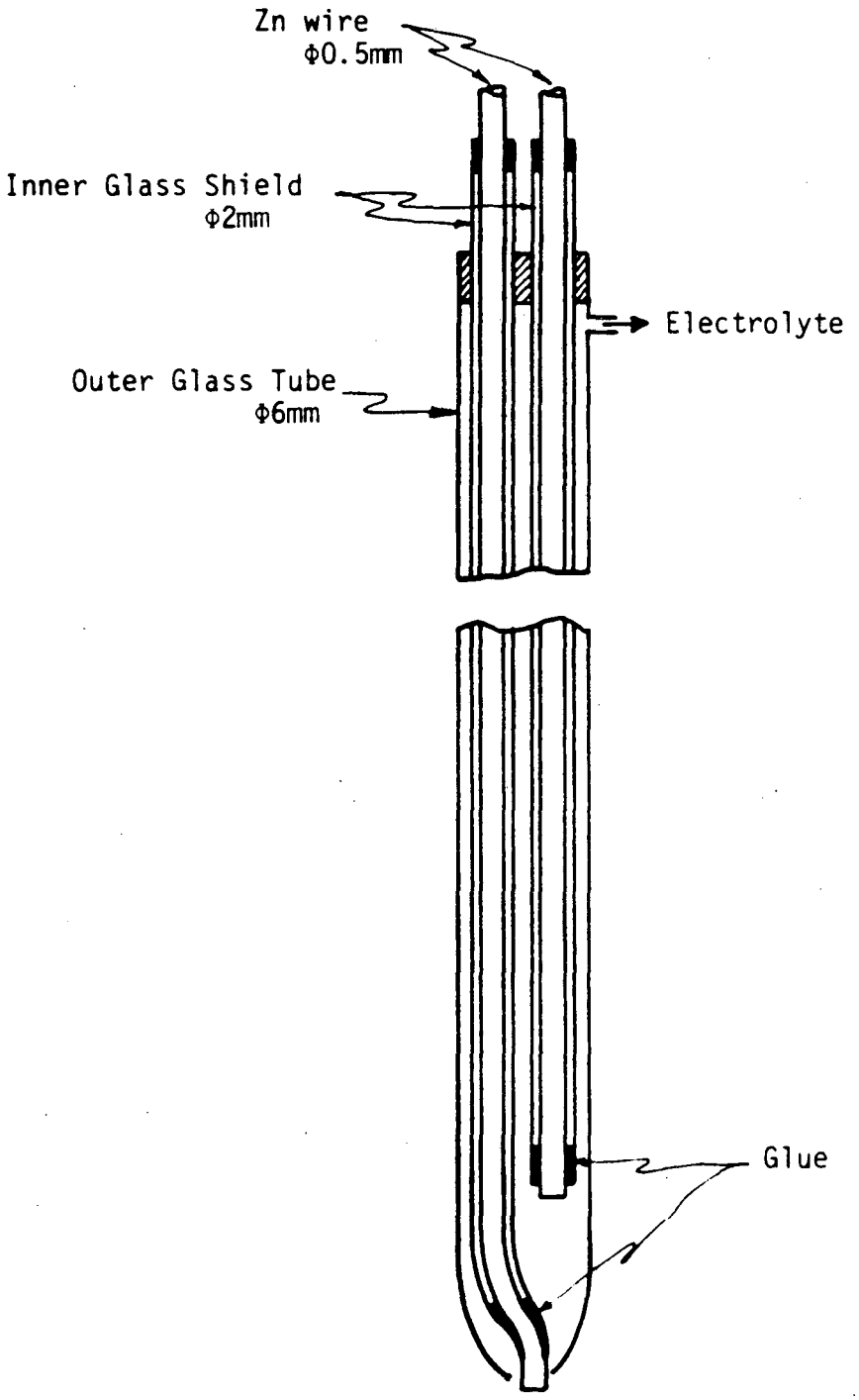

Figure IV-1 Schematic of potential measuring probe

$$\phi_p - \phi_e' = (\phi + \phi_e) - (\phi_o + \phi_e) = \phi - \phi_o = \eta \qquad \text{(IV-10)}$$

which is a local overpotential. By using this dual probe, the local overpotential can be measured directly.

This probe was mounted on a microscope stage, which was calibrated to 0.1mm so that it could be accurately positioned in horizontal directions and this microscope stage was connected with vertical jack, which was calibrated to 1mm to allow accurate vertical movement.

The signals detected by this probe were fed into two different channels of a Nicolet Model 2090 - III A digital storage oscilloscope and consequently saved on the floppy disk of an Apple - II micro computer. All the potentials were measured either with respect to the electrolyte potential adjacent to the diaphragm or with respect to the current feeder potential, i.e., particle potential at the current feeder.

In this investigation a somewhat wider cell than usual in these laboratories (45mm from current feeder to diaphragm) was used to permit insertion of a probe. An overall schematic of the apparatus is shown in Figure IV-2. For this investigation two different systems were studied. One was copper electrowinning from acidified concentrated copper sulfate solutions (Cu/H_2SO_4 system), and the other was anodic and cathodic behavior of zinc in concentrated potassium hydroxide solutions (Zn/KOH system). For the Cu/H_2SO_4 system, the probe was made with copper wire and the anode of the fluidized bed cell was a catalystic coated Ti mesh electrode(DSA, Eltech Corp.). The cathode was copper particles

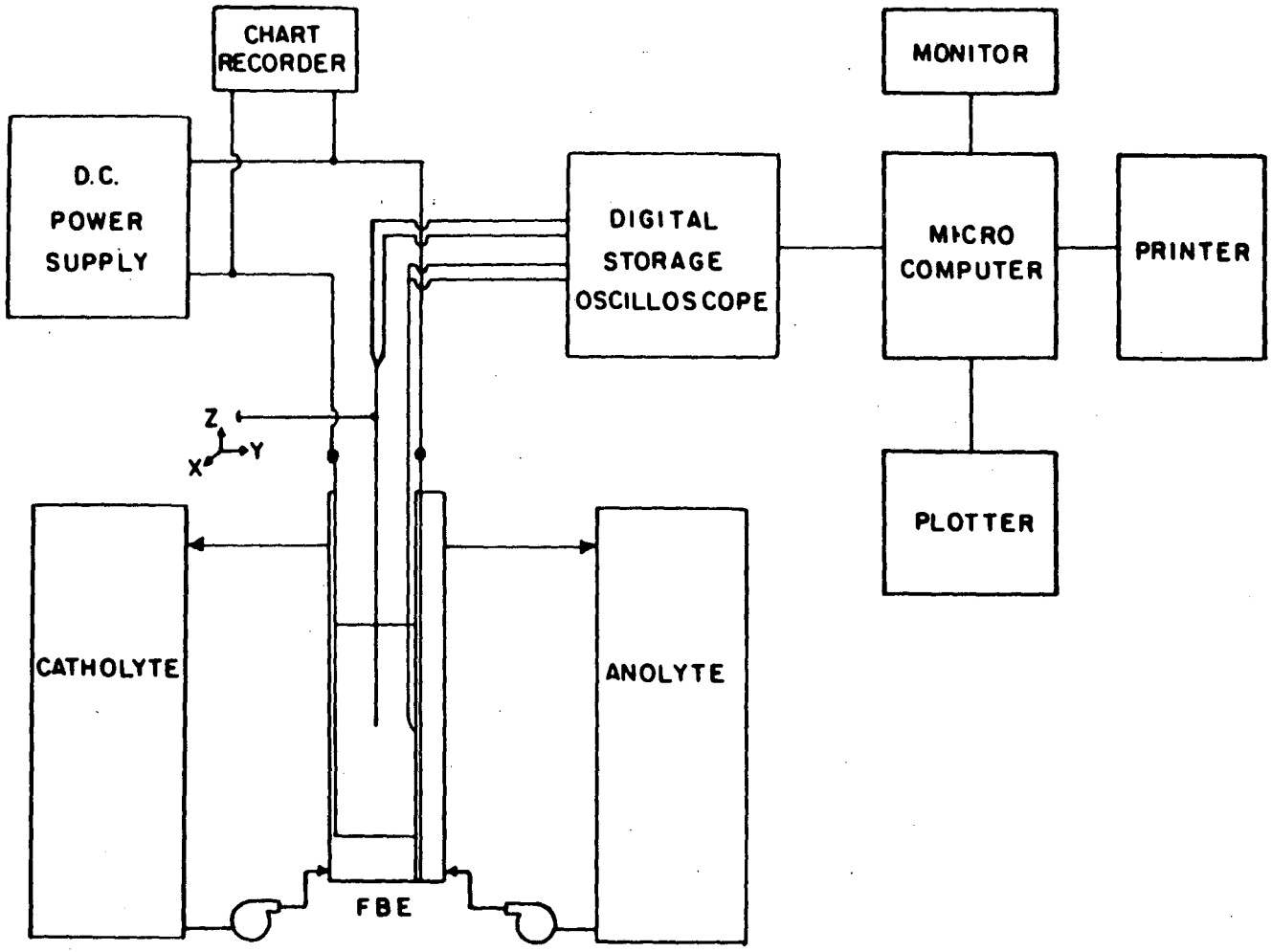

Figure IV-2 Apparatus schematic for potential transient measurement and analysis

(nominal diameter 0.5mm; Alkan Metal Powders) and the current feeder was made of 4mm thick graphite. The catholyte was prepared by dissolving copper sulfate (Reagent grade, Mallinckrodt Inc) in a known amount of distilled water which was acidified by sulfuric acid (Reagent grade, Mallinckrodt Inc). The catholyte concentration was kept at 25gr/l of Cu and 50gr/l of H_2SO_4 and the anolyte at 50g/l of H_2SO_4 at the beginning of electrolysis.

For the study of Zn/KOH system, zinc coated copper particles and Sorapec particles were used. The latter were zinc coated polymer particles under commercial development by this French company for battery applications. According to the manufacturer, onto the 300 - 400 μm plastic slurry 1 μm of nickel was deposited by an electroless process and 1 μm of cadmium followed by upto 125 μm of zinc was deposited electrochemically. Because the size range of these particles was wide, particles within the size range of -28 +35 mesh were selected by sieve analysis and used. The measured bulk density of the particles was around 3 gr/cm^3. Figure IV-3 shows the Sorapec particles as received from the manufacturer. The potential measuring probe was made either with zinc wires or the copper wires in which case the tips were coated with zinc electrochemically. The counter electrode of the fluidized bed was a platinized titanium mesh anode and both electrolytes were 5M potassium hydroxide solutions.

b. Data Collecting and Processing

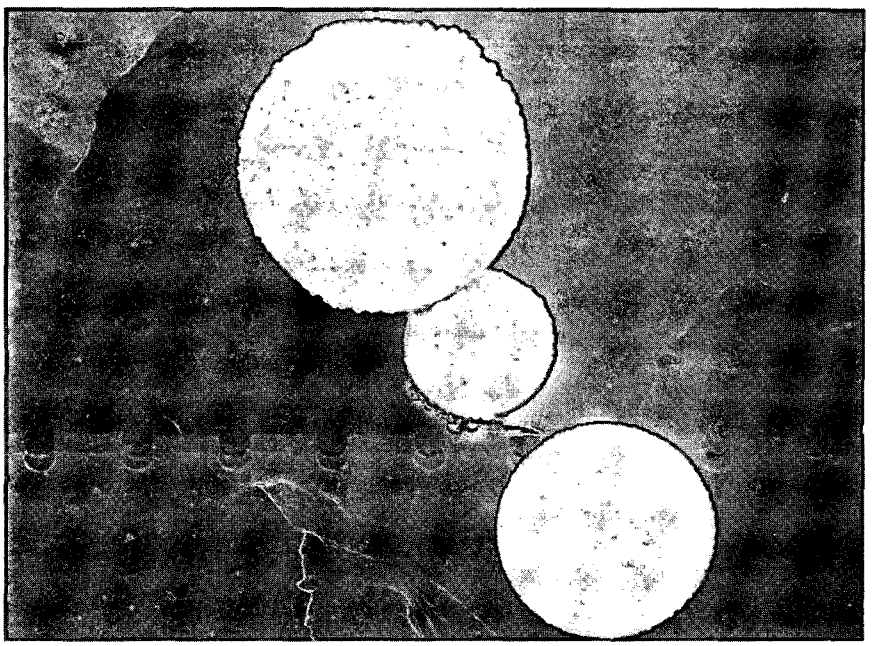

XBB 854-2751

Figure IV-3 Scanning Electron Microscope photograph of the Sorapec particles. (x50)

To analyze the measured potential traces, three different kinds of statistical functions were calculated initially. The probability density function (amplitude domain analysis), the autocorrelation function (time domain analysis) and it's Fourier transform, the power spectral density function (frequency domain analysis) were calculated by using the Blackmann-Tukey method [81,82]. Later, to reduce the resolution bandwidth and increase the calculation speed the fast Fourier transformation method[83-87] was employed to calculate the power spectral density function directly from the raw data set.

The probability density function defined as

$$P(x) = \lim_{\Delta x \to 0} \frac{\text{Prob}[x<x(t)<x+\Delta x]}{\Delta x} = \lim_{\Delta x \to 0} \frac{1}{\Delta x} \left[\lim_{T \to \infty} \frac{T_x}{T} \right] \qquad \text{(IV-11)}$$

where T is the observation time and T_x is the total time that $x(t)$ falls inside the range of $(x, x+\Delta x)$ during observation time T

describes the probability that the data will assume a value within some defined range at any instant of time.

The autocorrelation function defined as

$$R_x(\tau) = \lim_{T \to \infty} \frac{1}{T} \int_0^T x(t)\, x(t+\tau)\, dt \qquad \text{(IV-12)}$$

where τ is the lag time

describes the general dependence of the values of the data at one time to the value at another time. The quantity of $R_x(\tau)$ is always a real-valued even function with a maximum at $\tau=0$ and may be positive or negative.

The power spectral density function which also called the autospectral density function describes the general frequency composition of the data in terms of the spectral density of it's mean square value. This can be defined as

$$G_x(f)= \lim_{\Delta f\to 0} \frac{\Psi_x^2(f,\Delta f)}{\Delta f} = \lim_{\Delta f\to 0} \frac{1}{\Delta f}\{\lim_{\tau\to 0} \frac{1}{T} \int_0^T x^2(t,f,\Delta f)\} \qquad \text{(IV-13)}$$

and this is related to the autocorrelation function by a Fourier transform as follows

$$G_x(f)= 2 \int_{-\infty}^{\infty} R_x(\tau)\, e^{-j2\pi f\tau} d\tau = 4 \int_0^{\infty} R_x(\tau) \cos 2\pi f\tau \, d\tau \qquad \text{(IV-14)}$$

For the digitized data, the finite discrete Fourier transform is most important. Here the procedures of Blackmann-Tukey method and fast Fourier transformation method will be reviewed briefly for the digitized data set.

Let a data set contain N data points, $Y_1, \ldots, Y_N$, each of which

was sampled with a certain time interval Δt with an average $\bar{Y}$.

The procedure of the Blackman-Tukey method first computes the correlation function and then takes its Fourier transform and is described as follows:

1. Transfer the raw data set to zero mean values set by substracting the average from original values.

$$X_i = Y_i - \bar{Y} \qquad i = 1,\ldots,N \tag{IV-15}$$

2. Calculate the autocorrelation function

$$R_r = \frac{1}{N-r} \sum_{i=0}^{N-r} X_i \cdot X_{i+r} \tag{IV-16}$$

$r = 0, \ldots, m$

where m is the maximum number of lag

3. Calculate the power spectral density of X_i

$$G_k = 2\Delta t \left(R_0 + 2 \sum_{r=1}^{m-1} R_r \cos\frac{\pi kr}{m} + R_m \cos\frac{\pi k}{m}\right) \tag{IV-17}$$

$k = 0, \ldots, m$

where G_k corresponds to the power near $k/2m\Delta t$ Hz.

Here the maximum detectable frequency, $f_m = 1/2\Delta t$ is broken into m parts, and for this procedure, recommended number of lag time, m, is 0.1N. Therefore the frequency resolution bandwidth of power spectrum will be $5/N\Delta t$.

The starting procedure of fast Fourier transformation method is the same as the Blackman-Tukey method.

1. Transfer the raw data set to zero mean values set by substracting average from original values

$$X_i = Y_i - \bar{Y} \qquad i = 1,\ldots,N \tag{IV-15}$$

for fast Fourier transformation method N should be a power of 2, if not, 0s should be added to the original data set to make $N=2^n$

2. Calculate the Fourier transform of each data

$$X_k = \sum_{i=0}^{N-1} X_i \exp(-j\frac{2\pi ik}{N}) \tag{IV-18}$$

$k = 0, \ldots, N-1$

3. Calculate the power spectral density of X_i

$$G_k = \frac{2\Delta t}{N}|X_k|^2 \tag{IV-19}$$

$k = 0, \ldots, N+1/2$

where G_k corresponds to the power near $k/N\Delta t$ Hz.

Here the maximum detectable frequency is broken into N/2 parts so that the frequency resolution bandwidth, Δf, will be $1/N\Delta t$.

The following set of programs were run on the APPLE microcomputer to gather and process the data: BEGIN, OSCI.DATA, CALC, FFT. A brief

description of the operation of the system is as follows:

BEGIN clears the old files on the data disc and reinitializes the disc.

OSCI.DATA interacts with the oscilloscope and sets up the communication with APPLE via IEEE-488 interface and collects the data. Most of the data set consisted of 1024 data points. After collecting one data set, OSCI.DATA saves it in the data disc. After finishing a measurement at one position of the bed OSCI.DATA asks the operator to proceed to the next step. This process repeats until the operator stops taking measurements.

CALC runs after all the data set has been taken. It reads the data from the disc, calculates the probability density distribution, autocorrelation coefficients and normalized power spectral densities, saves all the results on a result disc for future plotting and gives a print out.

FFT functions similar to CALC but calculates probability density distribution and power spectral densities directly from the original data set.

c. Procedure

The general experimental procedure was rather simple and almost similar to what was described in Chapter III. It consisted of filling each reservoir with electrolyte, turning on the pumps, adjusting probe position and adding particles to the cathode chamber. Then catholyte flow rate was adjusted to bring the desired bed expansion. Then the

current was switched on, some time was allowed to elapse and data acquisition commenced.

Before inserting the potential measuring probe into the bed, it was treated with dilute sulfuric acid to remove any oxide layer present.

For the study of Zn in KOH electrolyte, Zn was first anodically dissolved in pure KOH electrolyte and then current was reversed to redeposit it. By doing this both the dissolution and deposition behavior was studied in pure KOH solutions. Samples were taken periodically to determined the zincate concentration by titration with EDTA.

2. Effective Resistivity Measurement.

a. Apparatus

The fluidized bed electrode employed during this study was the same as that used for the silver electrowinning study. This electrode was modified to put two current feeders at both sides of the bed and the anode chamber plus diaphragm eliminated.

Alternating current was supplied by a sine wave generator (IG - 18 Sine -Square Audio Generator, Heathkit Co.) with the desired frequencies. The potential drops across a known resistor(8.7 ohms), R_k, and the bed were detected simultaneously by both channels of the digital storage oscilloscope. Figure IV-4 shows the schematic diagragm of the system used in this study. The electrolytes were prepared by adding sulfuric acid or potassium hydroxide to a known amount of distilled

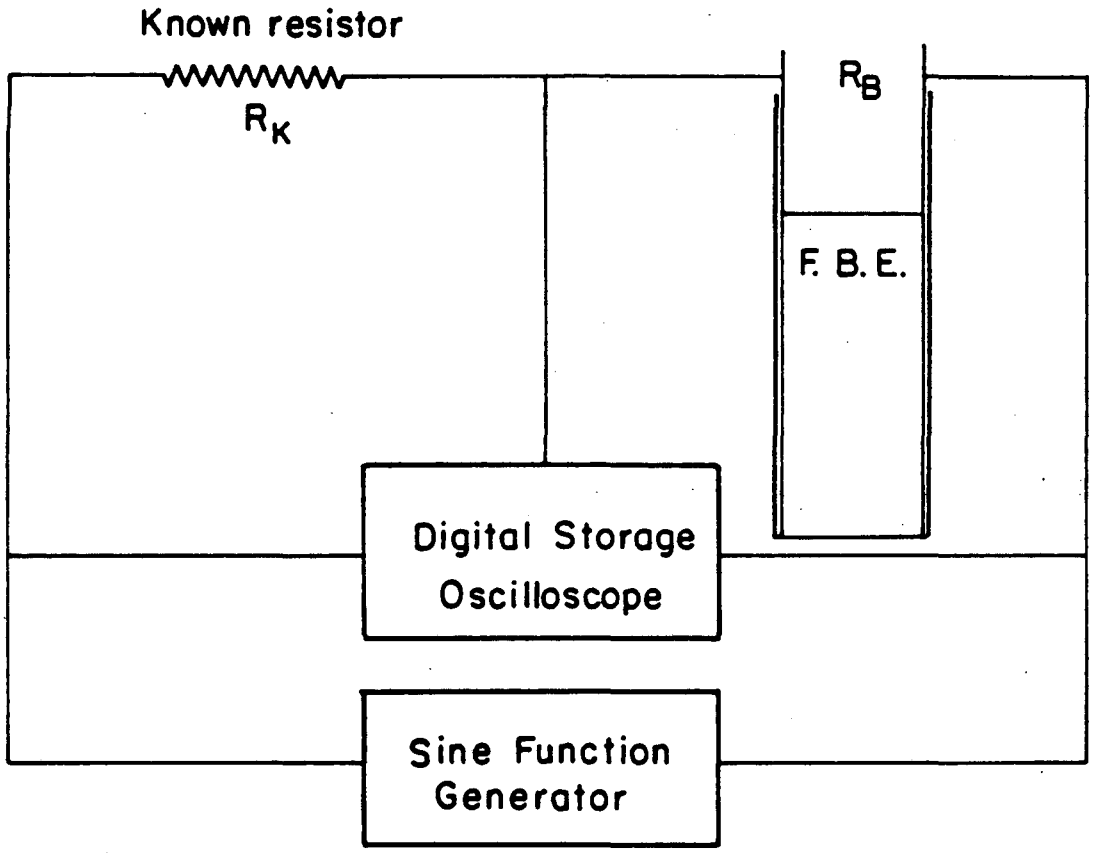

Figure IV-4 Apparatus schematic for effective bed resistivity measurement

water to obtain desired conductivity.

b. Data Collecting and Processing.

The procedure of data collection and storage were the same as those described in Chapter IV.B.1.b. Each data set was processed to calculate the amplitude and phase angle. The least square method was used for this calculation.

The bed resistance, R_b, can be calculated from the equation

$$R_b = R_k \frac{V_b}{V_k \cos\theta} \qquad \text{(IV-20)}$$

where R_k = resistance of the known resistor

V_k = potential drop across the known resistor

V_b = potential drop across the fluidized bed

θ = phase angle difference

which assume that any capacitance and inductance associated with the electrode are in parallel with its resistance.

For the geometry under consideration, the effective resistivity of the bed can be calculated using the equation

$$\sigma_b = \frac{R_b \cdot A}{L} \qquad \text{(IV-21)}$$

where A = active area of the current feeder

L = distance between current feeders

This equation is derived assuming that the macroscopic current distribution is uniform, i.e., perpendicular to the current feeder, a situation which is closely approximated in the bed used.

The following set of programs run on the Apple-II to process the data: FITTING, RES. A brief description of the operation of the system is as follows:

FITTING runs after all the data set has been taken. It reads the data file one at a time from the disc, calculates the amplitude and phase angle by using a least square method and saves the results in memory. After finishing calculation for all the data files, it calls RES.

RES runs immediately after the completion of FITTING to calculate the effective resistivities by recalling two corresponding results, one for the known resistor and one for the fluidized bed.

c. Procedure

The general procedure will not be repeated here. To be consistent with potential transient study, an active window area was made at the same location as before. After adjusting the bed expansion the current was switched on and some time was allowed to elapse and the measurement was performed.

C. Results and Discussions

During the part of this study concerned with potential transients, the fluidized bed electrode was driven with a constant current. Hence superficial current density and bed expansion were the main operating parameters. For each run, new solutions were prepared. During the experiments the cell potential was recorded continuosly by the chart recorder and intermittently by the oscilloscope. There was no change of cell potential observable on the strip chart recorder during the course of a run.

In the beginning of this study various sampling rates were tried to find the optimum sampling rate. Because the maximum detectable frequency, also called Nyquist Cutoff Frequency, is automatically set by sampling rate according to

$$f_{max}\ (Hz) = \frac{1}{2\Delta t} \qquad \text{(IV-22)}$$

where Δt = sampling interval (in seconds)

Table IV-2 shows an example of the effect due to sampling rate. Most of the experiments were performed with relatively slow sampling rate because it was found during preliminary experiments that only within the low frequency range, does the power spectrum show significant effects. The study was focused on that frequency range.

1. Cu/H_2SO_4 System

Table IV-2 : The Effect of Sampling Rate on the Potential Transient Measurement

Δt	$\bar{\phi}_p$	S_p	$\bar{\phi}_e$	S_e	$\bar{\eta}$	S_η
			(all are in mV)			
100 μs	137.1 ±16.6	7.33 ±0.41	140.1 ±16.6	6.77 ±0.41	-3.1 ±4.6	1.48 ±0.24
1 ms	129.0 ±11.4	9.90 ±1.86	130.1 ±11.3	10.31 ±1.84	-1.1 ±1.5	4.82 ±0.83
10 ms	141.4 ±4.4	23.94 ±2.07	142.9 ±4.4	23.72 ±2.06	-1.5 ±0.2	12.31 ±1.28

Bed Expansion : 25%
Superficial Current Density : 100 mA/cm^2
Cathodic Reaction of Cu/H_2SO_4 system

$\bar{\phi}_p$: Time Averaged Particle Potential

S_p : Standard Deviation of Particle Potential

$\bar{\phi}_e$: Time Averaged Electrolyte Potential

S_e : Standard Deviation of Electrolyte Potential

$\bar{\eta}$: Time Averaged Local Overpotential

S_η : Standard Deviation of Local Overpotential

Meaning of symbol is same for the following Tables.

The transients of particle potential and electrolyte potential (actually it is electrolyte potential plus local equilibrium potential but from now on, for brevity, this is just referred to as electrolyte potential) were measured with respect to the current feeder potential. This means the measured values represent the potential drop from the measuring position, within either particle phase or electrolyte phase, to the current feeder.

The measuring position was changed subject to the requirement of the experiment. But most of the data was collected from the center of the active window area unless otherwise noted.

a. General Behavior

Figure IV-5 shows the typical potential transients which were collected with sampling interval, Δt, of 10 ms from the center of the bed with the superficial current density of 200 mA/cm^2 and bed expansion of 25%. It shows traces of particle potential fluctuation, electrolyte potential fluctuation and local overpotential fluctuation. Figure IV-6 shows the analysis of particle potential trace of Figure IV-5 by the Blackmann-Tukey method and Figure IV-7 is the result of FFT method. The short vertical line in probability density distribution represents the mean value. The power spectral densities of Blackmann-Tukey method were divided by the maximum value and those normalized values were plotted. For FFT method, the calculated power spectral densities were plotted directly in log scale. In Figure IV-6, it can be seen that the particle potential transients show an approximately normal probability

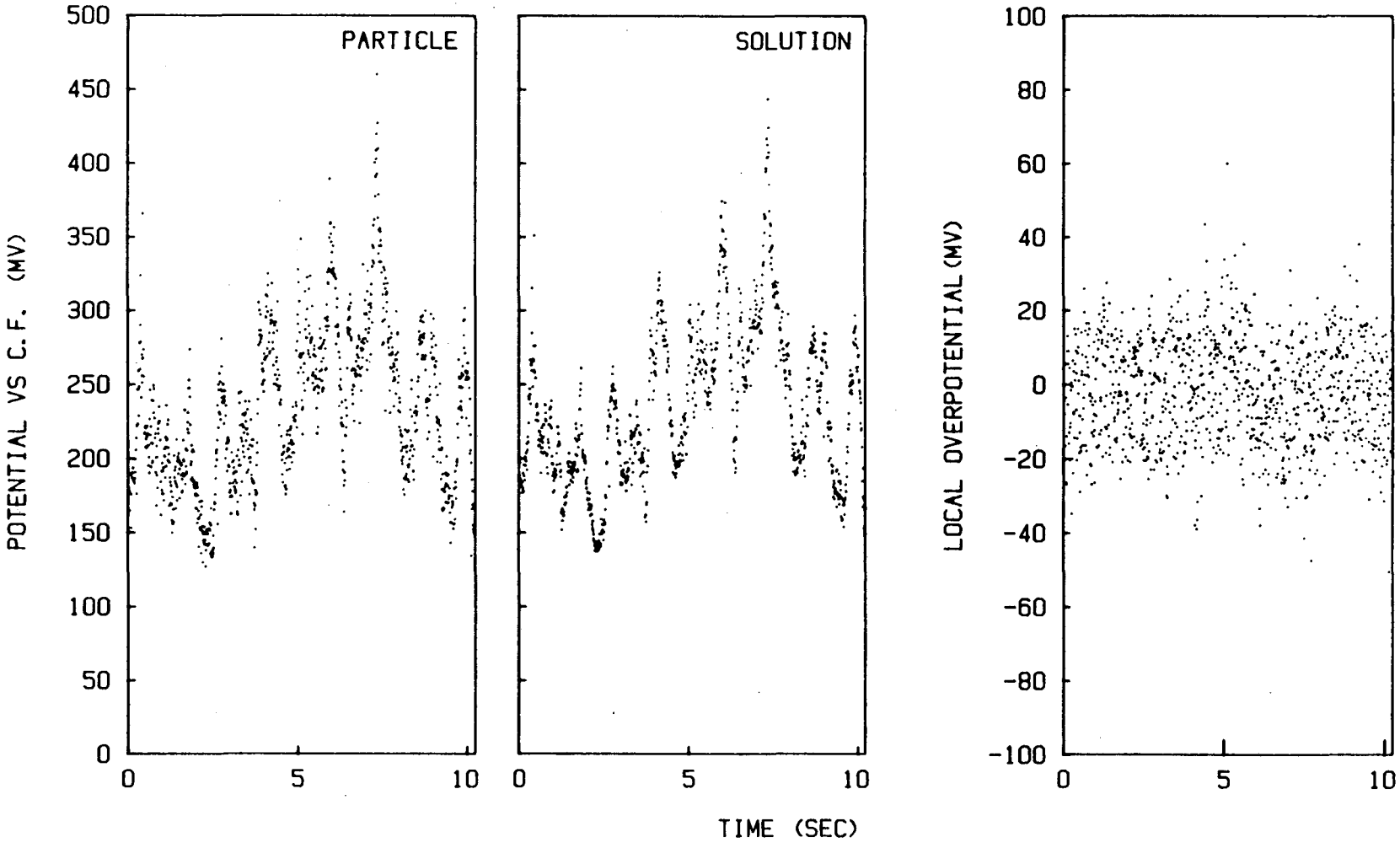

Figure IV-5 Potential transients from center of the bed
(Bed expansion: 25%, Superficial current density: 200 mA/cm^2)

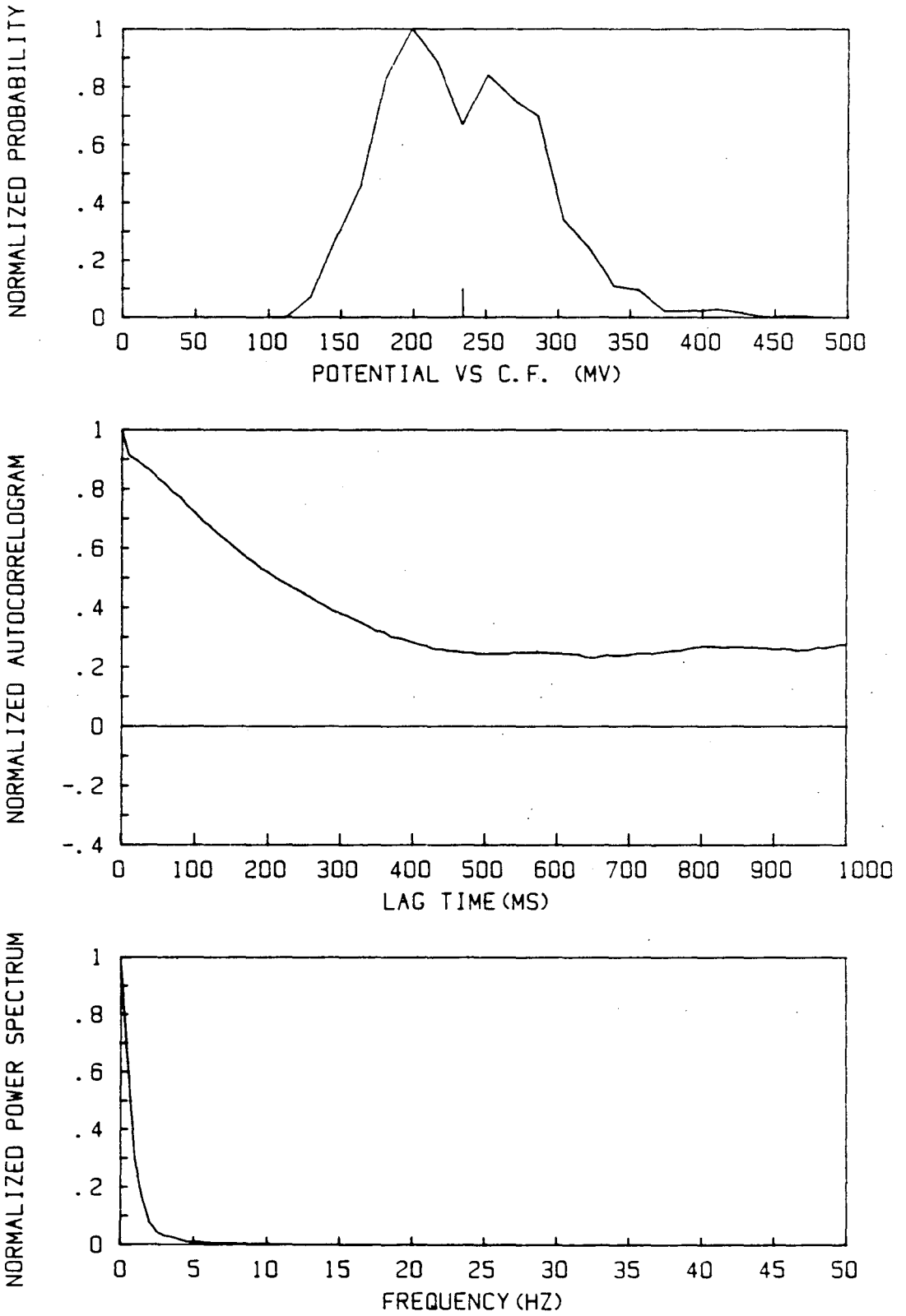

Figure IV-6 Result of Blackmann-Tukey method of particle potential trace of Figure IV-5

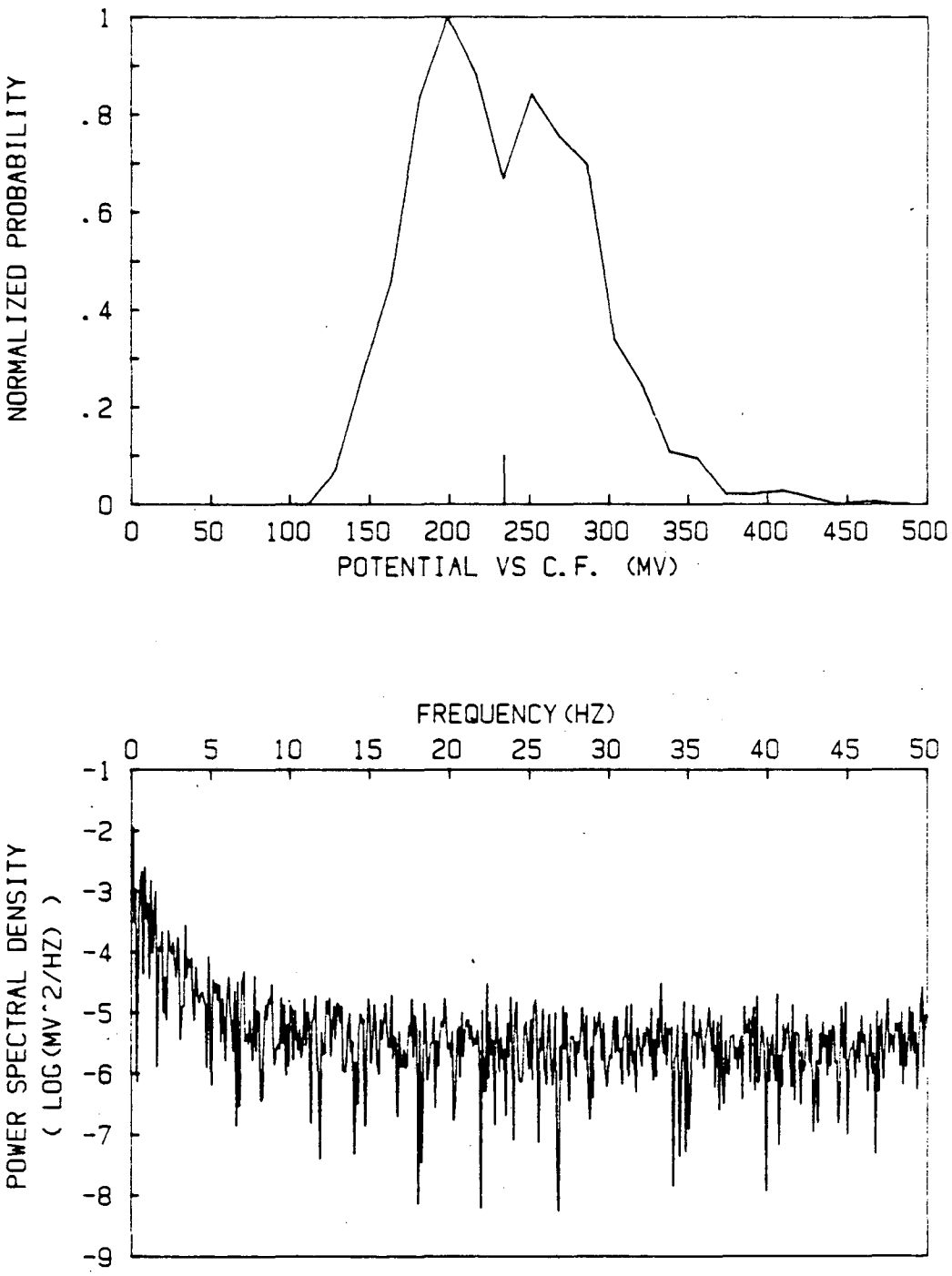

Figure IV-7 Result of FFT method of particle potential trace of Figure IV-5

density distribution and a fast decay of the autocorrelation. In the normalized power spectrum it is really hard to see any phenomena except at low frequency. Figure IV-7 shows that at low frequency power density decreases with increasing frequency, and at high frequency appears independent of frequency. From the view point of noise analysis[89-91] it is said that this spectrum consists of two kinds of noise, one is low frequency domain "flicker noise" and the other "white noise" over a wide frequency range.

The term white noise refers to the random data with energy distributed uniformly over all frequencies. It has a constant distribution across the frequency spectrum but looks as if it is heavily oriented to the higher frequencies. Flicker noise is characterized by random jumping of data which is due to fluctuations in the effectiveness of the barrier. Since the fluctuations are due to changes in a barrier, and these will in general be slow, the spectrum of flicker noise is expected to show strong low frequency components.

Figures IV-8 and 9 show the analysis of electrolyte potential transients and Figures IV-10 and 11 show those of local overpotential transients. By comparing Figures IV-6 and 7 with 8 and 9, it is observed that both potential transients are similar to each other as the raw data sets of Figure IV-4 look synchronous. Figures IV-10 and 11 show that local overpotential transient is a white noise over the detected frequency range except at very low frequencies. Note that the horizontal scale in the upper half and the vertical scale in the lower half of Figure IV-11 is different from that in Figures IV-7 and 9.

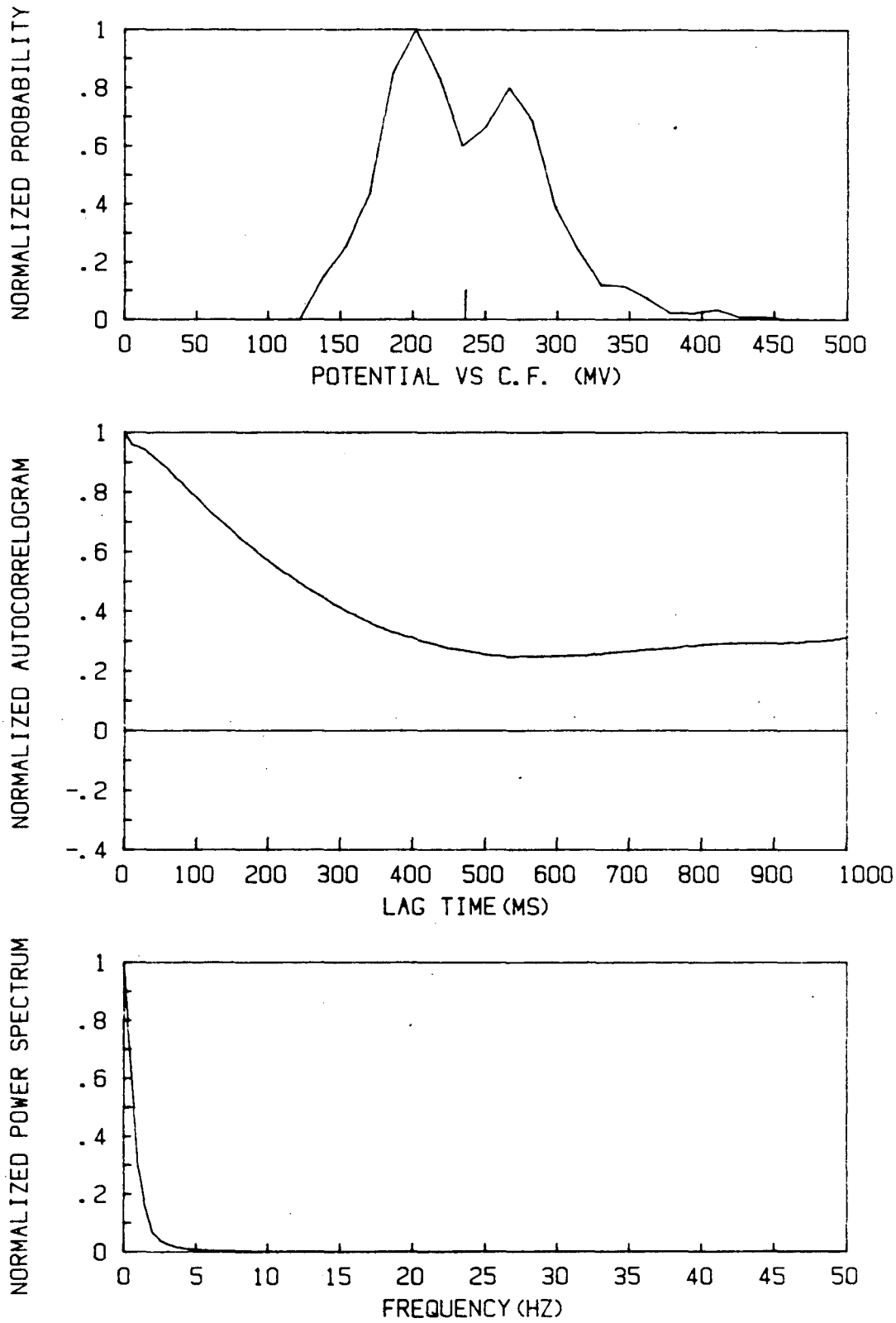

Figure IV-8 Result of B-T method of electrolyte potential trace of Figure IV-5

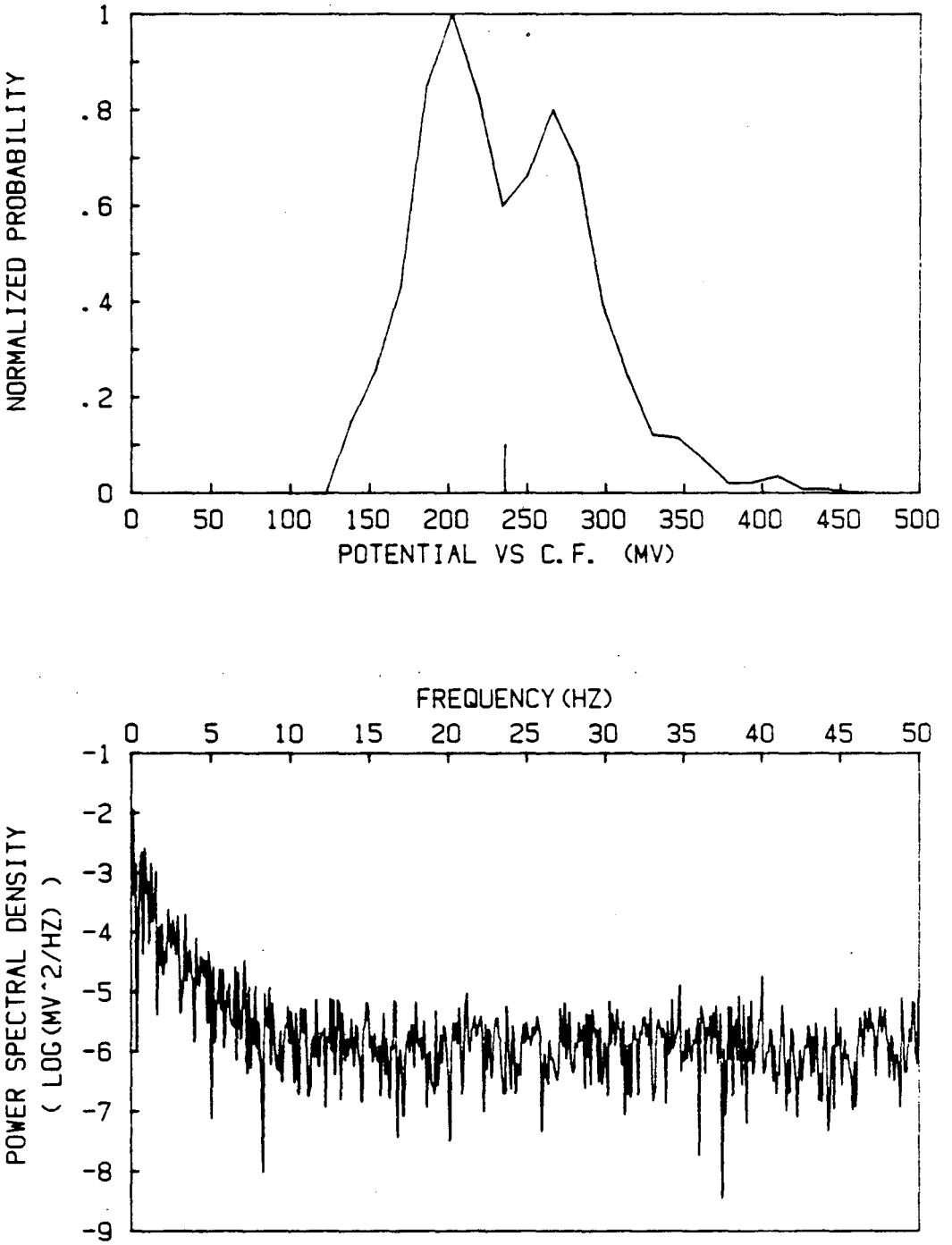

Figure IV-9 Result of FFT method of electrolyte potential trace of Figure IV-5

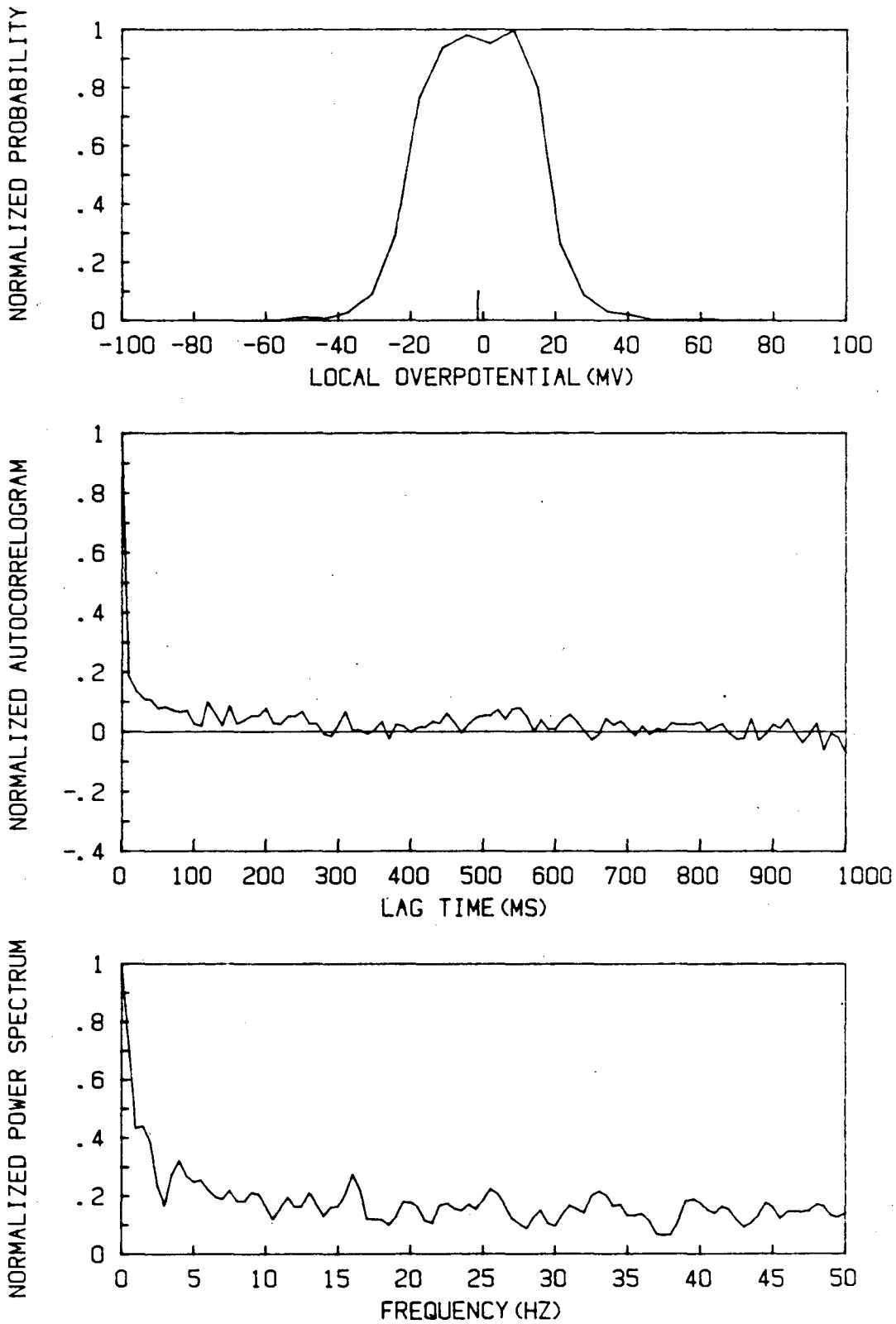

Figure IV-10 Result of B-T method of local overpotential trace of Figure IV-5

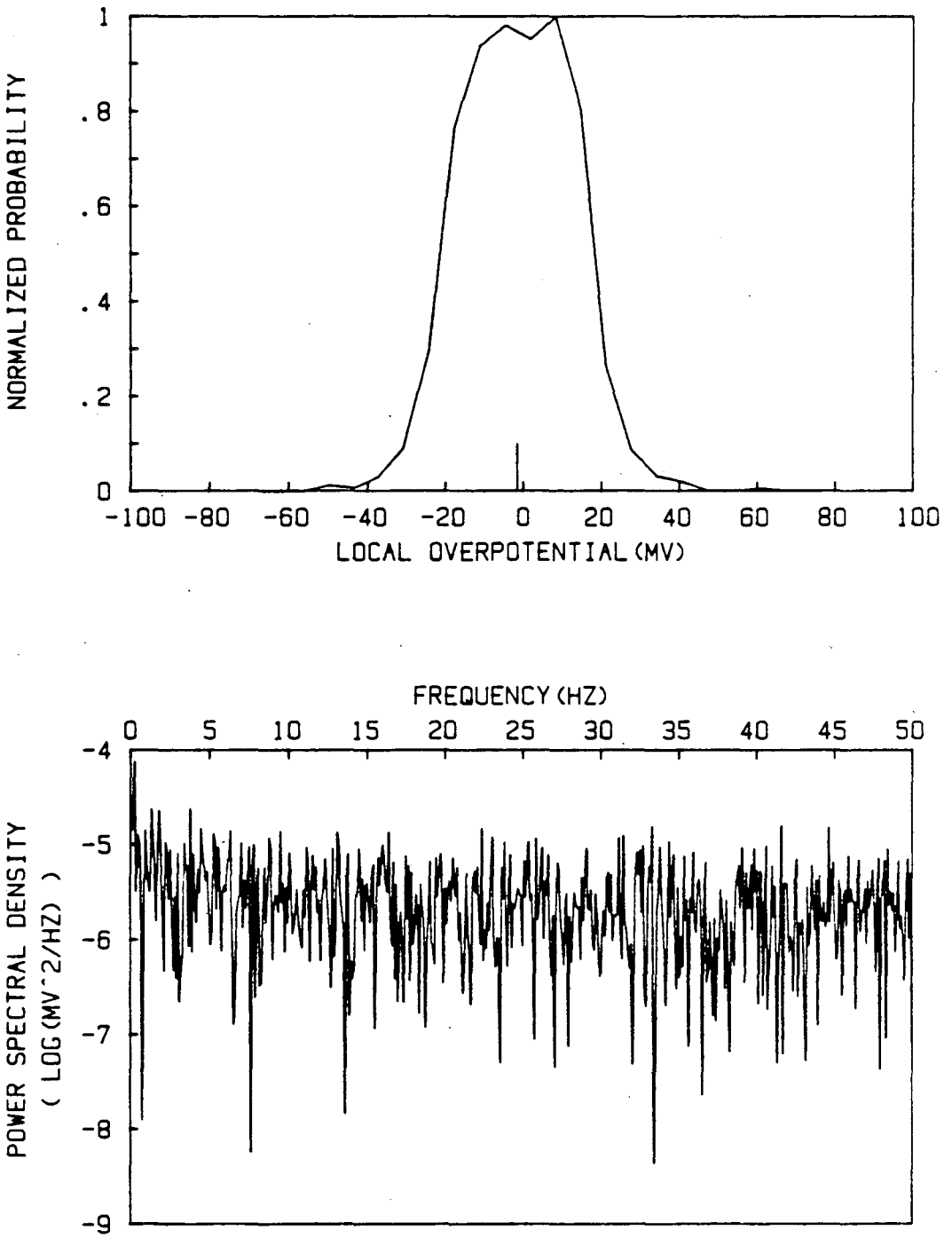

Figure IV-11 Result of FFT method of local overpotential trace of Figure IV-5

In addition to that, it is appropriate to examine the local overpotential transient behavior more closely. Even the fluidized bed was under cathodic reaction, i.e. local overpotential should be a negative value, the probability density shows approximately even distribution around the mean which is a negative number. This can be interpreted by the bipolar behavior of a fluidized bed electrode. Let the particle or particle cluster be isolated from the current feeder together with surrounding electrolyte with the particle potential of ϕ_p and electrolyte potential of ϕ_e. The relative values of electrical conductivity associated with electrolyte and particle will develop an equipotential distribution within the particulate phase while the electrolyte is characterized by a potential gradient. These different potential distributions will develop an anodic region on one side of a particle and a cathodic region on the other. When the captive particle of the potential measuring probe contacts the anodic region of the particle it senses the anodic overpotential even when the overall reaction is cathodic. This behavior generates the local overpotential fluctuation around the mean value within a certain range, which may depend upon the various operating conditions. And this fluctuation, which continuously reverse the directions of electrochemical reaction at the particle surface, will give a same effect as current reversing on the electrodeposit morphology.

It will now be shown that the autocorrelation and power spectral density function contain equivalent information. Consider the wide band random noise assuming the power spectrum, $G_x(f)$, of these data to be

uniform over a wide frequency bandwidth B, that is

$$G_x(f) = G \qquad 0 < f \leq B \qquad \text{(IV-23)}$$

$$= 0 \qquad f > B \qquad \text{(IV-24)}$$

From equation IV-14, the autocorrelation function is then given by

$$R_x(\tau) = \int_0^B G \cos 2\pi f\tau \, df = GB\left(\frac{\sin 2\pi B\tau}{2\pi B\tau}\right) \qquad \text{(IV-25)}$$

This correlation function diminishes very rapidly with a zero crossing at $\tau = 1/2B$.

Conversely, when the autocorrelation diminishes rapidly, the data are predicted as a wide band white noise. Autocorrelation and power spectrum therefore give the same information, even though their analysis domains are different. Because of this and because the FFT gives a small resolution bandwidth of the spectrum, only the FFT was used to process the data presented from now on.

Early in this study, there was some difficulty in reproducibility when the data were collected at a fast sampling rate. Figure IV-12 shows three sets of particle potential measurements with t=100μs, superficial current density of 100 mA/cm^2 and approximately 17% bed expansion. This shows that even if all the conditions are kept same the results are different. The experiment is repeated with a superficial current density of 200 mA/cm^2 and the result is plotted in Figure IV-13. There is a significant difference between the average values of the

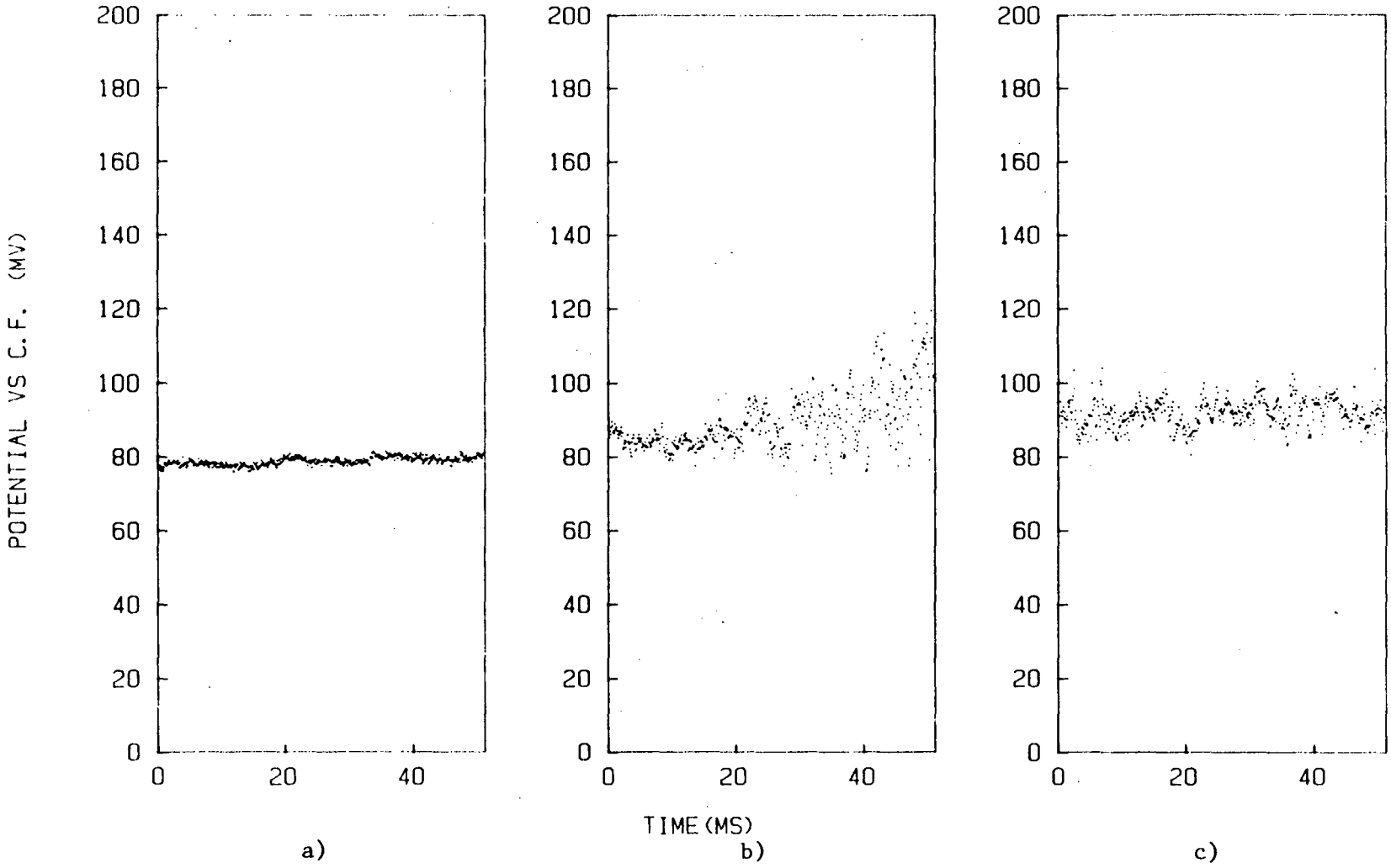

Figure IV-12 Particle potential transients at same operating condition (B.E. = 17%, S.C.D. = 100 mA/cm^2)

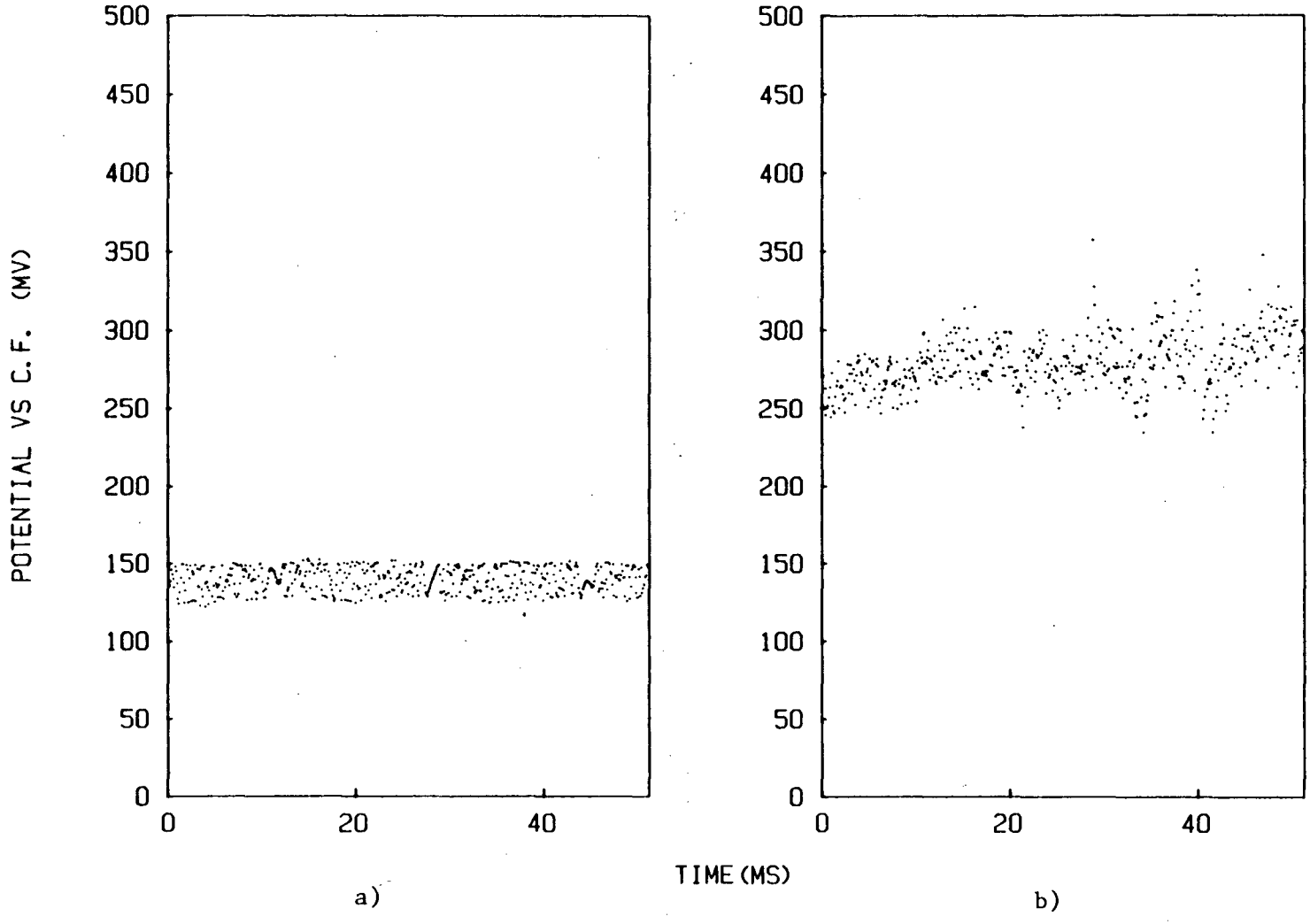

Figure IV-13 Particle potential transients at same operating condition (B.E. = 17%, S.C.D. = 200 mA/cm^2)

potentials, 139.4mV for a) and 279.9mV for b), in the two cases depicted in Figure IV-13 compared to that of Figure IV-12.

To find out the reason for this behavior, data were collected under the same condition as Figure IV-13 for a relatively long time. Figure IV-14 shows the measurements, each of which consists of 2048 data points with a sampling interval of 10 ms. Approximately 5 data points of Figure IV-14 represent the whole period of 50ms appearing as the horizontal axis in Figure IV-13. It can be seen that there are two kind of particle (or electrolyte) potential fluctuations: fluctuation of a few tens of millivolts about the time average value (these fluctuations appearing rapid and of broad frequency distribution) and occasional pulses of the order of 100mV that occur simultaneously in both the particle and electrolyte potential and are therefore not observed in the overpotential. The non-reproducibility encountered with too high a sampling rate is due to the happenstance of encountering (or not encountering) one of the large low frequency peaks during a 50 ms data collection interval. Figure IV-13a) shows a 50ms interval when the first kind of potential fluctuation is occuring while Figure IV-13b) shows a 50ms interval during one of the high amplitude low frequency "bursts". These bursts result in the "shoulder" at potential much different from the mean in the normalized probability density distribution for the particles and electrolytes (Figure IV-15). They also result in the low frequency flicker noise in the power spectrum for the particles and electrolytes. These features are almost absent from the corresponding plots for the overpotential (Figure IV-16). The low

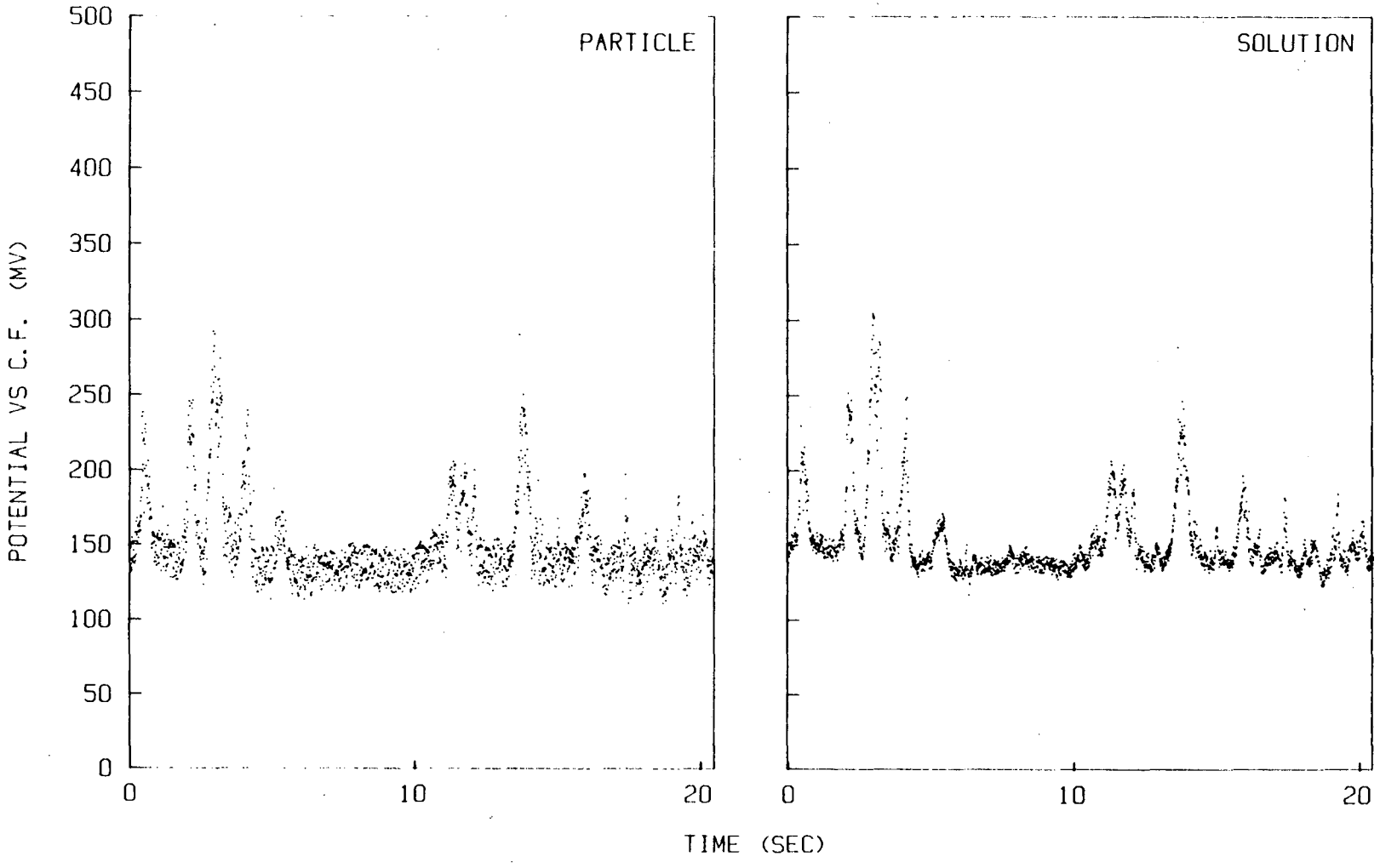

Figure IV-14 a) Potential transients from center of the bed
(B.E. = 17%, S.C.D. = 200 mA/cm^2)

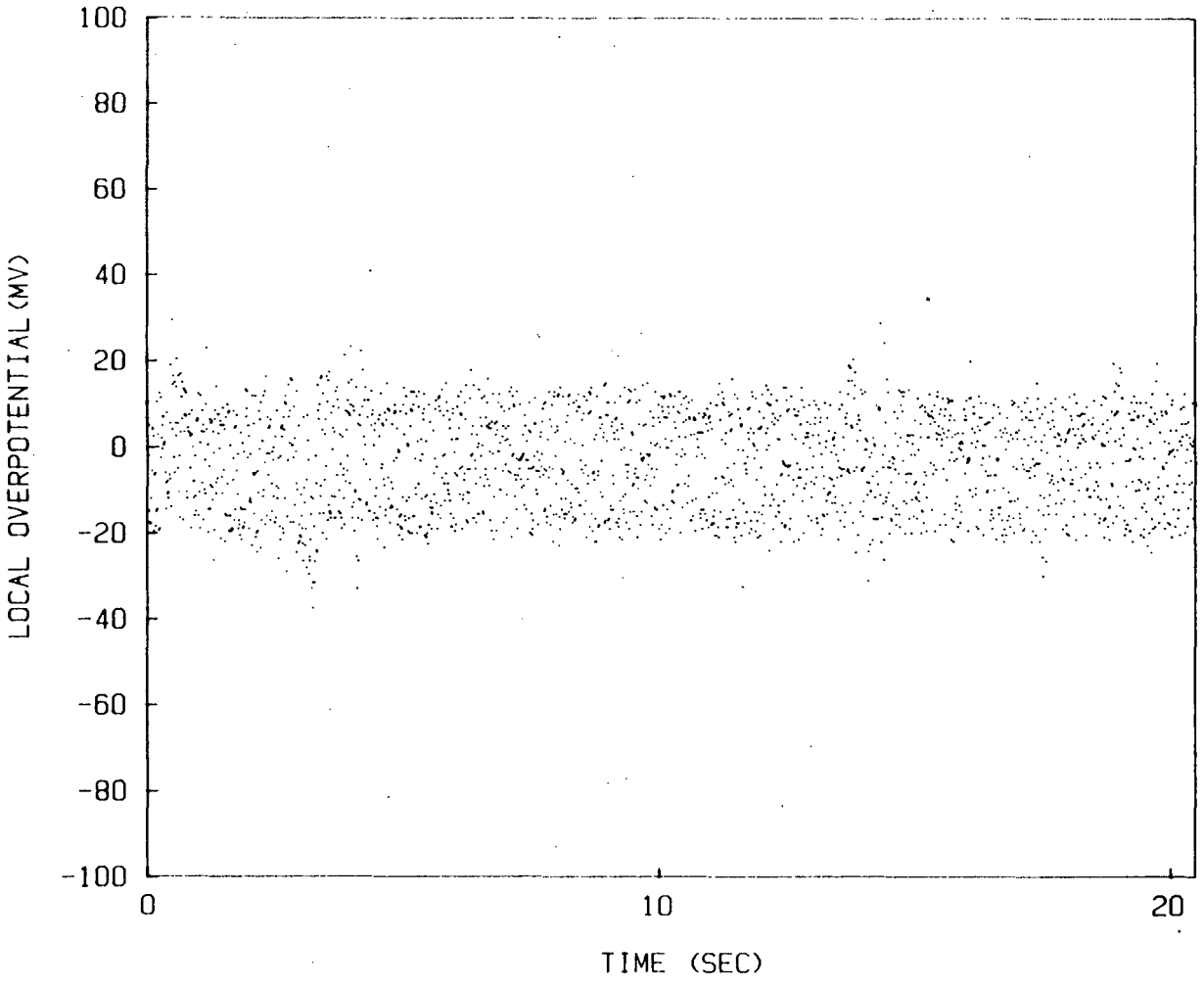

Figure IV-14 b) Corresponding local overpotential transient with Figure IV-14 a)

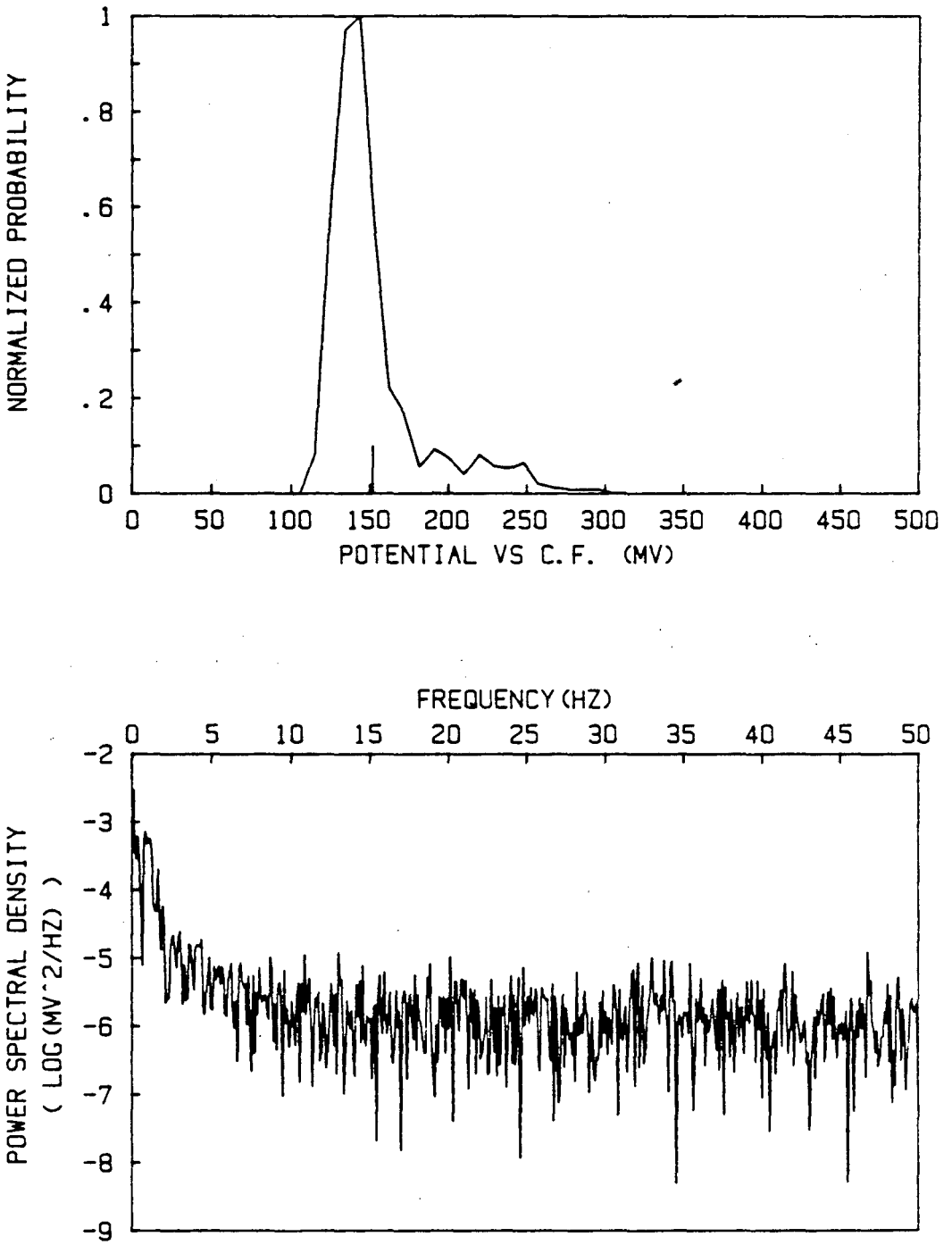

Figure IV-15 FFT analysis of particle potential transient of Figure IV-14 a)

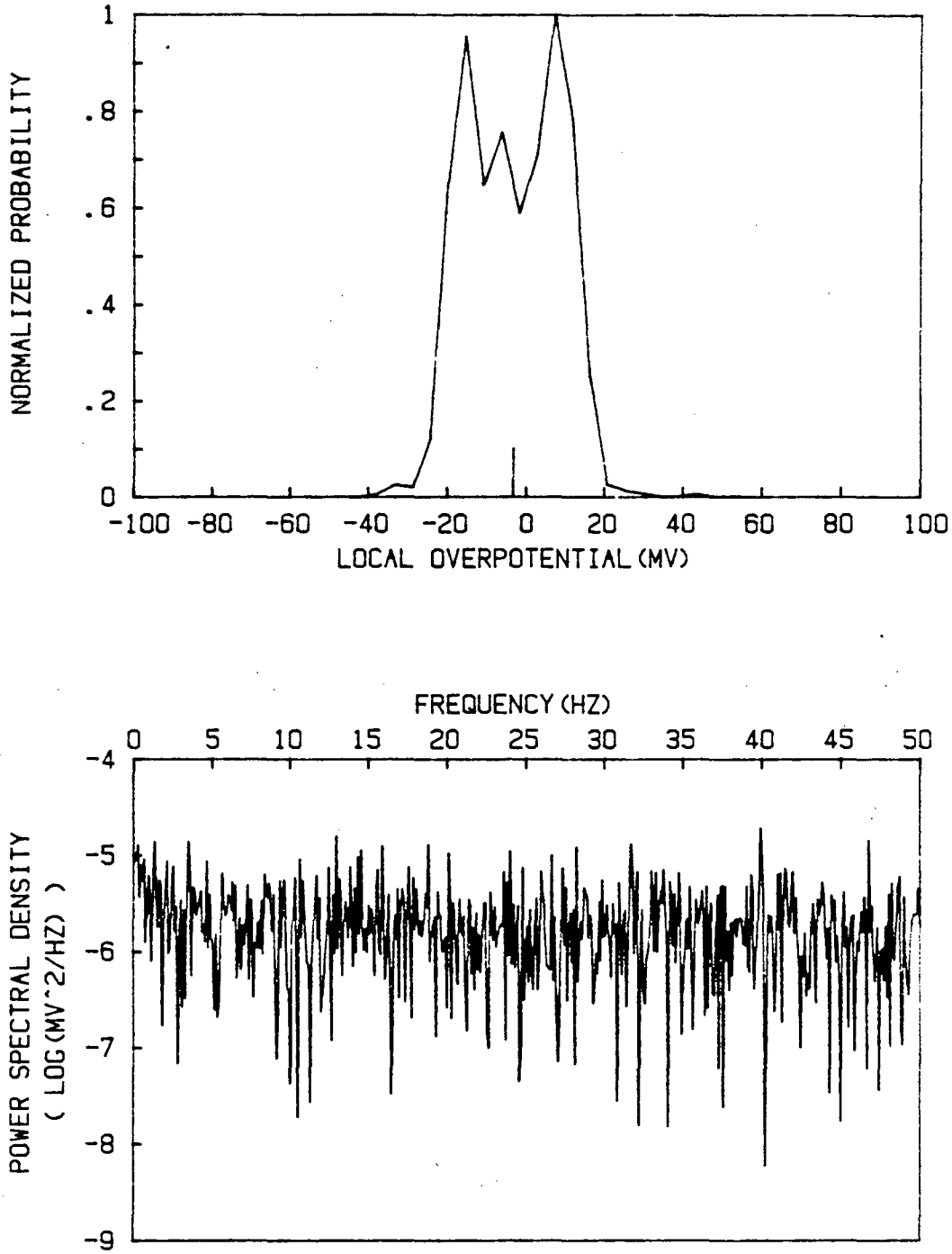

Figure IV-16 FFT analysis of local overpotential transient of Figure IV-14 b)

amplitude white noise can be seen in the plots for particle, electrolyte and overpotential.

These results suggest that the potential fluctuations of a fluidized bed electrode are affected to some extent by hydrodynamic behavior of the two media. In this regard a brief description of the hydrodynamics of fluidized beds is appropriate. Consider a bed of particles up through which a fluid is flowing. Starting from zero flow rate (or zero superficial fluid velocity = flow rate/bed cross section) the pressure drop from bottom to top of the bed increases as flow rate is increased. At a certain flow rate this pressure differential becomes sufficient to support the weight of the bed and the bed becomes fluidized. The superficial velocity of the fluid at this point is the "minimum fluidization velocity". If the flow rate (superficial velocity) is increased beyond this point the volume occupied by the bed increases. The percentage of volume increase (above that at minimum fluidization) is the bed expansion. Frequently, at fluid velocities above the minimum fluidization velocity, the bed exhibits what has become referred to "bubbling" behavior. The "bubbles" referred to are regions of the bed where there are little or no particles; these regions rise through the bed in much the same way that a gas bubble rises through a liquid.

These "bubbles" in fluidized beds have been studied by a large number of investigators (see for example the book by Kunni and Levenspiel, Fluidization Engineering[92]) and Davidson and Harrison[93] have provided a figure (copied here as Figure IV-17) which quantifies the

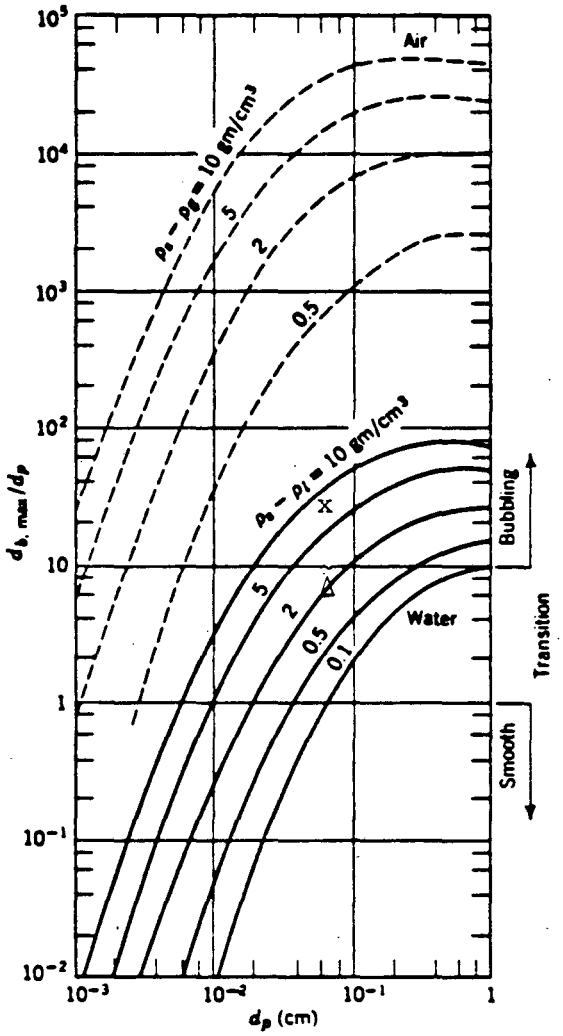

Figure IV-17 Maximum stable bubble size and conditions for bubbling and smooth fluidization (after Davidson and Harrison [93]) (x experimental condition for copper particle, Δ for Sorapec particle)

conditions under which bubbling behavior occurs and predicts the maximum stable bubble size. The term "maximum stable bubble size" refers to the fact that bubbles are typically smaller than this size in the region of the distributor (unless the distributor openings are unusually large) and grow to a maximum size by coalescence as they rise through the bed. Conditions for the two kinds of particles used in this investigation are marked on this figure and it is seen that for copper particles bubbling should occur while for the Sorapec particles the bed is in a transition regime between "smooth fluidization"(free of bubbles) and bubbling fluidization (a predominance of bubbles). In the liquid fluidized bed the relationship between bubble diameter, d_b, and bubble velocity, U_b, is

$$d_b = 1.978\ U_b^2 / g \qquad \text{(IV-26)}$$

where g is acceleration gravity

and the maximum size of stable bubble exists when bubble velocity is same as terminal velocity of the fluidizing particles. By this the maximum stable bubble size is predicted to be around 10mm for the bed of copper particles which is about 20 times larger than the average particle size and approaching the width of the bed. It is hypothesized that the low frequency flicker noise of the particle and electrolyte potential are a consequence of the occurence of bubbles. This is consistent with the observation that as the electrolyte flow rate is increased (bed expansion increased and the bubble volume in the bed increased) the flicker noise increases.

b. Effect of Bed Expansion

It has been known that bed expansion affects the performance of fluidized bed electrodes by changing the void fraction of the bed. Figure IV-18 is the potential transients at superficial current density of 200 mA/cm^2 and bed expansion of 13%. By comparing with Figure IV-5, where data were collected under the same condition as Figure IV-18 (except that the bed expansion was 25%), the effect of bed expansion on the potential transients can be seen. All the potential fluctuations are affected significantly. The statistical analysis for this data collected at low bed expansion appears in Figures IV-19 and 20 which should be contrasted with Figures IV-7 and 11 with due note of differences in scale. It is apparent that at low bed expansion the mean particle potential is closer to that of the current feeder for the same cell current (indicative of a higher effective conductivity of the particulate phase). Furthermore, particle potential variations (both the flicker noise and the white noise) are much diminished. Turning to the overpotential, a diminution in its fluctuations is observed although the effect is not as marked as for the particle potential. Table IV-3 summarizes the effect of bed expansion on the potential transients. The table reveals that both the time averaged particle potential and its standard deviation increase with bed expansion, the latter to a much greater extent than the former. In contrast the time averaged overpotential shows no significant variation with bed expansion while its standard deviation appears to show a modest increase.

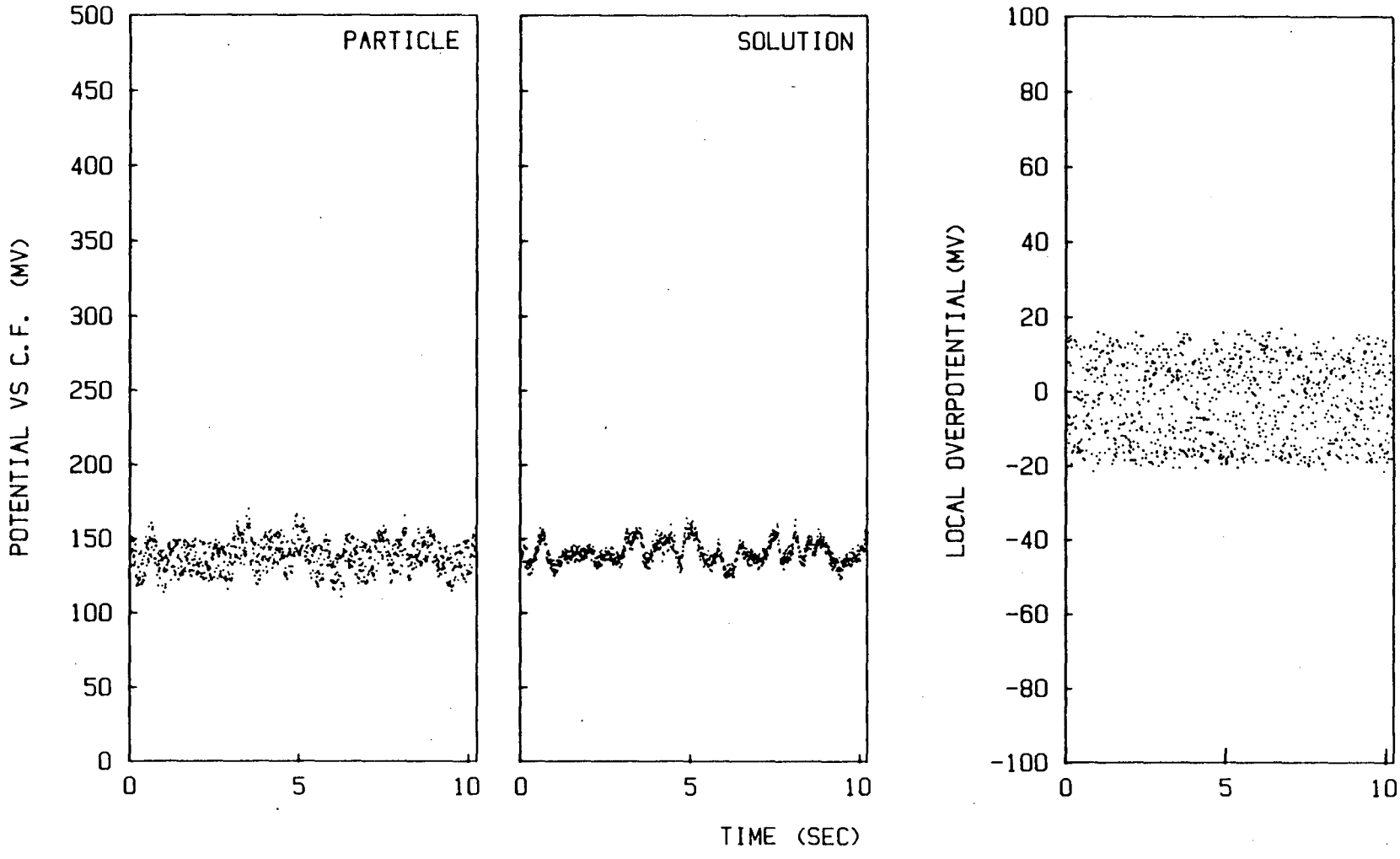

Figure IV-18 Potential transients from center of the bed (B.E. = 13%, S.C.D. = 200 mA/cm^2)

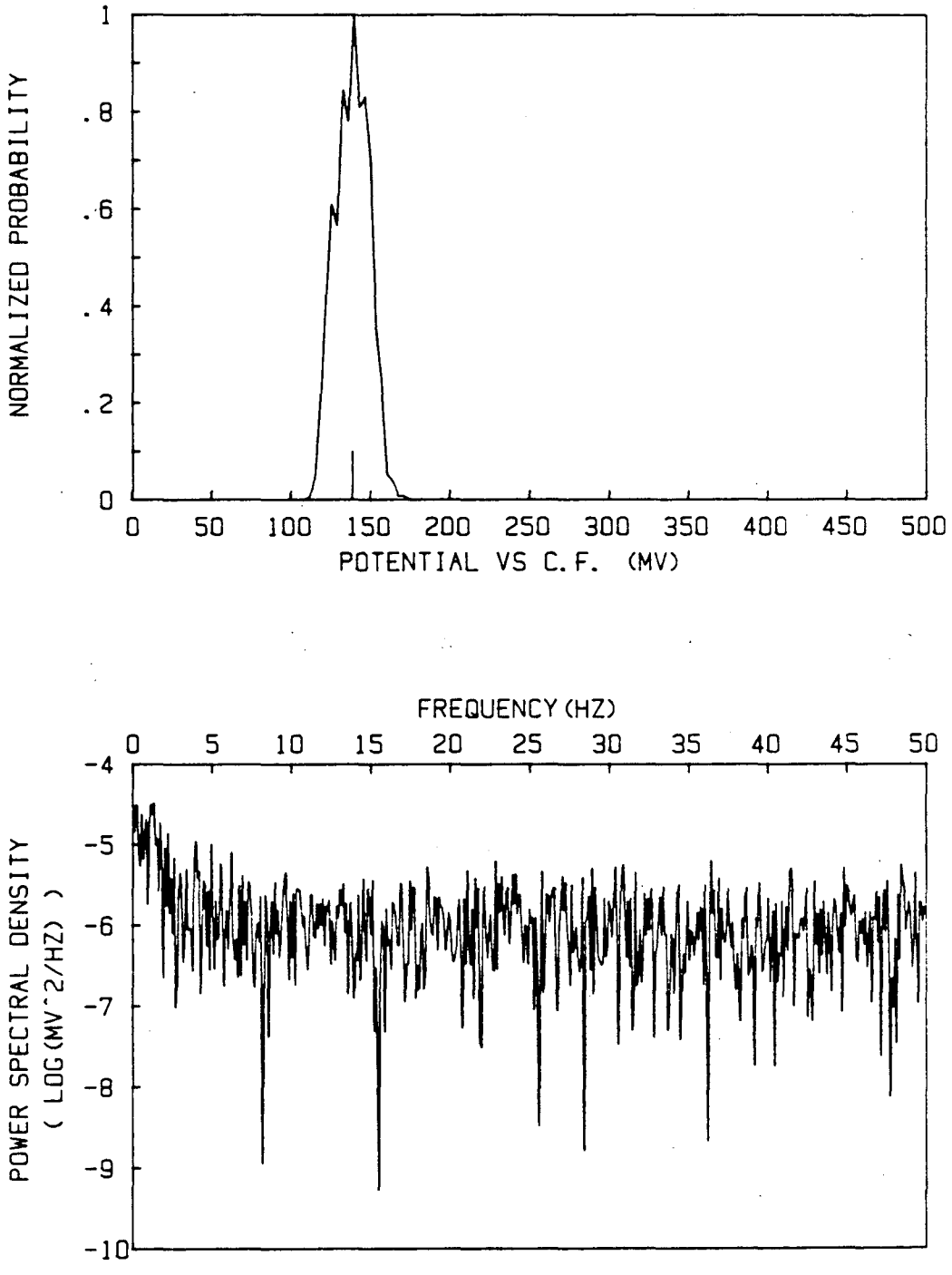

Figure IV-19 FFT analysis of particle potential trace of Figure IV-18

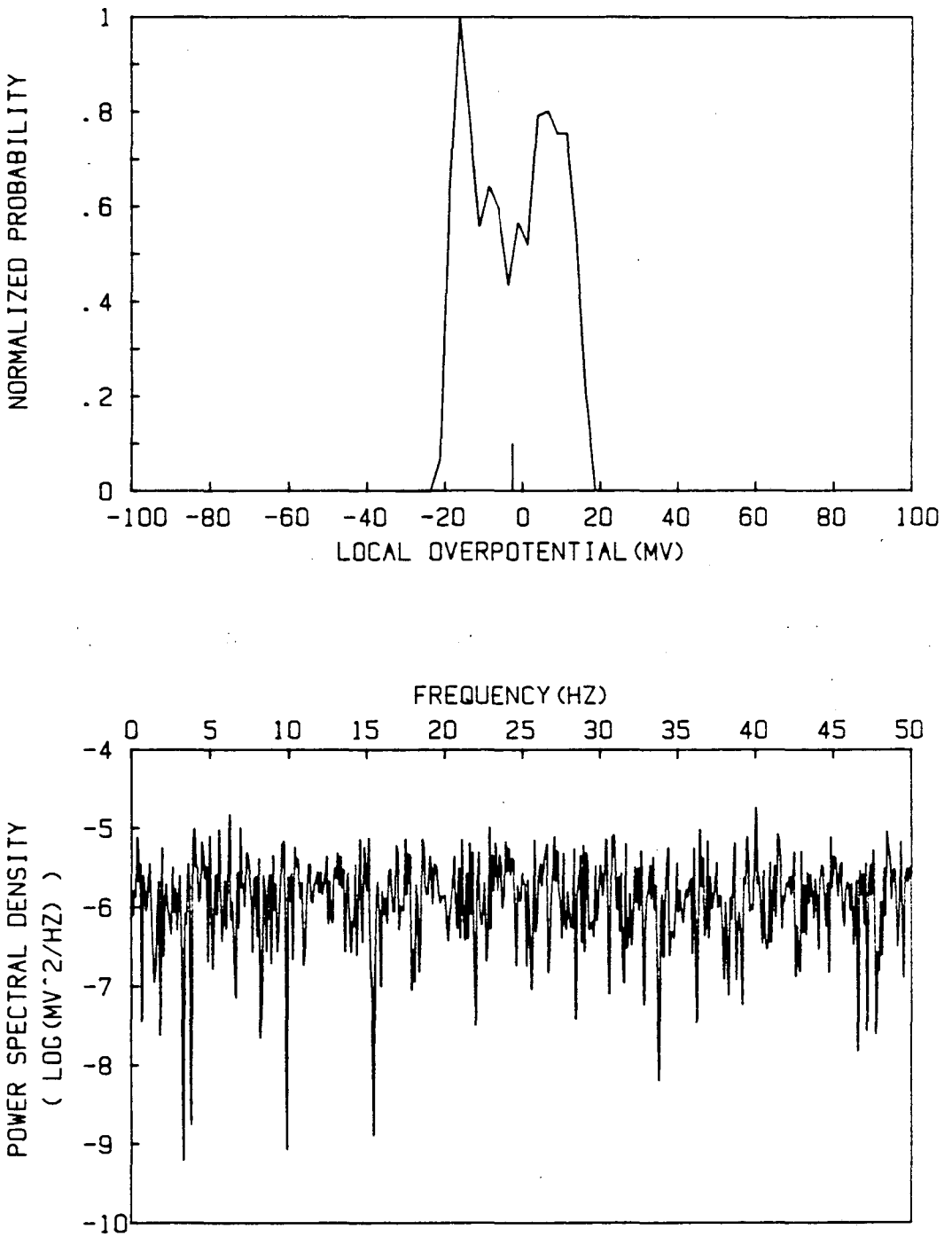

Figure IV-20 FFT analysis of local overpotential trace of Figure IV-18

Table IV-3 : Effect of Bed Expansion on Potential Transients

B.E. (%)	ϕ_p	S_p	$\bar{\eta}$	S_η
		(all are in mV)		
13	138.28	10.98	-1.54	10.33
17	160.24	31.05	-1.45	12.68
25	234.09	52.95	-1.71	13.96

Superficial Current Density : 200 mA/cm^2

Sampling Interval : 10 ms

Cathodic reaction of Cu/H_2SO_4 system

c. Vertical Variation of Potential Transients

During the operation of the copper fluidized bed electrode, it was seen that the particles are not uniformly distributed from bottom to top, the number of particles per unit volume being higher at the bottom. The effect of this non-uniformity on potential transients was studied by moving the potential measuring probe in the vertical direction.

Figure IV-21 shows the potential transients measured at 6cm above the center of the bed and Figure IV-24 depicts data collected 6cm below the center. These data sets should be contrasted with those of Figure IV-5 taken at the center of the bed. Because the size of the active window area was 5 x 10cm, the first position was 1cm above the upper edge of the active window area while the second position was 1 cm below its lower edge. Figures IV-22 and 23 are statistical analyses of particle potential and the local overpotential transients of Figure IV-21 and Figures IV-25 and 26 are the analyses of Figure IV-24. Data from other vertical positions in the bed are presented in Table IV-4 and Figures IV-27 and 28. One possible explanation of these results is as follows. Due to the "fringing" of the current, the region of highest current density in the bed is at mid height, consequently this is the region of highest time average particle and electrolyte potentials. Fluctuations in these potentials show a similar pattern being highest at mid height. In fact the ratio of the standard deviation to the time average value (coefficient of variation) is 0.19 ± 0.04 except for the lowest two measurement points. At the bottom of the bed this ratio is much smaler and we see from Figure IV-25 (compared, say, to Figure IV-7)

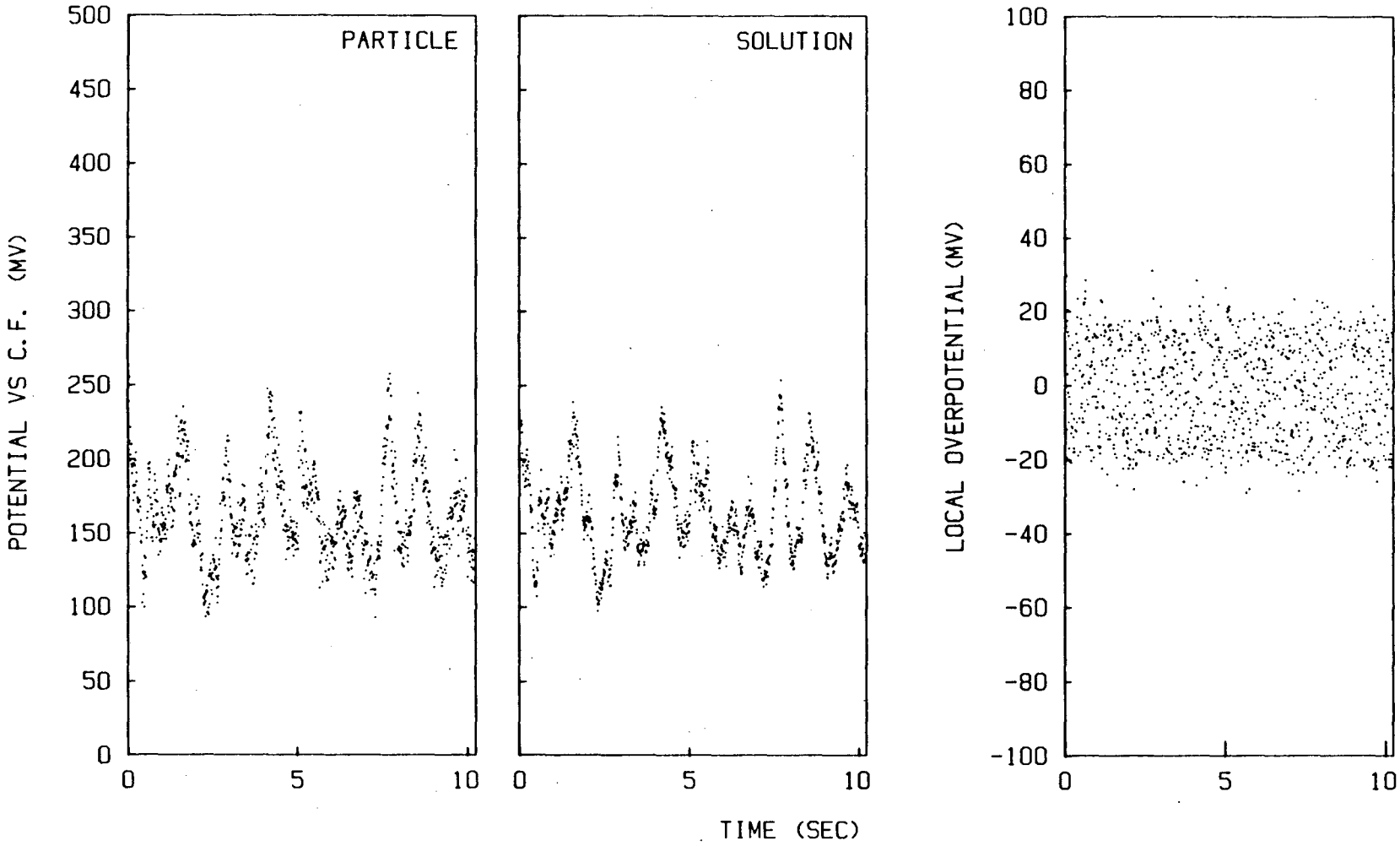

Figure IV-21 Potential transients from 6 cm above the center of the bed (B.E. = 25%, S.C.D. = 200 mA/cm^2)

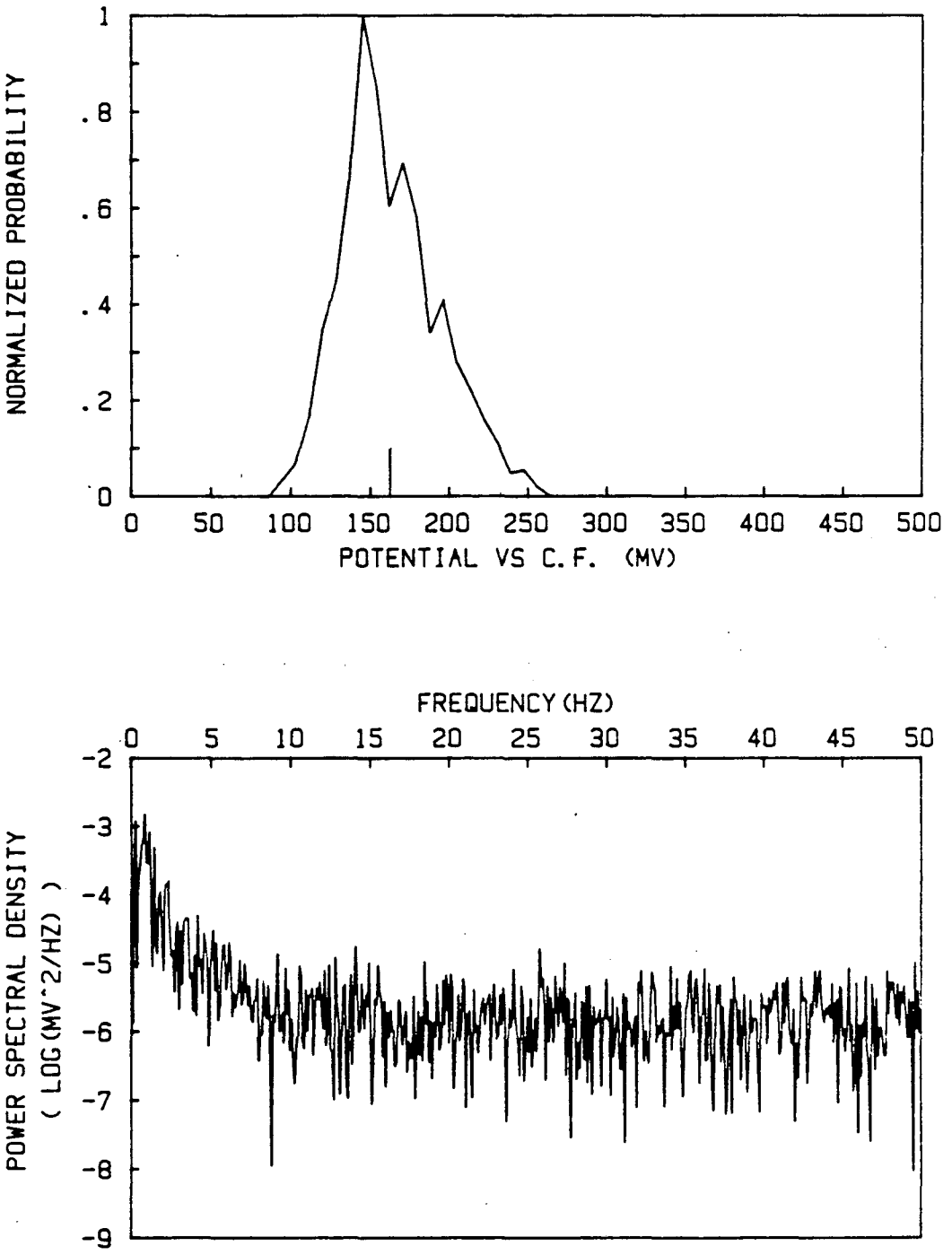

Figure IV-22 FFT result of particle potential trace of Figure IV-21

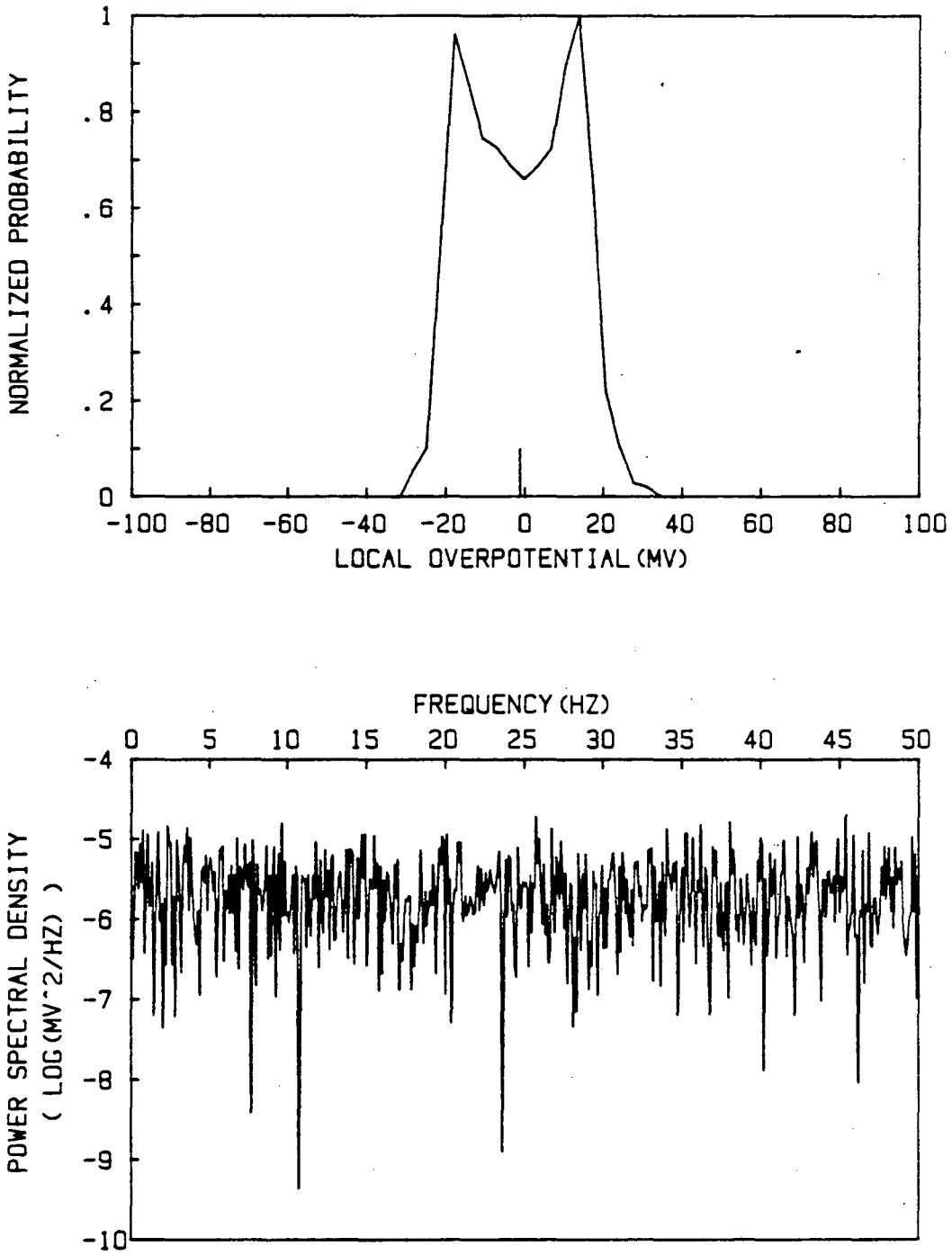

Figure IV-23 FFT result of local overpotential trace of Figure IV-21

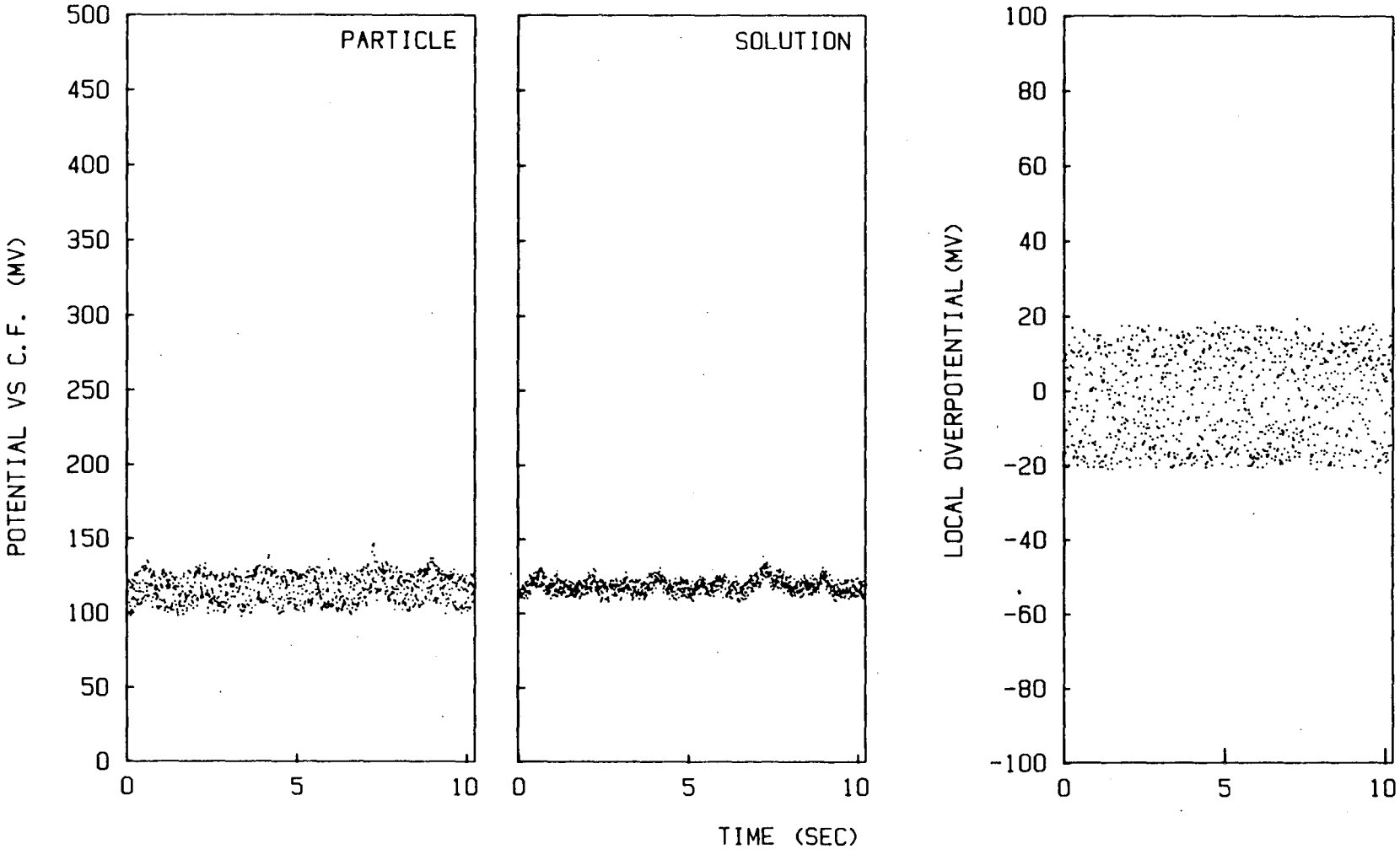

Figure IV-24 Potential transients from 6 cm below the center of the bed (B.E. = 25%, S.C.D. = 200 mA/cm^2)

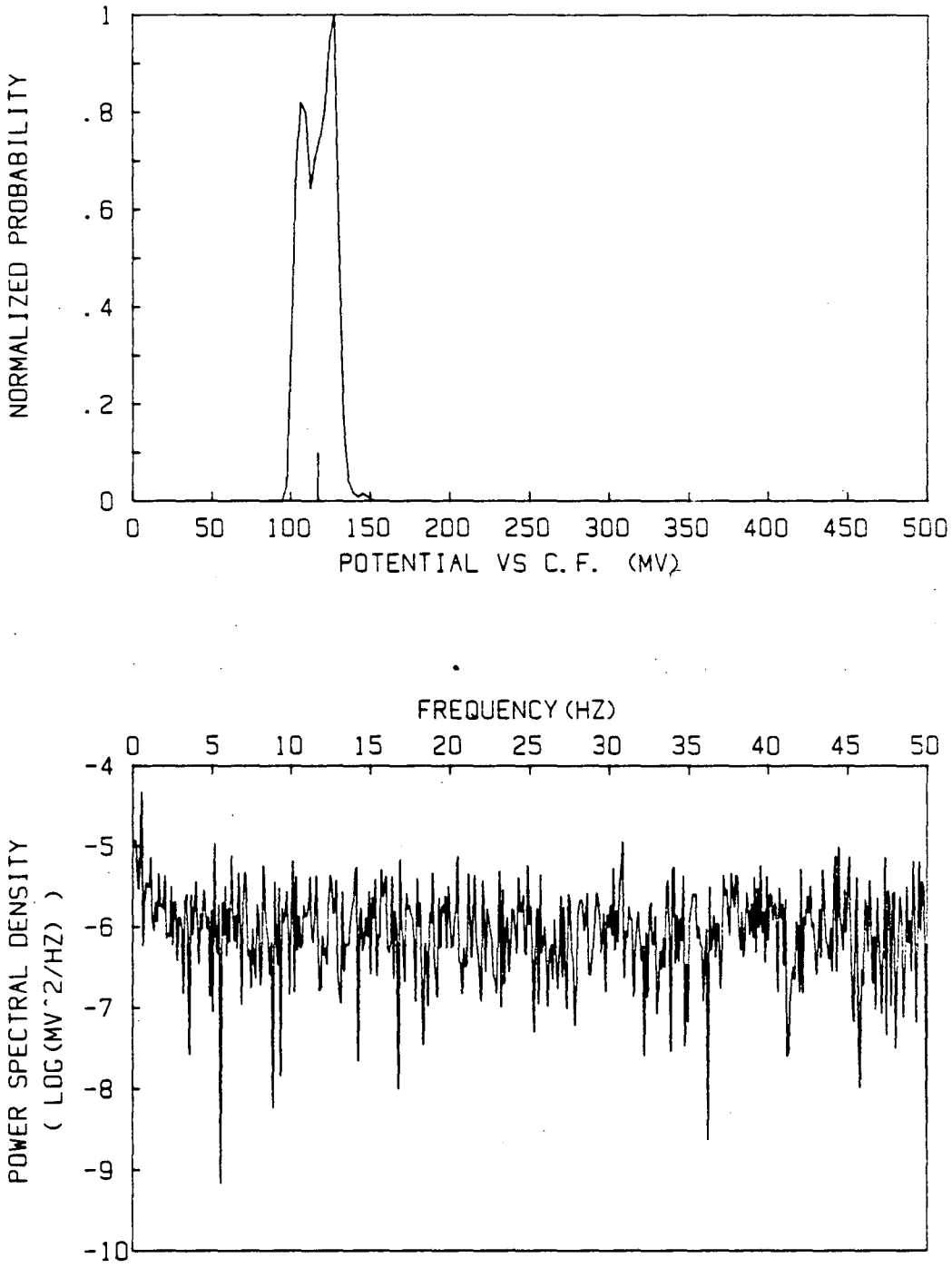

Figure IV-25 FFT result of particle potential trace of Figure IV-24

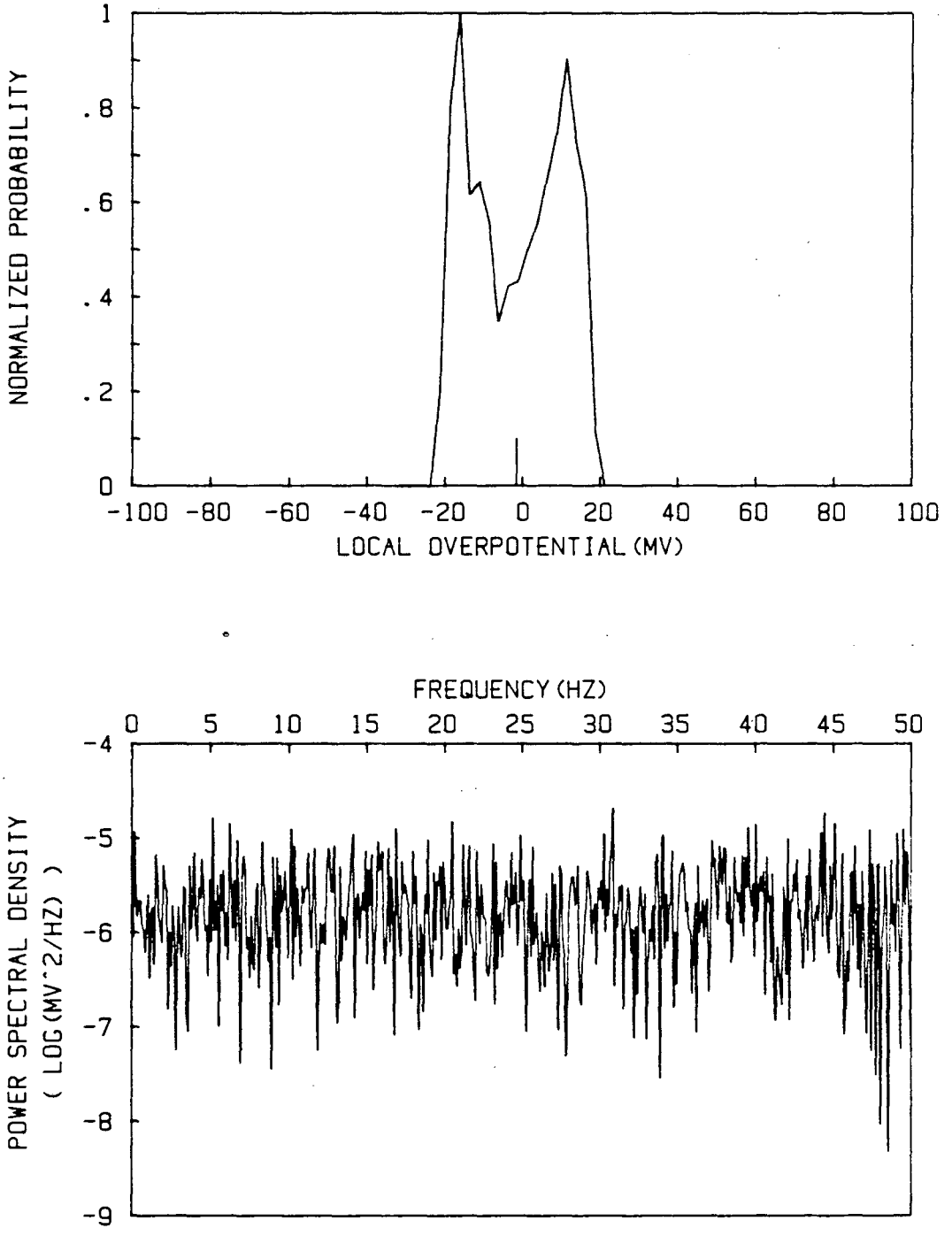

Figure IV-26 FFT result of local overpotential trace of Figure IV-24

Table IV-4 ; Vertical Variation of Potential Transients

Distance* (cm)	$\bar{\phi}_p$	S_p	$S_p/\bar{\phi}_p$ **	$\bar{\eta}$	S_η
	(all are in mV except **)				
8	132.1	19.37	0.15	0.1	12.79
6	162.5	30.67	0.19	-0.3	13.07
4	234.5	37.83	0.16	-1.0	13.76
2	277.5	54.40	0.19	-1.4	14.72
0	234.1	52.95	0.23	-1.7	13.96
-2	189.6	36.18	0.19	-2.4	12.20
-4	138.3	10.32	0.07	-2.8	10.72
-6	116.9	9.48	0.08	-1.8	12.02

* Distance from the center of active window area which is 7cm above distributor.

** Dimensionless Coefficient of Variation

Bed Expansion : 25%

Superficial Current Density : 200 mA/cm^2

Sampling Interval : 10 ms

Cathodic reaction of Cu/H_2SO_4 system

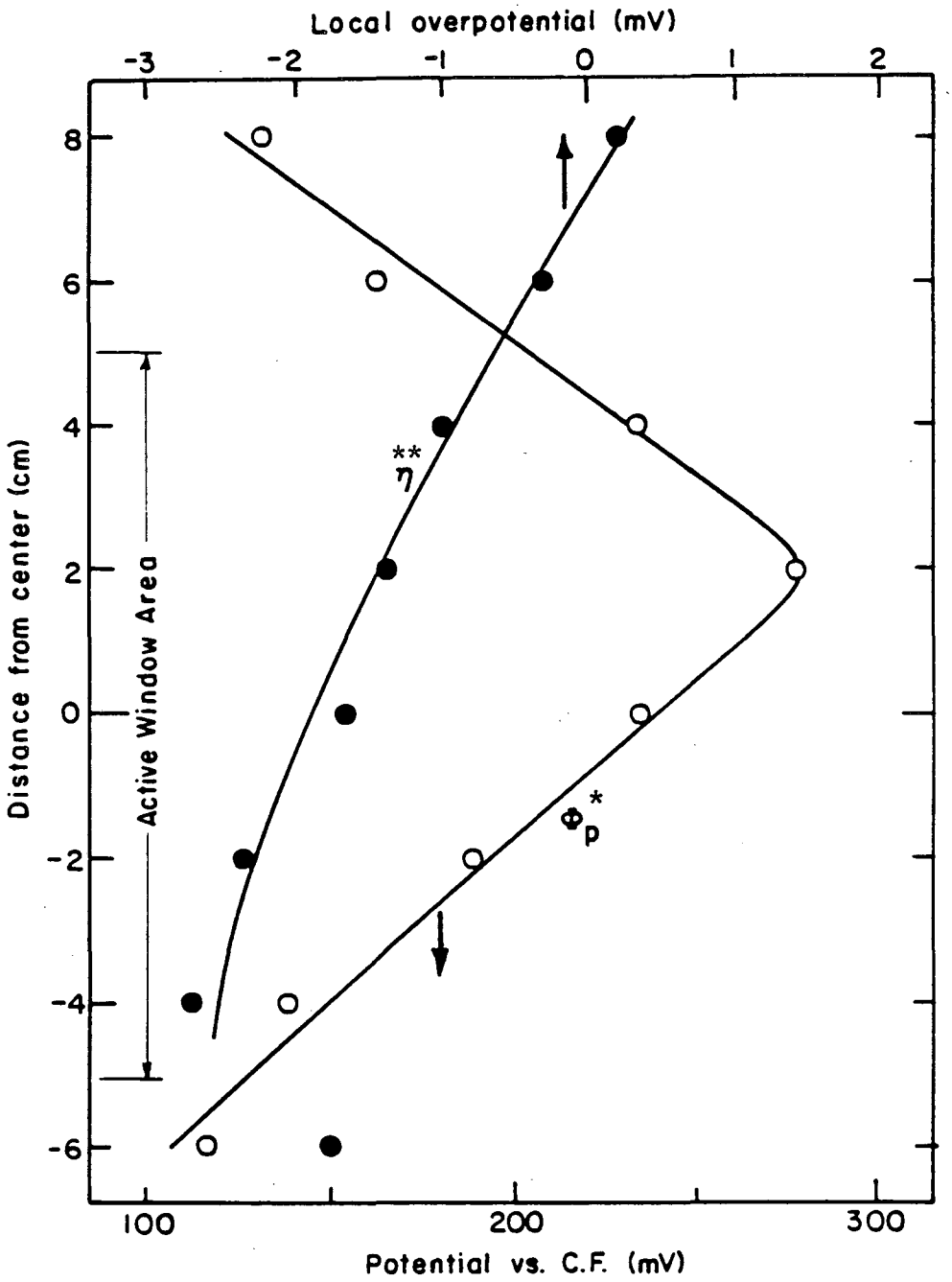

Figure IV-27 Time averaged potential distributions in vertical direction of the bed (B.E. = 25%, S.C.D. = 200 mA/cm^2)

* Particle potential

** Local overpotential

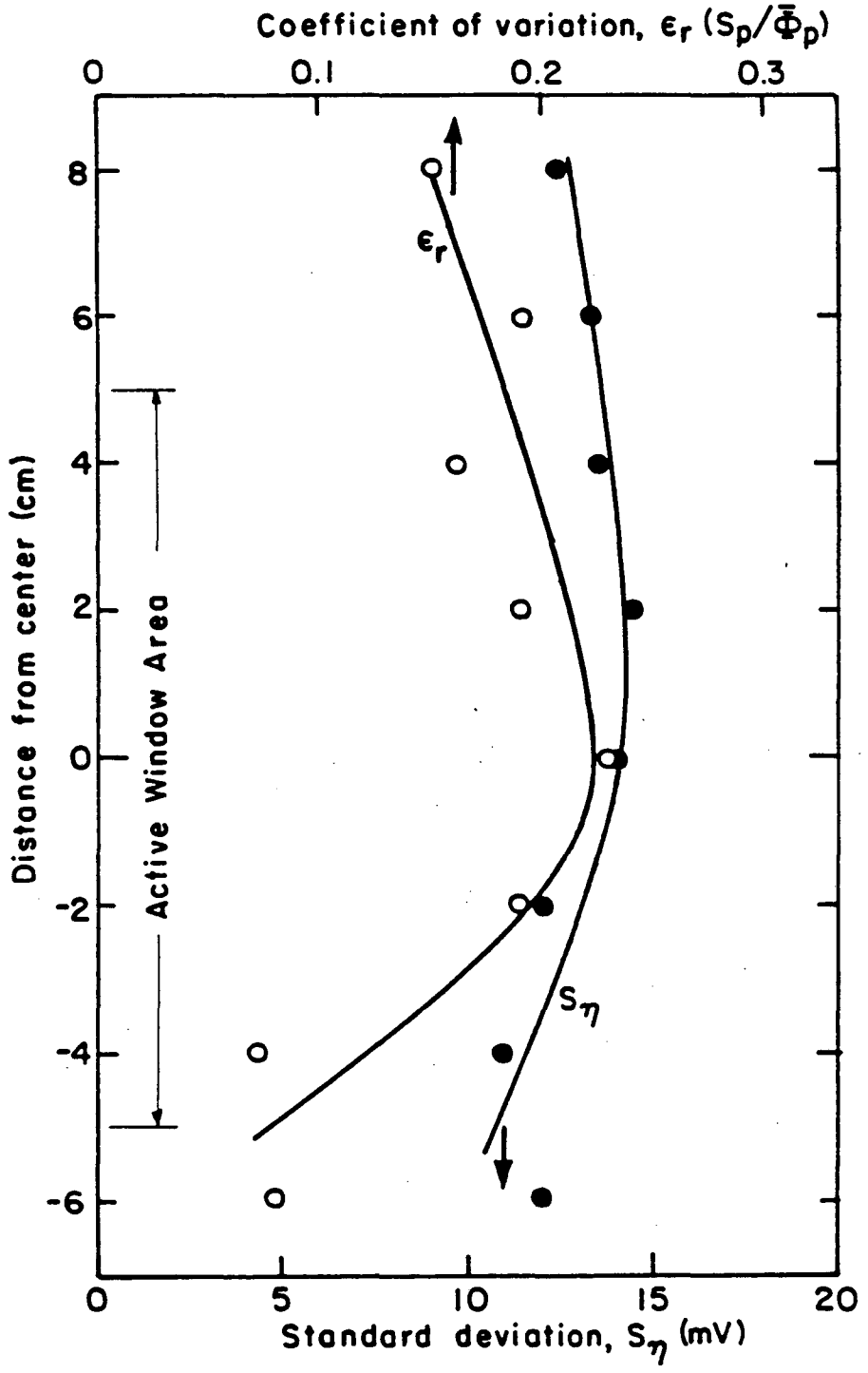

Figure IV-28 Standard deviation of local overpotential measurement and coefficient of variation of particle potential measurement distribution in vertical direction of the bed (B.E.= 25%, S.C.D. = 200 mA/cm^2)

Table IV-5 : Effect of Applied Current Density on Potential Transients

C.D.*	$\bar{\phi}_p$	S_p	$\bar{\eta}$	S_η
		(all are in mV)		
200	234.09	52.95	-1.71	13.96
100	160.14	15.32	-1.07	9.93

* Superficial Current Density in mA/cm^2

Bed Expansion : 25%

Sampling Interval : 10 ms

Cathodic Reaction of Cu/H_2SO_4 system

that flicker noise is almost absent at the bottom of the bed. This is consistent with the earlier hypothesis that low frequency potential transients are due to bubbles. Such bubbles grow by coalescence as they move up from the distributor and it is likely that at the bottom of the bed they are of insufficient size to effect the potentials.

The effect of the bubbles higher in the bed can be interpreted as a change in the local effective resistivity in the bed. The magnitude of a potential fluctuation due to a resistivity fluctuation will depend on the local current density, presumably in the same way that the time average potential depends on the local current density. Hence the approximately constant ratio of the standard deviation of the potential to its time averaged value over most of the bed is explained.

There is a gradual rise in the absolute value of time averaged overpotential on moving down through the bed. One explanation is the change of effective electrode surface area along the vertical direction of the bed. Due to higher particle volume fraction at the bottom of the bed, less electrode surface is exposed to electrolyte and undergoes electrochemical reaction than at the top of the bed. Within the active window area, for a given flux of current, higher reaction rate per unit effective electrode area is expected at the bottom of the bed. Outside of the active window area the particulate electrode is not totally protected cathodically and shows small values of local overpotential.

d. Effective Bed Resistivity

Prior investigations[8,9] have indicated that the void fraction (bed

expansion) has a significant effect on the effective electrical conductivity of the particulate phase. To examine this effect for the electrodes employed in this study, the effective bed resistivity was measured as a function of electrolyte conductivity and bed expansion.

Figure IV-29 shows the example of various sine waves of potentials across the known resistor and the bed at different bed expansions, a) is across the known resistor, b) is across the bed at 33% bed expansion, c) is 25%, d) is 20%, e) is 15% and f) is 10%. This gives a clear idea of the large scale resistivity fluctuation over the total active volume of the bed.

The different vertical scale for Figure IV-29 e) and f) should be noted. The results presented in this figure can be explained as follows. Conduction of an AC current through the fluidized bed can be regarded as via two parallel paths: through the electrolyte or through the particulate phase. At high bed expansion the conductivity of the latter is low and the majority of the current passes through the elctrolyte. The resistance is therefore high and little affected by variations in the resistance of the particulate phase. At intermediate bed expansions (20 - 25%) the particulate phase is more conductive and the resistance (potential drop across the bed) is less, on average. Now, since a significant fraction of the current is carried by the particulate phase, fluctuation of the effective resistance of the particulate phase results in significant variation in the amplitude of the sine wave of potential. As the bed expansion is lowered further (to

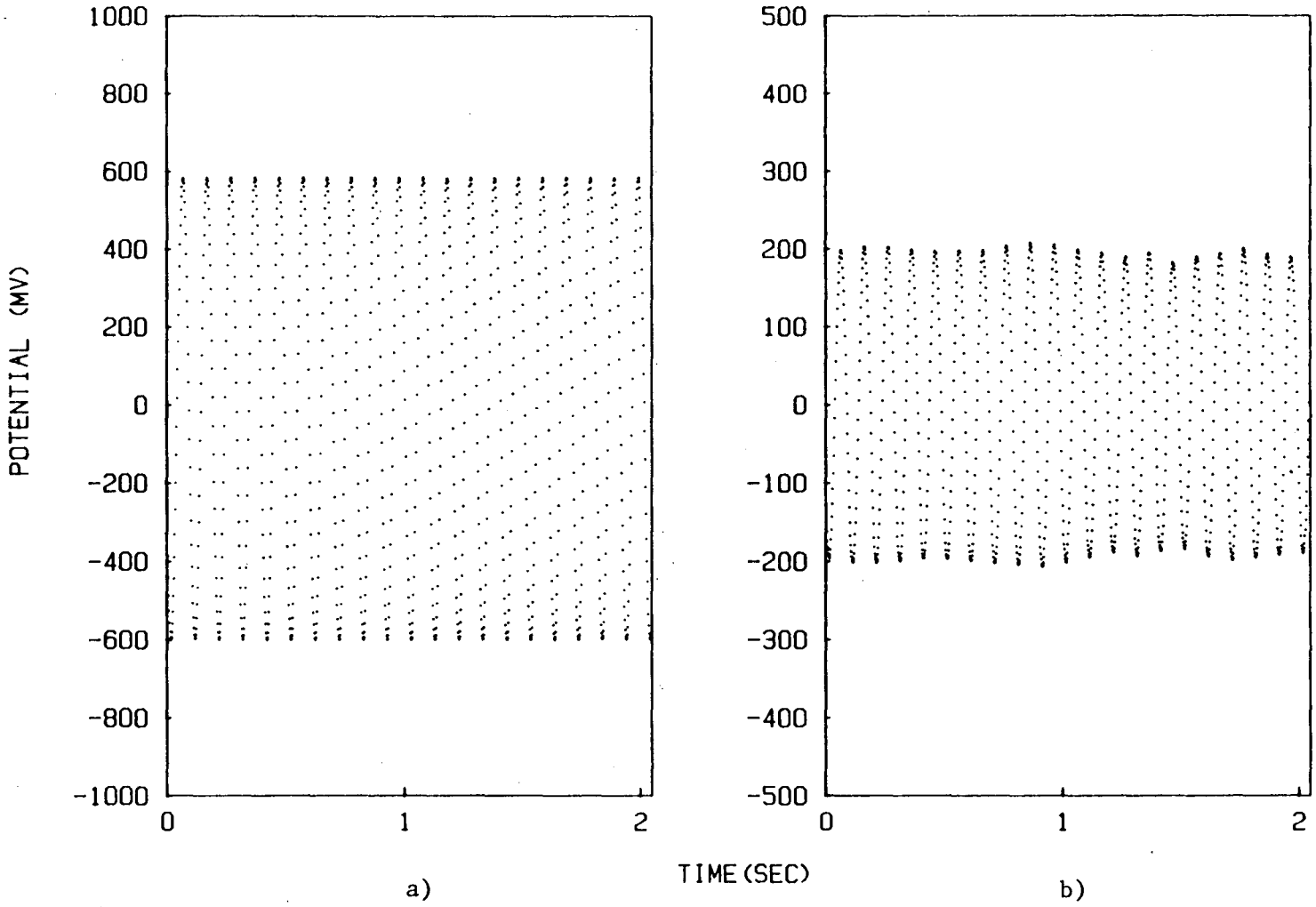

Figure IV-29 Various sine waves of potentials across the known resistor and the bed at different bed expansion
a) known resistor
b) at bed expansion of 33%

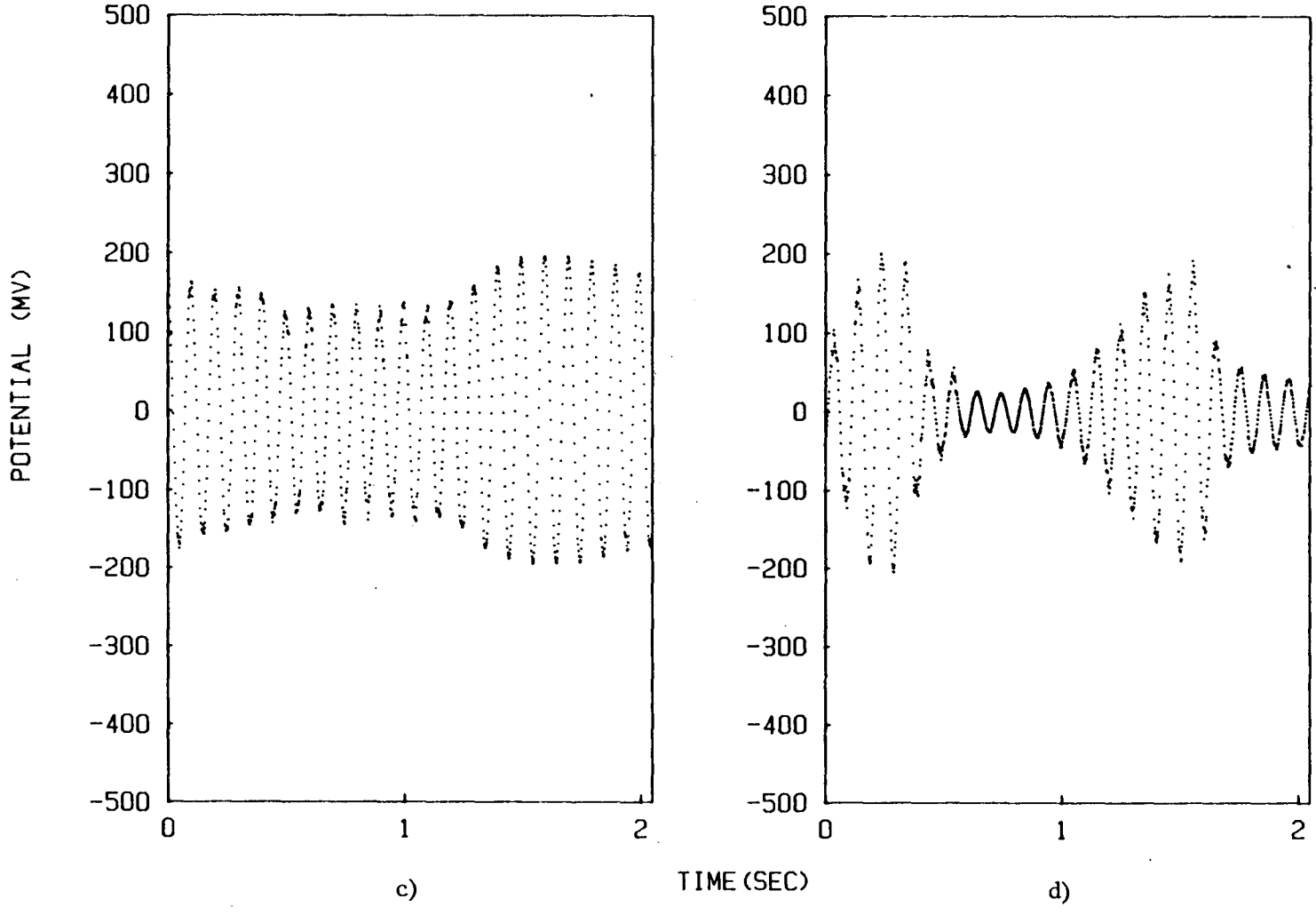

Figure IV-29 c) 25% d) 20%

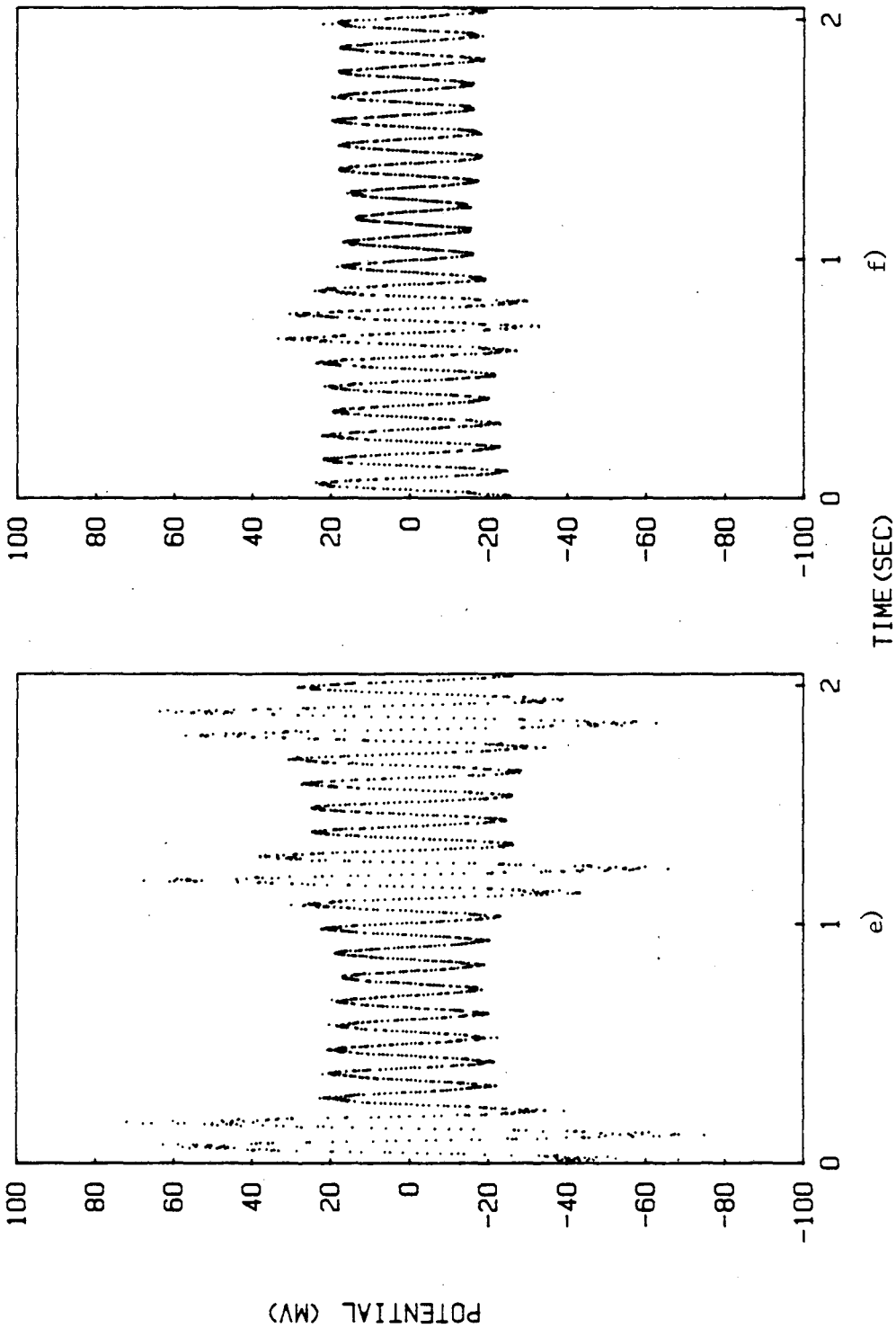

Figure IV-29 e) 15% f) 10%

15%) the effective particulate phase resistivity drops further, further lowering the amplitude of the sine wave. Finally at 10% bed expansion the amount of bubbles in the bed is low and effective resistivity fluctuations are less, resulting in much lower fluctuations of the amplitude of the sine wave.

The ratio of the potential across the bed to that across the known resistor yields the effective resistance of the bed and this can be time averaged for any bed expansion. From the geometry of the bed a time averaged effective resistivity can then be calculated.

Figure IV-30 shows the time averaged values of measured effective resistivities with AC frequency of 1000 Hz, and the results from previous studies. Resistivities measured in this study are a little higher than those of Sabacky's[8], because of using the active window area which blocks the current path at the bottom portion of the bed, but dependency on bed expansion agreed quite well. The higher values obtained in this study are due to the blocking of the current path at the bottom portion of the bed, where usually particle density is high. The bars shown in Figure IV-30 represent the range of measured resistivities. As shown in Figure IV-29, even for the same conditions, the potential across the bed, which is directly related to the calculated resistivity, is expected to vary over a wide range.

To summarize, results from both potential measurements and resistivity measurements suggest the following for a fluidized bed electrode of copper particles. Charge transport within the bed is both through the electrolyte and through chains of particles in electrical

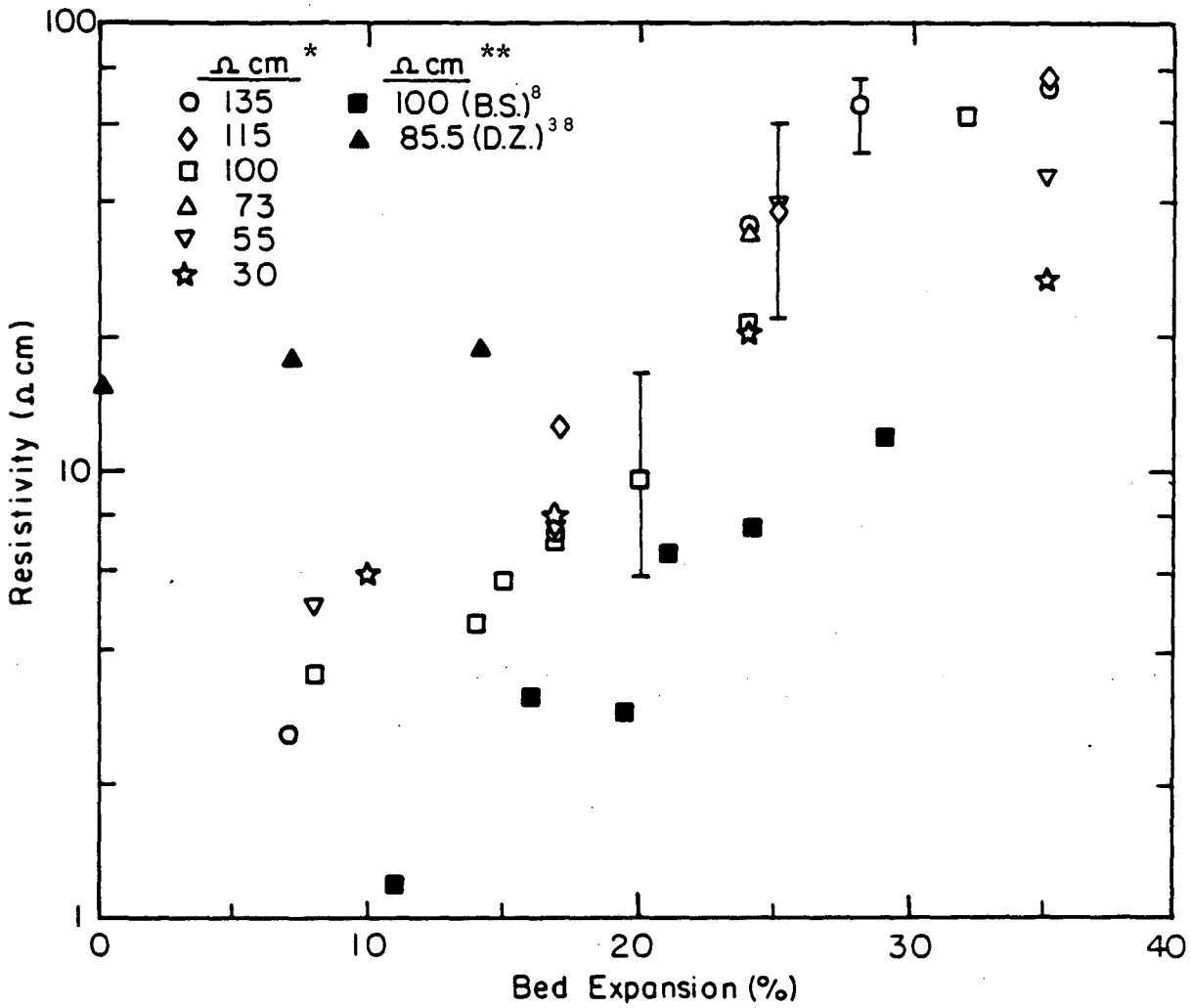

Figure IV-30 Dependency of time averaged bed resistivity on bed expansion

* electrolyte resistivities used in this investigation

** electrolyte resistivities from previous investigation

contact. In those instances where the chain is in contact with the current feeder the whole chain is likely to be cathodic (for a cathodic current feeder). If the chain is separated from the current feeder then it will be bipolar, i.e., have anodic as well as cathodic regions. Bubbles exist in the fluidized electrode; because they are regions free of particles (and therefore of chains) these bubbles have an effect on the local resistivity of the elctrode. Because the bubbles coalesce as they move up through the bed, approaching dimensions comparable to the bed width, their effect is more noticeable higher in the bed. The effect of the bubbles also varies with bed expansion because they are absent at minimum fluidization velocity and increase as the electrolyte velocity (and bed expansion) are increased beyond this point.

2. Zn/KOH System

During the course of this study, the particle and electrolyte potential transients were measured with respect to the electrolyte potential at the vicinity of the fluidized bed side of the diaphragm, which was measured by a luggin capillary with a zinc wire inside. This wire was the same as that used for the potential measuring probe and was insulated except for the exposed tip at one end.

Figure IV-32 shows the equilibrium potential of this wire in 5M KOH solution. Figure IV-33 shows the cell potential vs superficial curent density and Figure IV-34 shows the relationship between potential drop across the fluidized bed and superficial current density. The

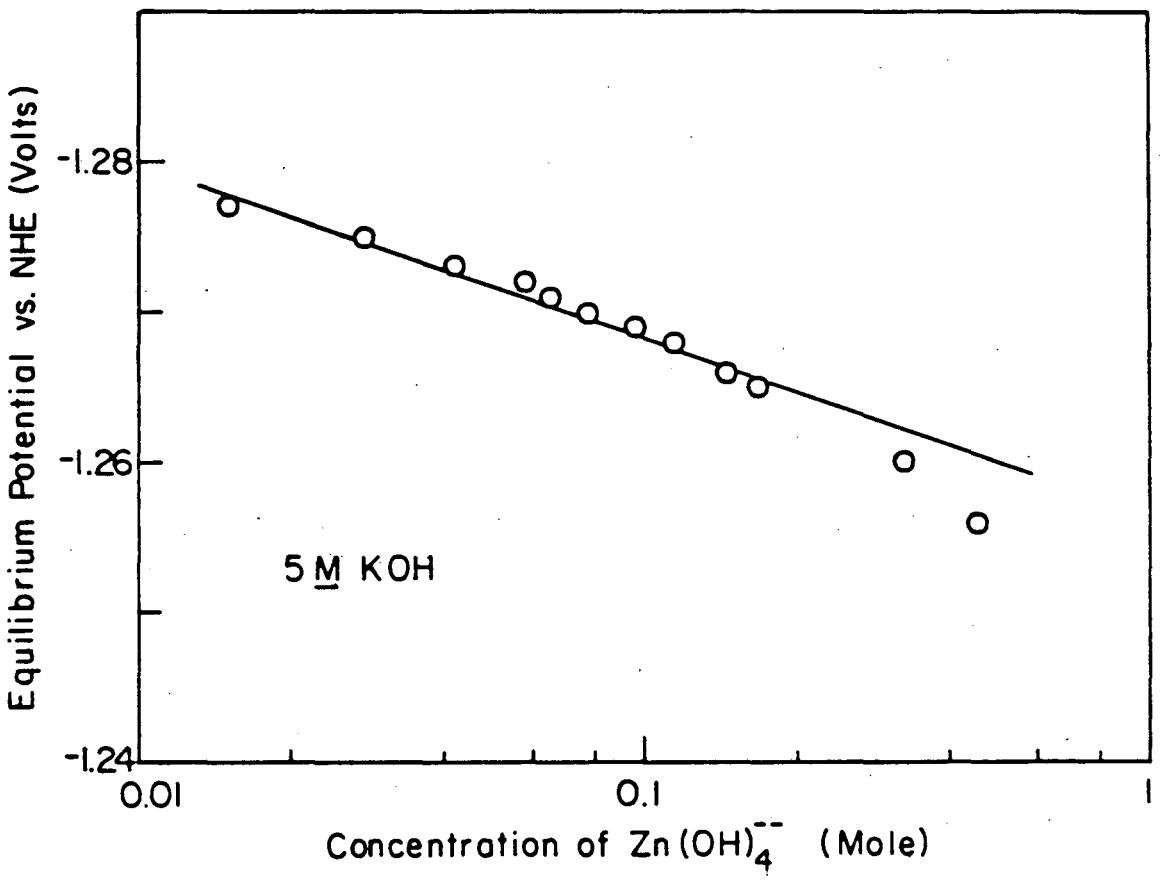

XBL 847-3272

Figure IV-32 Dependency of equilibrium potential of zinc wire with 5M KOH solution on zincate concentration

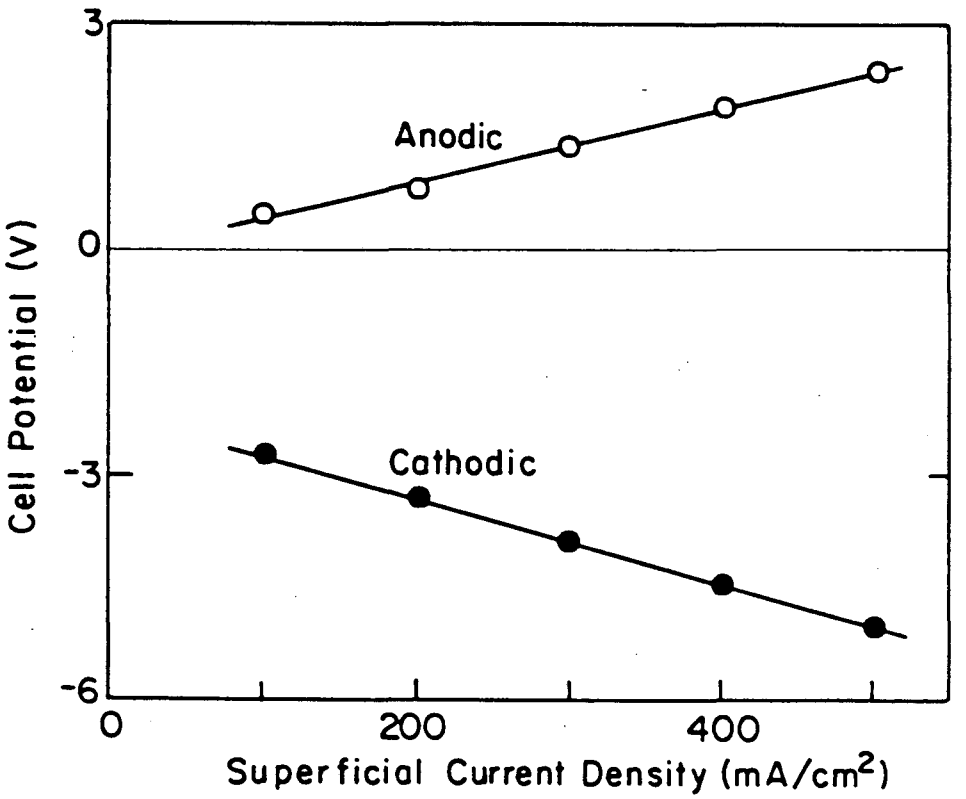

Figure IV-33 Dependency of Sorapec fluidized bed cell potential on superficial current density during anodic and cathodic reactions (counter electrode: platinized Ti mesh, B.E. = 25%)

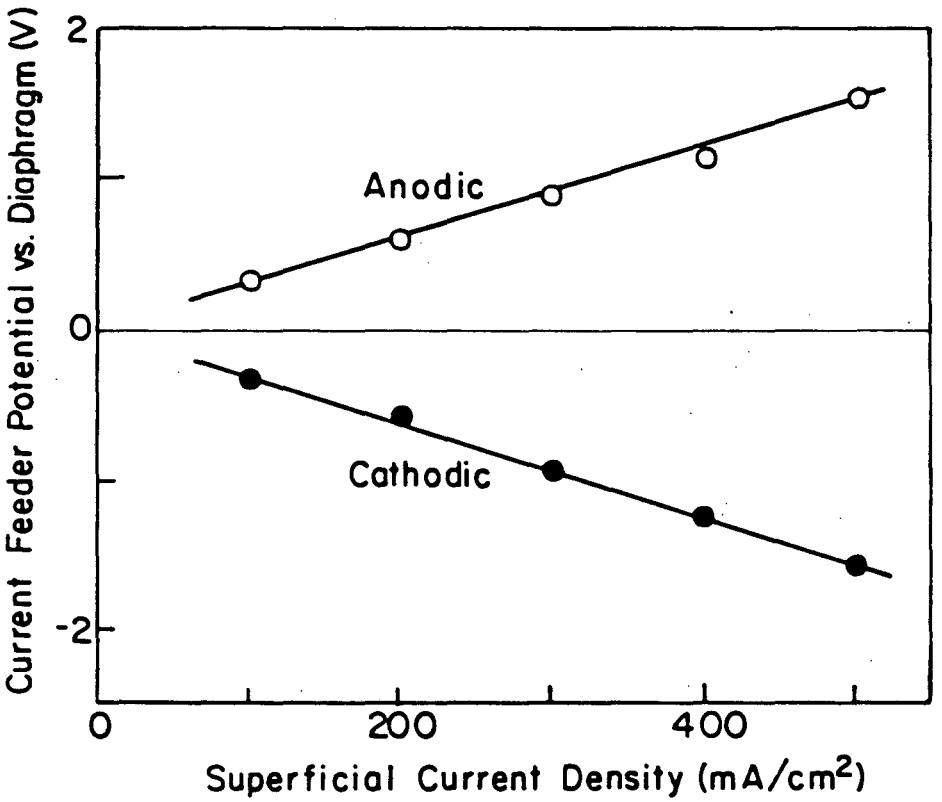

Figure IV-34 Potential drop across Sorapec fluidized bed during anodic and cathodic reactions at various superficial current densities (B.E.= 25%)

electrolyte during this measurement consisted of 5M KOH solution with 15 g/l of zincate in the fluidized bed chamber and pure 5M KOH in the other. The higher cell potential during the cathodic reaction compared to the anodic reaction is due to the high oxygen overpotenial at the platinized titanium mesh anode. This is evident from the fact that the potential difference between current feeder and diaphragm is the same (apart from the obvious change of sign) whether the bed is operated as an anode or cathode (Figure IV-34).

a. General Behavior

Figure IV-35 shows the potential transients of Sorapec particles, electrolyte and local overpotential during cathodic reaction with superficial current density of 100 mA/cm^2 and bed expansion of 25%.

Contrast the different appearance of Figure IV-35 with that of Figure IV-5 (recognizing a difference of scale and of current density). The particle and electrolyte potentials are scattered within a narrow range but the local overpotential fluctuates sharply around the mean value. Power spectra and probability plots for the data of Figure IV-35 appear in Figure IV-36 through 38. In contrast to copper, there is relatively little low frequency flicker noise in the particle potential; comparing Figure IV-36 with Figure IV-7. Nor is there significant flicker noise in the electrolyte potential for the Sorapec bed. However, in contrast with the case of copper there is flicker noise in the overpotential.

Figure IV-39 shows the potential transients of cathodic reaction

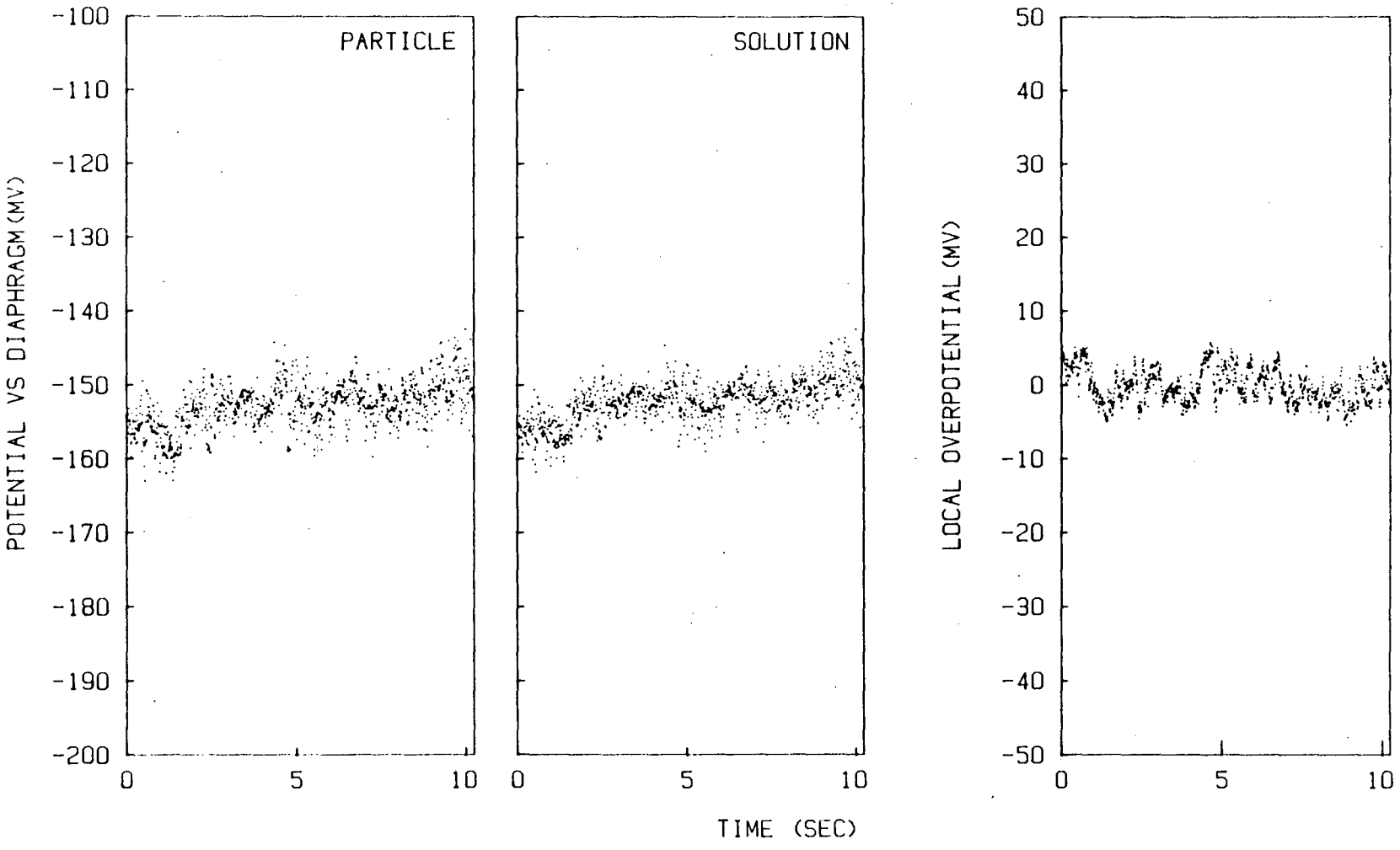

Figure IV-35 Potential transient from center of the Sorapec fluidized bed (B.E. = 25%, S.C.D. = 100 mA/cm^2, cathodic reaction)

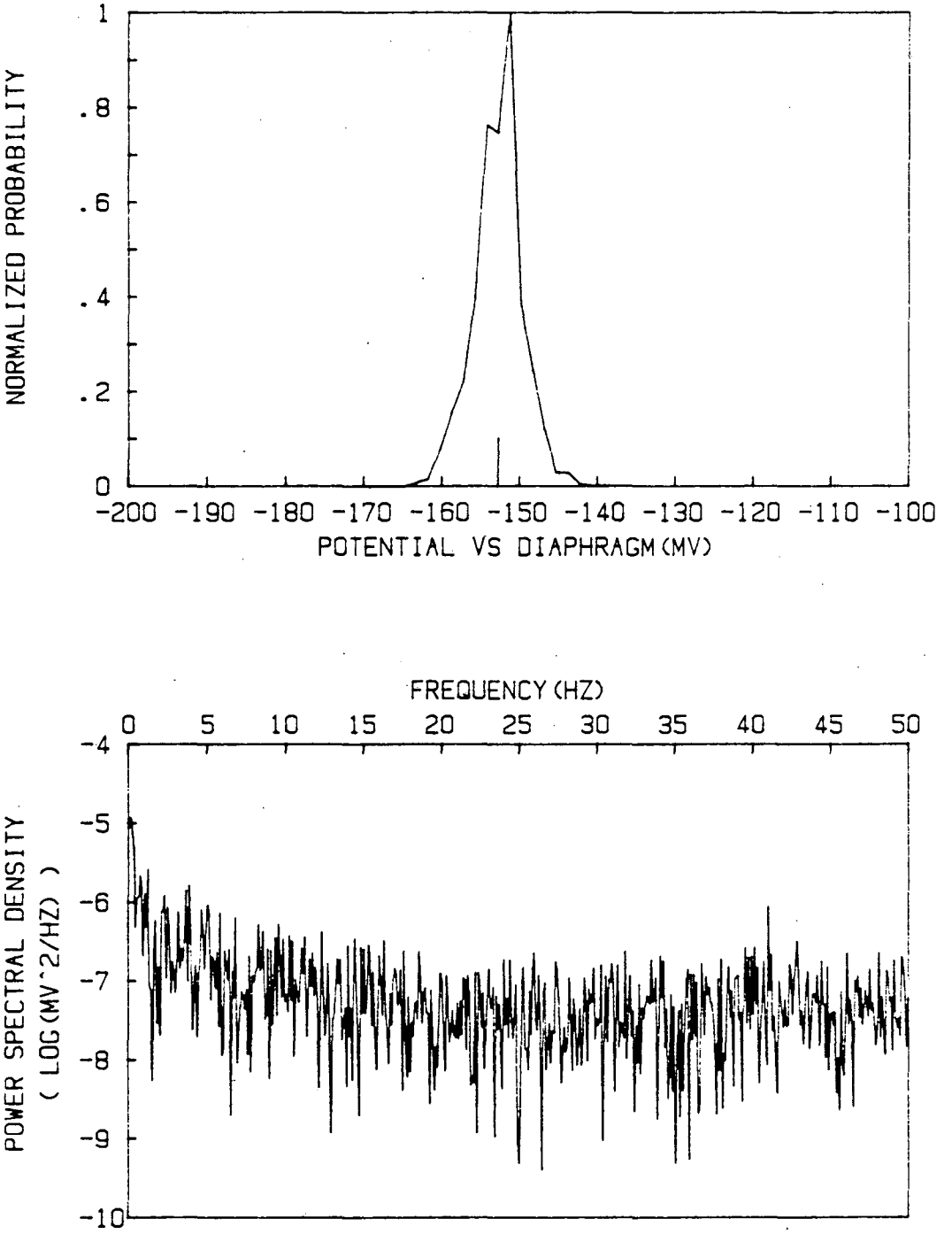

Figure IV-36 FFT result of particle potential trace of Figure IV-35

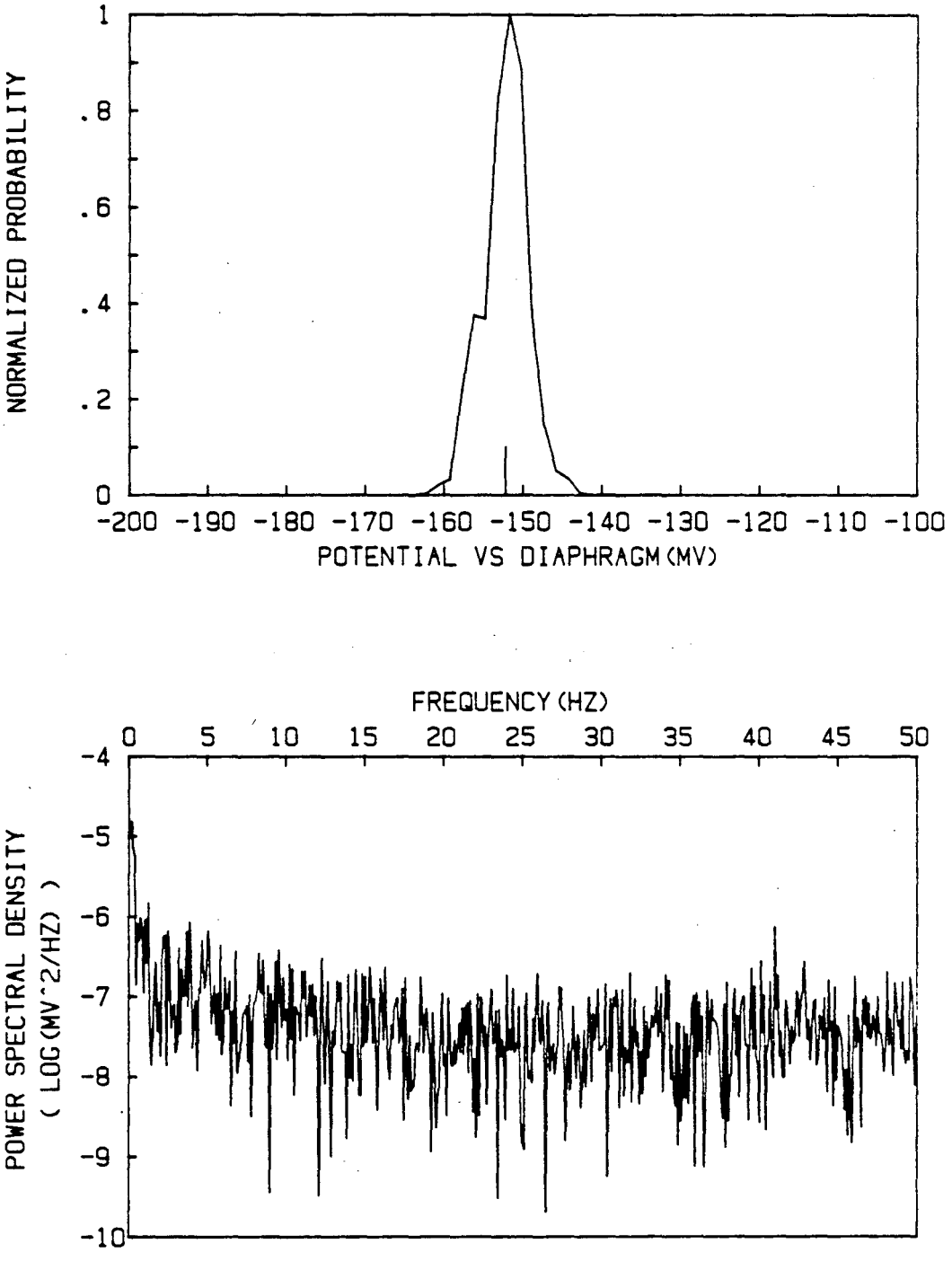

Figure IV-37 FFT result of electrolyte potential trace of Figure IV-35

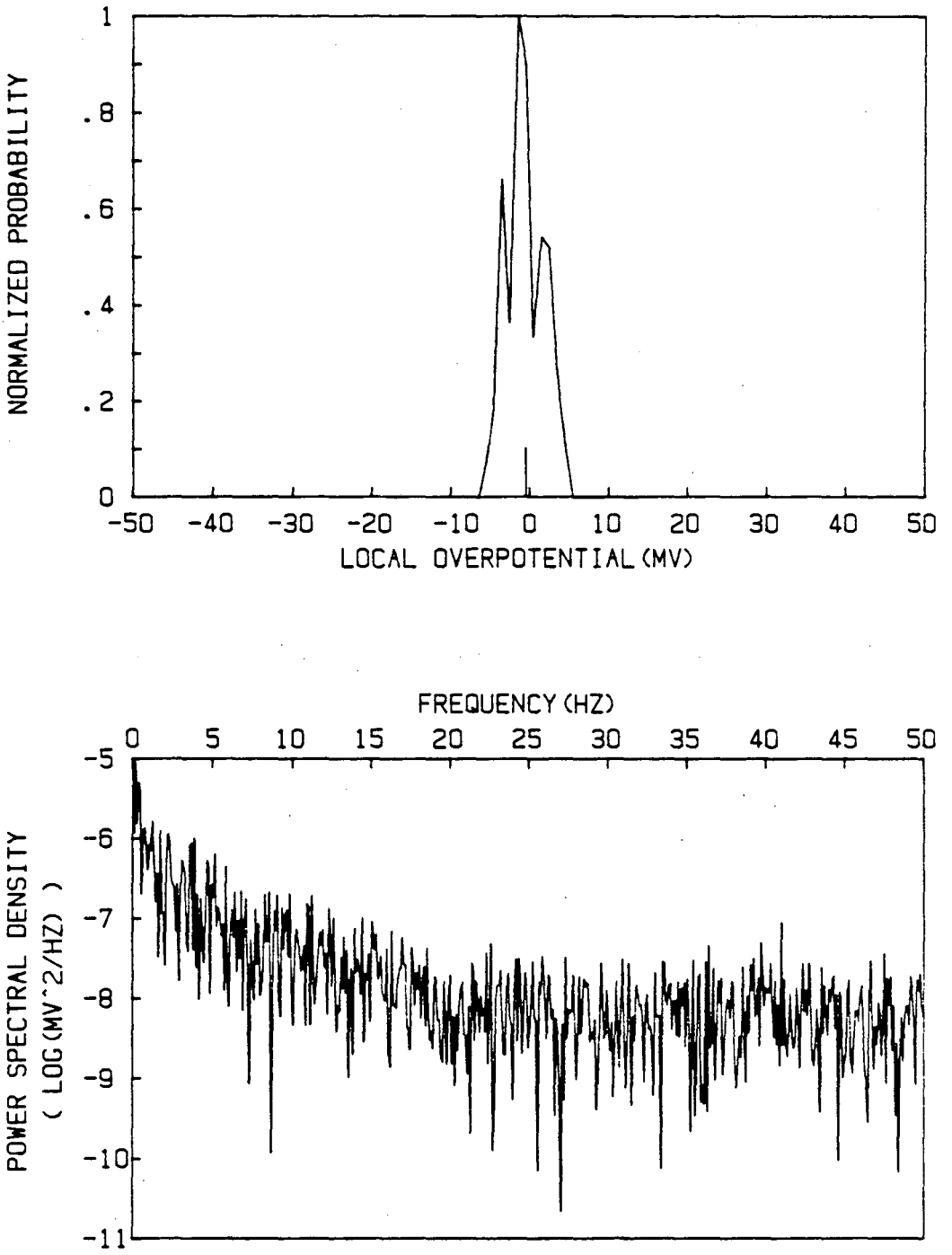

Figure IV-38 FFT result of local overpotential trace of Figure IV-35

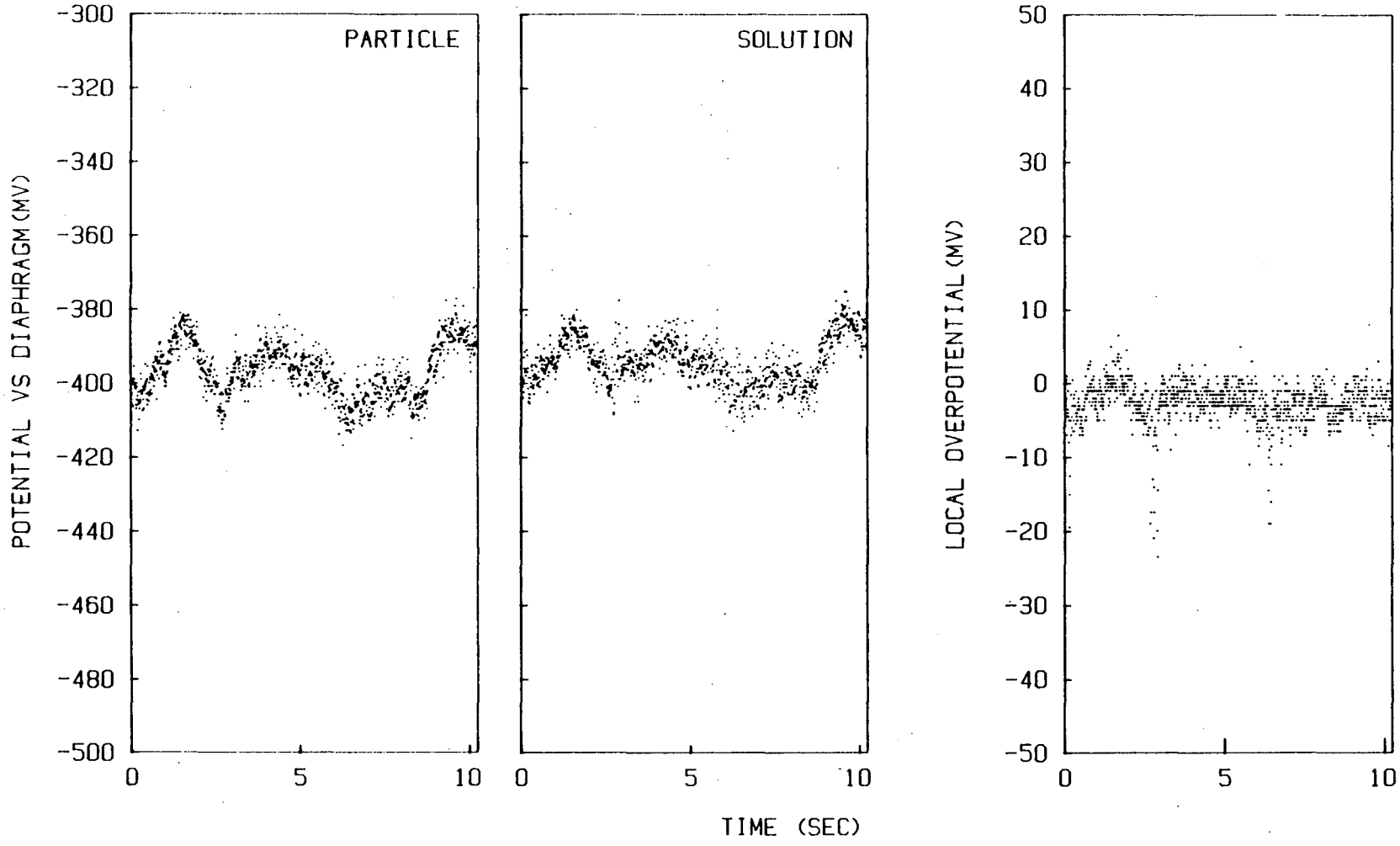

XBL 851-1032

Figure IV-39 Potential transient from center of the Sorapec fluidized bed (B.E. = 30%, S.C.D. = 200 mA/cm^2, cathodic reaction)

with superficial current density of 200 mA/cm^2 and bed expansion of 30%. The potential fluctuations are wider than in Figure IV-35 but the power spectra do not differ significantly. The local overpotential (see Figure IV-41) is distributed over a broader range than in Figure IV-38 and shows both flicker noise and white noise.

In explaining the difference in behavior between the Cu/H_2SO_4 bed and the Zn/KOH two important differences should be recognized. The two types of particles have different densities ($\rho_{Cu} = 8$ g/cm^3 while $\rho_{Sorapec} \simeq 3$ g/cm^3) which results in different fluidization velocity and different hydrodynamic characteristics of the fluidized bed (presence or absence of bubbles). Second, the electrochemical reactions are different.

The Sorapec bed was observed to be relatively free of bubbles and uniformly fluidized from top to bottom. This is consistent with the low level of flicker noise in the particle and electrolyte potential. The overpotential data for Sorapec particles have two characteristics that require explanation: the relatively light distribution about the time averaged value (contrast the upper half of Figure IV-41 with Figure IV-11, for example) and some flicker noise appearing in the overpotential (contrasting lower halves of these figures.)

The former may be explained in terms of the exchange current densities. The instantaneous overpotential of a particle in the bed is a consequence of two phenomena: the departure from equilibrium (zero overpotential) due to fleeting indirect electrical contact with the current feeder and the electrochemical reaction at the particle surface

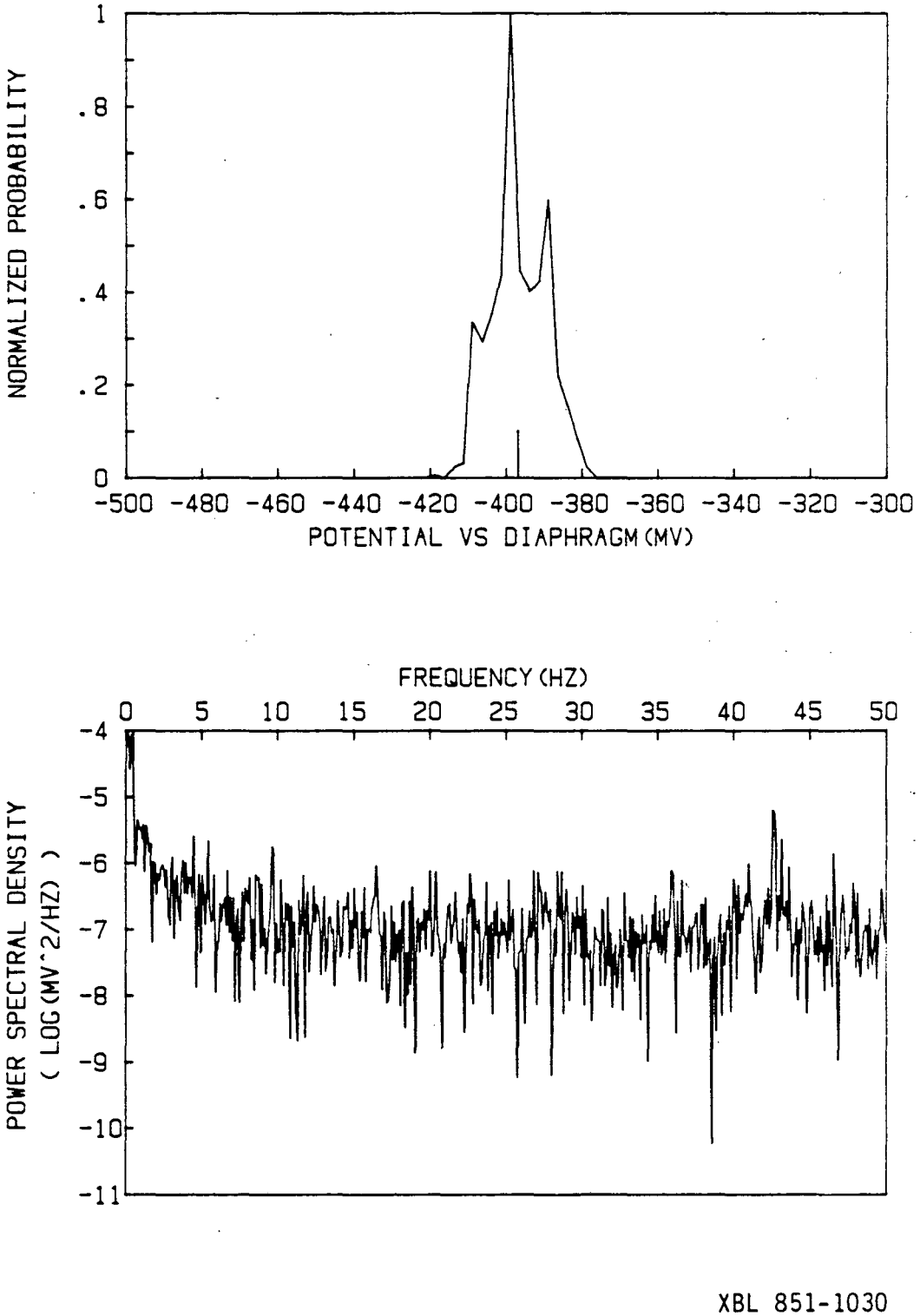

Figure IV-40 FFT result of particle potential trace of Figure IV-39

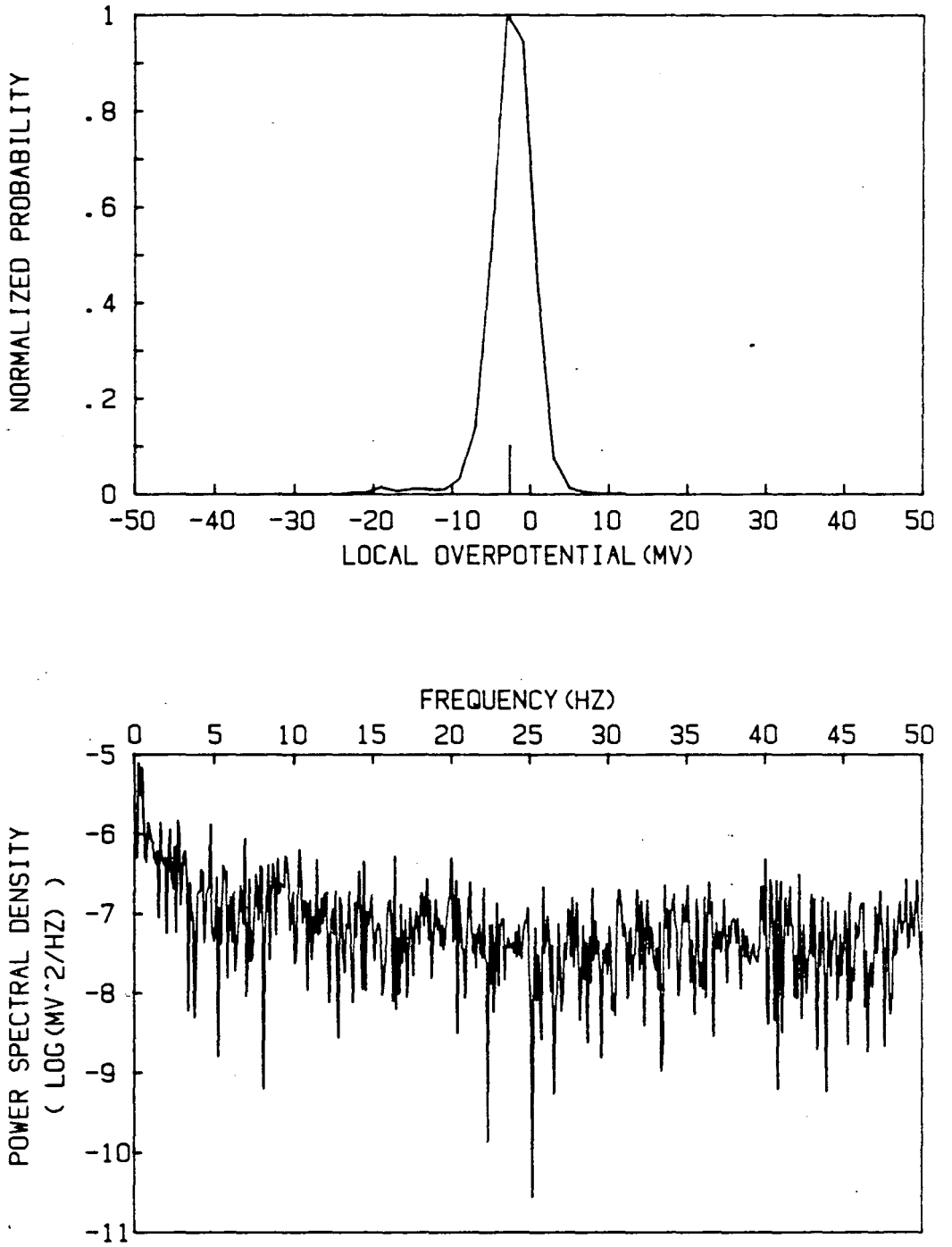

Figure IV-41 FFT result of local overpotential trace of Figure IV-39

Table IV-6 : Vertical Variation of Potential Transients

Distance* (cm)	ϕ_p	S_p	$\bar{\eta}$	S_η
		(all are in mV)		
9	-151.4	4.08	-0.8	2.38
7	-153.6	4.14	-0.7	2.24
5	-154.2	3.99	-1.0	2.45
3	-155.8	4.18	-0.9	2.23
1	-152.7	3.96	-1.0	1.99

* Distance from lower edge of active window area which is 2cm above distributor.

Bed Expansion : 25%

Sampling Interval : 10 ms

Superficial Current Density : 100 mA/cm^2

Cathodic reaction of Zn/KOH system with Sorapec particles

which tends to restore the particle to equilibrium. The magnitude of the potential fluctuations will therefore be less if the electrochemical reaction is faster. Zinc deposition from zincate solution has a higher exchange current density, reportedly in the range 8-370 mA/cm^2 [7], than copper (approximately 3 mA/cm^2) [88]. In other words, for the same overpotential there is a much greater tendency to reduce the overpotential for Sorapec particles, than for copper particles.

Only a tentative hypothesis can be offered for the presence of flicker noise in the overpotential for Sorapec particles. The white noise observed for both copper and Sorapec particles is presumed to be due to the stochastic nature of particle-particle collisions and the effect of these collisions on particle chain formation. It seems likely that such noise would be distributed throughout a broad frequency range, the nature of that distribution and its breadth being dependent on those particle characteristics (density, elasticity, size) that are involved in the dynamics of motion and collision. The apparent uniformity of the white noise for copper particles up to 50 Hz need not imply uniformity much beyond 50 Hz. The hypothesis then is that the low frequency noise evident in the lower part of Figure IV-38 is merely a consequence of the relatively slow collision process for Sorapec particles.

Figure IV-42 shows the potential transients under similar condition as that of Figure IV-35 except that the current was reversed. Statistical analysis are shown in Figures IV-43 through 45. The potential transients are not affected by reversing the current. This is consistent with Bockris' report[73] that the mechanism of the anodic and

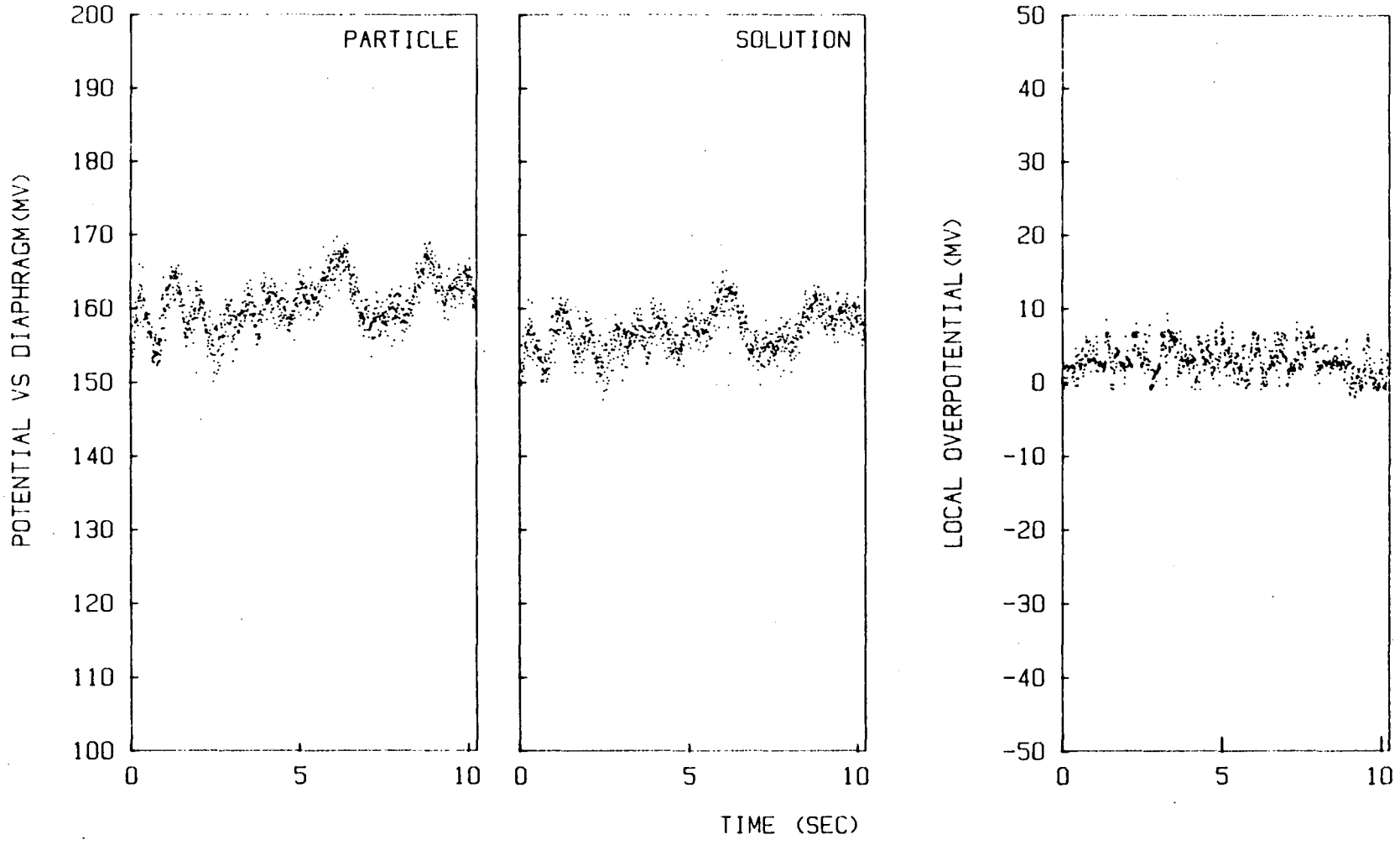

Figure IV-42 Potential transient from center of the Sorapec fluidized bed (B.E. = 25%, S.C.D. = 100 mA/cm^2, anodic reaction)

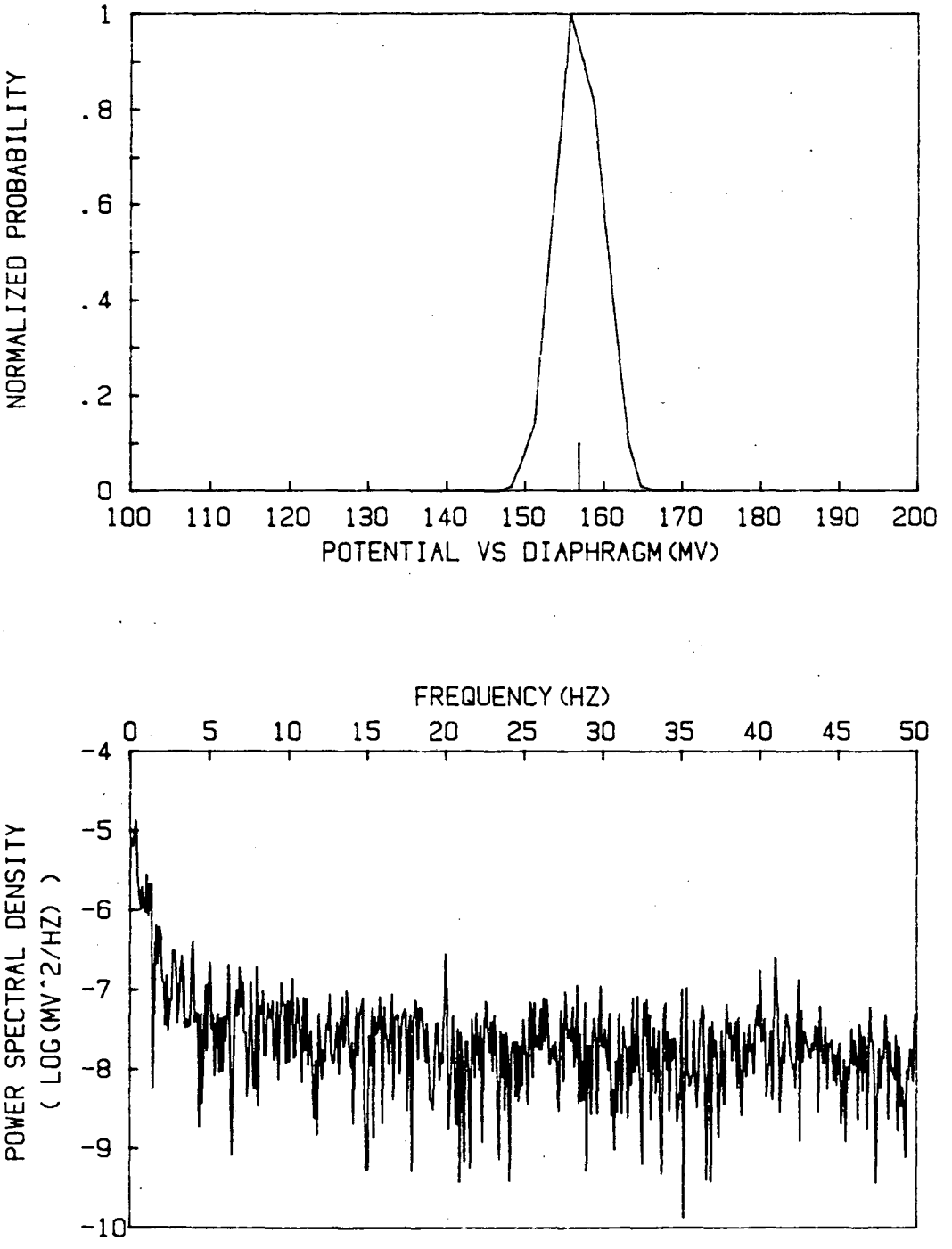

Figure IV-43 FFT result of particle potential trace of Figure IV-42

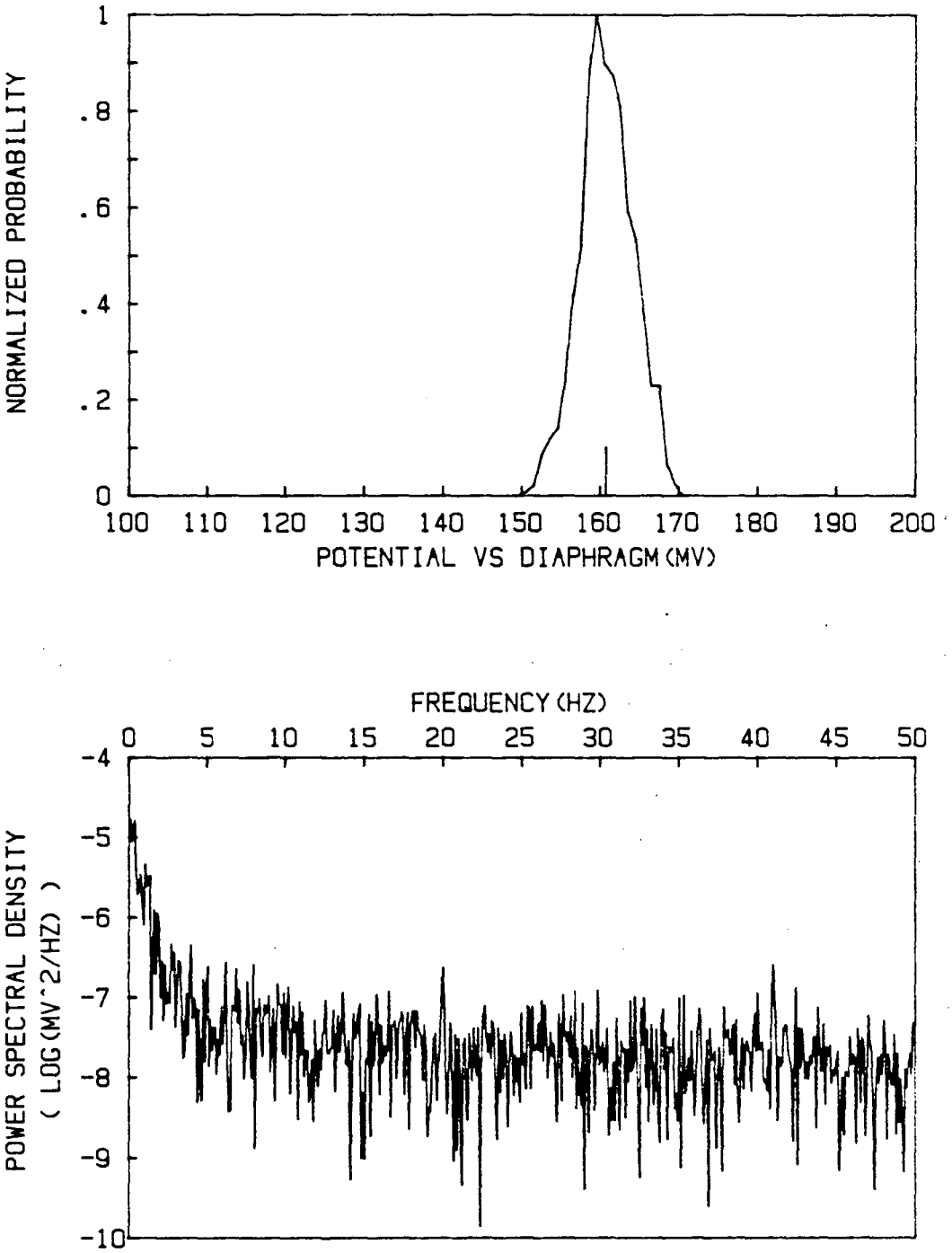

Figure IV-44 FFT result of electrolyte potential trace of Figure IV-42

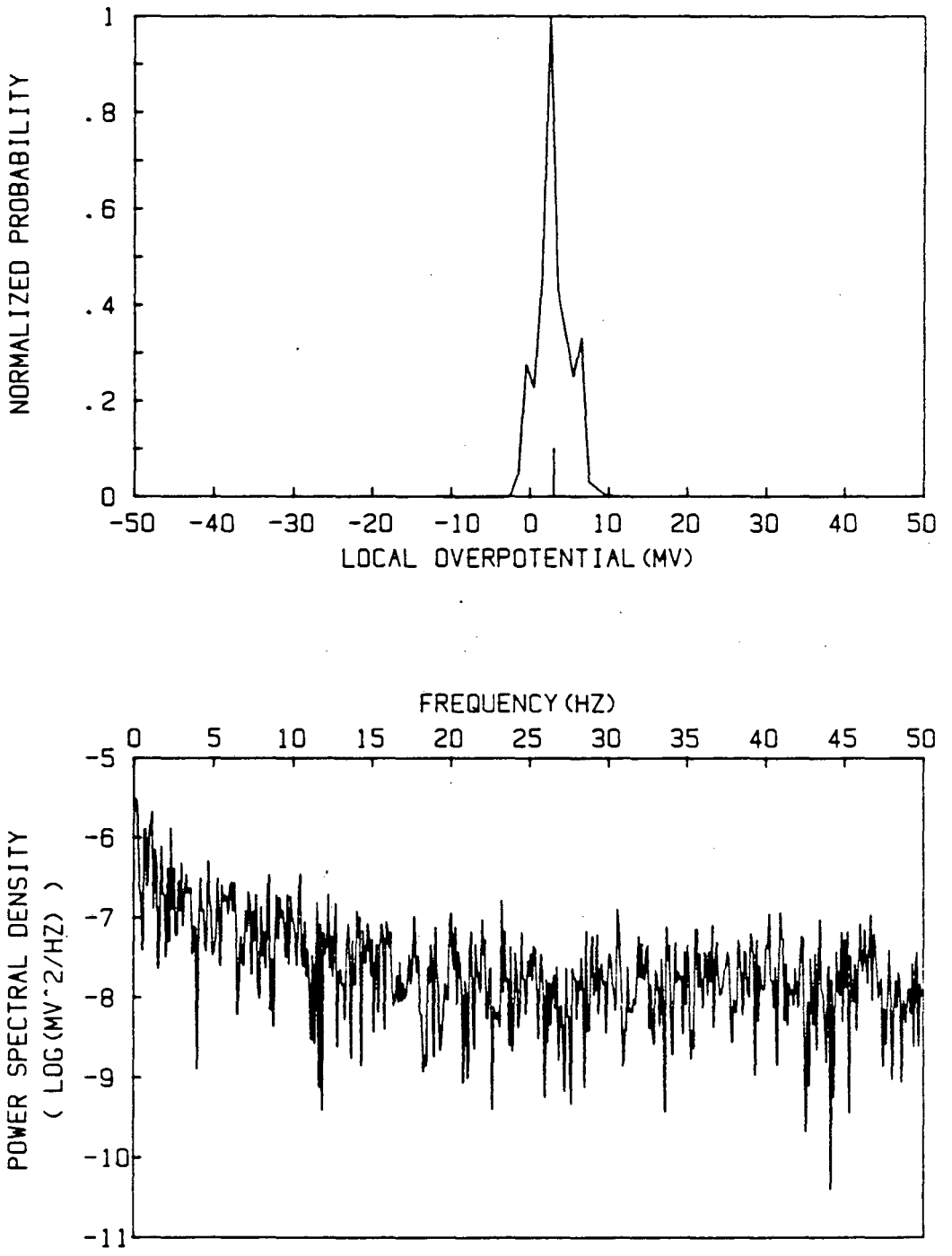

Figure IV-45 FFT result of local overpotential trace of Figure IV-42

cathodic reaction of zinc in alkaline solution is the same.

No sudden jump of local overpotential occurred during the course of the anodic dissolution study of zinc. That is, the zinc fluidized bed electrode was not passivated under experimental conditions. And also no gas evolution was observed from the bed during the cathodic reaction even when the zincate concentration was as low as 5 g/l.

The investigator also tried to determine the effect of potential fluctuation on zinc electrodeposit morphology, but due to the difficulty of monitoring a certain particle, no intensive study was performed. Figure IV-46 shows microstructures of a) Sorapec particles as received and b) Sorapec particles after several cycling experiments. This preliminary study indicates that the fluctuating potential of the particle surface gives smooth deposit morphology.

b. Effect of Bed Expansion

Figure IV-47 shows the effect of bed expansion on Sorapec particle potential transients with cathodic superficial current density of 100 mA/cm^2. Bed expansions are 15% for a) and 35% for b) respectively. The zincate concentration was around 10 g/l. The general trend of transients remains quite similar, though the data is scattered slightly over a wide band in the case of 35% bed expansion. This is confirmed by the wide spread in probability density distribution in the following two figures, Figures IV-48 and 49. Power spectra also look similar except for a slightly higher power density over the entire frequency range at 35% bed expansion. Note that even at 35% bed expansion, there was

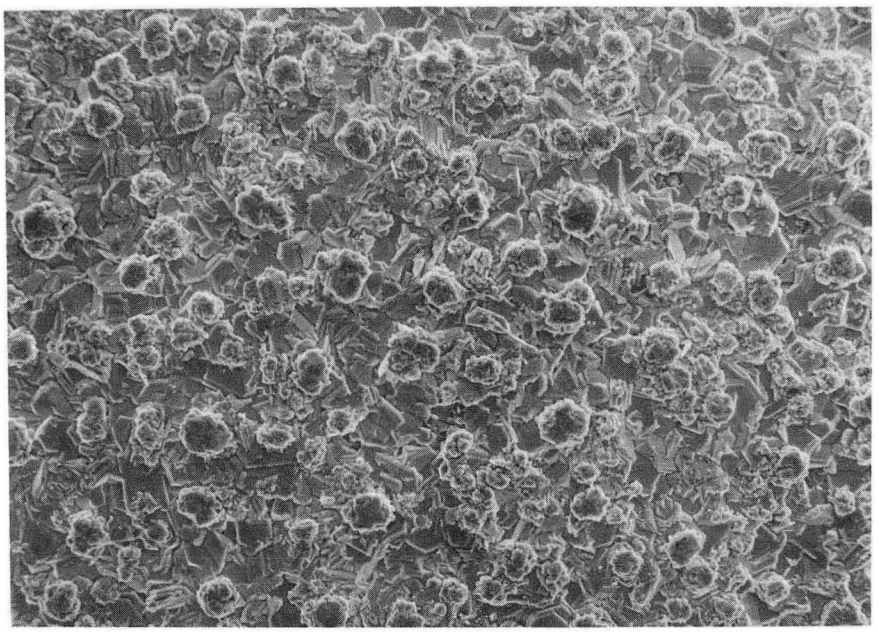

a)

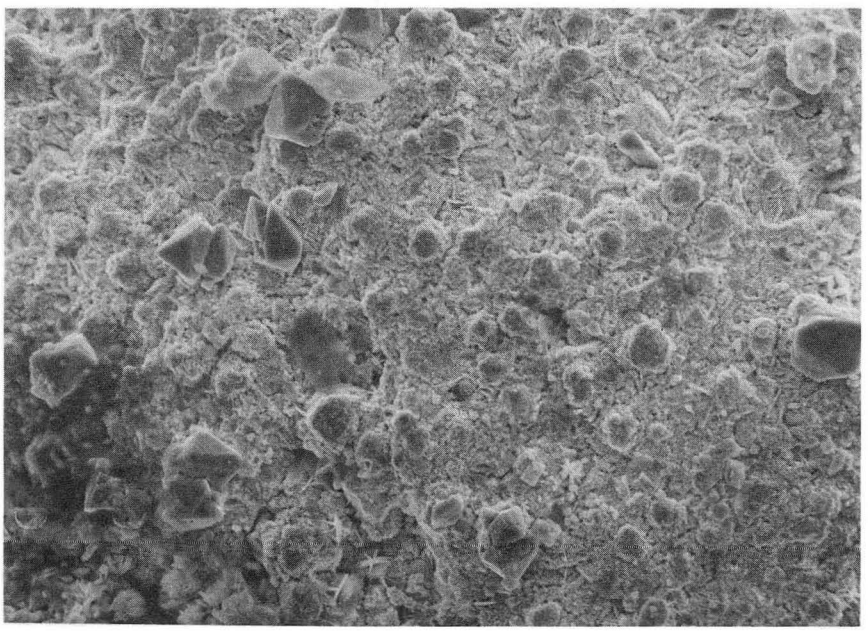

b)

XBB 854-2750

Figure IV-46 Microstructure of Sorapec particles (x500)
a) before experiment, b) after several cycle of experiments

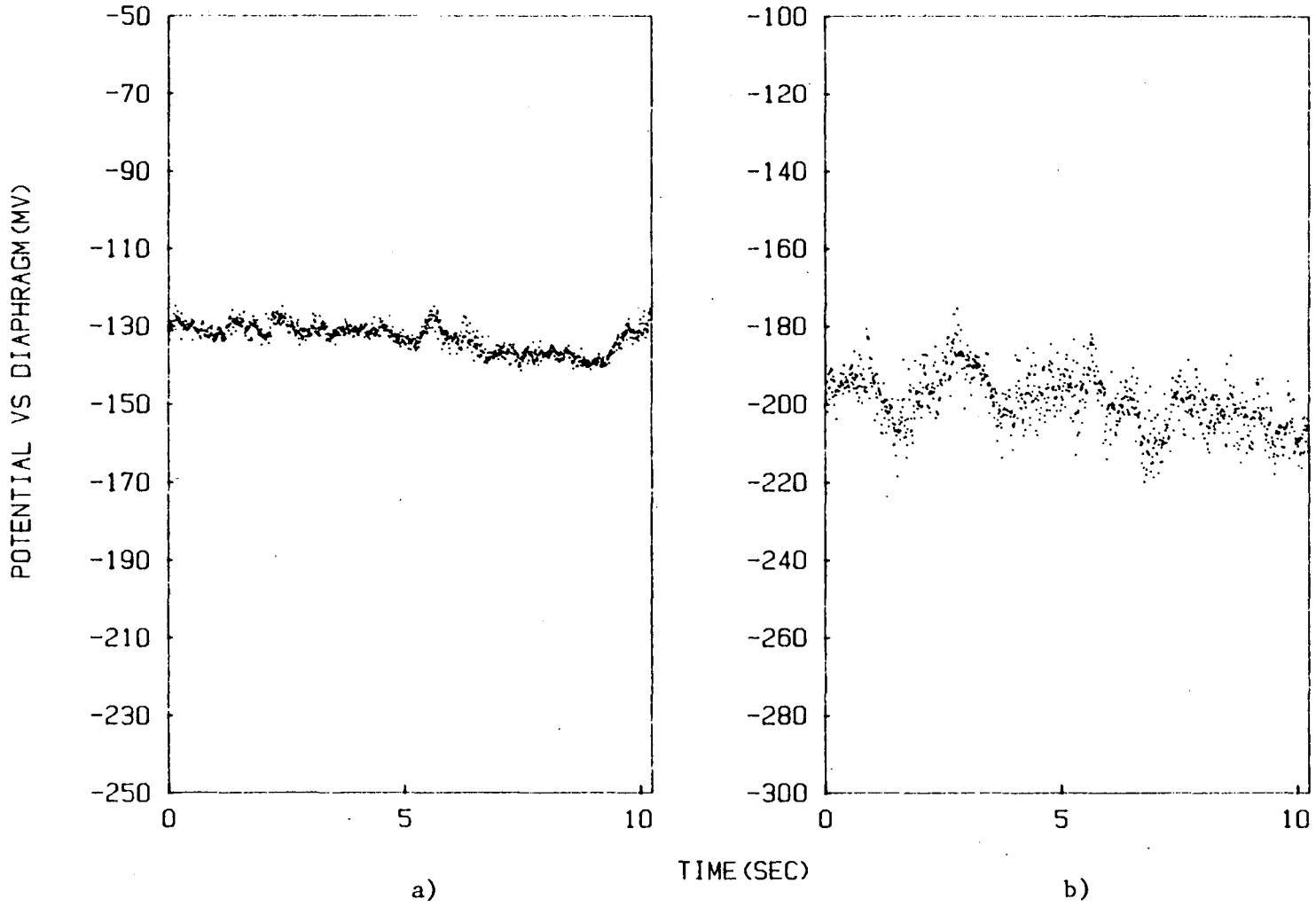

Figure IV-47 Effect of bed expansion on Sorapec particle potential transient (S.C.D. = 100 mA/cm^2, B.E. = a) 15%, b) 35%, cathodic reaction)

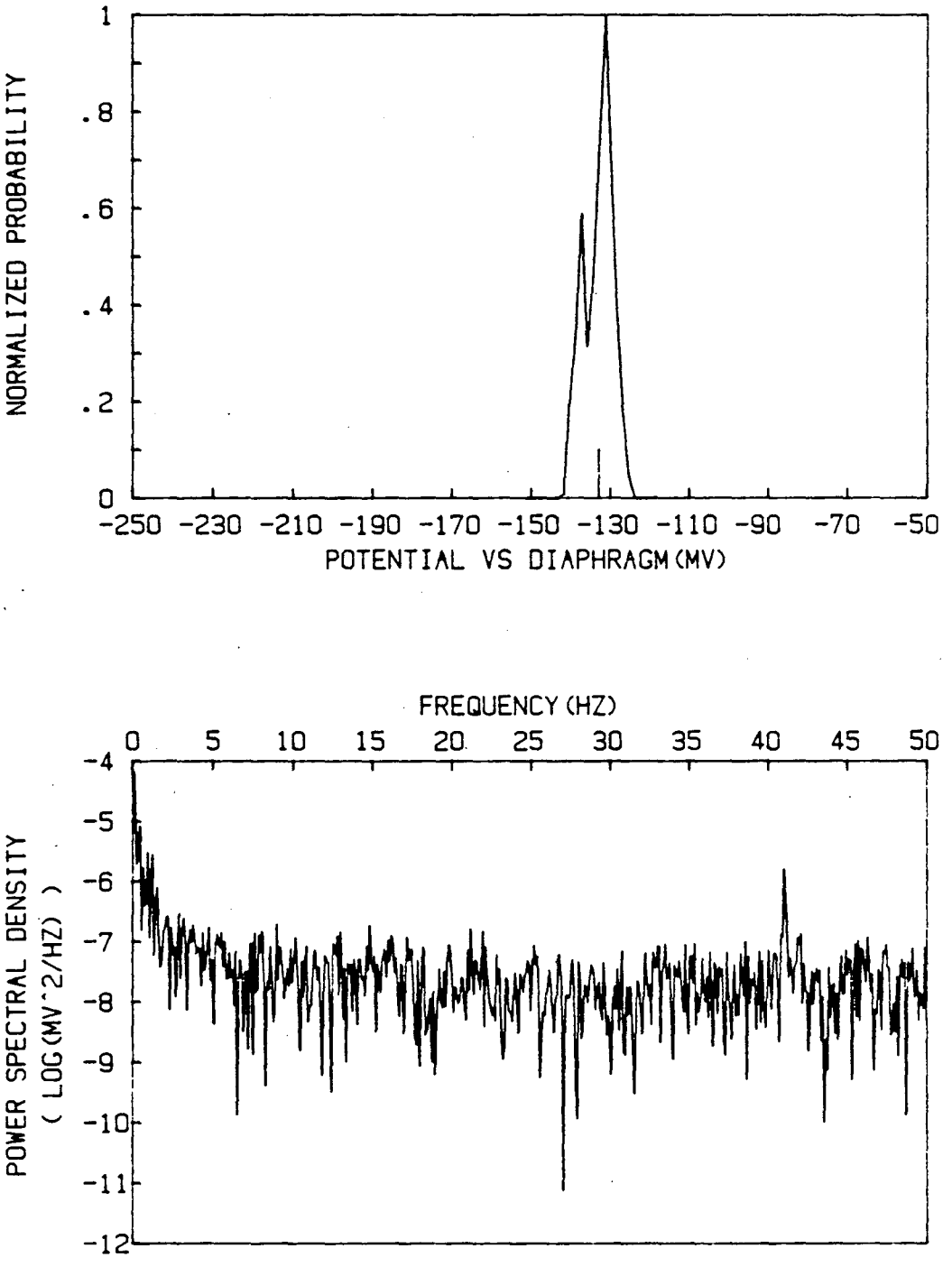

Figure IV-48 FFT result of Figure IV-47 a)

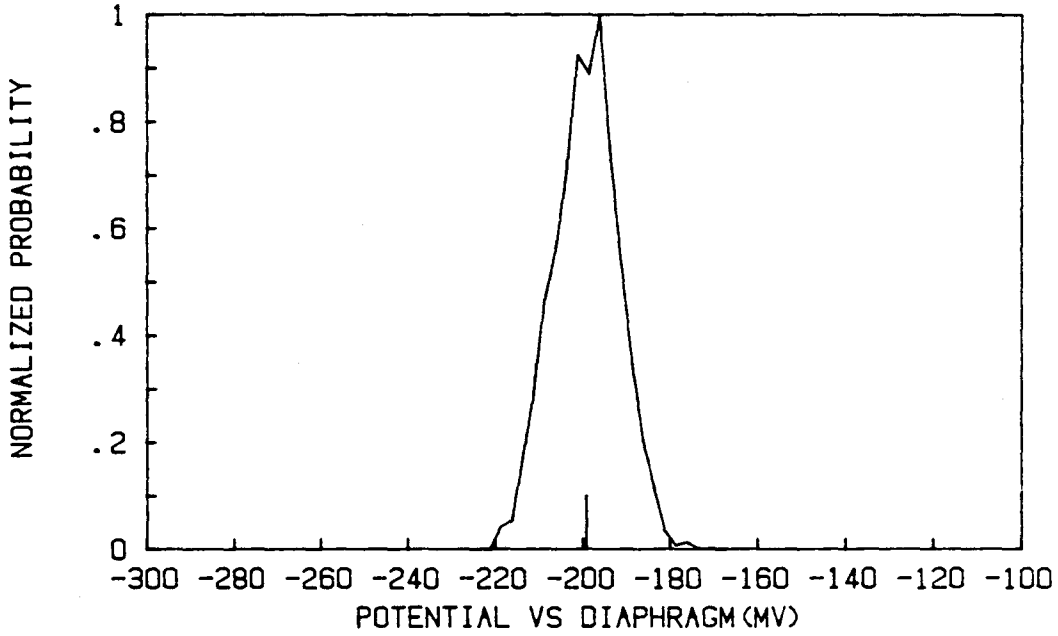

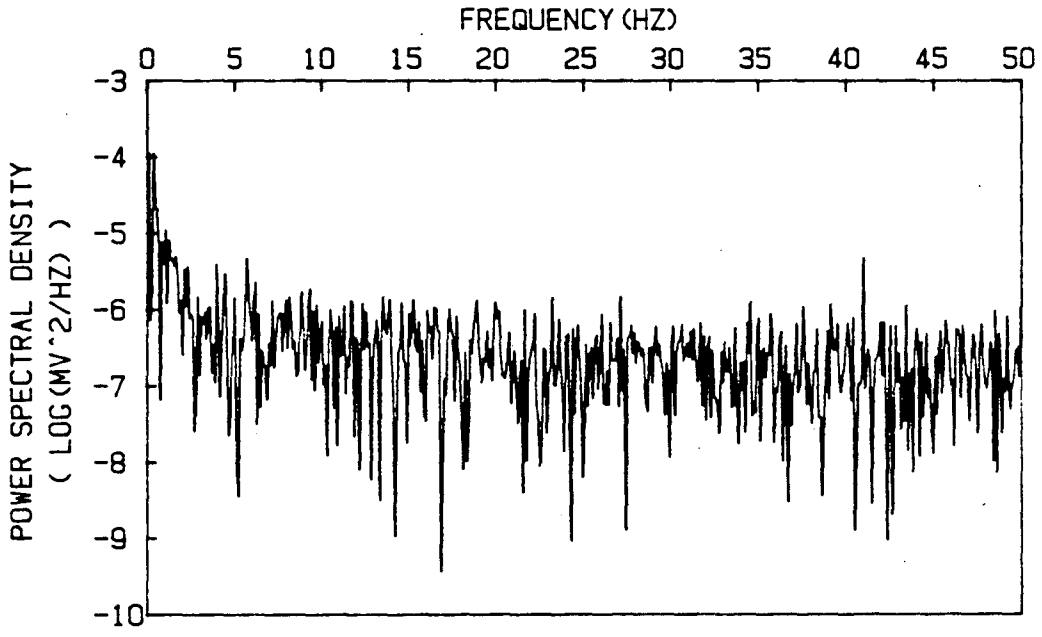

Figure IV-49 FFT result of Figure IV-47 b)

relatively little flicker noise in the particle potential.

Figure IV-50 shows the same effect on local overpotential transients. As expected, the overpotential transients are not greatly effected by bed expansion. It is seen that the potential transients of the Sorapec bed are not affected by bed expansion as much as those of the copper bed. This is mainly due to the difference in fluidization regime. The Sorapec bed is in the uniform fluidization regime, i.e. bubbles are not present in significant numbers, and so the local void fraction is constant after the onset of fluidization. When the bed is expanded further, the overall void fraction increases and consequently local resistivity increases. However, the fluidization regime remains the same.

Figure IV-53 compares the transients of two different particles, Sorapec and zinc coated copper, under the same conditions. It shows the three different potential transients in anodic reactions of a) zinc coated copper particles with superficial current density of 100 mA/cm^2 and Sorapec particles with superficial current densities of b) 100 mA/cm^2 and c) 200 mA/cm^2 respectively. The bed expansion was 30% in all cases. Power spectra and probability plots appear in Figures IV-54 through 56. As expected, there are relatively little flicker noise in Figures IV-55 and 56 as compared with Figure IV-54.

c. Effect of Applied Current Density

Figure IV-57 shows the potential fluctuations of zinc coated copper particles at different applied current densities, a) 100 mA/cm^2, b) 200

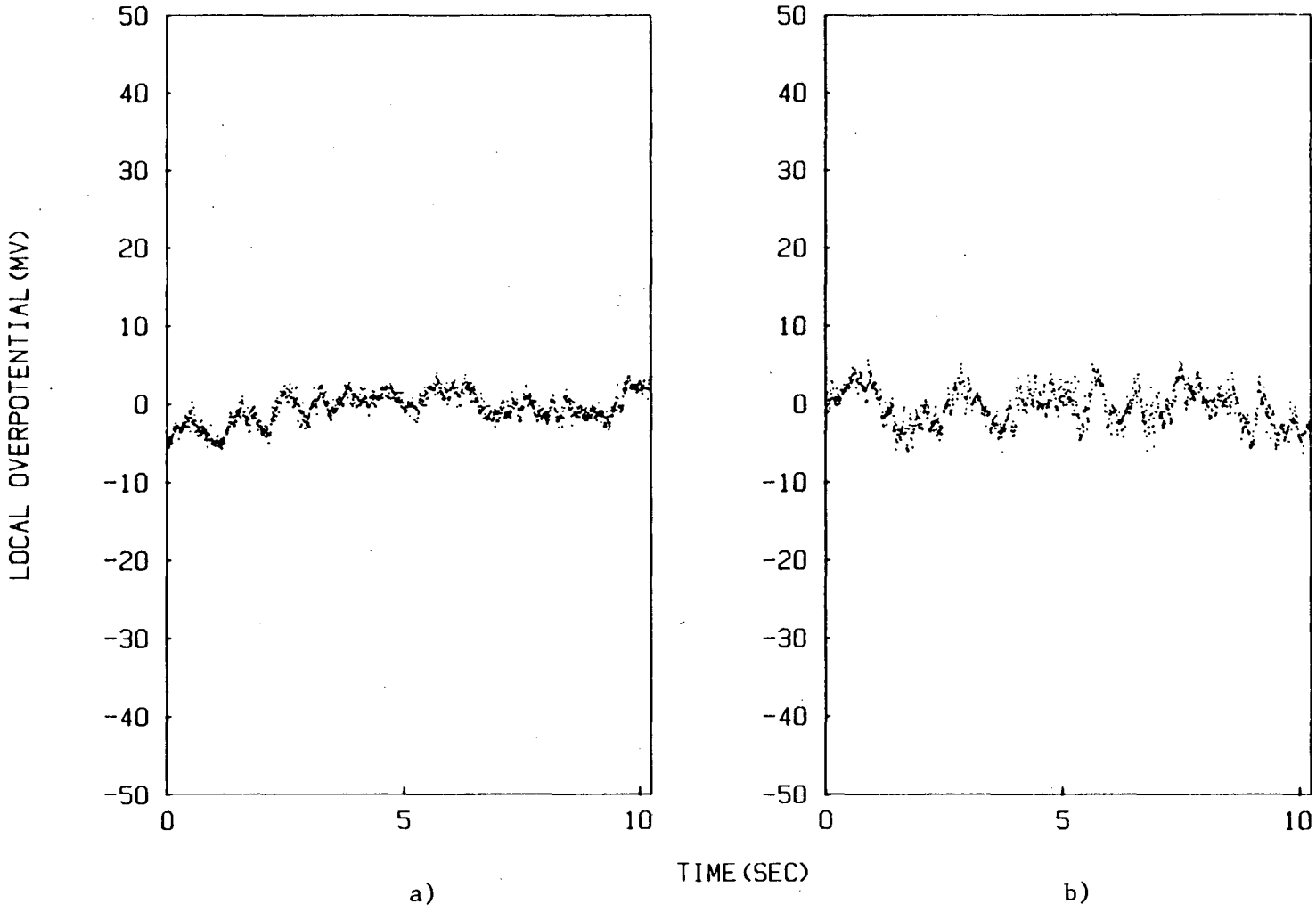

Figure IV-50 Effect of bed expansion on local overpotential transient (S.C.D. = 100 mA/cm^2, B.E. = a) 15%, b) 35%, cathodic reaction)

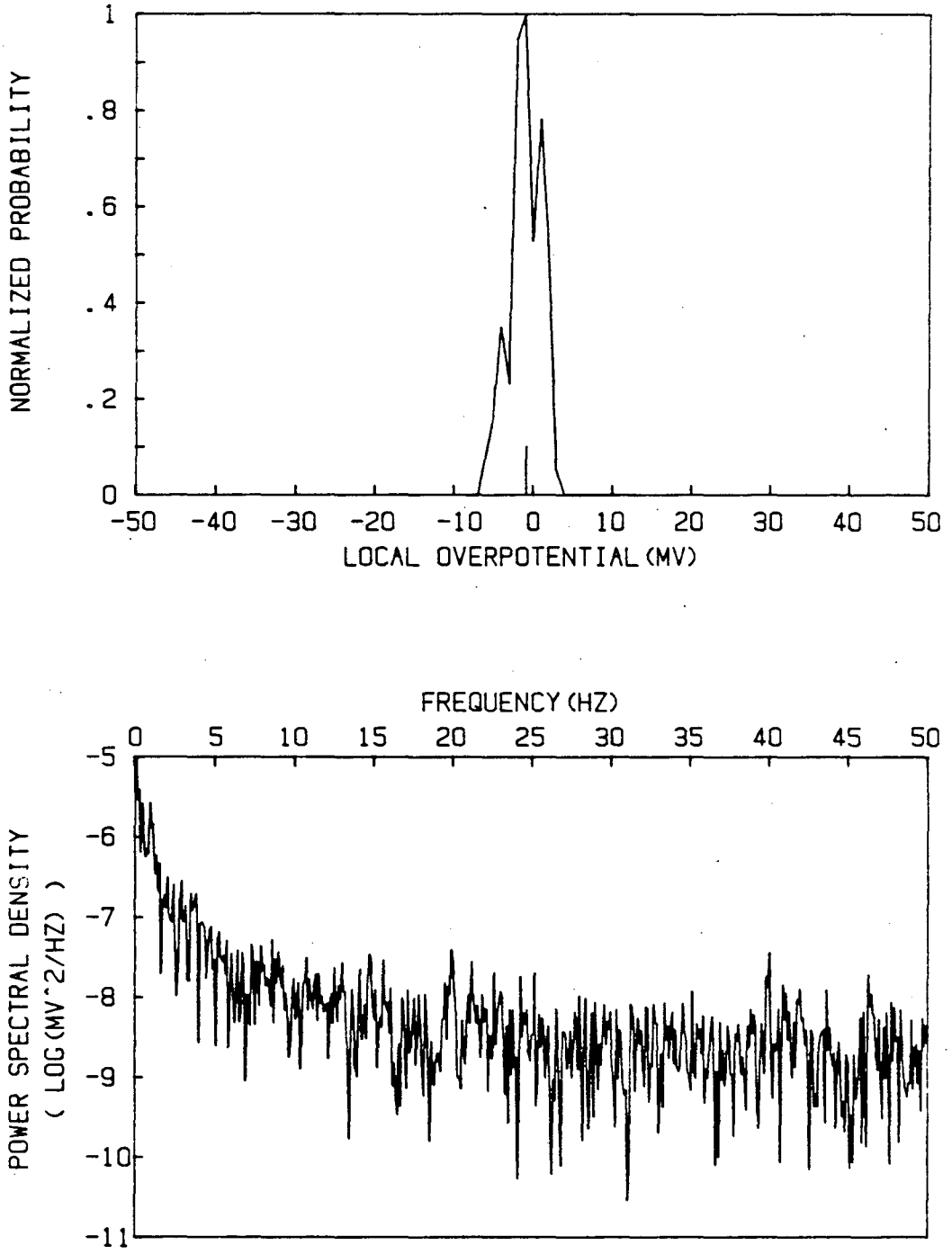

Figure IV-51 FFT result of Figure IV-50 a)

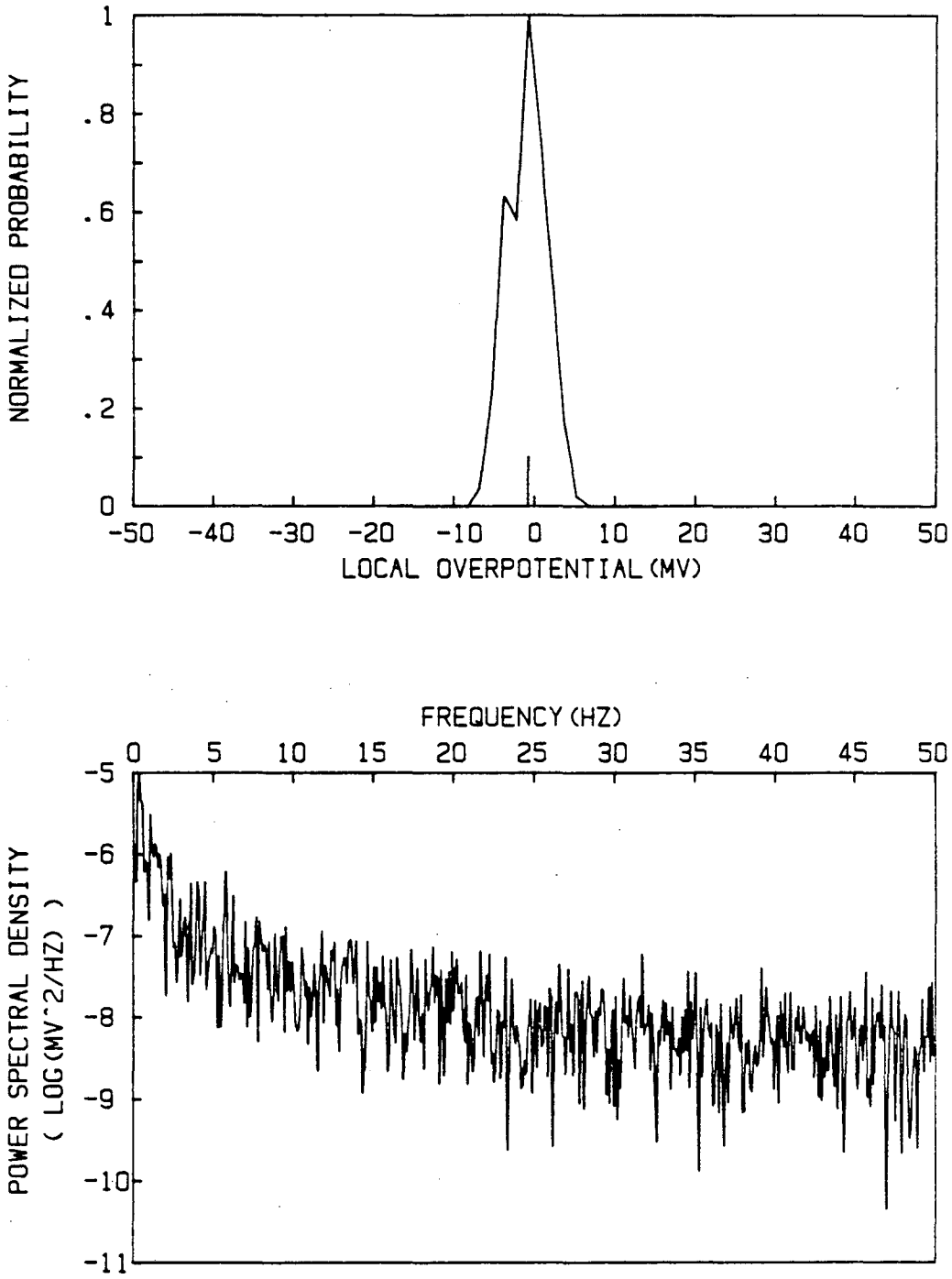

Figure IV-52 FFT result of Figure IV-50 b)

Table IV-7 : Effect of Bed Expansion on Potential Transients

B.E. (%)	$\bar{\phi}$	S_p	$\bar{\eta}$	S_η
		(all are in mV)		
15	-137.2	3.58	-0.9	1.95
35	-198.7	7.31	-1.0	2.36

Superficial Current Density : 100 mA/cm^2

Cathodic reaction of Zn/KOH system with Sorapec particles

Sampling Interval : 10 ms

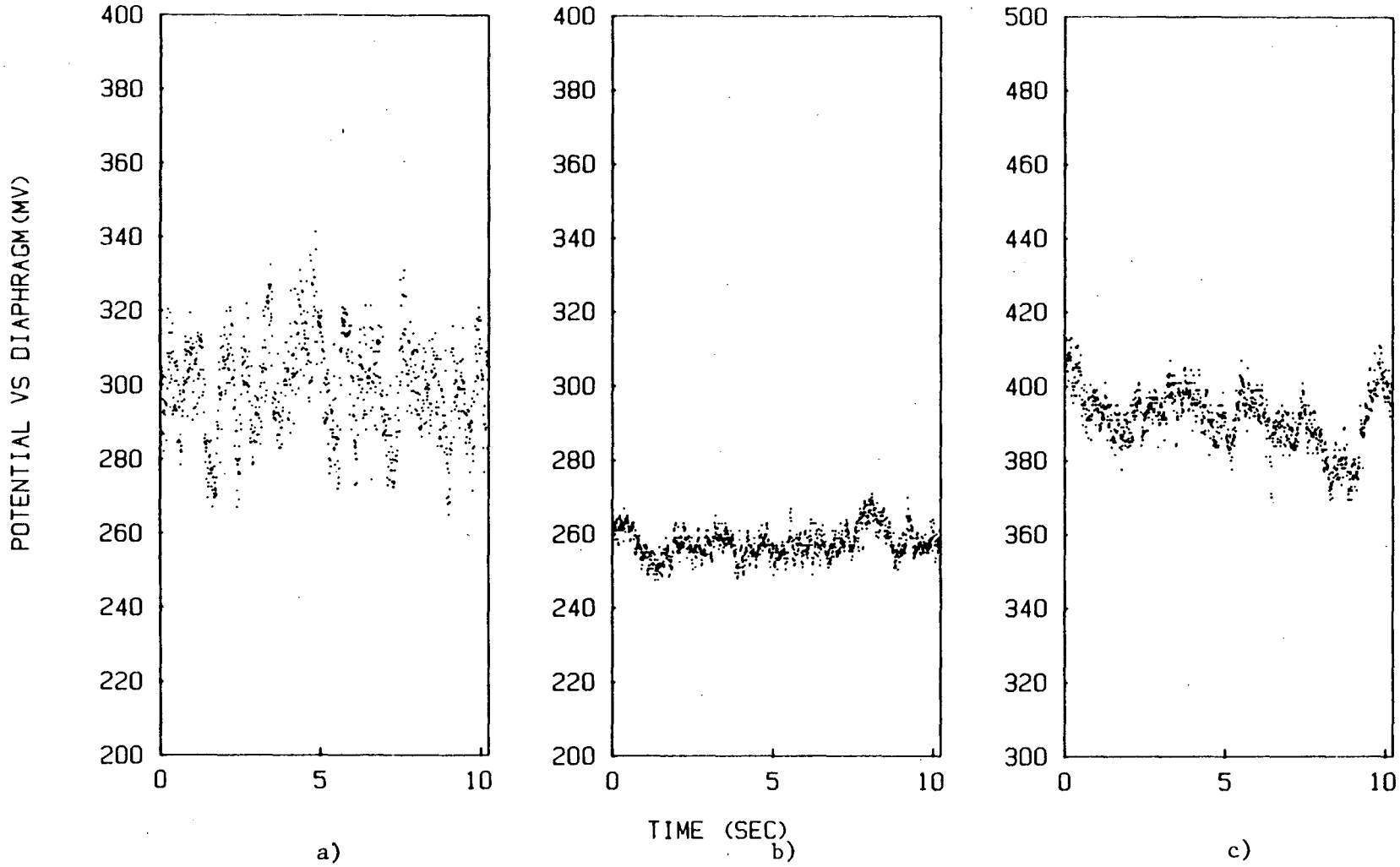

Figure IV-53 Particle potential transients during anodic reaction, B.E. = 30%
a) Zn coated Cu, S.C.D. = 100 mA/cm^2, b) Sorapec, S.C.D. = 100 mA/cm^2
c) Sorapec, S.C.D. = 200 mA/cm^2

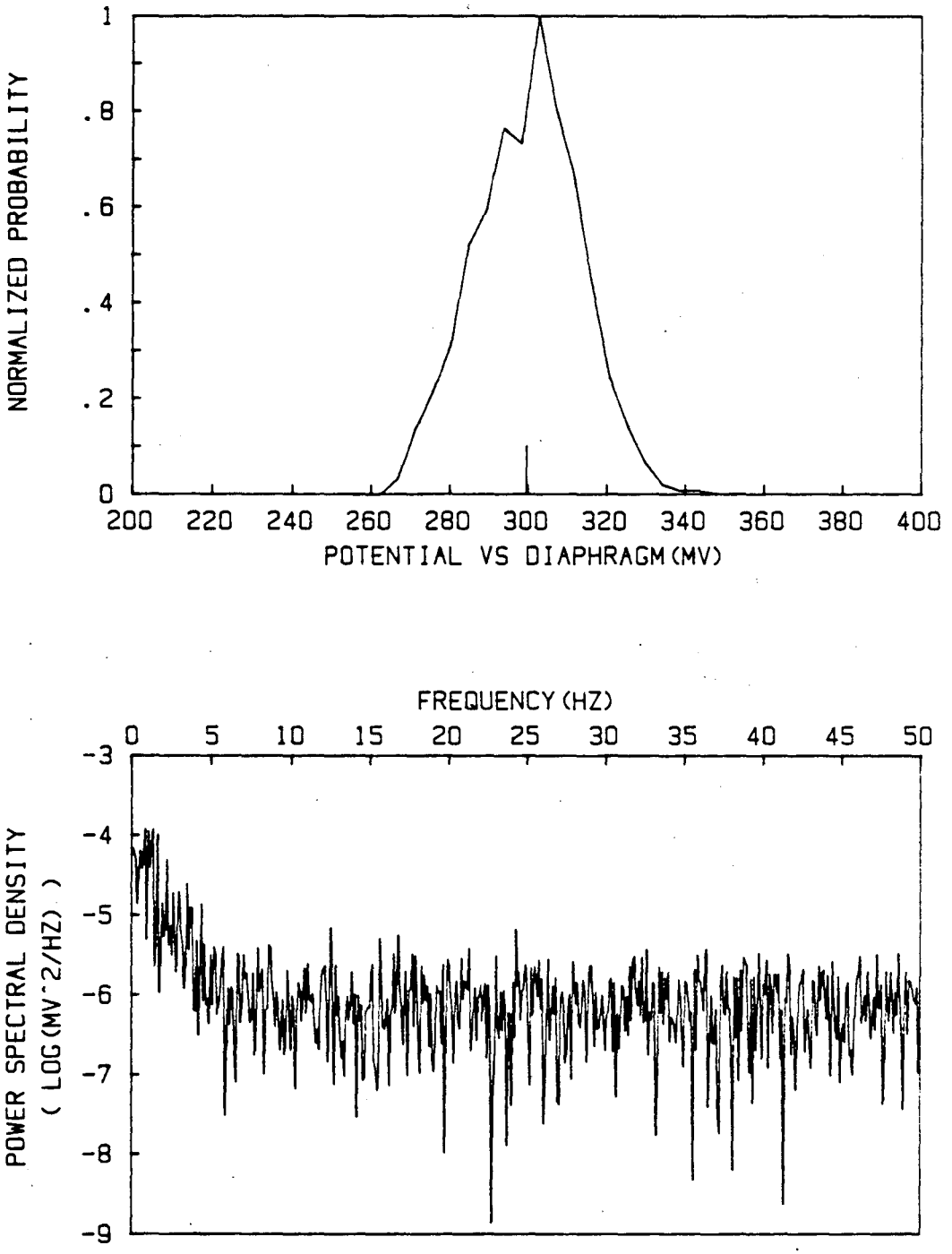

Figure IV-54 FFT result of Figure IV-53 a)

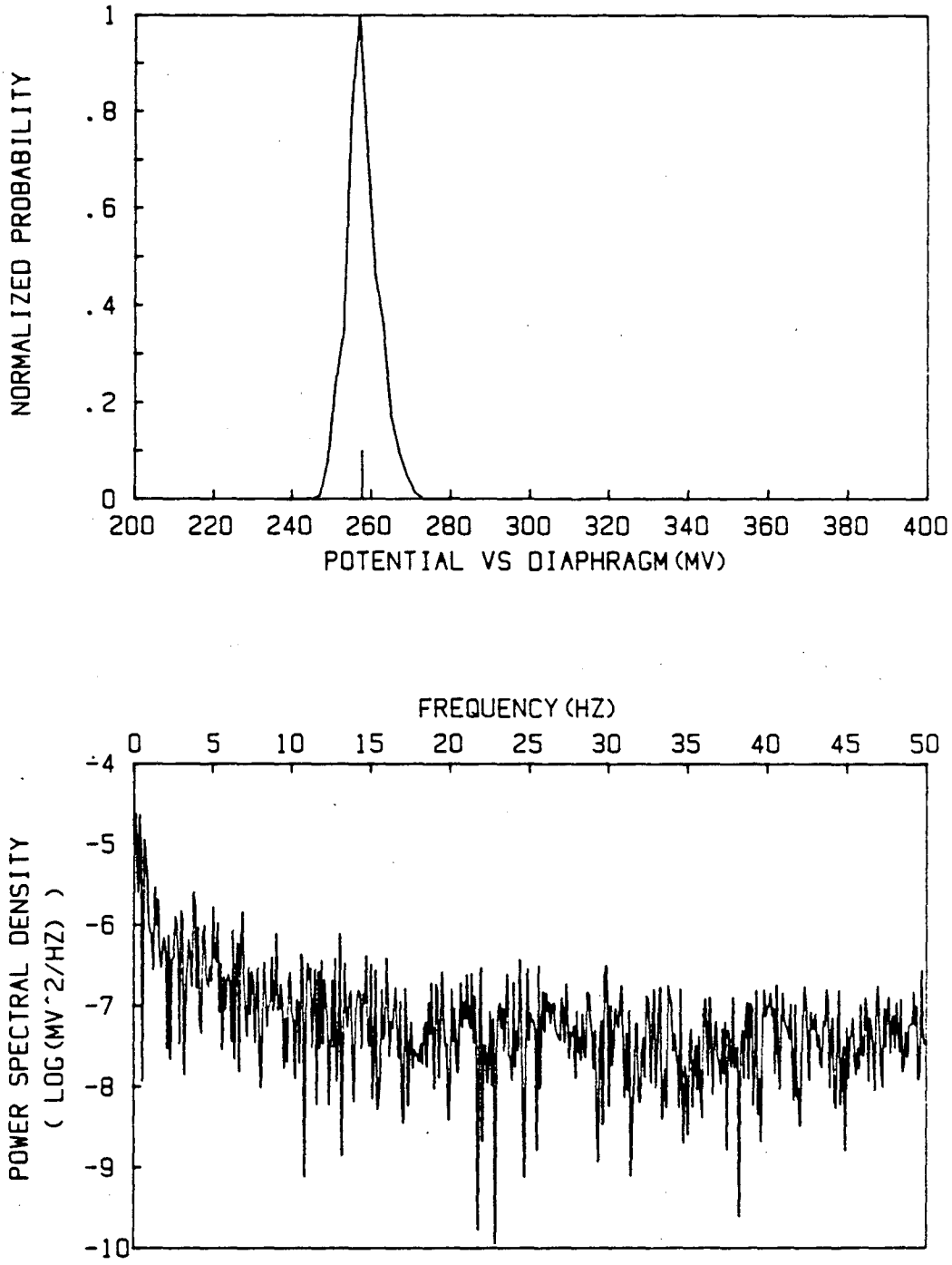

Figure IV-55 FFT results of Figure IV-53 b)

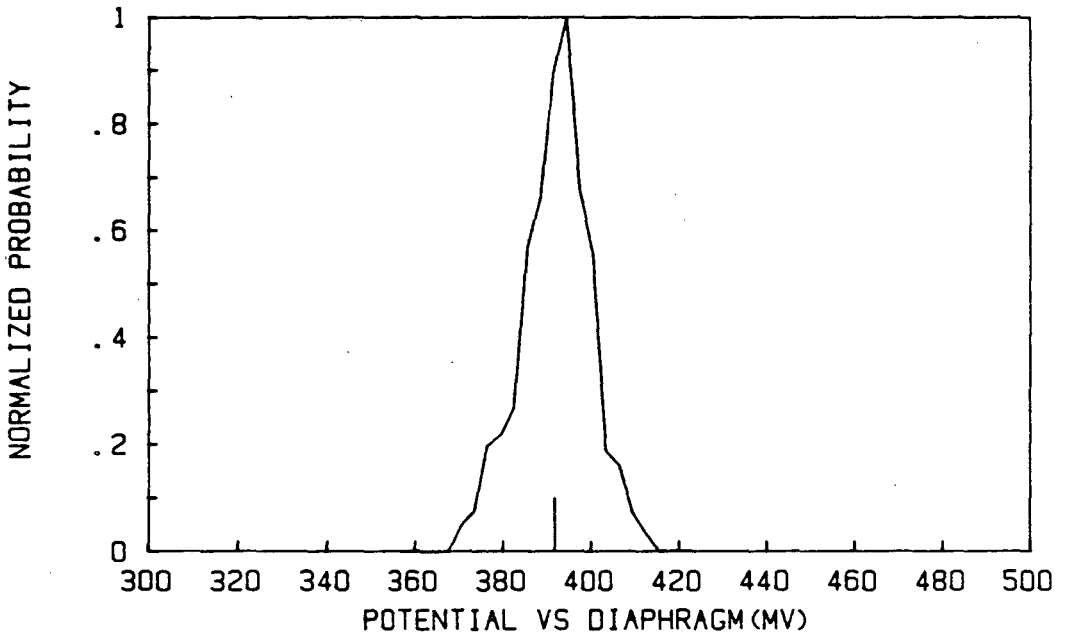

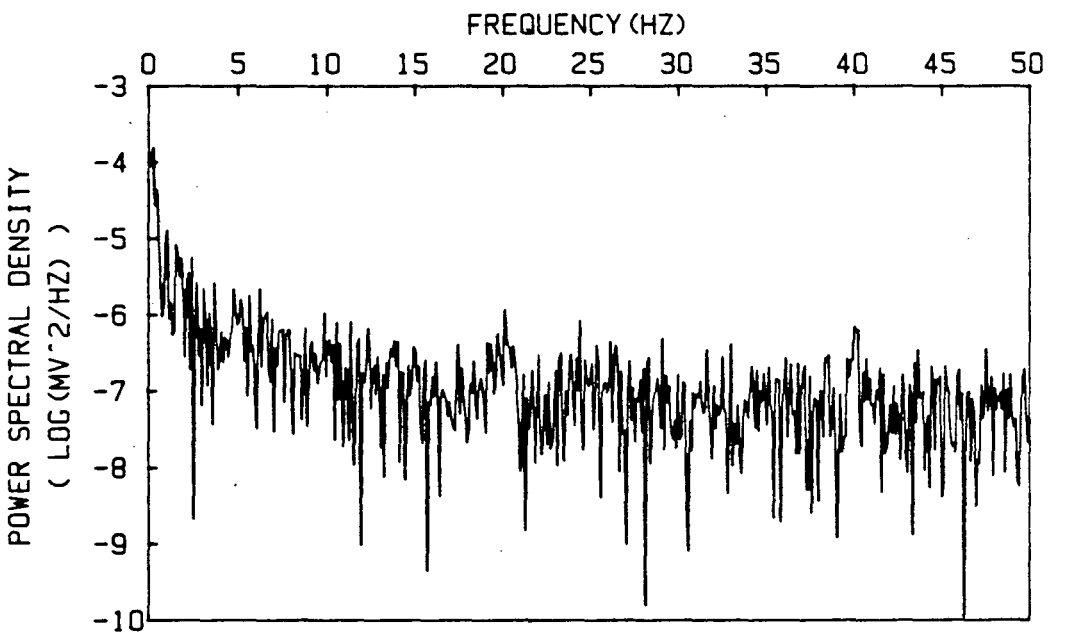

Figure IV-56 FFT result of Figure IV-53 c)

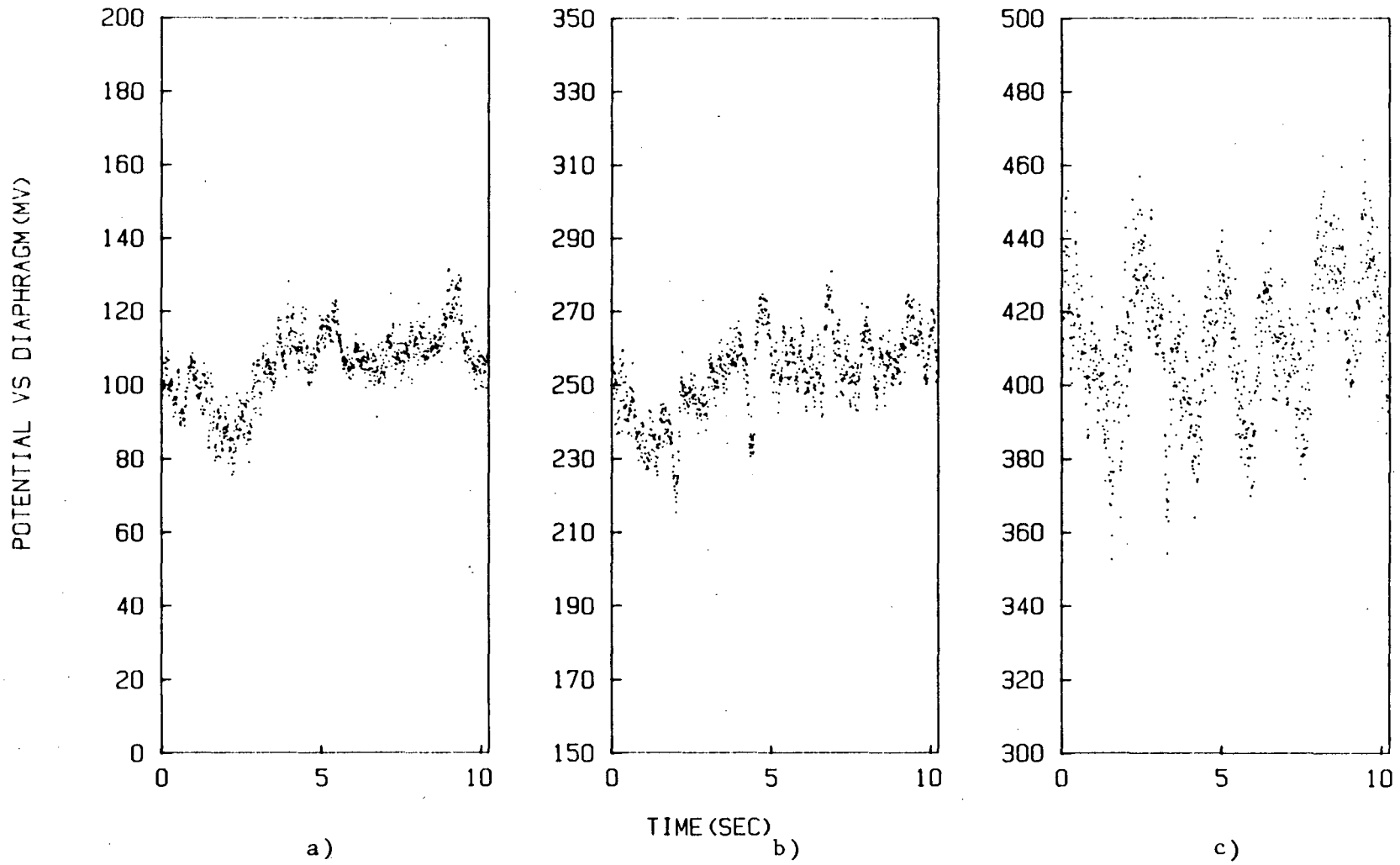

Figure IV-57 Effect of superficial current density on Zn coated copper particle potential transients during anodic reaction, B.E. = 15%, S.C.D. = a) 100 mA/cm^2, b) 200 mA/cm^2, c) 400 mA/cm^2

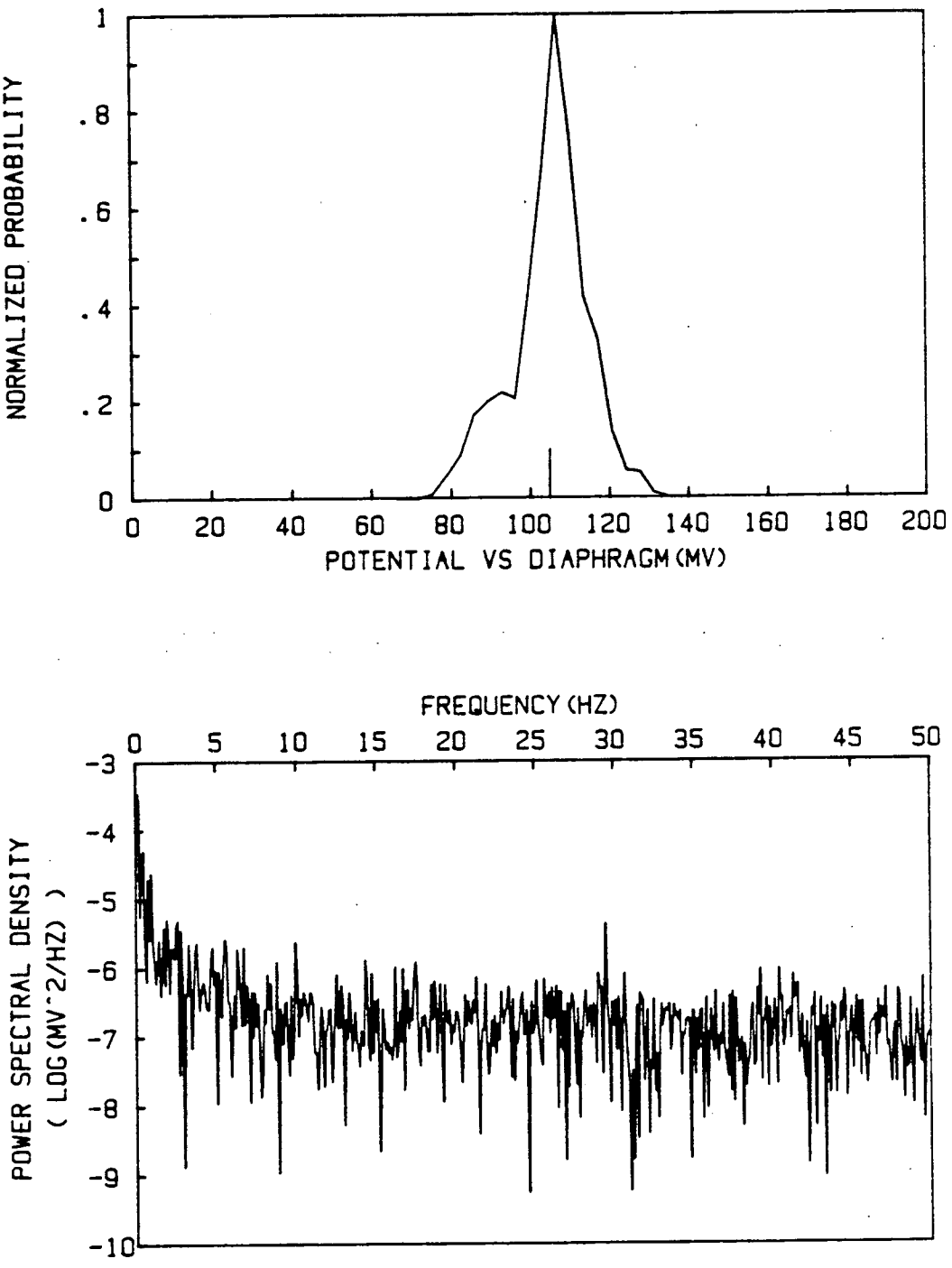

Figure IV-58 FFT result of Figure IV-57 a)

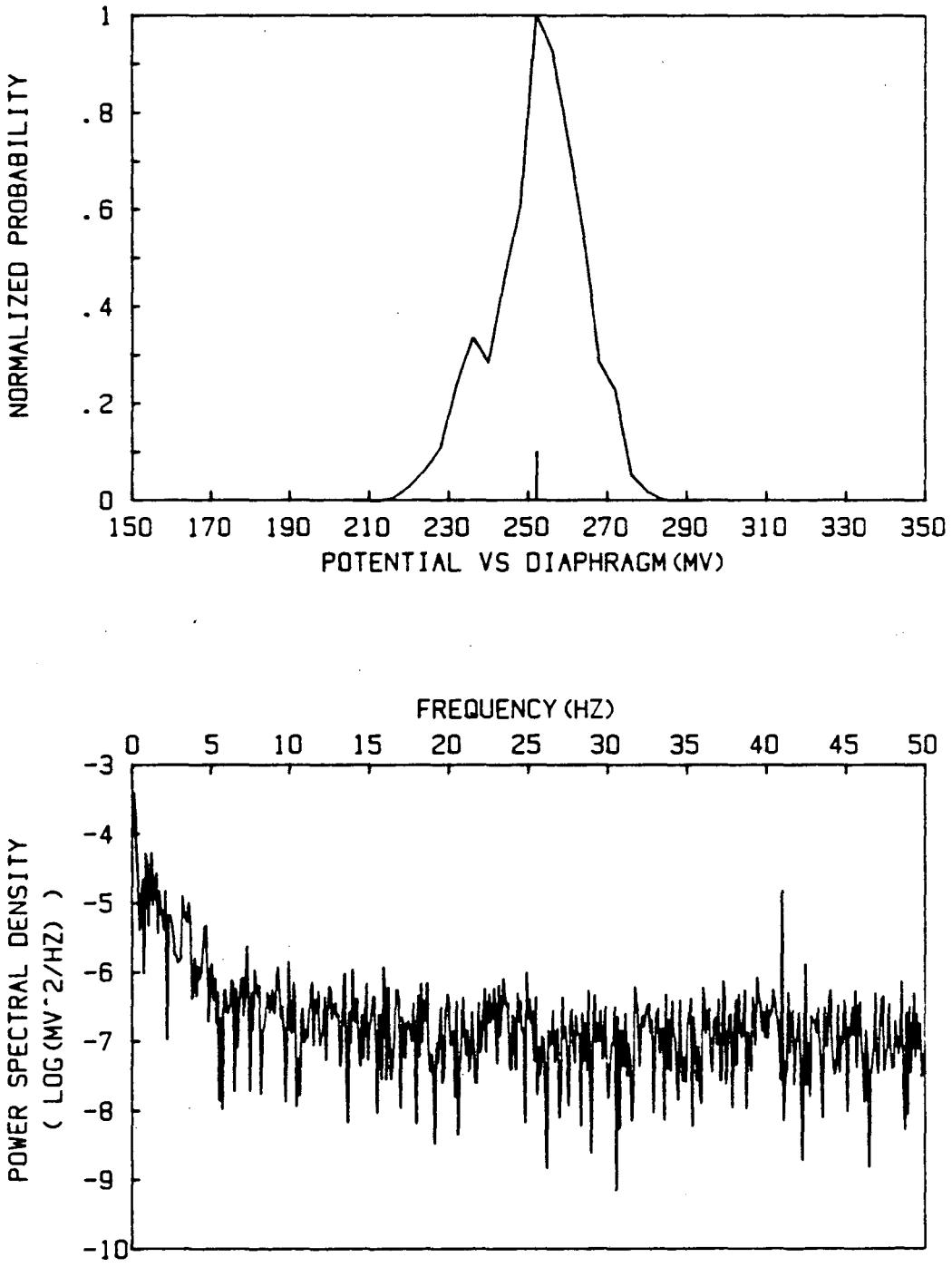

Figure IV-59 FFT result of Figure IV-57 b)

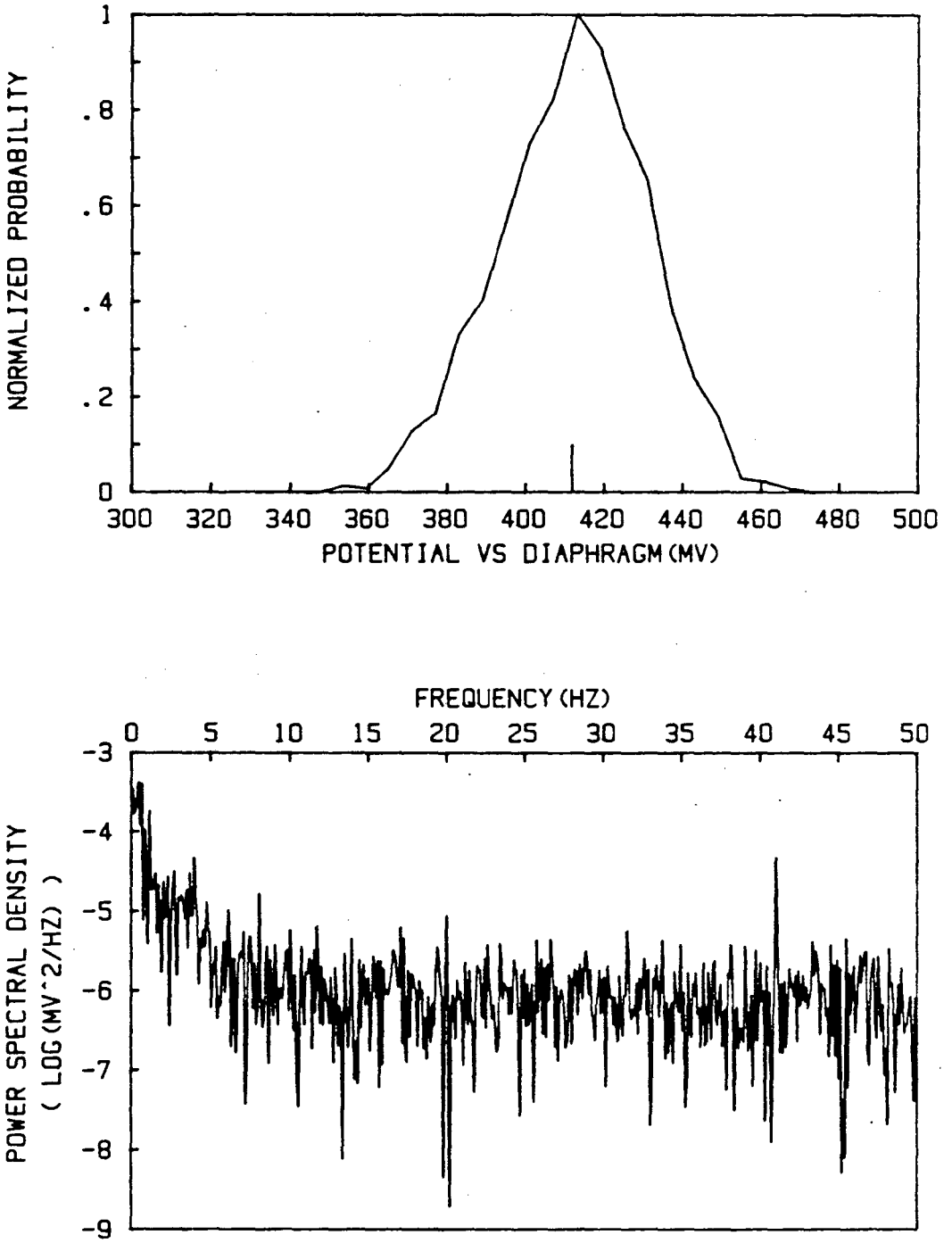

Figure IV-60 FFT result of Figure IV-57 c)

mA/cm^2, c) 400 mA/cm^2, and with 15% bed expansion during the anodic reaction. Figure IV-61 shows the corresponding local overpotential fluctuations. The transients become more scattered and the average value becomes larger as applied current density increases. The local overpotential seems to be affected. The general shape remains unchanged but scattering becomes severe. An increase in actual current density on the particle surface causes an increase in the time averaged value of local overpotential transients, i.e., increase in the local electrochemical reaction rate.

In addition, the particle potential transient of zinc coated copper particles looks similar to that of the Cu/H_2SO_4 system, while the local overpotential transient is that of the Sorapec bed. This also indicates that the particle and electrolyte potential transients are affected by hydrodynamic conditions which mainly arise from the interrelation of the two phases but the local overpotential transient is depend on the characteristics of electrochemical reaction at the particle surface, which is not changed by changing operating parameters.

d. Potential Distribution

Time averaged particle potential and local overpotential distribution through the bed are shown in Figures IV-65 and 66 respectively. Both were measured with a Sorapec bed during cathodic reaction with a superficial current density of 100 mA/cm^2 and a bed expansion of 25%.

Although this dissertation has been focused on potential transients, it is recognized that time averaged values are of interest

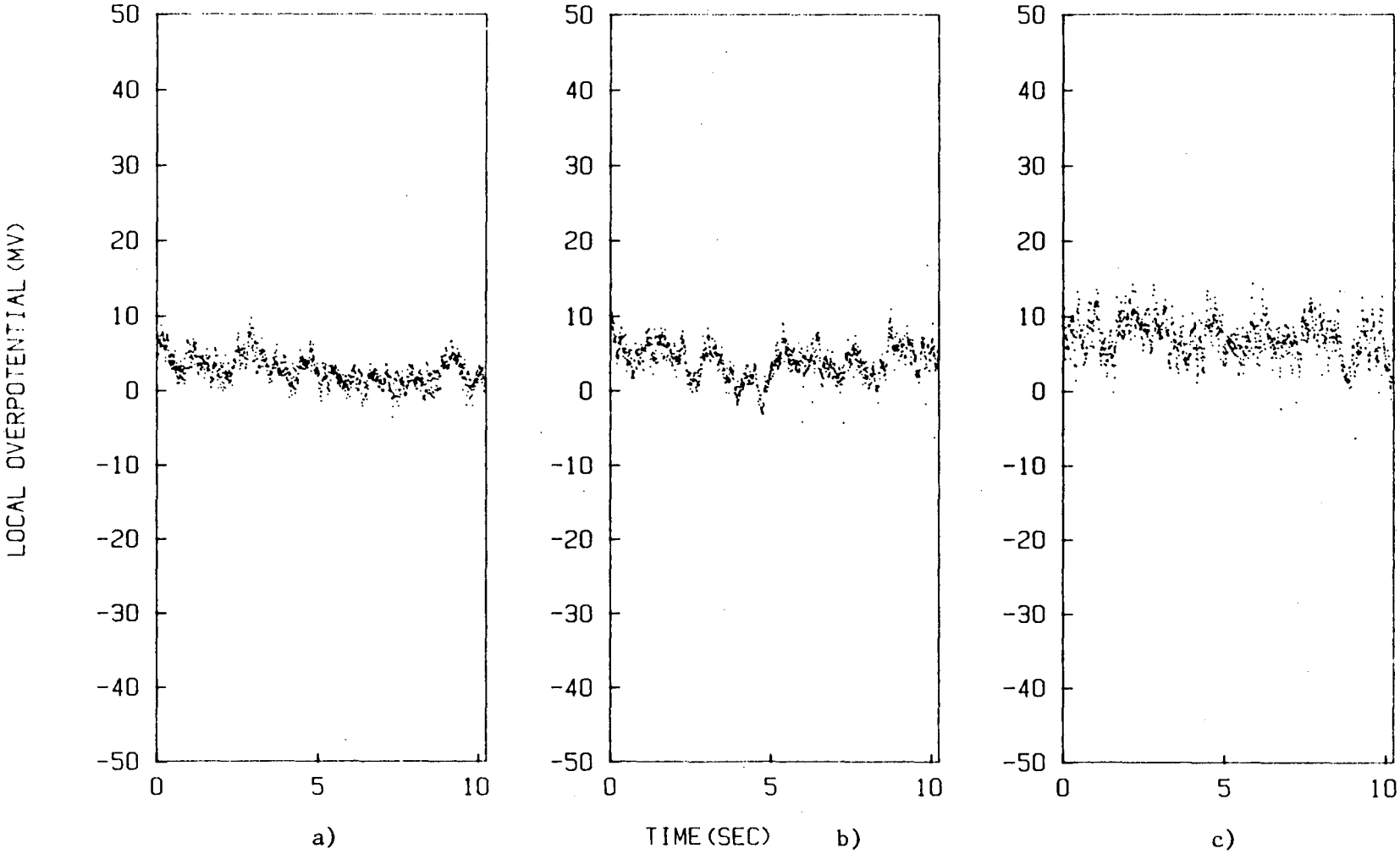

Figure IV-61 Effect of superficial current density on local overpotential transient, Zn coated Cu particles, anodic reaction, B.E. = 15%, S.C.D.: a) 100 mA/cm^2, b) 200 mA/cm^2, c) 400 mA/cm^2

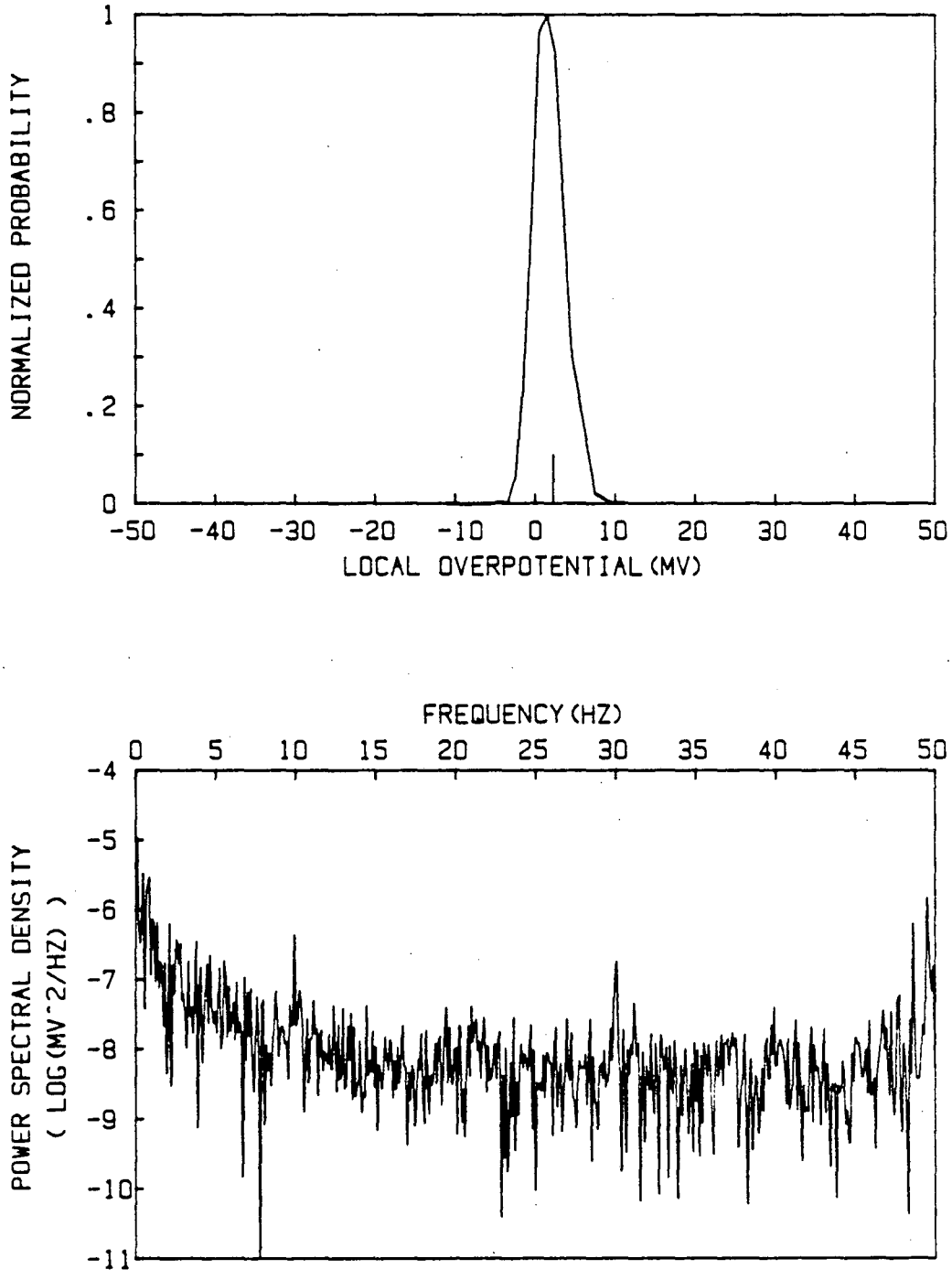

Figure IV-62 FFT result of Figure IV-61 a)

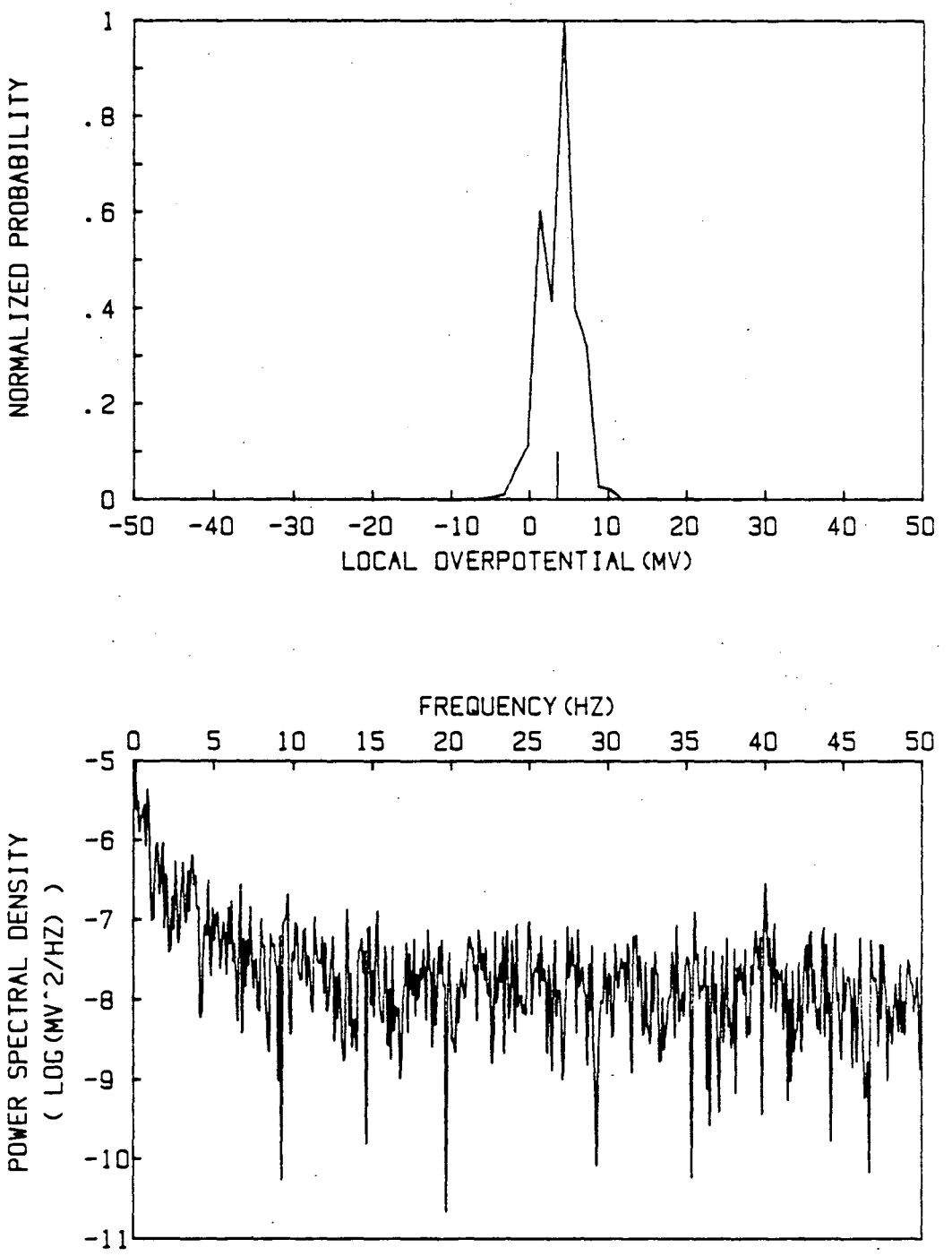

Figure IV-63 FFT result of Figure IV-61 b)

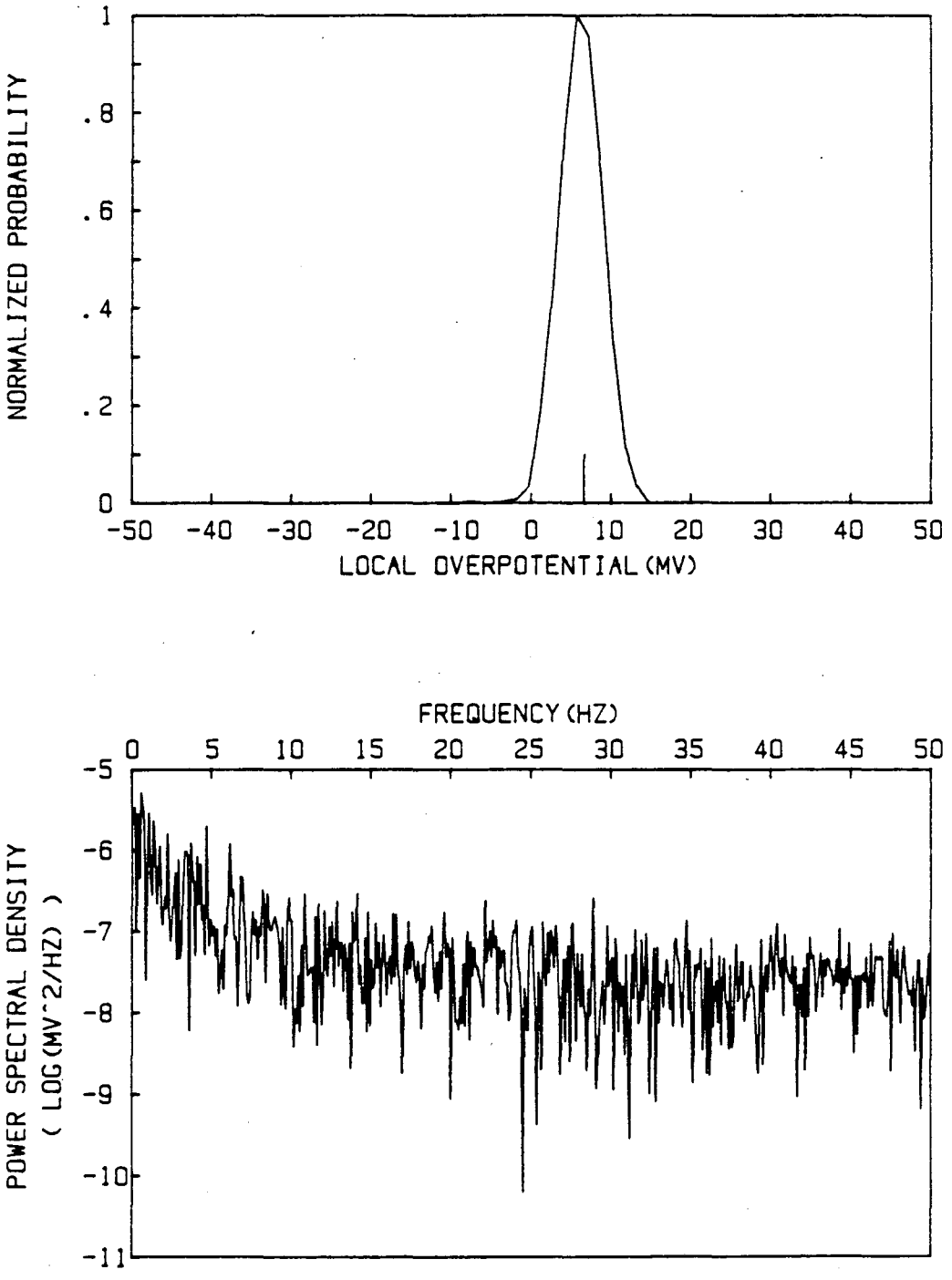

Figure IV-64 FFT result of Figure IV-61 c)

Table IV-8 : Effect of Applied Current Density on Potential Transients

C.D.*	$\overline{\phi}_p$	S_p	$\overline{\eta}$	S_η
		(all are in mV)		
100	104.8	9.7	2.2	1.98
200	252.0	11.2	3.5	2.36
400	411.7	18.7	6.6	2.66

* Superficial Current Density in mA/cm^2

Bed Expansion : 15%

Sampling Interval : 10ms

Anodic reaction of Zn/KOH system with Zn coated Cu particle

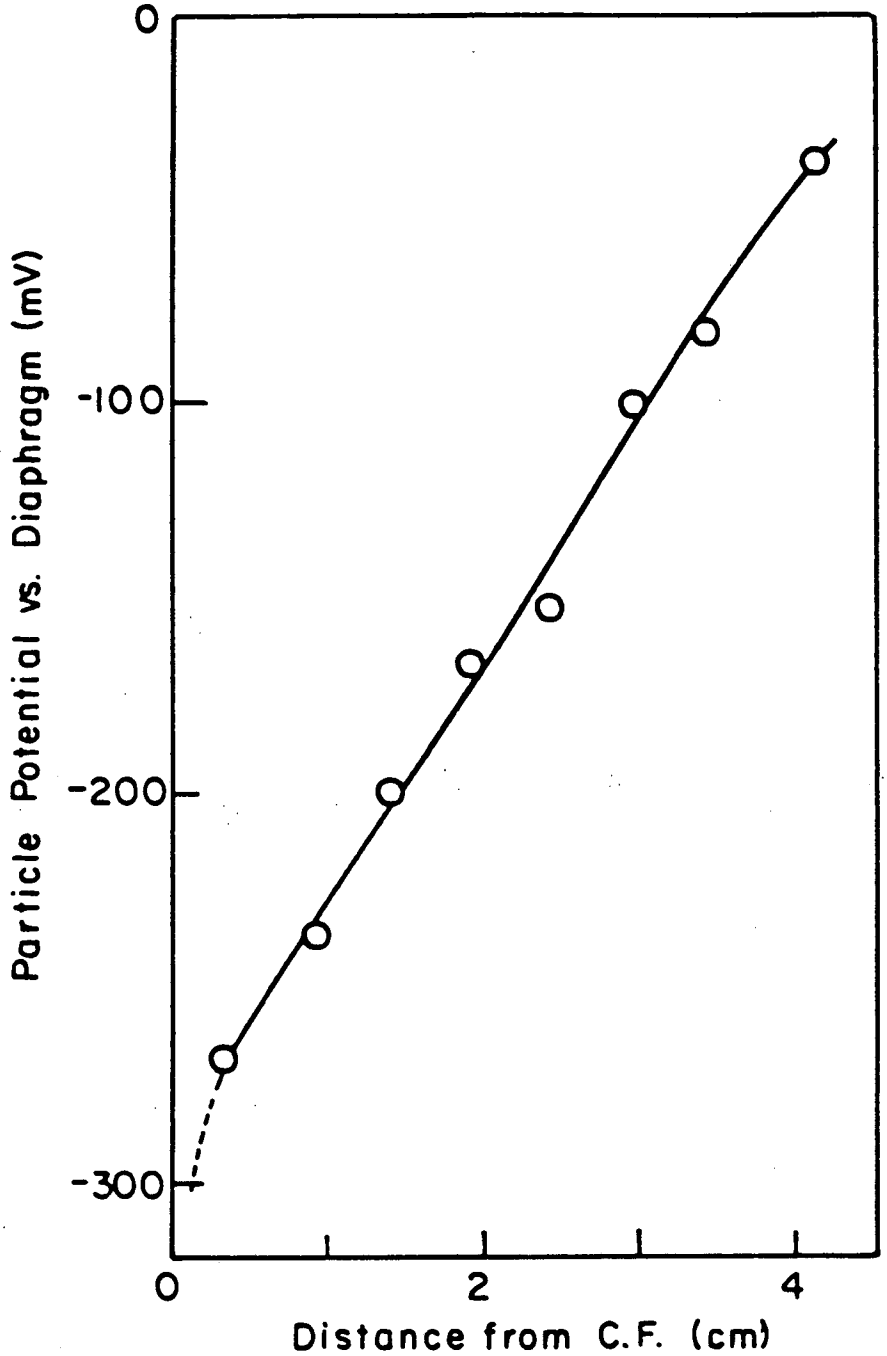

Figure IV-65 Time averaged Sorapec particle potential distribution during cathodic reaction, B.E. = 25%, S.C.D. = 100 mA/cm^2

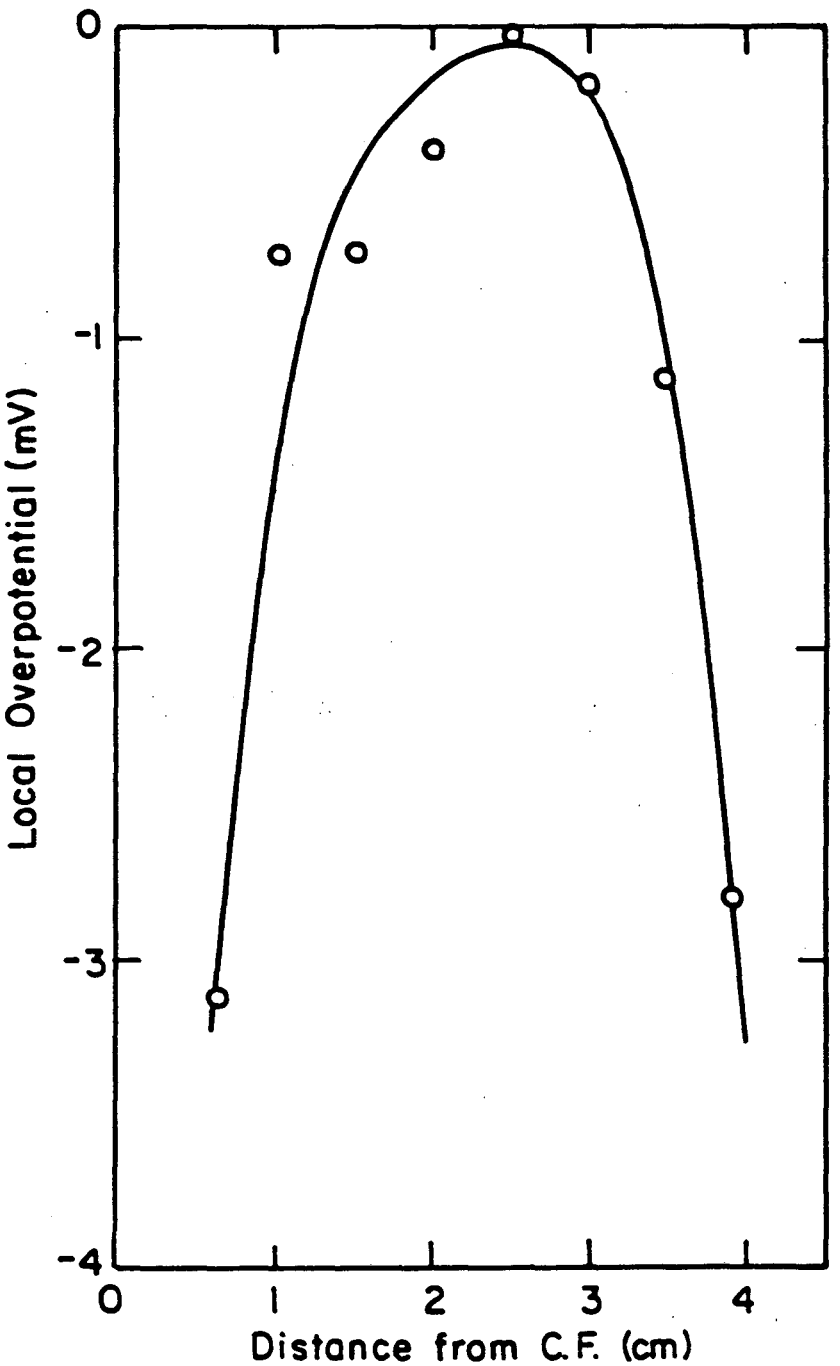

XBL 851-1031

Figure IV-66 Time averaged local overpotential distribution, cathodic reaction, B.E. = 25%, S.C.D. = 100 mA/cm^2

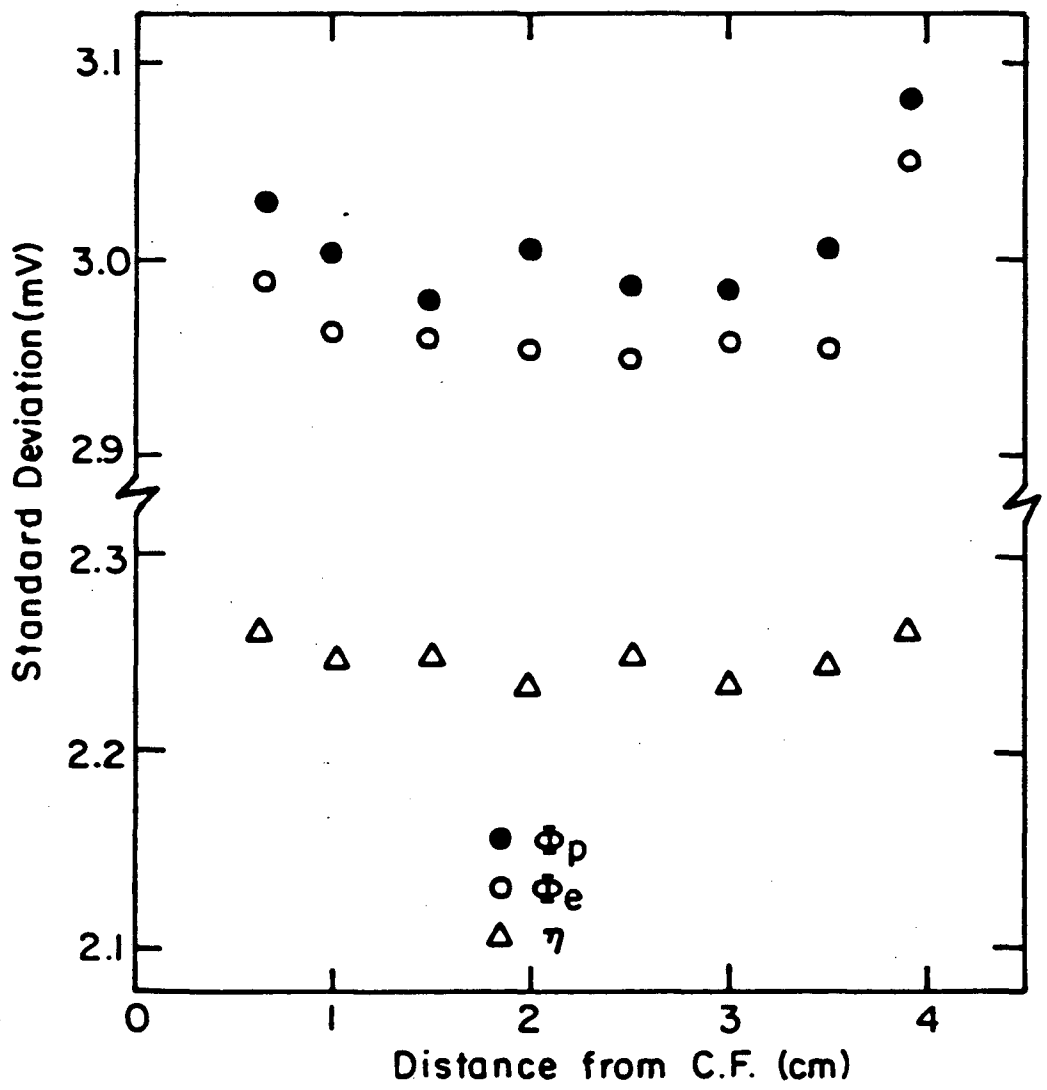

Figure IV-67 Standard deviations of time averaged potentials, corresponding with Figures IV-65 and 66.

in designing and understanding fluidized bed electrodes.

The local overpotential is important because it is directly related to the local electrochemical reaction rate (an important factor in the determination of bed performance). For this study, 2048 data were collected with a sampling interval of 10 ms for each data set and averaged to represent one time averaged value.

The shape of the overpotential distribution of Figure IV-66 implies that the electrochemical reaction (zinc deposition) occurs mainly in regions close to the current feeder and close to the diaphragm, whereas the center of the bed is almost inactive. This is consistent with mathematical models for porous electrodes, e.g. that of Newman and Tobias[11], or fluidized bed electrodes, e.g. that of Sabacky and Evans[9,10]. Figure IV-68 is taken from the former worker while Figure IV-69 is taken from the latter. An attempt was made to obtain a quantitative fit between the Sabacky and Evans model and the overpotential distribution of Figure IV-66. This was unsuccessful, perhaps because of the lack of consistent values for the exchange current density for zinc deposition.

e. Effective Bed Resistivity Measurements

Figure IV-70 shows the sinusoidal potential across the known resistor (8.7 ohms) and the fluidized bed of Sorapec particles at various bed expansions. These figures should be contrasted with Figure IV-29 for the copper particles. A steady sinusoidal voltage is evident for the Sorapec particles, in contrast to the fluctuating sine wave

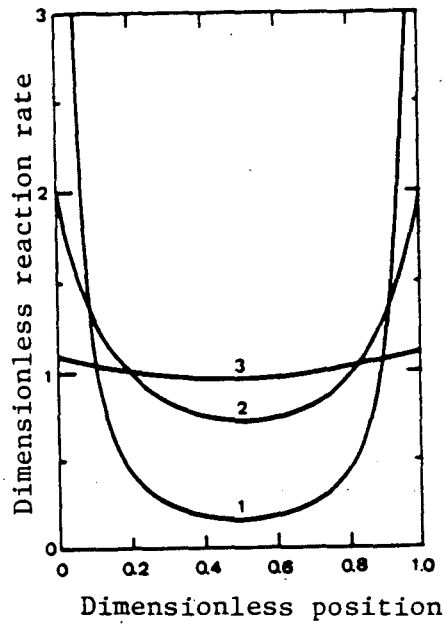

Figure IV-68 Dimensionless reaction rate distributions through the one-dimensional porous electrode for Tafel polarization with $\kappa = \sigma$, $\delta = 100$ for curve 1, 10 for curve 2 and 1 for curve 3, where $\delta = \beta|I|L(1/\kappa + 1/\sigma)$ and

κ = effective conductivity of pore electrolyte
σ = conductivity of matrix
β = reciprocal potential
I = current density
L = thickness

after Newman and Tobias[11]

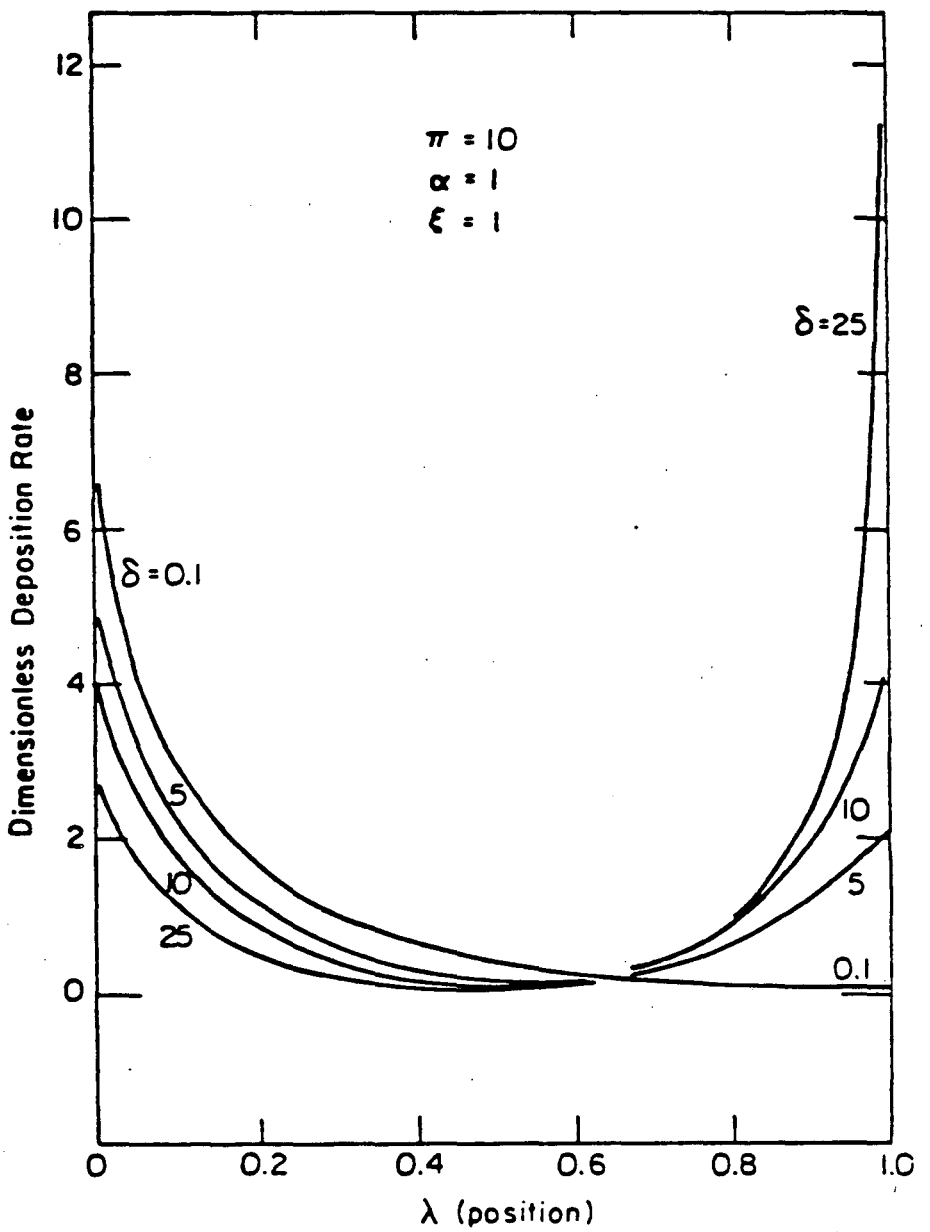

Figure IV-69 Variation of local deposition rate with distance from diaphragm, π = dimensionless electrolyte resistivity, α = dimensionless kinetic parameter, ξ = dimensionless concentration and δ = dimensionless particulate matrix resistivity. After B. Sabacky[9]

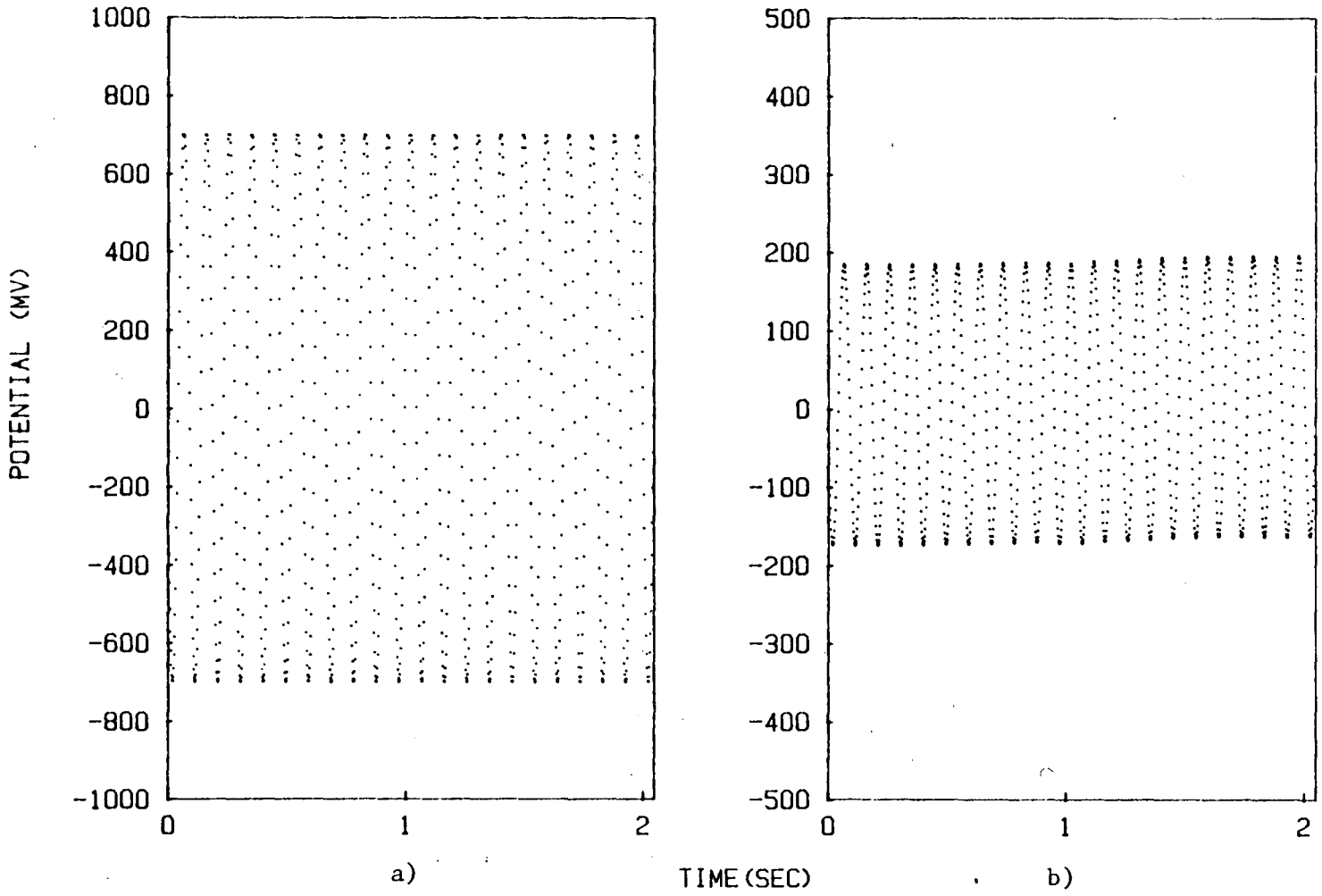

Figure IV-70 Output of sinusoidal potentials across the known resistor and bed at different bed expansions a) known resistor, b) at bed expansion of 40%

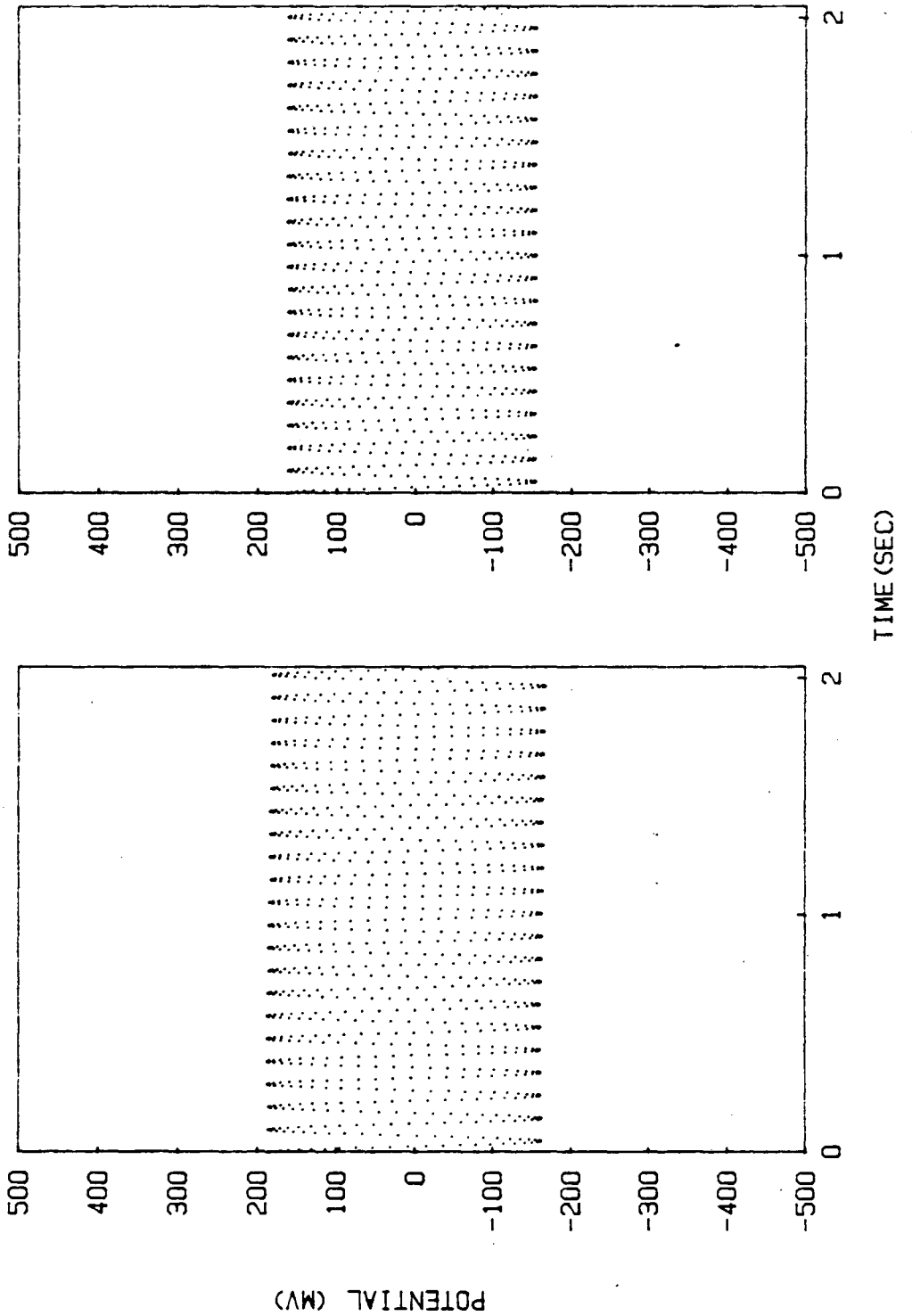

Figure IV-70 e) 25%, d) 10%

obtained with copper particles. This is further evidence of the absence of large bubbles in the Sorapec bed.

From the amplitudes of the sine waves and the geometry of the bed, the effective bed resistivity can be determined. The results are ploted in Figure IV-68. In these resistivity experiments a fraction of the current passes through the electrolyte; this fraction is significant for the wave conductive electrolyte. This is the reason for the dependence on electrolyte resistivity seen in Figure IV-71. Note that for the most conductive electrolyte, the bed resistivity approaches the electrolyte resistivity, for bed expansions over 10%, indicating that for these conditions the majority of the current is carried by the electrolyte. Figure IV-71 should be compared with Figure IV-30 for the copper particles. The bed resistivities of Sorapec particles are shown to be higher than those of copper particles under the same conditions. The resistivity of the copper bed depends more strongly on bed expansion than does the resistivity of the Sorapec bed. This can be explained by the conductivity difference (Cu = 5.96×10^5/ohm-cm versus Zn = 1.67×10^5/ohm-cm) and the surface morphology difference (see Figures IV-5 and IV-3) between the two kinds of particles. The porous surface of the Sorapec particles may provide insufficient contact between particles (also the pores are filled with electrolyte), resulting in high resistivity at low bed expansion (less than 10%). This can also explain the relatively stronger dependency of Sorapec bed resistivity on electrolyte conductivity than bed expansion.

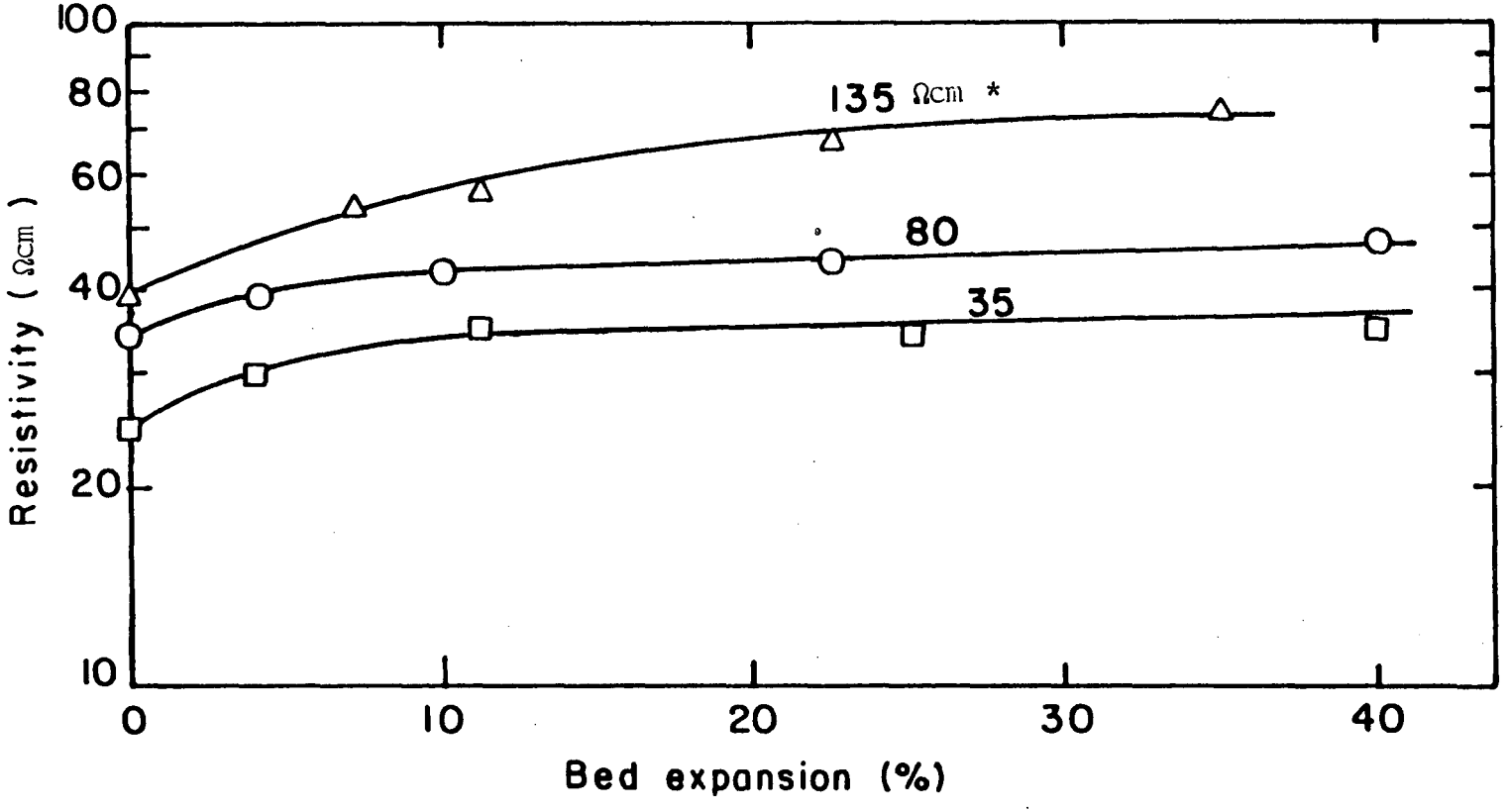

Figure IV-71 Dependency of time averaged Sorapec fluidized bed resistivity on bed expansion and on electrolyte resistivity. * = electrolyte resistivities

V. CONCLUSIONS

A. Silver Electrowinning

This investigation, carried out on a bench scale, has established that silver can be electrowon from solutions akin to those in a commercial plant by using a fluidized electrode. The performance of a fluidized bed cell was free of operating problems and superior to the Zadra type cell. Except when the cell is driven at too high a current or too low a silver concentration, the current efficiency of the cell appears higher than that reported for the Zadra type cell. Solutions can be stripped of silver down to the level of a few ppm (although this may not be the optimum mode of operation). During the operation, silver seed particles have performed successfully. Three anode materials that show the required performance and that do not appear to deteriorate have been identified. The cell voltage has been found to depend to a great extent on anolyte conductivity. Daramic has performed well as a diaphragm material in the cell. The silver deposited in the cell appears to be free of impurities down to the detection level of these experiments.

B. Transient Behavior of Fluidized Bed Electrodes

The potentials of particle and electrolyte and local overpotential in fluidized bed electrodes of two types of particles have been measured

and are observed to depend on current, bed expansion and position in the bed (for copper particles). Each potential can be regarded as a time average value onto which "noise" is added. In the case of copper particles, two kinds of noise are evident in the potential fluctuations of the particles and electrolyte, low frequency ("flicker") noise and white noise. The former is absent in the overpotential signal. The flicker noise is thought to be due to the formation of bubbles in the fluidized bed electrode. The existence of such bubbles is predicted by a bed behavior diagram in the literature and confirmed by resistance measurements on the bed of fluidized copper particles.
Resistance measurements yielded effective resistivity values for copper particles in the range reported by previous investigators and these were found to increase with increasing bed expansion.

In the case of the zinc coated Sorapec particles, much less flicker noise was observed in the particle and electrolyte potential signals, although some low frequency noise appeared in the overpotential. The bed behavior diagram predicts that a fluidized bed of Sorapec particles should be in a transition regime (few bubbles), which is consistent with visual observation of the bed and the bed resistance measurements. The distribution of the time averaged overpotential within an electrode of Sorapec particles is in qualitative agreement with predictions of prior mathematical models.

APPENDIX A: MOVING BED ELECTRODE

The other type of particulate electrode was first tested with the Cu/H_2SO_4 system. Figure A-1 is a schematic of the moving bed electrode used during this study. The advantages of this electrode compared to the fluidized bed electrode are

i) less pumping power

ii) less potential drop across the particualte bed(due to high particle packing density)

iii) no severe potential fluctuations

The bed of particles moved down very slowly and uniformly during operation as expected. It behaves like a packed bed but moves.

Figure A-2 shows the potential transients (it is hard to say transients) of such an electrode at the center of the bed with 200 mA/cm^2 of superficial current density when catholyte concentration was 25 g/l of Cu^{++} and 50 g/l of H_2SO_4. Even the current and electrolyte composition are same, this is not comparable with the potential transients of the fluidized bed electrode at low bed expansion (Figure IV-18).

Figures A-3 and 4 show distributions of time averaged particle potential and overpotential respectively. These results look like those of the packed bed electrode previously reported.

The moving bed electrode was found to be an alternative to the fluidized bed electrode, with the advantages mentioned. Further study is necessary, however, especially with regard to the feasibility of long

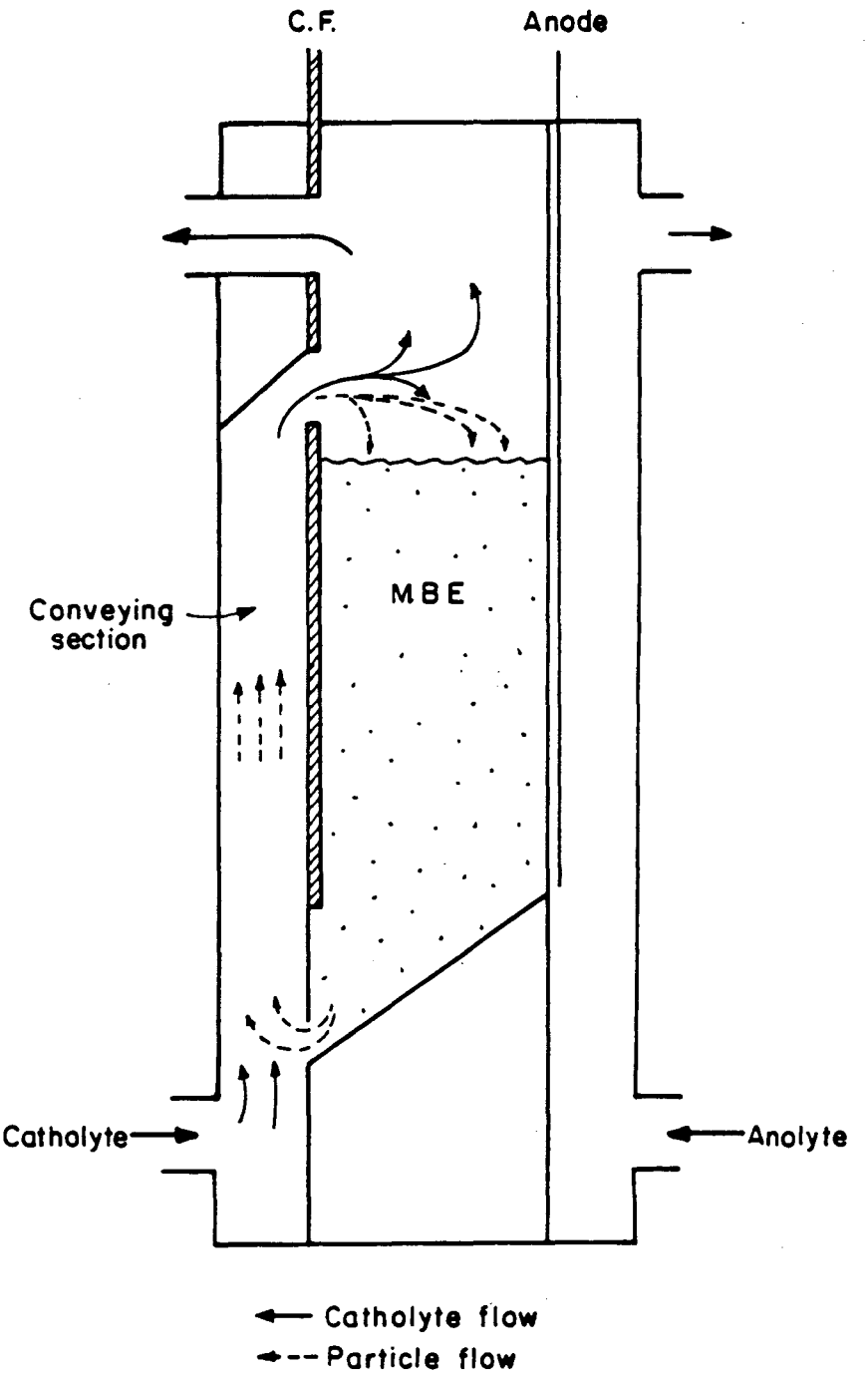

Figure A-1 Schematic side view of moving bed electrode

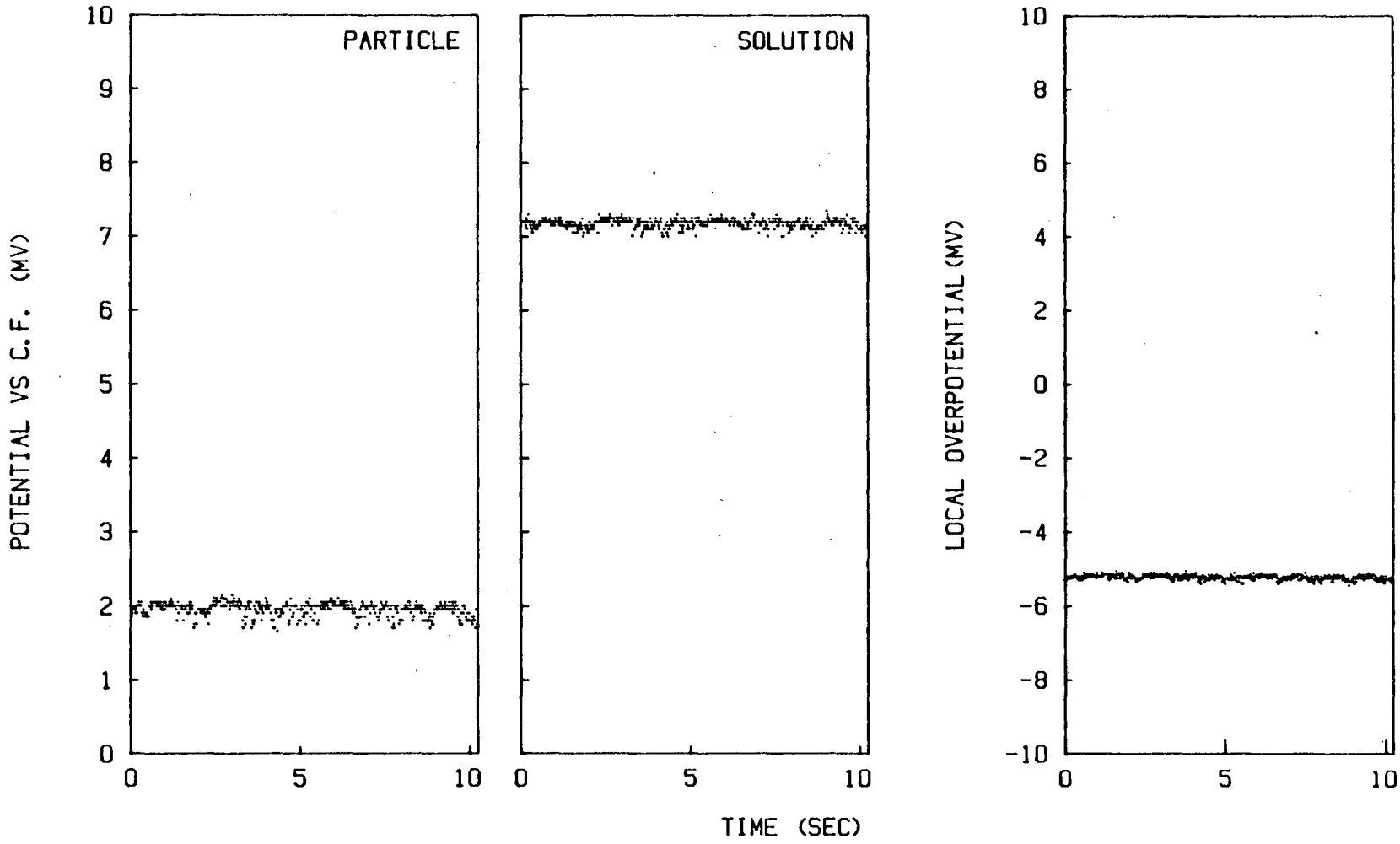

Figure A-2 Potential transients from center of the moving bed electrode S.C.D. = 200 mA/cm^2

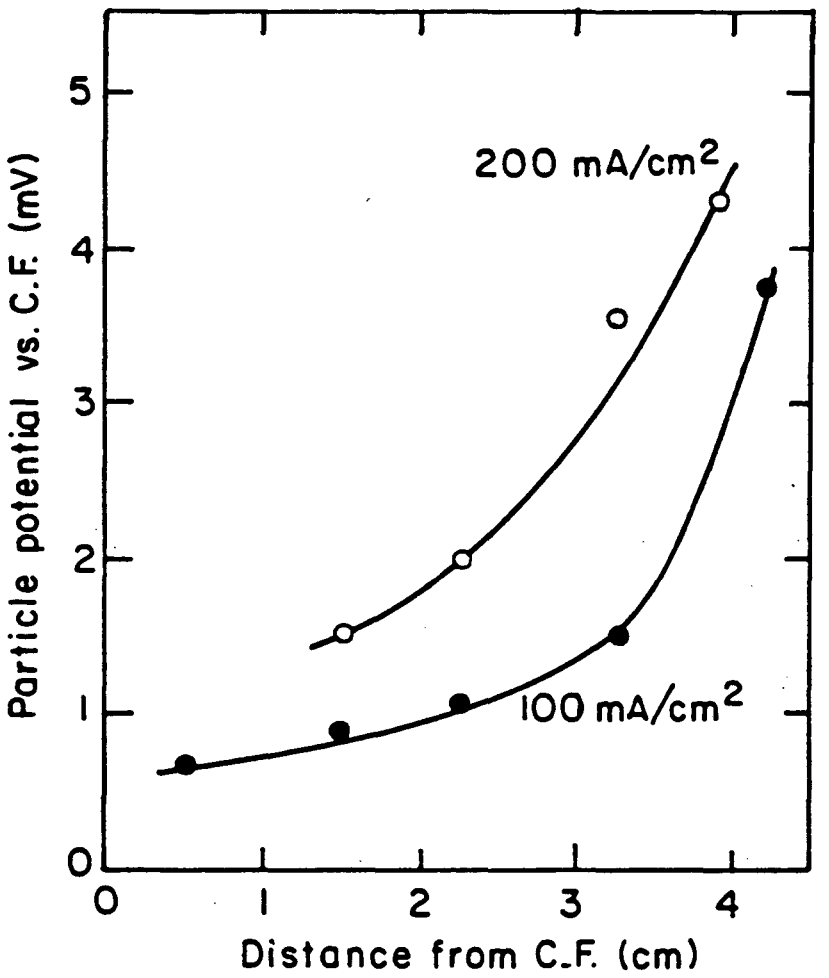

Figure A-3 Time averaged particle potential distribution through moving bed electrode at two different superficial current densities

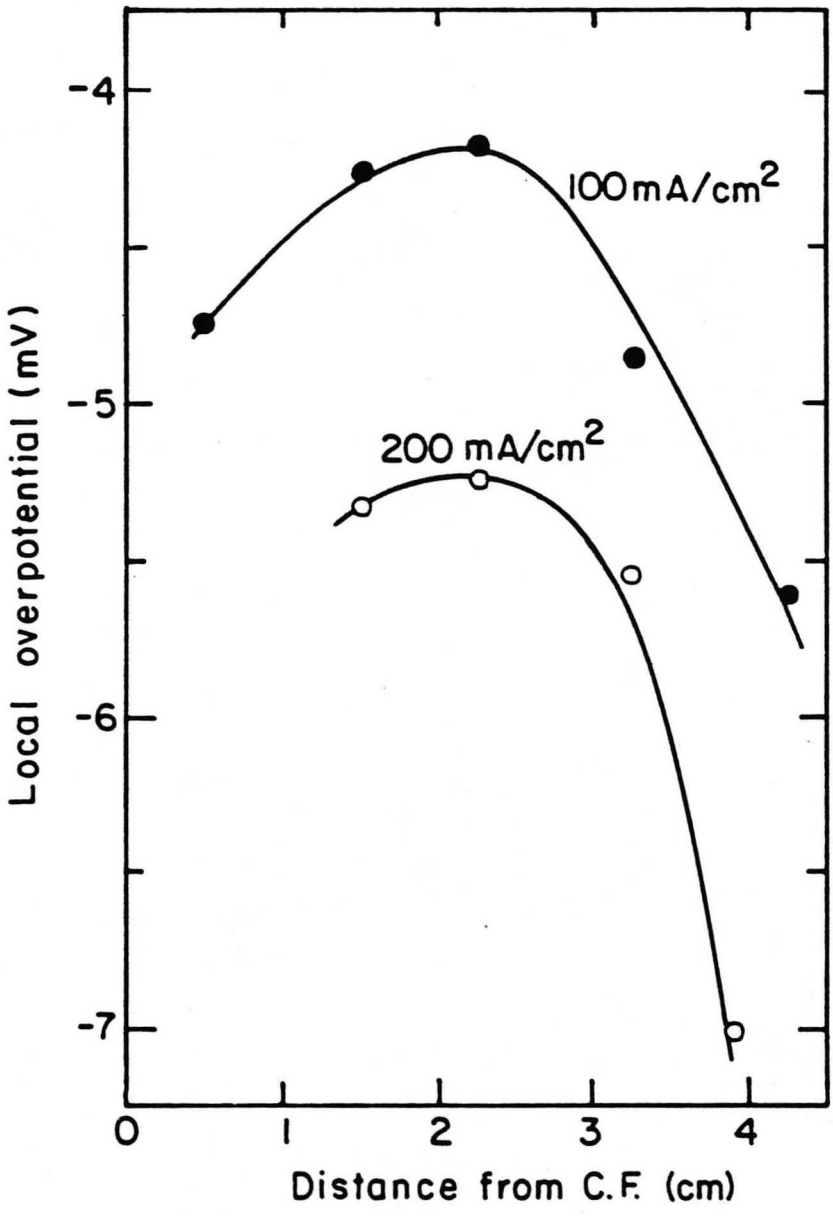

Figure A-4 Time averaged local overpotential distribution through moving bed electrode at two different superficial current densities

term operation.

APPENDIX B: APPARATUS FOR STUDYING THE EFFECT OF FLUCTUATING CURRENT/POTENTIAL ON ZINC DEPOSIT MORPHOLOGY.

For further studies of zinc morphology with fluctuating potential akin to those of the fluidized bed electrode, the following system was designed and is under operation now. The collected overpotential traces from the fluidized bed electrode are applied from a microcomputer through a programmable potentiostat to the rotating disc electrode, which is kept at the same hydrodynamic conditions as the fluidized bed electrode.

The apparatus is shown in Figure B-1.

This study is ongoing, and while it was found that fluctuating current affects zinc electrodeposit morphology significantly, no attempt is made to present detailed results.

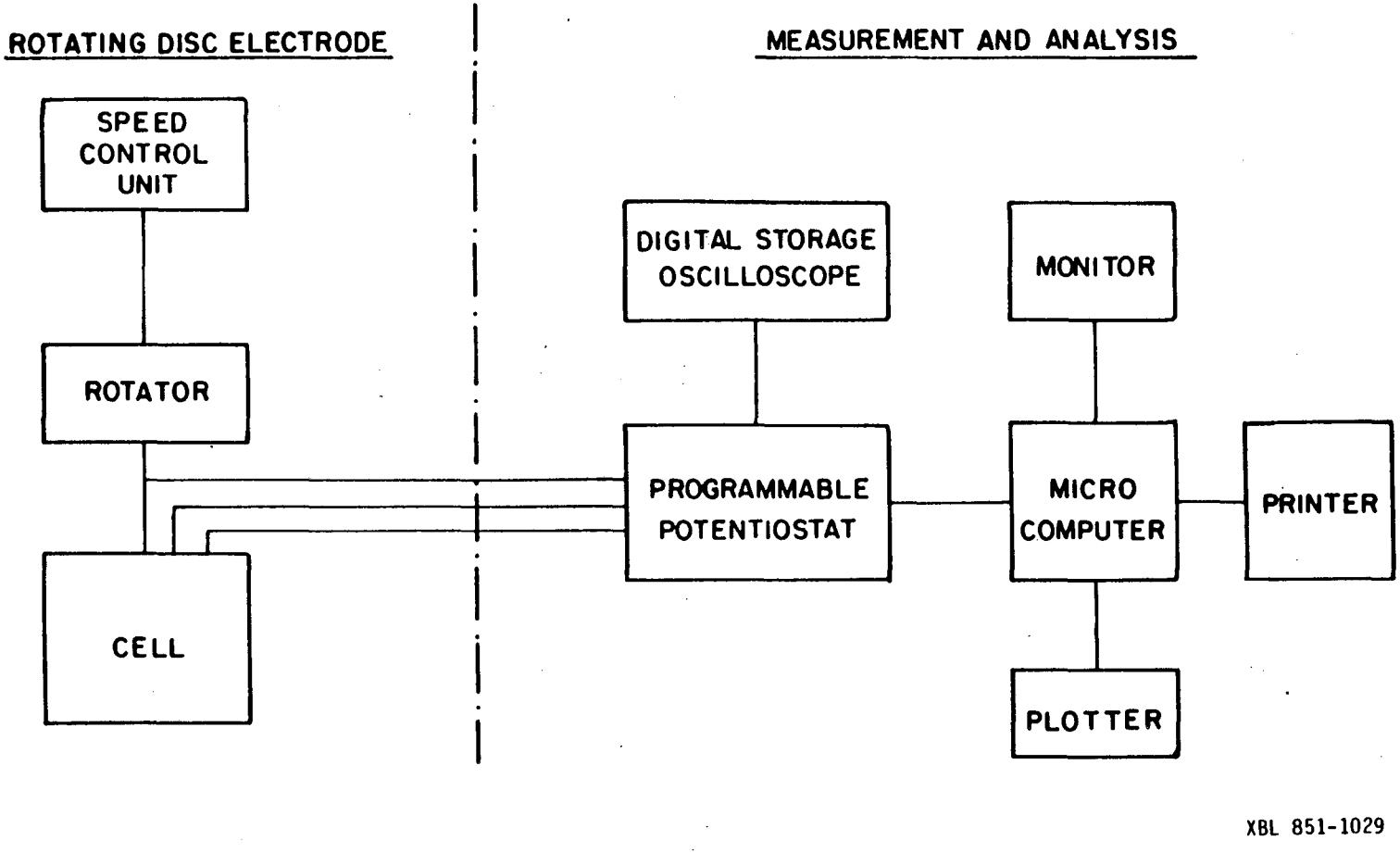

Figure B-1 Apparatus schematic for the study of effect of fluctuating potential/current on zinc electrodeposit morphology

REFERENCES

1. A. C. Trupp, "Dynamics of Liquid Fluidized Beds of Spheres", I. Chem. Eng. Symposium Series (1968) 30, 182
2. J. Bordet, O. Borlai, F. Vergnes and P. LeGoff, "Direct Measurement of the Kinetic Energy of Particles and their Frequency of Collision against a Wall in a Liquid-Solids Fluidized Bed", I. Chem. Eng. Symposium Series (1968) 30, 165
3. P. LeGoff, F. Vergnes, E. Coeuret and J. Bordet, "Applications of Fluidized Beds in Electrochemistry", Ind. and Eng. Chem. 61 (1969) 10, 8
4. J. R. Backhurst, J. M. Coulson, F. Goodridge, R. E. Plimley and M. Fleischmann, "A Preliminary Investigation of Fluidized Bed Electrodes", J. Electrochem. Soc 116 (1969) 1600
5. M. Fleischmann, J. W. Oldfield and L. Tennakoon, "Fluidized Bed Electrodes, Part I. Polarization Predicted by Simplified Models", J. Electroanal. Chem. 29 (1971) 211
6. M. Fleischmann and J. W. Oldfield, "Fluidized Bed Electrodes, Part II. The Effective Resistivity of the Discontinuous Metal Phases", ibid 29 (1971) 231
7. F. Goodridge, D. I. Holden, H. D. Murray and R. E. Plimley, "Fluidized Bed Electrodes, Part I: A Mathematical Model Of the Fluidized Bed Electrode", Trans. Instn. Chem. Engrs. 49 (1971) 128
8. B. J. Sabacky, "A Study on the Electrowinning of Metals Using A Fluidized Bed Electrode", Ph.D. dissertation (1978) University of

California, Berkeley

9. B. J. Sabacky and J. W. Evans, "The Electrical Conductivity of Fluidized Bed Electrodes-It's Significance and Some Experimental Measurements", Met. Trans. 8B (1977) 5

10. B. J. Sabacky and J. W. Evans, "Electrodeposition of Metals in Fluidized Bed Electrodes Part 1. Mathematical Model", J. Electrochem. Soc. 126 (1979) 1176

11 J. S. Newman and C. W. Tobias, "Theoretical Analysis of Current Distribution in Porous Electrodes" ibid 109 (1962) 1183

12 A. A. C. M. Beenakers, W. P. van Swaaij, A. Welmers and T. H. Twente, "Charge Transfer in a Fluidized Bed Electrode", I. S. E. 27th Meeting, Zurich (1976) Extended Abstracts No.18

13 F. Goodridge, "Some Recent Developments of Monopolar and Bipolar Fluidized Bed Electrodes", Electrochim Acta 22 (1977) 929

14 F. Goodridge, C. J. H. King and A. R. Wright, "Performance Studies on a Bipolar Fluidized Bed Electrode", ibid 22 (1977) 1087

15 R. L. Plimley and A. R. Wright, "A Bipolar Mechanism for Charge Transfer in a Fluidized Bed Electrode", Chem. Eng. Sci. 39 (1984) 395

16 J. C. R. Turner, "Electrical Conductivity of Liquid Fluidized Beds", American Inst. Chem. Eng. Symp. Series 69 (1973) 115

17 D. Handley and C. D. Eardley, "Bipolar Electrolysis with Intraphase Conduction in Fluidized Beds", Chem. and Ind. (1975) 8, 330

18 F. W. Salt, "Electrodeposition of an Adherent Coating onto Stainless Steel Powder", Proc. Chem. Eng. Conf. (1968) 169

19 D. S. Flett, "Methods, Apparatus: New Product Research, Process Development and Design", Chem. and Ind. 51 (1971) 300

20 M. Fleischmann, J. W. Oldfield and D. F. Porter, "Fluidized Bed Electrodes, Part III. The Cathodic Reduction of Oxygen on Silver in a Fluidized Bed Electrode", J. Electroanal. Chem 29 (1971) 241

21 M. Fleischmann, J. W. Oldfield and L. Tennakoon, "Fluidized Bed Electrodes, Part IV. Electrodeposition of Copper in a Fluidized Bed of Copper Coated Spheres", J. App. Electrochem. 1 (1971) 103

22 F. Goodridge, D. I. Holden, H. D. Murray and R. F. Plimley, "Fluidized Bed Electrodes, Part II. Non-Uniform Behavior of the Hydrodynamic Entrance Region", Trans. Inst. Chem. Eng. 49 (1971) 137

23 S. Germain and F. Goodridge, "Copper Deposition in a Fluidized Bed Cell", Electrochim. Acta 21 (1976) 545

24 F. Goodridge and C. J. Vance, "Copper Deposition in a Pilot Plant Scale Fluidized Bed Cell", ibid 24 (1979) 1237

25 D. S. Flett, "The Fluidized Bed Electrode in Extractive Metallurgy", Chem. and Ind. 52 (1972) 983

26 J. A. E. Wilkinson and K. P. Haines, "Feasibility Study on the Electrowinning of Copper with Fluidized Bed Electrodes", 81 (1972) C157

27 ibid, 82 (1973) C119

28 D. C. Carbin and D. R. Gabe, "Electrodeposition from a Fluidized Bed Electrolytes-II.", J. of Applied Electrochem 5 (1975) 129

29 ibid, 137

30 A. J. Monhemius and P. L. N. Costa, "Interactions of Variables in

the Fluidized Bed Electrowinning of Copper", Hydromet. 1 (1975) 183

31 F. Goodridge, letter to the editor, Hydromet. 1 (1976) 393

32 C. C. Simpson Jr, "Purity of Copper Produced by Fluid Bed Electrolysis of a Heap-Leach Solution", J. Metals 29 (1977) 7, 7

33 D. Hutin and F. Coeuret, "Experimental Study of Copper Deposition in a Fluidized Bed Electrode", J. Applied Electrochem. 7 (1977) 463

34 B. J. Sabacky and J. W. Evans, "Electrodeposition of Metals in Fluidized Bed Electrodes, Part II. An Experimental Investigation of Copper Electrodeposition at High Current Density", J. Electrochem. Soc. 126 (1979) 1180

35 I. F. Masterson, " The Use of Fluidized Bed Electrodes for Electrowinning Metals from Aqueous Solution in a 1000 Ampere and Other Cells", Ph.D. Dissertation (1980) University of California, Berkeley

36 I. F. Masterson and J. W. Evans, "Fluidized Bed Electrowinning of Copper; Experiments using 150 Ampere and 1000 Ampere Cells and Some Mathematical Modelling", Met. Trans. 13B (1982) 3

37 D. P. Ziegler, "Anodes for Use in Fluidized Bed Electrowinning ", M.S. Thesis (1980) University of California, Berkeley

38 D. P. Ziegler, M. Dubrovsky and J. W. Evans, "A Preliminary Investigation of Some Anodes for Use in Fluidized Bed Electro-deposition of Metals", J. Applied Electrochem. 11 (1981) 625

39 M. Dubrovsky, D. P. Ziegler, I. F. Masterson and J. W. Evans, "Electrowinning of Copper and of Cobalt using Fluidized Bed Cathodes", Ext. Met (1981) Inst. Min. Met. London

40 W. G. Sherwood, P. B. Queneau, C. Nikolic and D. R. Hedges, "Fluid Bed Electrolysis of Nickel", Met. Trans. 10B (1979) 659

41 M. Dubrovsky and J. W. Evans, "An Investigation of Fluidized Bed Electrowinning of Cobalt Using 50 Ampere and 1000 Amp Cells", Met. Trans. 13B (1982) 293

42 F. Goodridge and C. J. Vance, "The Electrowinning of Zinc Using a Circulating Bed Electrode", Electrochim. Acta. 22 (1977) 1073

43 V. Jiricny and J. W. Evans, "Fluidized Bed Electrodeposition of Zinc", Met. Trans 15B (1984)

44 R. C. Reloy, "Fluidized Bed Electrowinning-I. General Modes of Operation", Electrochim. Acta. 23 (1978) 815

45 R. L. Reloy, "Fluidized Bed Electrowinning-II. Operation at Constant Current Density", ibid, 827

46 D. C. Carbin and D. R. Gabe, "Electrodeposition from Fluidized Bed Electrolytes-I.", Electrochim. Acta. 19 (1974) C119

47 D. J. Pickett, "An Approximate Design Relationship for a Fluidized Bed Electrode Operating Under Condition of Mass Transfer Control", J. Applied Electrochem. 5 (1975) 101

48 D. R. Gabe and D. C. Carbin, "Optimisation of Mass Transport in Fluidized Bed Electrolytes", Chem. and Ind. 55 (1975) 335

49 Editor, "Fluidized Bed Electrolysis System Debuts", Chem. Eng. 77 (1978)

50 B. J. Zadra, A. L. Engels and H. J. Heinen, "Process for Recovering Gold and Silver from Activated Carbon by Leaching and Electrolysis", U. S. B. M. Report 4843 (1952)

51 K. B. Hall, "Homestake's Bulldog Mountain Carbon-In-Pulp Silver Plant", World Mining 27 (1974) 12 44

52 G. Kreysa and E. Heitz, "Kinetic Investigation into Silver Deposition in a Fluidized and Packed Particle Electrode", Chem. and Ind. April 19 (1975) 332

53 R. L. Paul, A. O. Filmer and M. J. Nicol, "The Recovering of Gold from Concentrated Aurocyanide Solutions", Hydrometallurgy Research, Development and Plant Practice, TMS-AIME (1983) 689

54 B. Watterman, F. A. Olson and T. N. Anderson, "The Electrowinning of Gold with Fluidized Bed Electrode", Proceedings of the International Symposium of Electrochemistry in Mineral and Metal Processing, Cincinati, Ohio (1984), 661

55 D. Doniat, "Electrochemical Generator Comprising an Electrode in the Form of a Suspension", U. S. Patent 4,126,733 (1978)

56 M. Fleischmann and G. H. Kelsall, "An Investigation of the Local Behavior of a Copper Fluidized Bed Electrode", Chem. and Ind. April 19 (1975) 329

57 J. McBreen and E. J. Cairns, "The Zinc Electrode", Advances in Electrochemistry and Electrochemical Engineering Vol. 11, Interscience, NY (1979)

58 J. S. Fordyce and R. L. Baum, "Vibrational Spectra of Solutions of Zinc Oxide in Potassium Hydroxide", J. Chem. Phy 43 (1965) 3 843

59 N. A. Hampton and M. J. Tarbox, "The Anodic Behavior of Zinc in Potassium Hydroxide Solution, 1. Horizontal Anode", J. Electrochem. Soc 110 (1963) 95

60 J. P. Elder, "The Electrochemical Behavior of Zinc in Alkaline Media", ibid, 116 (1969) 757

61 T. P. Dirkse and N. A. Hampson, "The Anodic Behavior of Zinc in Aqueous KOH Solution-I. Passivation Experiments at Very High Current Densities", Electrochim. Acta. 16 (1971) 2049

62 G. Coates, N. A. Hampton, A. Marshall and D. F Porter, "The Anodic Behavior of Porous Zinc Electrodes. II. The Effects of Specific Surface Area of the Zinc Compact Materials", J. Applied Electrochem. 4 (1974) 75

63 R. W. Powers and M. W. Breiter, "The Anodic Dissolution and Passivation of Zinc in Concentrated Potassium Hydroxide Solutions", J. Electrochem. Soc. 116 (1969) 719

64 R. D. Amstrong and G. M. Bulman, "The Anodic Dissolution of Zinc in Alkaline Solutions", J. Electroanal. Chem. 25 (1970) 121

65 R. W. Powers, "Anodic Films on Zinc and the Formation of Cobwebs", 116 (1969) 1652

66 M. N. hull and J. E. Toni, "Formation and Reduction of Films on Amalgamated and Non-Amalgamated Zinc Electrodes in Alkaline Solutions", Trans. Fara. Soc. 67 (1971) 1128

67 B. N. Kabanov, "La Theorie de la Passivation du Zinc et la Possibilite de la Transition des Couches d'Adsorption Passivantes en Couches Epaisses", Electrochim. Acta 6 (1962) 253

68 C. M. Shepherd and H. C. Langelan, "High Rate Battery Electrodes", J. Electrochem. Soc. 114 (1967) 8

69 J. S. Drury, N. A. Hampton and A. Marshall, "The Anodic Behavior of

Zinc in Silicate-Containing Alkaline Solutions", J. Electroanal. Chem. 50 (1974) 292

70 A. Marshall, N. A. Hampton and J. S. Drury, "The Anodic Behavior of Zinc in Flowing Electrolyte System", ibid, 59 (1975) 19

71 S. Arouete, K. F. Blurton and H. G. Oswin, "Controlled Current Deposition of Zinc from Alkaline Solution", J. Electrochem. Soc. 116 (1969) 166

72 R. D. Naybour, "The Effect of Electrolyte Flow on the Morphology of Zinc Electrodeposited from Aqueous Alkaline Solution Containing Zincate Ions", ibid, 520

73 J. O'M. Bockris, Z. Nagy and A. Damjanovic, "On the Deposition and Dissolution of Zinc in Alkaline Solutions", ibid, 119 (1972) 285

74 R. A. Myers and J. M. Marchello, "Capacities of Zinc Potassium Hydroxide Interfaces", ibid, 116 (1969) 790

75 N. A. Hampton, G. A. Herman and R. Taylor, "Some Kinetic and Thermodynamic Studies of the System Zn/Zn(II), OH^-", J. Electroanal. Chem. 25 (1970) 9

76 A. Marshall, N. A. Hampton and J. S. Drury, "The Discharge Behavior of The Zinc/Air Slurry Cell", J. Electroanal. Chem 59 (1975) 33

77 T. Yoshimura, H. Fukuda and M. Yamashita, "Discharge Behavior of Zinc-Bed Electrode", (1975) 1148

78 A. J. Appleby and M. Jacquier, "The C.G.E. Circulating Zinc/Air BAttery: A Practical Vehicle Power Source", J. Power Sources 1 (1976/77) 17

79 A. J. Appleby, J. Jacquelin and J. P. Pompon, "Charge-Discharge

Behavior of the C.G.E. Circulating Zinc-Air Vehicle Battery", SAE Paper 770381, SAE Auto. Eng. Conf. Detroit (1977)

80 R. L. Clarke and A. R. Wasson, "Zinc-Air-Hydrogen, An Alternative Battery System for Electric Vehicles", Extended Abstracts of the 35th Meeting of the International Society of Electrochemistry, Berkeley (1984) 222

81 G. E. P. Box and G. M. Jenkins, "Time Series Analysis, Forecasting and Control", Holden-Day, San Francisco (1970)

82 J. S. Bendat and A. G. Piersol, "Random Data: Analysis and Measurement Procedures", Wiley-Interscience, NY (1971)

83 E. A. Robinson, "Multichannel Time Series Analysis with Digital Computer Programs, 2nd Ed.", Holden-Day, SF (1983)

84 E. A. Robinson and M. T. Silvia, "Digital Foundations of Time Series Analysis, Vol. 2. Wave-Equation, Space-Time Processing", Holden-Day, SF (1979)

85 E. A. Robinson, "Time Series Analysis and Application", Goose Pond Press, Houston (1979)

86 R. N. Bracewell, "The Fourier Transformation and its Applications, 2nd Ed.", McGraw-Hill, NY (1978)

87 R. K. Otnes and L. Enchson, "Digital Time Series Analysis", Johnson & Sons, NY (1972)

88 N. Tanaka and R. Tamamuchi, "Kinetic Parameters of Electrode Reactions", Electrochim. Acta. 9 (1964) 963

89 F. N. H. Robinson, "Noise in Electrical Circuit", Oxford University Press (1962)

90 J. S. Bendat, "Principles and Applications of Random Noise Theory", John Wiley & Sons, NY (1958)

91 A. Ryan and T. Scranton, "D-C Amplifier Noise Revisited; Understanding, Measuring and Testing for Random Noise", Anal. Dial. 18 (1984) 1, 3

92 D. Kunni and O. Levenspiel, "Fluidization Engineering", John Wiley & Sons, NY (1969)

93 J. F. Davidson and D. Harrison, "Fluidized Particles", Cambridge University Press, NY (1963)

This report was done with support from the Department of Energy. Any conclusions or opinions expressed in this report represent solely those of the author(s) and not necessarily those of The Regents of the University of California, the Lawrence Berkeley Laboratory or the Department of Energy.

Reference to a company or product name does not imply approval or recommendation of the product by the University of California or the U.S. Department of Energy to the exclusion of others that may be suitable.

LAWRENCE BERKELEY LABORATORY
TECHNICAL INFORMATION DEPARTMENT
UNIVERSITY OF CALIFORNIA
BERKELEY, CALIFORNIA 94720